

# COMPUTATIONAL FLUID DYNAMICS MODELLING OF DISSOLVED OXYGEN IN OXIDATION DITCHES

---

TOM MATKO

DOCTOR OF ENGINEERING

Centre for Digital Entertainment  
Bournemouth University

July 2020



Water Innovation  
& Research  
Centre



Wessex Water  
YTL GROUP



## Copyright Statement

*This copy of the thesis has been supplied on condition that anyone who consults it is understood to recognise that its copyright rests with its author and due acknowledgement must always be made of the use of any material contained in, or derived from, this thesis.*

SUPERVISORS:

Prof Jian Chang, Bournemouth University

Prof Jan Hofman, University of Bath

## **Abstract**

This research aims to reveal new knowledge about the factors that affect the hydrodynamics, dissolved oxygen (DO) and aeration performance of a wastewater oxidation ditch. The literature is reviewed on the Computational Fluid Dynamics (CFD) modelling of wastewater aeration tanks. This study develops a CFD model of an aerated oxidation ditch, by taking into account two-phase gas-liquid flow, inter-phase oxygen mass transfer and dissolved oxygen. The main contributions to knowledge are the effect of bubble size distribution (BSD) and biochemical oxygen demand (BOD) distribution on the DO distribution. Species transport modelling predicts the BOD and DO distribution in the ditch. De-oxygenation of local dissolved oxygen by BOD is modelled by an oxygen sink that depends on the local BOD concentration. This is a novel approach to flow modelling for the prediction of the DO distribution. The local BOD concentration in the ditch may depend on either the local DO concentration or the local residence time. The numerical residence time distribution (RTD), heterogeneous flow pattern and DO distribution indicate that the flow behaviour in the ditch is non-ideal. Dissolved oxygen is affected by BOD distribution, bubble size, BSD, mechanical surface aeration and temperature. There is good agreement between the numerical simulation and both the observation of flow pattern and the measurement of mean DO. The BSD predicts a mean bubble size of around 2 mm, which is also the bubble size that best agrees with the measurements of DO. This study identifies that the BOD distribution and the BSD are key parameters that affect the DO distribution and improve the accuracy of the agreement with experimental data. In decreasing order of aeration performance are the air membrane diffuser, Fuch air jet aerator, Kessener brush surface aerator and Maguire hydro-jet aerator.

## Acknowledgments

There are organisations I wish to thank for their help and support. The research is supported, managed and funded by the Centre for Digital Entertainment (CDE) and the Engineering and Physical Sciences Research Council (EPSRC). The project is supported by Wessex Water, that has close links to the Water Innovation and Research Centre (WIRC) in the University of Bath. I wish to thank everyone in the NCCA in Bournemouth University and in the chemical and process engineering department in the University of Bath for their help in training, resources, seminars, management and advice in this project. I wish to thank engineers in Wessex Water for their help in acquiring data and during the experiments at Potterne WWTP.

My supervisor Professor Jian Chang at Bournemouth University has given me encouragement and technical advice for the full four year length of the doctorate. Dr Zhidong Xiao at Bournemouth University has helped me in my first year. My supervisor Professor Jan Hofman at the University of Bath has helped me technically in CFD and aeration wastewater treatment. I thank John Leonard from Wessex Water who has been enthusiastic in our meetings and shares a common interest in running. Acknowledgments to Professor John Chew and Dr Jannis Wenk from the chemical engineering department at the University of Bath, who attended meetings and gave me useful technical advice. Most important is my wife Emal who encouraged me and gave me advice in her unique caring way. Her own work is on radar engineering, remote sensing and space engineering.

During my doctorate I ran my 100th 10K and 350th race in the world's most northern race in Svalbard. I have already completed 100 half marathons races. There are only a few runners who have reached these major milestones. Here are transcendental, philosophical and inspiring quotes which apply to both running and research: "run when you can, walk if you have to, crawl if you must, just never give up", "crossing the start line may be an act of courage, but crossing the finish line is an act of faith", "joy was in the act of running and in the journey, not in the destination".

Copyright Statement.....	II
Abstract .....	III
Acknowledgments .....	IV
List of Figures and Tables .....	VII
List of Symbols.....	XI
1. Introduction .....	1
1.1 Background.....	1
1.2 Motivation.....	2
1.3 Aims and objectives .....	3
1.4 Contribution to knowledge.....	4
1.5 Thesis structure.....	5
2. Literature review.....	7
2.1 Introduction .....	7
2.2 Aeration design and fluid dynamics.....	11
2.3 Theory.....	23
2.4 CFD modelling .....	39
2.5 Experimental validation .....	59
2.6 CFD application to aeration design .....	65
2.7 Summary.....	68
3. Numerical model of single-phase flow.....	72
3.1 Introduction .....	72
3.2 Theory.....	73
3.3 Numerical methods .....	76
3.4 Results and discussion .....	86
3.5 Summary.....	99
4. Numerical model of multi-phase flow .....	101
4.1 Introduction .....	101
4.2 Theory.....	102
4.3 Numerical methods .....	104
4.4 Results and discussion .....	107
4.5 Summary.....	134

5.	Numerical model of dissolved oxygen .....	136
5.1	Introduction .....	136
5.2	Theory .....	137
5.3	Numerical methods .....	141
5.4	Results and discussion .....	145
5.5	Summary.....	164
6.	Parameter study.....	165
6.1	Introduction .....	165
6.2	Theory.....	166
6.3	Numerical methods .....	166
6.4	Results and discussion .....	169
6.5	Summary.....	185
7.	Experimental validation .....	186
7.1	Introduction .....	186
7.2	Method .....	187
7.3	Results and discussion .....	189
7.4	Summary.....	201
8.	Aeration system design.....	203
8.1	Introduction .....	203
8.2	Theory.....	204
8.3	Method.....	205
8.4	Results and discussion .....	206
8.4	Summary.....	218
9.	Conclusions and future work .....	219
9.1	Conclusions.....	219
9.2	Future work .....	221
	References.....	223
	Appendix .....	237

## List of Figures and Tables

Figure 2.1	Activated sludge treatment process (Degremont, 2007).....	8
Figure 2.2	Wastewater treatment plant with oxidation ditches (Karpinska, 2013)....	8
Figure 2.3	Energy requirements of aeration (Rosso et al, 2008) .....	9
Figure 2.4	Reactor types (Jin et al, 2004).....	11
Figure 2.5	Channel with full floor coverage aeration (Le Moullec et al, 2008a) .....	12
Figure 2.6	Channel with centrally distributed aeration (Le Moullec et al, 2008b)...	12
Figure 2.7	Aeration tank design (Potier et al, 2005) .....	14
Figure 2.8	Oxidation ditch with horizontal surface aerators (Pereira et al, 2012) ..	14
Figure 2.9	Vertical shaft surface aerator profile (Stenstrom and Rosso, 2010) .....	20
Figure 2.10	Horizontal shaft surface aerator profile (Stenstrom and Rosso, 2010) .	20
Figure 2.11	Bubble size variation (Nopens et al, 2015).....	21
Figure 2.12	Bubble breakup and coalescence (Wang et al, 2011).....	22
Figure 2.13	Particle aggregation and breakup (Nopens et al, 2015) .....	22
Figure 3.1	Maguire jet aerator in OD1 .....	76
Figure 3.2	Surface brush aerators in OD1 .....	76
Figure 3.3	Grid membrane diffusers in OD1 and OD2.....	77
Figure 3.4	Fuch jet aerators in OD2.....	77
Figure 3.5	Propeller in flow booster in OD2 .....	78
Figure 3.6	Geometry of oxidation ditch 1 .....	79
Figure 3.7	Geometry of oxidation ditch 2 .....	80
Figure 3.8	Computational mesh of oxidation ditch 1 .....	82
Figure 3.9	Computational mesh of oxidation ditch 2 .....	83
Figure 3.10	Numerical residuals of case S4.....	85
Figure 3.11	Water velocity in OD2 with no devices .....	87
Figure 3.12	Water velocity in both ditches with no devices .....	88
Figure 3.13	Water velocity in OD1 with Maguire jet aerator .....	89
Figure 3.14	Water velocity in OD1 caused by Maguire jet aerator .....	90
Figure 3.15	Water velocity in OD1 with surface aerators only .....	91
Figure 3.16	Water velocity in OD1 caused by surface aerators .....	92
Figure 3.17	Water velocity vectors in OD1 with surface and jet aeration .....	93
Figure 3.18	Water velocity contours in OD1 with surface and jet aeration .....	94
Figure 3.19	Water velocity in OD2 with flow booster - mid depth .....	95
Figure 3.20	Water velocity in OD2 caused by flow booster .....	96
Figure 3.21	Water velocity in OD1 and OD2 - different cases.....	97
Figure 4.1	Numerical residuals of case M5.....	106
Figure 4.2	Volume fraction of air in OD2 with no aerators .....	108
Figure 4.3	Water velocity in OD1 with Maguire jet aerator.....	109
Figure 4.4	Water velocity in OD1 caused by Maguire jet aerator.....	110
Figure 4.5	Volume fraction of air in OD1 caused by Maguire jet aerator .....	110
Figure 4.6	Water velocity in OD1 with surface aerators only .....	111
Figure 4.7	Volume fraction of air in OD1 caused by surface aerators.....	112
Figure 4.8	Water velocity in OD1 with diffuser only .....	113

Figure 4.9	Water velocity in OD1 caused by diffuser.....	113
Figure 4.10	Volume fraction of air in OD1 caused by diffuser .....	114
Figure 4.11	Water flow patterns in OD1 - operating conditions at WWTP.....	115
Figure 4.12	Volume fraction of air in OD1 - operating conditions .....	116
Figure 4.13	Water velocity in OD2 with flow booster .....	117
Figure 4.14	Water velocity and air volume fraction in OD2 with Fuch aerators .....	118
Figure 4.15	Volume fraction of air in OD2 caused by Fuch jet aerator .....	119
Figure 4.16	Water velocity and air volume fraction in OD2 with diffusers.....	120
Figure 4.17	Water velocity in OD2 caused by diffuser.....	121
Figure 4.18	Water flow pattern in OD2 - operating conditions at WWTP.....	122
Figure 4.19	Water velocity in OD2 near diffuser - ditch length .....	124
Figure 4.20	Water velocity in OD2 near Fuch jet aerators in parallel .....	124
Figure 4.21	Volume fraction of air in OD2 .....	124
Figure 4.22	Volume fraction of air in OD2 near diffusers and Fuch jet aerator.....	124
Figure 4.23	Volume fraction of air in OD1 (case M5 - without TDF).....	125
Figure 4.24	Volume fraction of air in OD1 (case M5 - with TDF).....	125
Figure 4.25	Multi-phase water flow pattern in OD1 with mesh refinement .....	127
Figure 4.26	Multi-phase water flow pattern in OD2 with mesh refinement .....	128
Figure 4.27	RTD of OD1 and OD2 without aerators (case S1) .....	131
Figure 4.28	RTD of OD1 with Maguire jet aerator only (case S2) .....	131
Figure 4.29	RTD of OD1 with surface aerators only (case S3) .....	131
Figure 4.30	RTD of OD1 with Maguire jet and surface aerators (case S4) .....	131
Figure 4.31	RTD of OD2 with flow booster (case S5) .....	131
Figure 4.32	RTD of OD1 - operating conditions (case M5) .....	132
Figure 4.33	RTD of OD2 - operating conditions (case M9) .....	132
Figure 5.1	Numerical residuals of scalar equations .....	144
Figure 5.2	Water velocity in OD1 without devices .....	149
Figure 5.3	Water velocity in OD1 with surface aerators only .....	149
Figure 5.4	DO concentration in OD1 with surface aerators only .....	149
Figure 5.5	Water velocity in OD1 with diffuser only .....	150
Figure 5.6	DO concentration in OD1 with diffuser only .....	150
Figure 5.7	Water velocity in OD1 with Maguire jet aerator only .....	150
Figure 5.8	DO concentration in OD1 with Maguire jet aerator only.....	151
Figure 5.9	Water velocity in OD1 - operating conditions at WWTP .....	151
Figure 5.10	Air velocity in OD1 - operating.....	151
Figure 5.11	Volume fraction of air in OD1 - operating .....	152
Figure 5.12	Mass fraction of oxygen in air phase in OD1 - operating.....	152
Figure 5.13	Mass transfer coefficient in OD1 - operating .....	152
Figure 5.14	Mass fraction of oxygen in water phase in OD1 - operating.....	153
Figure 5.15	DO concentration in OD1 - operating .....	153
Figure 5.16	DO percentage saturation in OD1 - operating .....	153
Figure 5.17	Water velocity in OD2 with flow booster .....	154
Figure 5.18	Water velocity in OD2 with diffusers only .....	154
Figure 5.19	DO concentration in OD2 with diffusers only.....	154

Figure 5.20	Water velocity in OD2 with Fuch jet aerators only.....	155
Figure 5.21	DO concentration in OD2 with Fuch jet aerators only .....	155
Figure 5.22	Water velocity in OD2 - operating conditions .....	156
Figure 5.23	DO concentration in OD2 - operating conditions.....	156
Figure 5.24	Residence time in OD1 - operating conditions .....	157
Figure 5.25	BOD concentration in OD1 depends on residence time .....	157
Figure 5.26	BOD concentration in OD1 depends on DO.....	158
Figure 5.27	Water velocity in OD1 - operating conditions .....	161
Figure 5.28	DO concentration in OD1 - operating - uniform BOD (15 mg/l) .....	161
Figure 5.29	DO concentration in OD1 - operating - distributed BOD.....	161
Figure 5.30	Water velocity in OD2 - operating conditions .....	162
Figure 5.31	Air velocity in OD2 - operating.....	162
Figure 5.32	Volume fraction of air in OD2 - operating .....	162
Figure 5.33	Mass transfer coefficient in OD2 - operating .....	163
Figure 5.34	DO concentration in OD2 - operating - uniform BOD (15 mg/l) .....	163
Figure 6.1	Water velocity in OD1 - standard model.....	173
Figure 6.2	Mass transfer coefficient in OD1 without BOD - standard.....	173
Figure 6.3	DO concentration in OD1 without BOD - standard .....	173
Figure 6.4	DO concentration without BOD - summer (20 °C) .....	174
Figure 6.5	Water velocity - surface aeration (12 h <sup>-1</sup> ).....	174
Figure 6.6	DO concentration without BOD - surface aeration (12 h <sup>-1</sup> ) .....	174
Figure 6.7	DO without BOD - bubble diameter (3 mm).....	175
Figure 6.8	DO without BOD - bubble diameter (2 mm).....	175
Figure 6.9	DO without BOD - bubble diameter (1 mm).....	175
Figure 6.10	Air velocity - bubble diameter (1 mm).....	176
Figure 6.11	BSD without BOD - equal diameter discretisation .....	176
Figure 6.12	BSD without BOD - equal mass discretisation .....	176
Figure 6.13	Water velocity - BSD - equal diameter discretisation .....	177
Figure 6.14	Mass transfer without BOD - equal diameter discretisation.....	177
Figure 6.15	Mass transfer without BOD - equal mass discretisation .....	177
Figure 6.16	DO without BOD - equal diameter discretisation.....	178
Figure 6.17	DO without BOD - molar fraction Henry coefficient (x 0.5) .....	178
Figure 6.18	DO without BOD - mass diffusivity of oxygen in water (x 2) .....	178
Figure 6.19	DO with uniform BOD - standard model.....	181
Figure 6.20	DO with distributed BOD - standard model .....	181
Figure 6.21	DO with uniform BOD - summer (20 °C) .....	181
Figure 6.22	DO with distributed BOD - summer (20 °C).....	182
Figure 6.23	DO with uniform BOD - surface aeration (12 h <sup>-1</sup> ) .....	182
Figure 6.24	DO with distributed BOD - surface aeration (12 h <sup>-1</sup> ).....	182
Figure 6.25	DO with distributed BOD - bubble (3 mm).....	183
Figure 6.26	DO with distributed BOD - bubble (2 mm).....	183
Figure 6.27	DO with distributed BOD - bubble (1 mm).....	183
Figure 6.28	DO with uniform BOD - BSD - equal diameter discretisation.....	184
Figure 6.29	DO with distributed BOD - BSD - equal diameter discretisation .....	184

Figure 7.1	Multi-phase flow simulation of water velocity in OD1 .....	190
Figure 7.2	Sketches of water flow patterns in OD1 observed at WWTP .....	190
Figure 7.3	Multi-phase flow simulation of water velocity in OD2.....	191
Figure 7.4	Sketches of water flow patterns in OD2 observed at WWTP.....	191
Figure 7.5	Observed flow behaviour in OD1 .....	192
Figure 7.6	Observed flow behaviour in OD2.....	193
Figure 7.7	Numerical DO concentrations and measurement locations.....	194
Figure 7.8	DO for mean bubble sizes - distributed BOD in OD1.....	196
Figure 7.9	DO for BSD - distributed BOD in OD1 .....	196
Figure 7.10	DO for temperature and surface OTR - distributed BOD in OD1.....	196
Figure 7.11	DO for standard model - uniform and distributed BOD in OD1.....	197
Figure 7.12	DO for BSD - uniform and distributed BOD in OD1.....	197
Figure 7.13	DO for temperature - uniform and distributed BOD in OD1 .....	197
Figure 7.14	DO for standard model - uniform BOD in OD2.....	197
Figure 8.1	Water velocity in OD1 with surface aerators only .....	208
Figure 8.2	DO in OD1 with surface aerators only .....	208
Figure 8.3	Water velocity in OD1 with diffuser only .....	209
Figure 8.4	DO in OD1 with diffuser only .....	209
Figure 8.5	Water velocity in OD1 with Maguire jet aerator only .....	209
Figure 8.6	DO in OD1 with Maguire jet aerator only .....	210
Figure 8.7	Water velocity in OD1 - operating conditions.....	210
Figure 8.8	DO in OD1 - operating conditions.....	210
Figure 8.9	Water velocity in OD2 with flow booster only.....	212
Figure 8.10	Water velocity in OD2 with diffusers only .....	212
Figure 8.11	DO in OD2 with diffusers only .....	213
Figure 8.12	Water velocity in OD2 with Fuch jet aerators only.....	213
Figure 8.13	DO in OD2 with Fuch jet aerators only .....	213
Figure 8.14	Water velocities in OD2 - operating conditions.....	214
Figure 8.15	DO in OD2 - operating conditions .....	214
Table 2.1	Activated sludge modelling software .....	38
Table 3.1	Single-phase flow simulations .....	86
Table 3.2	Mean water velocity for single-phase flow .....	98
Table 4.1	Gas-liquid flow simulations .....	107
Table 4.2	Mesh convergence study.....	129
Table 4.3	Hydraulic parameters of residence time distribution .....	133
Table 5.1	Physical properties of dissolved oxygen modelling.....	145
Table 5.2	Dissolved oxygen concentrations without BOD .....	146
Table 6.1	Physical properties of parameter study in OD1 .....	169
Table 6.2	Effect of parameters on dissolved oxygen - without BOD in OD1.....	170
Table 6.3	Effect of parameters on dissolved oxygen - with BOD in OD1.....	179
Table 7.1	Dissolved oxygen compared to measurements at locations in OD1...	195
Table 7.2	Dissolved oxygen compared to measurements at locations in OD2...	195
Table 8.1	Dissolved oxygen and aerator efficiencies without BOD.....	206

## List of Symbols

Symbol	Description	Units
$a$	specific interfacial area	$m^{-1}$
$a$	bubble interfacial area	$m^2$
AE	aeration efficiency in clean water	$kgO_2 \cdot kW/h$
$b$	circular horizontal projected area of diameter	$m$
$B_{br}$	birth rate of bubble breakup	$kg/m^3s$
$B_{co}$	birth rate of bubble coalescence	$kg/m^3s$
$c$	vertical smaller axis	$m$
$C$	suspended solids concentration	$kg/m^3$
$C, C_0, C_{tr}$	tracer concentration	$kg/m^3$
$C'$	dimensionless tracer concentration	-
$C_0$	initial DO concentration in aeration tank	$mg/l$
$C_0$	influent BOD concentration	$mg/l$
$C_d$	drag coefficient of spherical bubbles in pure liquid	-
$C_{DLS}$	drag coefficient of solid phase in liquid phase	-
$C_{DS}, C_L^*, C_s$	saturation dissolved oxygen concentration in water	$kg/m^3$
$C_L, C_S, C_t$	dissolved oxygen concentration in water	$kg/m^3$
$C_{p1}, C_{p2}, C_1, C_2$	turbulent constants	-
$C_t$	BOD concentration in water phase at LMA	$mg/l$
$C_{td}$	turbulent dispersion force coefficient	-
$D$	molecular (mass) diffusion coefficient	$m^2/s$
$D_{br}$	death rate of bubble breakup	$kg/m^3s$
$D_{co}$	death rate of bubble coalescence	$kg/m^3s$
$D$	hydraulic diameter	$m$
$d$	floc diameter	$m$
$d$	distance from wall to boundary layer	$m$
$d_b$	bubble diameter	$m$
$D_b$	equivalent non-spherical bubble diameter	$m$
$d_i$	bubble diameter of phase i	$m$
$D_m$	mass diffusivity	$m^2/s$
$D_o$	standard mass diffusivity of oxygen at 20 °C	$m^2/s$
$D_{radius}$	drum radius	$m$
$D_{rotsp}$	drum rotational speed	$rpm$
$d_s, d_p$	particle diameter	$m$

E	aeration efficiency of spray water in air	%
E	bubble eccentricity with ellipsoid bubble shape	-
$E_o$	Eötvös number	-
$f_i$	ratio of total volume of bubbles of class i to all classes	-
$\overline{F}_q$	interfacial forces between phases	N
G	turbulent velocity gradient	$s^{-1}$
G	turbulence generation term	$kg/ms^3$
$H^x$	molar fraction Henry coefficient	Pa
K	von Karman constant	-
k	temperature dependent decay rate constant	$day^{-1}$
k, $k_{inl}$	velocity scale turbulent kinetic energy	$m^2/s^2$
$k_1$	floc settling parameter	$m^3/kg$
$k_2$	colloids settling parameter	$m^3/kg$
$K_G$	gas film mass transfer coefficient	m/s
$K_H$	molar concentration Henry coefficient	$Pa \cdot m^3/mol$
$K_L$	liquid film / local mass transfer coefficient	m/s
$K_L a$	overall / oxygen mass transfer coefficient	$s^{-1}, h^{-1}$
$K_L a_L$	mass transfer coefficient	$s^{-1}$
$K_L a_T$	$K_L a$ coefficient at temperature T	$s^{-1}$
$K_L a_{tw}$	oxygen mass transfer coefficient of tap water	$s^{-1}$
$K_L a_{ww}$	oxygen mass transfer coefficient of wastewater	$s^{-1}$
$L_k$	interfacial transfer of oxygen between phases	$kg/m^3s$
$M_{L,G}$	inter-phase momentum exchange of gas and liquid	$N/m^3$
$M_{L,S}$	inter-phase momentum exchange of solid and liquid	$N/m^3$
$m_{pq}^i, m_{qp}^i$	mass transfer from phase p to q and from phase q to p	$kg/s$
$M_t$	mass of tracer injected	kg
OTE	oxygen transfer efficiency	%
OTR	oxygen transfer rate	$kg/h$
$OTR_{sp}$	oxygen transfer rate of spray water	$mg/h$
P	power input	kW
p	pressure	$N/m^2$
$P_{Ag}$	partial pressure of component A in gas phase	Pa
$P_G$	partial pressure of oxygen in bulk gas phase	Pa
$P_i$	partial pressure of oxygen at interface	Pa
$Pr_a$	propeller area	$m^2$
$Pr_r$	propeller radius	m

$Pr_t$	propeller reaction thrust	N
$Pr_v$	propeller volume	$m^3$
Q	spray water flow rate	l/h
Q	volumetric flow rate	$m^3/s$
r	mass transfer rate per interfacial area per time	$kg/m^2s$
$Re_b$	bubble Reynolds number	-
$Re_m$	mixture Reynolds number	-
$Sc_t$	turbulent Schmidt number	-
$S_m$	fluid mass source	$kg/m^3s$
$S_o$	DO concentration in liquid phase	$g/m^3$
$S_{o(s)}$	saturation DO concentration in clean water	$g/m^3$
$S_p$	fluid momentum source	$kg/m^2s^2$
T	temperature	$^{\circ}C$
t	LMA in water phase	day
t'	dimensionless time	-
$t_o$	theoretical / hydraulic mean residence time	s
$u^*$	friction velocity	m/s
u, v, w	directional mean flow velocities	m/s
$u_g$	gas velocity	m/s
$u_{inl}$	inlet velocity	m/s
$u_l$	liquid velocity	m/s
$u_p$	particle velocity	m/s
$u_p$	flow velocity parallel to wall	m/s
$\overline{u_r}$	whirl velocity	m/s
V	tank fluid volume	$m^3$
$V, V_o$	terminal settling velocity of suspended solids floc	m/s
$V_a$	angular velocity	m/s
$V_b$	bubble volume	$m^3$
$v_i, v_j, v_k$	i, j, k directional velocities	m/s
$V_p$	fluid velocity	m/s
$V_r$	relative velocity between liquid and gas phases	m/s
$W_o$	maximum solids settling velocity	m/s
$V_s, W_s$	solids settling velocity	m/s
$V_t$	tangential velocity	m/s
$V_{tl}$	kinematic eddy viscosity of liquid phase	$m^2/s$
$wO_2$	oxygen supply	$kgO_2/h$

$X$	mixed liquor suspended solids concentration	mg/l
$x, x_i, x_j, x_k$	i, j, k directional distances	m
$X_{Al}$	mole fraction of component A in liquid phase	-
$y_p^+$	dimensionless wall distance	-
$y_p$	wall distance	m

### Greek letters

$\alpha_q, \rho_q$	effective density of phase q	kg/m <sup>3</sup>
$\sigma, \sigma_{dl}, \sigma_k, \sigma_\varepsilon$	turbulent Schmidt number	-
$\mu$	dynamic viscosity	kg/ms
$\mu_l$	liquid water viscosity	kg/ms
$\mu_m$	mixture viscosity	kg/ms
$\mu_t$	turbulent viscosity	kg/ms
$\mu_q$	shear viscosity of phase q	kg/ms
$C_\mu$	turbulent model constant	-
$u_\alpha$	terminal vertical bubble velocity	m/s
$\alpha$	oxygen transfer factor of wastewater and clean water	-
$\alpha_g$	gas holdup / gas volume fraction	-
$\alpha_i$	volume fraction of phase i	-
$\beta$	solids settling empirical constant	m <sup>3</sup> /kg
$\gamma$	solids settling empirical constant	s
$\gamma$	surface tension of bubble	N/m <sup>2</sup>
$\varepsilon, \varepsilon_{inl}$	turbulence length scale eddy dissipation rate	m <sup>2</sup> /s <sup>3</sup>
$\varepsilon_G$	gas hold up / gas volume fraction	-
$\varepsilon_s, \lambda_s$	solids volume fraction	-
$\theta$	temperature coefficient	-
$\lambda$	minimum compressive settling velocity	m/s
$\rho$	oxygen mass transfer rate from gas to liquid phase	g/m <sup>3</sup> s
$\rho_g$	air bubble density	kg/m <sup>3</sup>
$\rho_l, \rho_w$	liquid water density	kg/m <sup>3</sup>
$\rho_p$	primary particle density	kg/m <sup>3</sup>
$\rho_p, \rho_q$	density of phases p and q	kg/m <sup>3</sup>
$\omega$	specific frequency	s <sup>-1</sup>
$\overline{\omega}$	angular velocity	rad/s

## Acronyms

ADV	Acoustic Doppler Velocimetry
AE	Aeration Efficiency
ALOD	Air Lift Oxidation Ditch
ALR	Air Lift Reactor
ASM	Activated Sludge Model
ASM	Algebraic Stress Model
ASMM	Algebraic Slip Mixture Model
ASR	Aerated Stirred Reactor
BCR	Bubble Column Reactor
BNRM	Biological Nutrient Removal Model
BOD	Biochemical Oxygen Demand
BSD	Bubble Size Distribution
CAD	Computer Aided Design
CFD	Computational Fluid Dynamics
CFR	Cage Fin Rotor
COD	Chemical Oxygen Demand
CRWR	Cage Rope Wound Rotor
CSTR	Continuous Stirred Tank Reactor
DNS	Direct Numerical Simulation
DO	Dissolved Oxygen
E-E	Eulerian-Eulerian
EGSB	Expanded Granular Sludge Bed Reactor
E-L	Eulerian-Lagrangian
HRT	Hydraulic Residence Time
LDV	Laser Doppler Velocimetry
LES	Large Eddy Simulation
LMA	Local Mean Age
MLSS	Mixed Liquor Suspended Solids
MRF	Multiple Reference Frame
MSM	Momentum Source Model
MUSIG	Multiple Size Group Model
MWM	Moving Wall Model
OD	Oxidation Ditch

OTE	Oxygen Transfer Efficiency
OTR	Oxygen Transfer Rate
PAO	Phosphorus Accumulating Organism
PBM	Population Balance Model
PDA	Particle Doppler Anemometry
PFR	Plug Flow Reactor
PIV	Particle Image Velocimetry
PSD	Particle Size Distribution
RANS	Reynolds Averaged Navier-Stokes
RFR	Rotating Frame of Reference
RNG	Reynolds Normalisation Group
RPM	Revolutions Per Minute
RSM	Reynolds Stress Model
RTD	Residence Time Distribution
SBR	Sequencing Batch Reactor
SGBR	Static Granular Bed Reactor
SMM	Sliding Mesh Model
SST	Shear Stress Transport
TDF	Turbulent Dispersion Force
TN	Total Nitrogen
TP	Total Phosphorus
TSS	Total Suspended Solids
URANS	Unsteady Reynolds Averaged Navier-Stokes
VOF	Volume of Fluid
WWTP	Wastewater Treatment Plant

# 1. Introduction

## 1.1 Background

The research is about the computational fluid dynamics (CFD) modelling of dissolved oxygen (DO) in an aerated oxidation ditch in activated sludge wastewater treatment. The aeration bioreactor needs sufficient oxygen to allow the aerobic bacteria to reduce the biochemical oxygen demand (BOD) of the wastewater. Therefore an aeration system is always needed in the bioreactor (Metcalf et al, 2003). Aeration (Rosso et al, 2008) is usually the largest energy cost (45 - 90 %) in a waste water treatment plant (WWTP). Therefore reducing the energy consumption of aeration is usually the best step to minimise the total energy cost of a WWTP.

CFD is the numerical simulation of fluid flow, heat transfer, fluid turbulence, multi-phase components of droplets, bubbles and particles, species transport and chemical and biochemical reaction (Ranade, 2002). Developments in multiphase flow research have seen a steady growth in the CFD modelling of water and wastewater treatment for disinfection, dissolved air flotation, the activated sludge bioreactor, primary and secondary sedimentation and anaerobic digestion (Samstag et al, 2016). CFD simulation can be used to predict the multiphase flow pattern and the multi-component distribution of dissolved oxygen (DO) in an aeration tank. It can be used to investigate how aeration design affects the hydrodynamics, oxygen transfer and aeration efficiency (Brannock, 2003). It enables process design improvements for aeration technology (Karpinska et al, 2010).

## 1.2 Motivation

The long term motivation of the project is to reduce the considerable energy consumption of aeration in activated sludge treatment. Wessex Water invest in new state of the art oxidation ditches that enable better understanding of aeration treatment, and may lead to more efficient processing and significant cost reduction. However, these designs could have a detrimental effect, due to their curved geometry, shallow depth and different aeration devices. There is insufficient research and simulation and experimental data to support these designs.

The project therefore develops computational fluid dynamics (CFD) models to provide detailed understanding of the effects of aeration systems on aeration performance in Wessex Water's oxidation ditches at Potterne WWTP in Wiltshire, England. The project studies the factors that affect the hydrodynamics, dissolved oxygen (DO) and aeration performance. The numerical flow pattern and dissolved oxygen distribution is evaluated tangibly by comparison between computation and on-site measurement. CFD simulations are also used to evaluate the designs of different types of aeration devices. These CFD models can be used in the future by Wessex Water for more detailed design and energy costing of the aeration devices.

### **1.3 Aims and objectives**

The research hypothesis is that accurate flow modelling can help reveal the core factors that relate to dissolved oxygen in an aeration tank. The newly developed numerical models are able to handle complex multi-phase and multi-component fluid phenomena and make the prediction of dissolved oxygen more accurate. CFD models predominantly only consider a uniform bubble size and a uniform biochemical oxygen demand (BOD) concentration. Determining the effects of bubble size, bubble size distribution (BSD), BOD distribution and other parameters on dissolved oxygen can help reveal new knowledge. CFD simulation used for aeration design retrofitting can improve the aeration performance and lead to energy savings.

#### **Aims**

- Reveal the core factors that relate to dissolved oxygen in an oxidation ditch.
- Develop new knowledge about the effects of bubble size, BSD, BOD distribution and aeration design on the hydrodynamics and dissolved oxygen.

#### **Objectives**

- Develop knowledge about the hydrodynamics and dissolved oxygen distribution of an oxidation ditch.
- Reveal new knowledge about the effects of parameters on the hydrodynamics and dissolved oxygen distribution in an oxidation ditch.
- Determine the level of accuracy of fluid simulation by validation with experimental data.
- Determine if there is better accuracy of prediction of the dissolved oxygen distribution, when comparing BSD with a uniform bubble size.
- Determine if there is better accuracy of prediction of the dissolved oxygen distribution, when comparing BOD distribution with a uniform BOD.
- Reveal new knowledge about the effects of aeration system design on the hydrodynamics and aeration performance of an oxidation ditch.

## 1.4 Contribution to knowledge

Here is a summary of the main contributions to knowledge of this research.

- Dissolved oxygen can be affected by BOD distribution, temperature, surface aeration, mean bubble size, bubble size distribution and transport properties.
- Decreasing bubble size increases the total interfacial bubble surface area which causes an increase in oxygen mass transfer and dissolved oxygen.
- The bubble size distribution when compared to a mean bubble size does improve the accuracy of the dissolved oxygen, in terms of better agreement with the measurements of the mean dissolved oxygen in the ditch.
- The bubble size distribution predicts a mean bubble size of 1.9 mm. The best agreement with the measurements of dissolved oxygen is a bubble size of 2 mm, suggesting this is the probable mean bubble size.
- The BOD distribution when compared to a mean BOD does improve the accuracy of the prediction of dissolved oxygen, in terms of better agreement with the measurements of the variation of dissolved oxygen in the ditch.
- There is good agreement between the numerical and physical observations of flow behaviour and between the numerical and measurements of mean DO.
- In decreasing order of aeration effectiveness are the membrane diffuser, Fuch air jet aerator, Kessener brush surface aerator and Maguire hydro-jet aerator.
- It is recommended that the flow booster, Maguire jet aerator and membrane diffusers are relocated to reduce the flow disturbance between the aerators.

## 1.5 Thesis structure

In **Chapter 2** the literature is reviewed about the CFD modelling of aeration tanks in activated sludge treatment. Numerical models, design applications and experimental validation are reviewed and the new opportunities for research are identified.

In **Chapter 3** single-phase flow simulations and the standard two equation k-epsilon turbulence model predict the water velocity distribution in two full-scale operational wastewater oxidation ditches. The commercial CFD software ANSYS-CFX is used for all CFD modelling. The rigid lid symmetry plane boundary condition models the water surface. The multiple reference frame (MRF) mixer model predicts the rotational mechanical solid-liquid interaction of the brush surface aerators. The momentum source model (MSM) predicts the flow dispersion of the flow booster.

In **Chapter 4** the Euler-Euler multi-fluid flow model predicts the two-phase gas-liquid flow velocity distribution and the volume fraction distribution. A uniform mean bubble size of 4 mm is an average value taken from the CFD studies in the literature. The suspended solids are ignored due to the complexity of modelling a three phase fluid system. The gas-liquid flow degassing plane boundary condition models the water surface. The residence time distribution (RTD) is predicted using a species transport equation of a passive tracer that is transported by the multi-phase flow pattern. A mesh independency and convergence study is conducted for a range of mesh sizes, that is also based on the multi-phase flow pattern.

In **Chapter 5** species transport simulation predicts the biochemical oxygen demand (BOD) distribution and dissolved oxygen (DO) concentration distribution, that are transported by the multi-phase flow pattern. The effect of BOD distribution on the DO distribution is studied. The local BOD concentration can either be solely dependent on the local DO concentration or the local residence time. The DO distribution is predicted by an oxygen mass transport equation, with source terms for aeration and a sink term for the oxygen consumption by BOD. There are two approaches: (1) uniform BOD and homogeneous oxygen sink, (2) BOD distribution and heterogeneous oxygen sink.

In **Chapter 6** a parameter study is conducted to see the effects of parameters on the dissolved oxygen distribution. The parameters are the BOD distribution, seasonal temperature, oxygen transfer rate (OTR) of surface aeration, bubble diameter, bubble size distribution (BSD) and species transport properties. To predict the BSD there are bubble break-up and coalescence models in the multiple size group (MUSIG) model. They are coupled to the multi-fluid multi-phase model by using population balance modelling (PBM).

In **Chapter 7** experimental validation of the CFD simulation is conducted. The physical observation of the flow pattern is conducted on two full-scale operational ditches at Potterne WWTP and compared to the numerical multi-phase flow pattern. The dissolved oxygen concentration measurements in the ditches using a portable DO meter are compared to species transport simulation of the dissolved oxygen.

In **Chapter 8** the performances of different types of aerators are evaluated. Design recommendations are given for the retrofitting of the aerators to improve the hydrodynamic and aeration performance of the ditch. In **Chapter 9** the conclusions of this study are presented and recommendations given for possible future study. In **Chapters 3 to 8**, where the CFD results are presented in figures, they are mostly shown on a plane that is near to the water surface. Where the location is different it is identified in the figure caption.

## **2. Literature review**

### **2.1 Introduction**

Aeration occurs in many water and wastewater treatment processes. Major advances in aeration technology came as a result of the activated sludge process (Arden and Lockett, 1914; Martin, 1927). Sludge suspension in the aeration bioreactor containing the purifying bacterial flora is called 'activated sludge'. Dissolved oxygen (DO) is one of the most important wastewater quality parameters in an activated sludge treatment process (Figure 2.1). Dissolved oxygen in the aeration bioreactor allows aerobic bacteria to remove the biochemical oxygen demand (BOD) of the wastewater. Due to the low rate of oxygen mass transfer from the gas to the liquid phase and the low solubility of oxygen in water, sufficient dissolved oxygen cannot be achieved naturally. Therefore an aeration system is always needed in the bioreactor (Metcalf et al, 2003). Reducing the energy usage of aeration is usually the best way to minimise the energy cost of a wastewater treatment plant (WWTP) (Figure 2.2). Aeration is usually the largest energy cost (Figure 2.3), as much as 45 - 90 % of the total energy requirements of a WWTP (Wasner et al, 1978; Rosso et al, 2008; US Water Environment Federation, 2009).

Activated sludge biological treatment in which wastewater is brought into contact with bacterial floc in the presence of oxygen is termed 'aeration'. The objective of aeration is to increase dissolved oxygen and remove substances by chemical and biological oxidation (Thakre et al, 2008). Aeration also provides mixing to ensure close contact between bacterial cells (biomass), polluting chemicals and wastewater (Degremont, 2007). The activated sludge process (Figure 2.1) usually includes biological treatment in an aeration tank, where there is a device for supplying oxygen to the biomass. There is also a mixing device to provide optimal contact between bacterial cells and nutrient, prevent solids deposits, and promote homogeneous distribution (Degremont, 2007). Distinct aerobic, anaerobic and anoxic regions in the bioreactor are for the removal of phosphorus and nitrogen (nutrients) and for better effluent quality. Simultaneous nitrification and denitrification may occur in different parts of the same tank. Aeration systems include oxidation ditches, anaerobic systems and biological nutrient removal (Mueller et al, 2002).

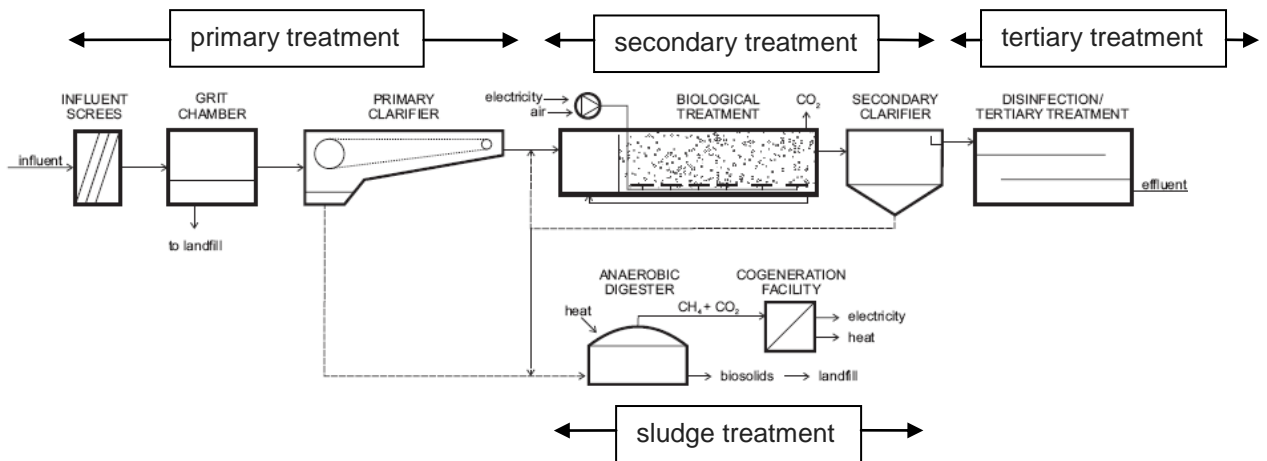


Figure 2.1 Activated sludge treatment process (Degremont, 2007)

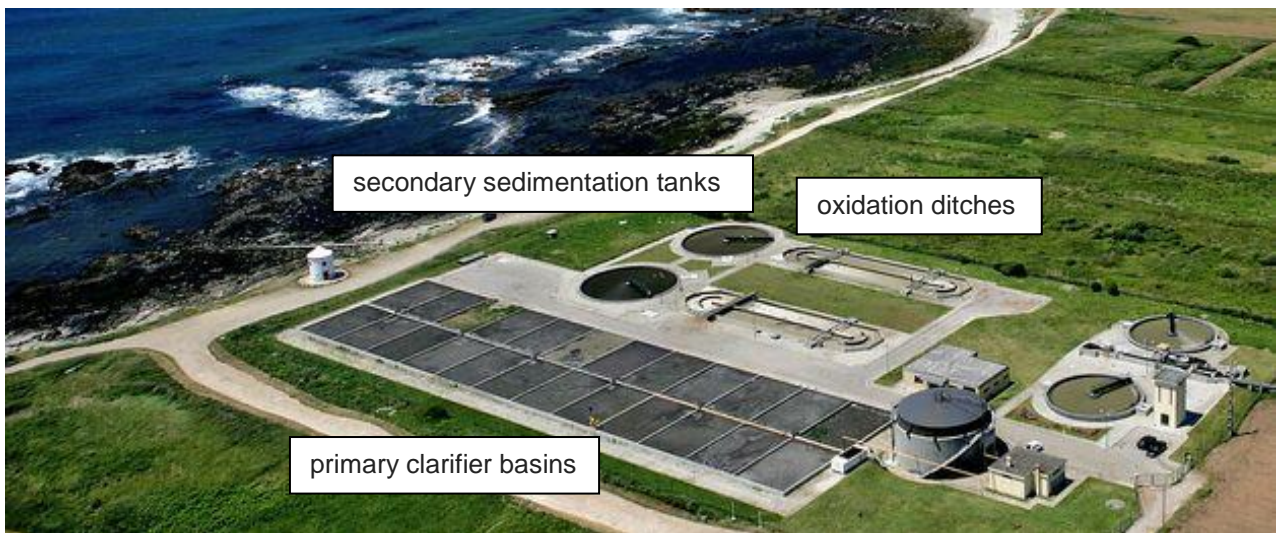


Figure 2.2 Wastewater treatment plant with oxidation ditches (Karpinska, 2013)

Wastewater is treated in three stages in Figure 2.1 (Metcalf et al, 2003). A typical WWTP with oxidation ditches is shown in Figure 2.2 (Karpinska, 2013). Primary treatment consists of screens, a grit chamber and a radial primary settler. Secondary treatment involves the activated sludge process, consisting of an oxidation ditch and a radial secondary clarifier. Tertiary treatment involves the final effluent that is disinfected and discharged into the receiving surface water (Karpinska, 2013). Secondary sedimentation is the separation of biological floc from the interstitial liquor. There is a recirculation stream where a large part of the sludge from the bottom of the secondary sedimentation tank is fed back into the aeration tank to support microorganisms in the biological floc (Degremont, 2007).

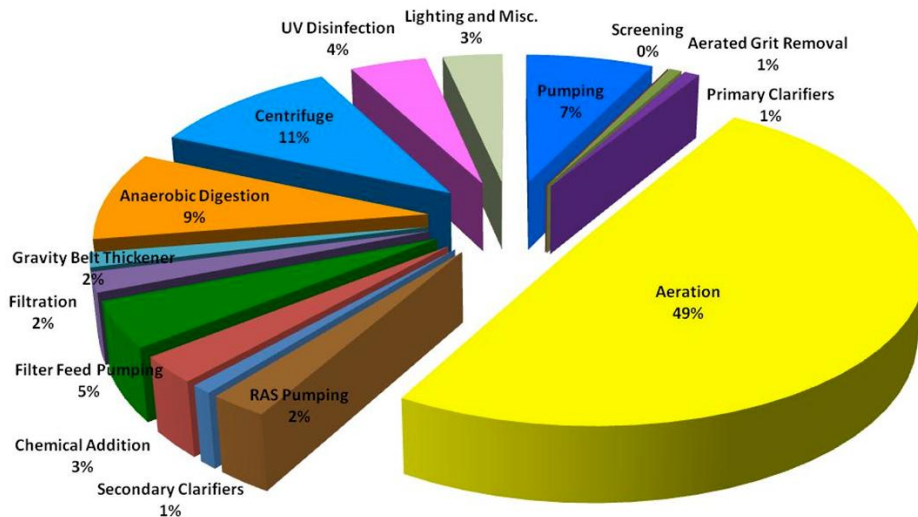


Figure 2.3 Energy requirements of aeration (Rosso et al, 2008)

Aeration bioreactors are complex physical-chemical-biological systems with gas-liquid-solid multi-phase flow. Aeration tank and aeration system design have an influence on the hydrodynamics, oxygen transfer and biological treatment (Jin et al, 2004). Hydrodynamic and hydraulic characteristics depend on the reactor geometry, physical properties and the aeration performance (Orhon et al, 1989). Important multiphase parameters are the gas-liquid interfacial area and the gas holdup (volume fraction of air), which affect the inter-phase mass and momentum transfer. They depend on the physical properties and the fluid flow regime (Jin et al, 2004).

Reactor modelling combines the hydrodynamics, inter-phase transfer processes and chemical kinetics, which are often coupled presenting a challenge (Ranade, 2002). The first step is hydrodynamics then transfer processes and then kinetics. Two different methods are used to model hydrodynamics. The first is hydraulic modelling often called systemic modelling (Levenspiel, 1998). It describes flow behaviour as a network of connected elementary reactors (plug flow and perfect mixed). Hydraulic modelling enables the global prediction of oxygen consumption, pollutant removal and biomass growth and decay. However, hydraulic models are empirical and heuristic, and neglect the detailed local component distribution within the reactor.

Computational fluid dynamics (CFD) is the mathematical solution of fluid flow by computer based simulation. It is the analysis of fluid flow, heat transfer, fluid turbulence, multi-phase components of droplets, bubbles and particles, species transport and chemical and biochemical reaction (Ranade, 2002). The fundamental Reynolds Averaged Navier-Stokes equations (RANS) of fluid flow are spatially discretised by using a geometric computational grid (equations 2.49 and 2.50).

CFD modelling is a powerful tool for predicting the local fluid behaviour within an aeration tank (Karpinska and Bridgeman, 2016). CFD models enable the prediction of the flow field, coupled with mass and heat transfer and chemical reactions, and the local distribution of components such as dissolved oxygen (Karpinska et al, 2010; Le Moullec et al, 2011). CFD can be used for reactor design to predict the effect of the hydrodynamics on aeration performance (Brannock, 2003).

CFD has found application with chemical engineers mainly for reactor design (Ranade, 2002). Recent developments in multiphase flow research have seen a steady growth in the application of CFD towards wastewater treatment, with a focus on the pumping station, grit chamber, flow splitter, disinfection tank, dissolved air flotation, activated sludge bioreactor, primary and secondary sedimentation tank and anaerobic digester (Karpinska and Bridgeman, 2015; Samstag et al, 2016).

## 2.2 Aeration design and fluid dynamics

### 2.2.1 Aeration bioreactor

Airlift, stirred and bubble columns are some of the designs of aeration bioreactors (Figure 2.4). Airlift reactors (ALR) are used in biochemical fermentation and in biological wastewater treatment, for example for the nitrification and denitrification of wastewater (Van Benthum et al, 1999). The main advantage is the liquid circulation has low shear stress on the particles where the biofilm grows (Van Baten et al, 2003). It has no moving parts, requires limited energy and has good mass and heat transfer (Mudde and Van den Akker, 2001). Air flow oxygenates the biomass and circulates the solid particles (Oey et al, 2001). Three phase airlift suspension reactors known as 'Circox' in wastewater treatment (Heijnen et al, 1997) are an alternative to slurry bubble column suspension reactors. In biofilm airlift suspension (BAS) reactors the solids phase consists of sand, which provides a large surface area, where biofilm is able to grow from the microorganisms.

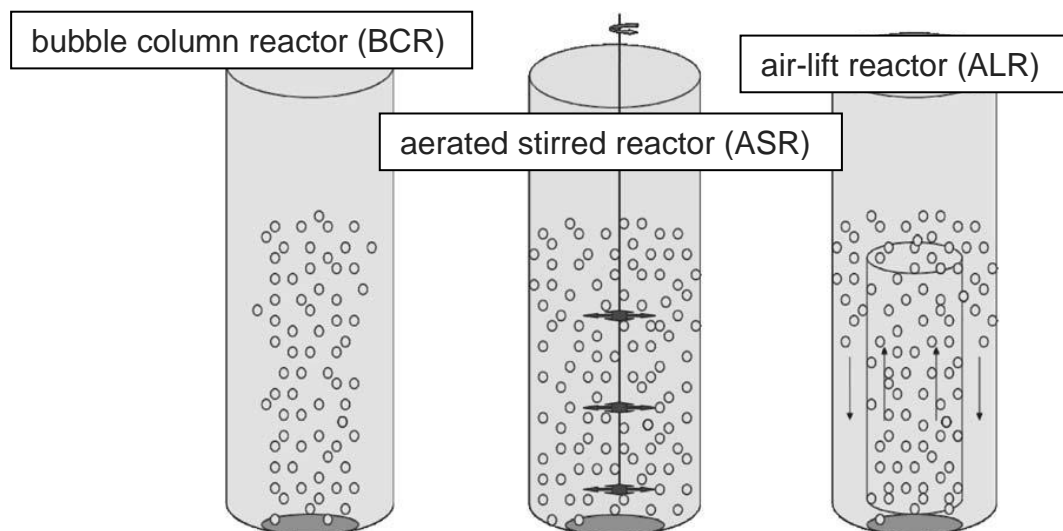


Figure 2.4 Reactor types (Jin et al, 2004)

Activated sludge reactors are mostly cross-flow in which the water flow is horizontal and the gas flow is vertical. The channel reactor with sparger aeration is one of the oldest systems and is well adapted to larger WWTPs (Figures 2.5, 2.6, 2.7). Due to its cuboid geometry there are concentration gradients for dissolved oxygen and nutrients (Dudley, 1995; Metcalf et al, 2003). CFD simulation of a channel reactor predicts hydrodynamics, oxygen mass transfer and biokinetic reactions (Le Moullec et al, 2008a (Figure 2.5); Le Moullec et al, 2008b (Figure 2.6)).

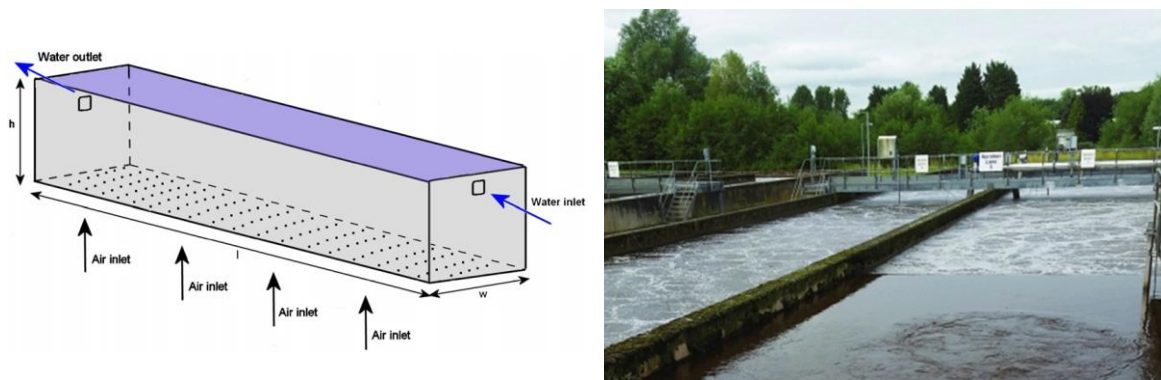


Figure 2.5 Channel with full floor coverage aeration (Le Moullec et al, 2008a)

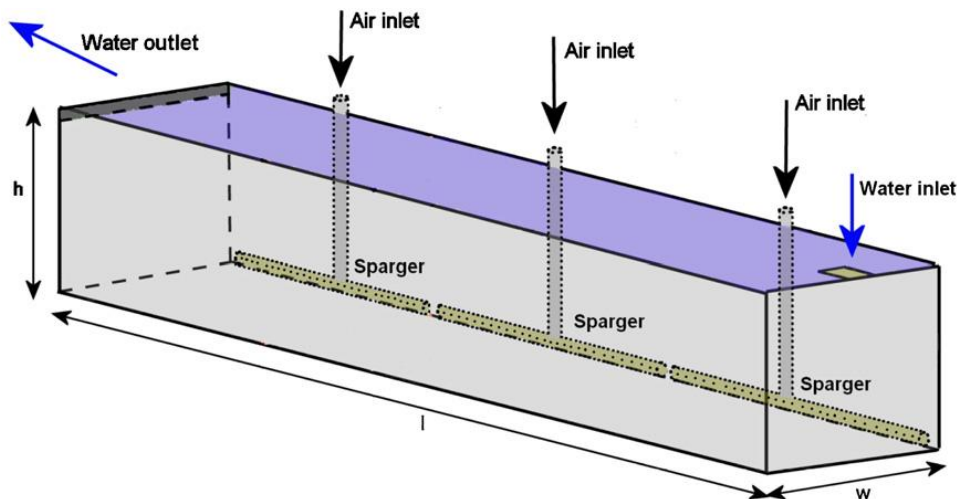


Figure 2.6 Channel with centrally distributed aeration (Le Moullec et al, 2008b)

The oxidation ditch (OD) is a modified activated sludge biological treatment process that utilises long solid retention times to remove biodegradable organics (Burrows et al, 2001; Yang et al, 2010). Typical oxidation ditches consist of a single or multichannel configuration within a ring, oval or horseshoe-shaped basin. Flow to the aeration ditch is aerated and mixed with return sludge from a secondary clarifier. Horizontally or vertically mounted aerators provide flow circulation, oxygen transfer and aeration in the ditch. The mixing process entrains oxygen into the mixed liquor for microbial growth. Aeration sharply increases the dissolved oxygen (DO) concentration, but DO decreases as the biomass uptakes the oxygen, as mixed liquor travels through the ditch. Solids are maintained in suspension as the mixed liquor circulates around the ditch. The oxidation ditch effluent is settled in a separate secondary clarifier (USEPA, 2000).

The oxidation ditch (OD) is a type of closed-loop open channel. Wastewater is driven by the impellers of the surface aerators and the fluid circulates within a 'racetrack'. Due to its curved geometry, shallow depth and local aeration sources, there are concentration gradients for dissolved oxygen and nutrients. There are design variations with anaerobic and anoxic zones and with mechanical mixers. They can be physically extended to facultative aerated lagoons. Channel reactors and closed-loop reactors have depths of up to a few meters. The air-lift oxidation ditch (ALOD) is much deeper (Xu et al, 2010).

These aeration tanks are called 'oxidation ditches' (Potier et al, 2005) when the aerators are horizontally oriented (Figure 2.7 and Figure 2.8 (Pereira et al, 2012)). They are called 'carrousel' when the aerators are vertically oriented (Figure 2.7). The Carrousel oxidation ditch is a closed looped channel, with a central dividing wall and a vertical rotating surface aerator at one or both ends of this wall. The mixed liquor in the Carrousel is oxygenated by low-speed vertical shaft aerators, to ensure proper mixing, and to generate the horizontal velocity and turbulence to mitigate against sludge settling. Aeration is concentrated at one vertical point in a carrousel, instead of being distributed over the length of an oxidation ditch. The mixed liquor is rich in oxygen as it flows out of the aeration zone, but low in oxygen as it returns back to the aeration zone (Koot and Zeper, 1972).

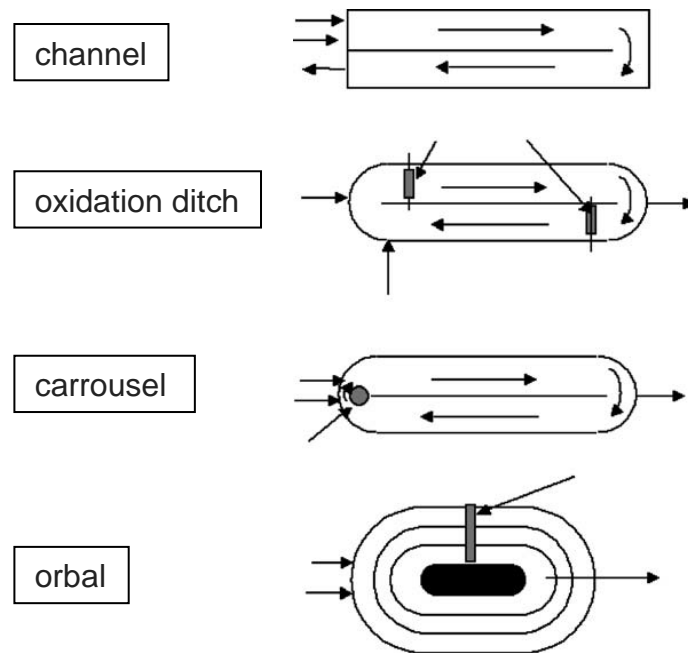


Figure 2.7 Aeration tank design (Potier et al, 2005)

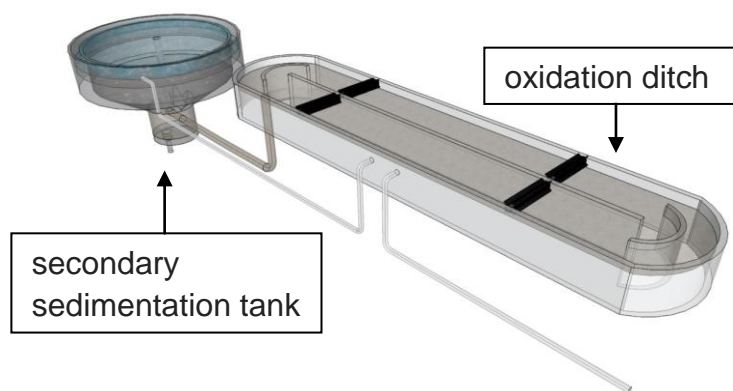


Figure 2.8 Oxidation ditch with horizontal surface aerators (Pereira et al, 2012)

The Orbal oxidation ditch is a special type of OD (Figure 2.7) which is subdivided into orbal concentric channels (Daigger and Littleton, 2000). Residence times are long and with increasing numbers of subdivisions the behaviour approaches that of the ideal plug flow regime (Drews et al, 1972, 1973). Dissolved oxygen concentrations are high downstream of the surface aerator and gradually decrease along the channel (Mandt and Bell, 1984; Metcalf et al, 2003; Guo et al, 2013).

The oxidation ditch was first developed in the Netherlands in 1959 (Pasveer, 1962). The first generation of oxidation ditch operates aeration and precipitation. The second generation has vertical surface aeration, nitrification and de-nitrification. The third generation has phosphorus and nitrogen removal. The fourth generation is the circulation ditch that improves efficiency and reduces plant labour (Wang et al, 2019). The ditch is commonly used in new WWTPs due to its high BOD, phosphorus and nitrogen removal, up to 75-95% (Benfield & Randall, 1980). By the late 1970s and mid 1980s in Europe, over 2,000 municipal WWTPs were using Pasveer horizontal aeration, with over 200 Carrousel vertical aeration systems (Mueller et al, 2002). In the USA alone, by the year 2000, ODs found application in more than 9,200 municipal WWTPs (USEPA, 2000). In China, the most commonly used technology is the OD in 32.1 % of WWTPs (Yang et al, 2008). Different reactor types are the Pasveers and Carrouseis (Koot and Zeper, 1972; Potier et al, 2005), Orbal, total barrier oxidation ditch and jet aeration channel (Mandt and Bell, 1984).

### **2.2.2 Aeration technology**

These are the types of aeration systems in aeration bioreactors (Thakre et al, 2008).

- Mechanical surface aeration is the transfer of oxygen to water by mechanical devices, to cause entrainment of atmospheric oxygen into the bulk liquid by surface agitation and mixing (Mueller et al, 2002). Surface aerators shear the water surface producing a spray of fine droplets that land on the surface.
- Diffusion aeration is the injection of air under pressure below a liquid surface (Mueller et al, 2002). This method releases smaller air bubbles at depth which rise and interact with the water surface. Diffusers are nozzles or porous surfaces that are usually located near the tank bottom.
- Jet aeration is a subset of diffusion aeration and produces small bubbles due to hydraulic shear (Mueller et al, 2002; Metcalf et al, 2003). It releases at depth a high velocity jet of water that is saturated with air or a high velocity jet of pure air. Jet nozzles can be near the tank bottom or at the mid water depth.

Early investigators were aware of the effect of bubble size, diffuser placement, flow circulation and gas flow rate on the oxygen transfer efficiency (OTE) (Martin, 1927). Mechanical aerators are widely used in WWTPs because of their better efficiency, operation and maintenance (Rao, 1999). They are divided into vertical axis or horizontal axis types (Thakre et al, 2008). Both of these are further subdivided into surface and submerged aerators. Surface mechanical aerators are often designed upon the original Kessener brush aerators, which has a cylinder with attached bristles. The bristles (or plastic bars or blades) are semi-submerged and the cylinder is rapidly rotated. Energy is transmitted through the top layer of the liquid and water is dispersed as small droplets (Thakre et al, 2008). Submerged horizontal axis aerators are similar except that they use disks or paddles (Metcalf et al, 2003).

Diffusion aeration systems blow compressed air into water at depth. Gas diffusers are categorised according to their bubble size (Degremont, 2007). Coarse bubble devices (bubble diameter > 6 mm) inject gas directly using vertical pressurised pipes and large orifices. Medium-bubble devices (4 to 5 mm) have smaller orifice openings. Fine-bubble devices (< 3 mm) use porous or finely perforated elastic membranes. Fine pore diffusers save at least half of the power of coarse bubble systems (Stenstrom and Rosso, 2010). Gas diffusers can also be categorised by (1) porous, (2) non-porous, (3) hybrid: jet, sparge turbine and U-tube (Karpinska, 2013). Due to its power efficiency, fine pore diffusion aeration with full floor coverage has become popular (Mueller et al, 2002). Another type uses jet aeration, where energy demand is mostly for pumping and air delivery. The energy from the jet keeps the solids in suspension and creates flow circulation (Karpinska et al, 2010). A more detailed history of aeration systems is in the literature (Karpinska, 2013).

### **2.2.3 Aeration energy requirement**

The oxygen transfer rate (OTR) is the mass of oxygen transfer per unit time and a key process design variable (equation 2.11). Another variable is the oxygen transfer per unit of oxygen supply. It is expressed as the oxygen transfer efficiency (OTE) and is equal to OTR divided by the oxygen supply rate (equation 2.12). The mass of oxygen transfer per unit of power input is the most important efficiency parameter. It is expressed as the aeration efficiency (AE) and is equal to the OTR divided by the

power input (equation 2.13). Since aeration systems are competitively bid on the basis of oxygen transfer per unit of power then the power requirement is important. The types of power are mechanical for rotors, air blowers and water pumps and conveyance for the motion of water. Conveyance relates to the effect of the device on the transport of water (Stenstrom and Rosso, 2010). The energy requirement of a device depends on its power, air and water supply. The device can therefore be evaluated by using process variables (OTR, OTE and AE). These variables can be determined by a CFD simulation that is able to predict the water velocity and dissolved oxygen in the aeration tank (Stenstrom and Rosso, 2010).

#### **2.2.4 Hydraulics**

Efficiency of the aeration bioreactor depends also on the liquid residence time distribution (Potier et al, 2005). There are two contrasting types of theoretical hydraulic behaviour: plug flow and completely mixed (Kjellstrand, 2006). Ideal plug flow is characterised by the fluid particles passing through the tank and discharged in the same sequence. Particles remain in the tank for a time equal to the theoretical detention or residence time (equation 2.46). This type of flow is approximated by long tanks or pipes with a high length-to-width ratio. These are known as plug flow reactors (PFR), with a one dimensional approximation of the material and energy balances (Levenspiel, 1998; Ranade, 2002; Metcalf et al, 2003). Velocity is uniform over all the planes normal to the flow direction. There is no mixing in the direction of flow. Therefore there is a maximum variation of concentration from the reactor inlet to the outlet (Ranade, 2002). On the contrary the most ideal reactor is one that is completely mixed with a zero dimensional equation (Ranade et al, 2002). There are no concentration gradients and composition is equal all over the tank. The effluent has the same composition as the influent and fluid inside the tank. Completely mixed reactors are known as continuous stirred tank reactors, CSTRs (Levenspiel, 1998; Ranade, 2002; Metcalf et al, 2003).

The actual behaviour of an aeration tank is non-ideal and falls somewhere between plug flow and completely mixed (Ranade, 2002). It is important to characterise the hydraulic behaviour of an aeration tank by its residence time distribution (Koot and Zeper, 1972; Kjellstrand, 2006). In real tanks there are various hydraulic phenomena. Short circuiting is where the incoming flow takes a short cut through the fluid domain. Short circuiting has a lower residence time than the theoretical mean residence time of the tank (equation 2.46). Dead fluid zones are regions of the tank where flow is stagnant. Typically the region near a corner may act as a dead volume. With dead zones the active reactor volume is smaller than expected, and therefore the residence time is also reduced (Ranade, 2002; Kjellstrand, 2006).

### **2.2.5 Hydrodynamics**

The hydrodynamics in an aeration tank is complex, due to multiphase (gas-liquid-solid) flow, and interaction between nano, micro and macro-scale components, such as the sludge flocs and gas bubbles (Karpinska et al, 2015). The movement of bubbles influences the dissolved oxygen distribution (Hu et al, 2013). There is also a high mixed liquor suspended solids concentration (MLSS) (Degremont, 2007). However, some investigators incorrectly simplify by regarding the mixed liquor as single phase water flow (Chen and Feng, 2014).

In an oxidation ditch oxygen is supplied to maintain the dissolved oxygen during the biological aerobic process (Fayolle et al, 2007). The mathematical model that does not take the gas phase into consideration cannot reasonably simulate oxygen mass transfer between the gas and liquid wastewater. Activated sludge comprises of a strongly hydrated solids phase and has different physical properties to pure water (Dammel and Schroder, 1991; Grijspeerdt and Verstraete, 1997; Schmid et al, 2003; Sears et al, 2006; Jin et al, 2014). An oxidation ditch includes transfer of oxygen from gas to liquid phase (equation 2.5), carbon oxidation and nitrification and denitrification (equations 2.47 and 2.48) in liquid and solid phases (Lei and Ni, 2014).

Dissolved oxygen changes with the distance from the aerator. Therefore there may be aerobic (free oxygen), anaerobic (absence of oxygen) and anoxic (oxygen from a chemical compound) zones in a reactor. Wastewater is purified after a long residence time in a ditch which make them different to other types of aeration tanks. Biological processes are reasonably well understood and are modelled using specialist software such as BioWin (Henze et al, 2000). However, the hydrodynamics is poorly understood. In oxidation ditches, mechanical surface aerators, submerged jet aerators and mixing devices promote unidirectional flow, with average velocities ranging from 0.25 - 0.40 m/s (Abusam et al, 2002; Metcalf et al, 2003). The velocity needs to be sufficient to maintain biomass suspension and create suitable turbulence (Wu et al, 2012; Fouad and Morsy, 2014). When water velocity is too low sludge can deposit to the bottom. Sludge settling not only decreases the working volume which causes flow short circuiting, but can also lead to a higher energy cost (Wu et al, 2012). Treatment efficiency also depends on the homogenisation of the flow pattern, mixed liquor, dissolved oxygen and chemical nutrients in the reactor. The mixing efficiency depends on the hydraulics and operation of the aeration and mixing devices (Karpinska et al, 2010). Oxidation ditches occupy large areas of land, consume substantial energy and produce uneven sludge deposits (Yang et al, 2011). Ditches have a bend geometry and relative shallow depth, and therefore their velocity distribution is heterogeneous and non-ideal. Because treatment efficiency depends on the hydrodynamics, ditch design cannot be successful unless there is good knowledge of the fluid behaviour (Littleton et al, 2007a; Yang et al, 2010).

### **Surface aeration**

In some oxidation ditches the surface aerator may produce the most oxygenation. Hydrodynamic effects are caused by the interaction of the surface solid rotor with the water, which creates circulation in one dominant direction around the ditch (Thakre et al, 2008). Oxygen transfer into the water (equation 2.14) is caused by the gas-water interface, surface water re-aeration and the air entrainment (McWhirter et al, 1995). Water ripples and surges form due to natural motion of the water surface. Surface aerators shear the liquid into small droplets, which are spread in a turbulent plume and then land and mix with the liquid. Air bubbles are introduced into the

mass of water. Surface aerators pump in a circulatory pattern, which means there is usually a dissolved oxygen gradient. Typical flow and dissolved oxygen patterns in a low speed vertical shaft surface aerator in a Carrousel oxidation ditch are shown in Figure 2.9 (Huang et al, 2009; Stenstrom and Rosso, 2010). Horizontal shaft aerators called brushes or rotors (Figure 2.10: Stenstrom and Rosso, 2010) find many applications in oxidation ditches. They provide aeration as well as imparting a circulation velocity. Their power input can be controlled by the submergence depth of the rotor (Stenstrom and Rosso, 2010). Furthermore, more knowledge is required of how the flow is affected by the submerged mixing impeller (Zhang et al, 2016).

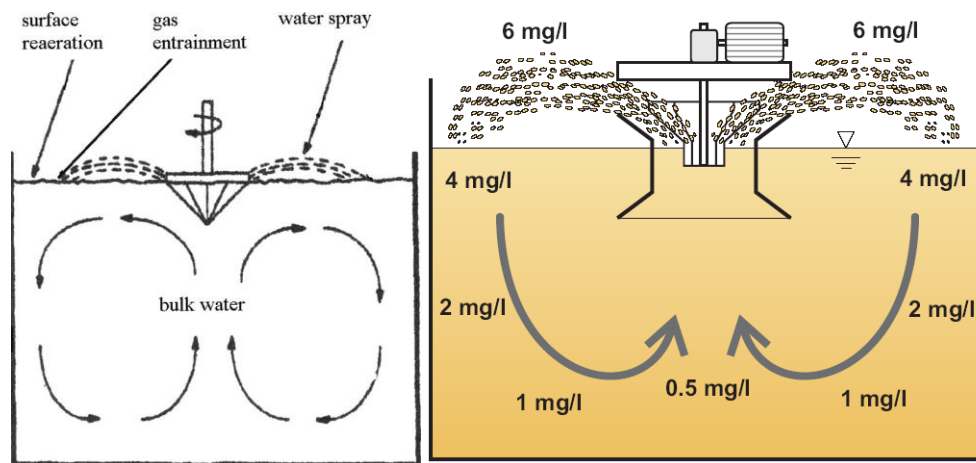


Figure 2.9 Vertical shaft surface aerator profile (Stenstrom and Rosso, 2010)

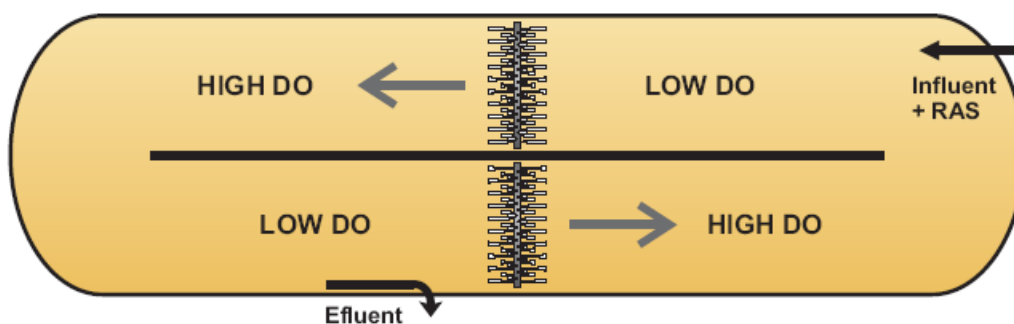


Figure 2.10 Horizontal shaft surface aerator profile (Stenstrom and Rosso, 2010)

## Diffusion aeration

Coarse bubble diffusers when installed in simple rows create spiral flow patterns. Water velocities can be as high as 2 m/s near the water surface (Stenstrom and Rosso, 2010). Diffusers are placed as uniformly as possible across the floor. Submerged diffusers release bubbles at depth, producing a free turbulent bubble plume that rises to the water surface through buoyancy. The ascending bubble plume entrains the water, causes vertical circulation and lateral surface spreading. Oxygen transfers into the water through the surface interfaces of the individual bubbles. Oxygen transfer also occurs at the water surface due to the fluid turbulence that is caused by the bubble plume and the flow circulation (De Moyer et al, 2003).

## Bubble coalescence and breakup

Many natural systems consist of populations (Nopens et al, 2015) of individual entities (flocs, bubbles, bacterial cells), which have specific properties (size, density). Individual entities interact with one another (coalescence and flocculation). One key assumption in almost all CFD models of aeration tanks in the literature is a single mean bubble size. This assumption is unrealistic since the total bubble interfacial area drives the oxygen mass transfer between the phases (Nopens et al, 2015). In reality the bubble size is spatially distributed (Figure 2.11) due to coalescence and breakup (Nopens et al, 2015). Another factor is the decrease of hydrostatic pressure from the bottom to the top of the reactor that increases the bubble size. Another factor is the increase in fluid viscosity that is caused by the presence of suspended solids, which promotes bubble coalescence (Nopens et al, 2015). Fluid viscosity is also affected by temperature (Degremont, 2007). Typical mechanisms of breakup and coalescence (Wang et al, 2011) are shown in Figure 2.12 and in equation 2.38.



Figure 2.11 Bubble size variation (Nopens et al, 2015)

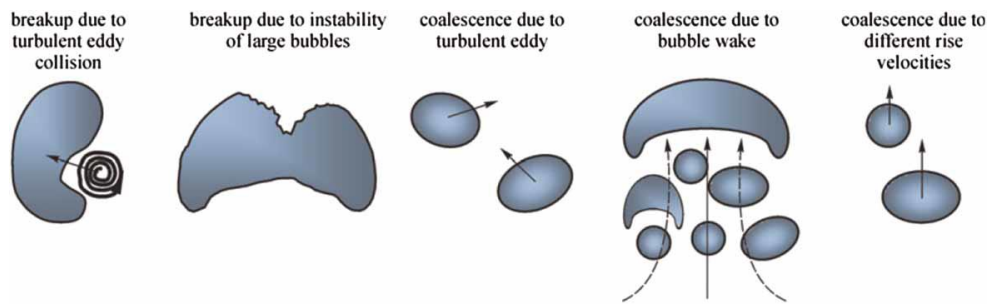


Figure 2.12 Bubble breakup and coalescence (Wang et al, 2011)

### Particle flocculation / aggregation and breakup

Agglomeration via flocculation of fine particles and colloids into larger particles is a proven method of removing impurities in WWTPs. Flocculation is the transformation of smaller destabilised particles into larger aggregates or flocs, which are subsequently removed by sedimentation or flotation (Degremont, 2007). For flocs in their initial growth phase, the formation process is a balance between the rate of collision induced aggregation and the rate of breakage that is caused by fluid shear (Bridgeman, 2009). Floc size may be considered a balance between the hydrodynamic forces that are exerted on a floc and the floc strength. Typical mechanisms for aggregation and breakup (Nopens et al, 2015) are in Figure 2.13.

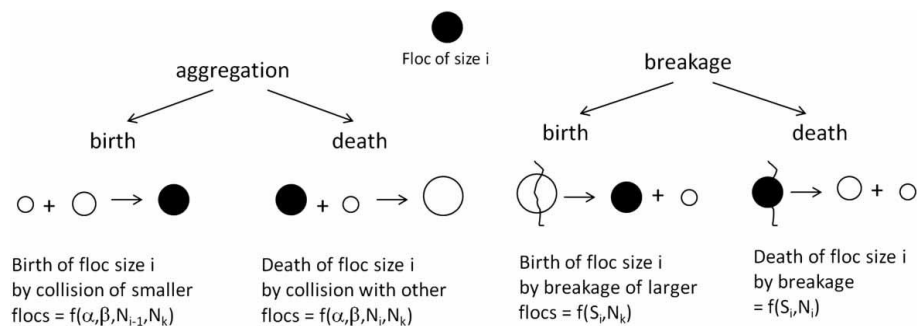


Figure 2.13 Particle aggregation and breakup (Nopens et al, 2015)

## 2.3 Theory

CFD modelling of an aeration tank includes inter-phase oxygen mass transfer (equations 2.1 to 2.10), oxygen transfer of the aeration system (equations 2.11 to 2.14), inter-phase momentum transfer (equations 2.15 to 2.33), settling velocity of suspended solids (equations 2.34 to 2.37), bubble breakup and coalescence (equations 2.38 to 2.40), residence time distribution (equations 2.41 to 2.46), biological kinetics (equations 2.47 and 2.48), fluid flow (equations 2.49 and 2.50) and fluid turbulence (equations 2.51 to 2.53).

### 2.3.1 Inter-phase oxygen mass transfer

Oxygen mass transfer is based on Fick's classic two film theory (Lewis and Whitman, 1924; Metcalf et al, 2003) that considers the interface between films of two phases: gas and liquid. The passage of gaseous phase through the interface occurs slowly due to molecular (mass) diffusion. In the case of gases of low solubility such as oxygen, the resistance of the gas film can be neglected, and therefore the entire resistance is due to the liquid film. It is assumed the concentration in the bulk liquid phase and the partial pressure in the bulk gas phase are uniform and completely mixed. Fick's first law of molecular diffusion for mass transfer (Degremont, 2007):

$$r = - D_m \left( \frac{\partial C}{\partial x} \right) \quad (2.1)$$

where,  $r$  denotes the mass transfer rate per unit interfacial area per unit time ( $\text{kg}/\text{m}^2\text{s}$ ),  $D_m$  (diffusivity) represents the mass diffusion coefficient ( $\text{m}^2/\text{s}$ ),  $\partial C/\partial x$  is the concentration gradient and  $x$  is the distance (m).

For oxygen transfer into water, the film mass transfer coefficients and concentration gradients are expressed in each phase for the bulk values to the interface values.

$$\text{oxygen layer:} \quad r = K_G (P_G - P_i) \quad (2.2)$$

$$\text{water layer:} \quad r = K_L (C_s - C_t) \quad (2.3)$$

where  $K_G$  denotes the gas film mass transfer coefficient (m/s),  $P_G$  is the partial pressure of oxygen in the bulk gas phase (Pa),  $P_i$  is the partial pressure of oxygen at the interface (Pa),  $C_S$  is the oxygen concentration in water (mg/l),  $K_L$  is the liquid film mass transfer coefficient (m/s), and  $C_t$  is the oxygen concentration in the bulk liquid phase (mg/l). Furthermore,  $A$  is the area through which mass is transferred ( $m^2$ ),  $V$  denotes volume ( $m^3$ ) and  $A/V$  denotes specific interfacial area,  $a$  ( $m^{-1}$ ), (equation 2.7). After rearrangement the volumetric oxygen mass transfer coefficient:

$$K_L a = \frac{r}{C_S - C_t} \quad (2.4)$$

CFD studies often use the general transport equation for the concentration of oxygen scalar in two phase flow (Fayolle et al, 2007) and the interfacial mass transfer of oxygen between the air phase (gas bubble) and the water phase (liquid):

$$L_k = K_L a (C_L^* - C_L) \quad (2.5)$$

where  $L_k$  is the interfacial transfer of oxygen concentration between two phases, ( $kg/m^3s$ ).  $K_L$  is the local mass transfer coefficient, m/s. The term 'a' is the bubble interfacial area,  $m^{-1}$ . The product of these two terms  $K_L a$  is the oxygen mass transfer coefficient,  $s^{-1}$ . Other terms are  $C_L$ , which is the DO concentration in water, ( $kg/m^3$ ), and  $C_L^*$  which is the saturation DO concentration in water at temperature  $T$ , ( $kg/m^3$ ). The term  $L_k$  therefore includes the bubble interfacial area term,  $a$ .

The oxygen mass transfer coefficient ( $K_L a$ ) is used to quantify interfacial (inter-phase) mass transfer between the gas and liquid phases (units of  $s^{-1}$ ). It is also used in equation 2.14 in this study to determine how much oxygen is transferred to the water from the surface brush aerators (units of  $h^{-1}$ ). The local mass transfer coefficient  $K_L$  depends on locally distributed quantities predicted by multi-phase flow modelling and is therefore a spatially distributed term (equation 2.6). These distributed quantities are the local relative velocity between phases (air and water velocity), the volume fraction of air (gas holdup) and the bubble diameter.

Oxygen mass transfer coefficient from air to water phase is mostly modelled in CFD studies of aeration tanks using Higbie's film penetration theory (Higbie, 1935; Cockx et al, 2001; Fayolle et al, 2007; Le Moullec et al, 2010b; Terashima et al, 2016):

$$K_L a = 2 \sqrt{D_o \frac{|u_g - u_l|}{d_b}} \frac{6 \alpha_g}{d_b} \quad (2.6)$$

where  $D_o$  is the standard mass diffusivity of oxygen in the water phase ( $1.97 \times 10^{-9} \text{ m}^2/\text{s}$  at  $20 \text{ }^\circ\text{C}$ ),  $d_b$  is the bubble diameter (m),  $\alpha_g$  is the gas volume fraction and  $u_g$  and  $u_l$  are the respective gas and liquid phase velocities (m/s).

The interfacial area,  $a$  is the ratio of total surface area of bubbles to liquid volume. Spherical bubbles with bubble diameter  $d_b$ , have the following interfacial area ( $\text{m}^{-1}$ ):

$$a = \frac{6}{d_b} \frac{\alpha_g}{1 - \alpha_g} \approx \frac{6 \alpha_g}{d_b} \quad (2.7)$$

Oxygen mass transfer is increased by the higher area of interface between the liquid volume and air, lower thickness of interfacial film and the higher driving force for the oxygen concentration difference (Degremont, 2007). This is the difference between dissolved oxygen (DO) concentration and saturation DO concentration (Degremont, 2007). A low DO concentration has a higher oxygen transfer driving force. There are physical limits to oxygen mass transfer such as bubble size. Bubble size also depends on the orifice size of the diffusion aerator. Smaller bubbles can be produced by a porous surface membrane diffuser. The oxygen mass transfer coefficient (equation 2.6) depends on the wastewater quality (suspended solids, chemicals), the aeration system and the reactor geometry (Degremont, 2007). There are numerous CFD studies that model a fixed mean bubble diameter (Cockx et al, 2001). Oxygen mass transfer is extensively described in the literature (Gillot and Heduit, 2000).

The influence of temperature on  $K_L a$ :

$$K_L a_T = K_L a_{20} \theta^{T-20} \quad (2.8)$$

where  $K_L a_T$  is the  $K_L a$  coefficient at temperature  $T$  ( $s^{-1}$ ),  $K_L a_{20}$  is the  $K_L a$  coefficient at the standard temperature of  $20^\circ C$  ( $s^{-1}$ ), and  $\theta$  is the temperature coefficient.

Dissolved organics, soaps, surfactants and other contaminants in wastewater have a significant impact on the  $K_L a$  (Degremont, 2007). An experimentally measured parameter -  $\alpha$  factor - accounts for the reduction in oxygen transfer rate by impurities:

$$\alpha = \frac{K_L a_{ww}}{K_L a_{tw}} \quad (2.9)$$

The  $\alpha$  factor is the most uncertain of oxygen transfer parameters. Typically,  $\alpha$  is 0.6 to 1.2 in mechanical aeration and 0.4 to 0.8 in diffusion aeration (Metcalf et al, 2003). The mass transfer coefficients of wastewater and tap water are  $K_L a_{ww}$  and  $K_L a_{tw}$ .

The activated sludge models (ASM) consider activated sludge to be soluble in the liquid phase. However, an activated sludge floc has different properties to water. It is better to treat the floc at least as a separate pseudo solid phase (Lei and Ni, 2014), with oxygen mass transfer (equation 2.10) between the gas and liquid phases modified in terms of the solids concentration (Mena et al, 2011). Therefore, a pseudo three-phase CFD simulation of a ditch (Lei and Ni, 2014) models the oxygen mass transfer rate,  $\rho$  from the gas to the liquid phase as follows (Kulkarni, 2007):

$$\rho = K_L a_L \left( \alpha (S_{o(s)} - S_o) \right) \quad (2.10)$$

where,  $K_L a_L$  is the mass transfer coefficient ( $s^{-1}$ ),  $S_{o(s)}$  is saturation DO concentration in clean water ( $g/m^3$ ),  $S_o$  is DO concentration in liquid phase ( $g/m^3$ ),  $\alpha$  is the ratio of saturation DO in wastewater between the suspended solids and the clean water.

## Oxygen transfer rate of aeration system

The oxygen transfer rate (OTR) is the oxygenation capability of an aeration system (Stenstrom and Rosso, 2010). It represents the mass of oxygen that is transferred per hour into deoxygenated water:

$$\text{OTR} = K_L a V C_s \quad (2.11)$$

where,  $K_L a$  is the overall mass transfer coefficient ( $\text{h}^{-1}$ ),  $V$  is the tank volume ( $\text{m}^3$ ),  $C_s$  is the oxygen saturation concentration in water ( $\text{kg}/\text{m}^3$ ).

The oxygen transfer efficiency (OTE) is used to define diffusion aeration (Stenstrom and Rosso, 2010):

$$\text{OTE} = \left( \frac{\text{OTR}}{w\text{O}_2} \right) \times 100 \quad (2.12)$$

where  $w\text{O}_2$  is the oxygen supply rate ( $\text{kgO}_2/\text{h}$ ).

Coarse bubbles have an efficiency of only 4 - 6 %, medium bubbles 5 - 10 %, while fine bubbles 15 - 30 % (Degremont, 2007). Although not strictly an efficiency, another criteria (Stenstrom and Rosso, 2010) is the aeration efficiency (AE), which is the oxygen transfer rate (OTR) ( $\text{kgO}_2/\text{h}$ ) per unit power consumed (kW):

$$\text{AE} = \frac{\text{OTR}}{P} \quad (2.13)$$

where, AE is aeration efficiency in clean water ( $\text{kgO}_2/\text{kW}/\text{h}$ ), P is power input (kW).

## OTR of surface aerator

The oxygen transfer rate of spray water in air is the main oxygen transfer process in high-speed surface aerators (McWhirter et al, 1995; Huang et al, 2009):

$$\text{OTR}_{\text{sp}} = K_L a V (C_{\text{DS}} - C_0) \approx Q E C_{\text{DS}} \quad (2.14)$$

where  $\text{OTR}_{\text{sp}}$  is the oxygen transfer rate of spray water ( $\text{mg}/\text{h}$ ),  $V$  is tank volume ( $\text{m}^3$ ),  $Q$  is spray water flow rate ( $\text{L}/\text{h}$ ),  $E$  is aeration efficiency of spray water in air (dimensionless),  $C_{\text{DS}}$  is saturation concentration of DO at the wet-bulb temperature of air ( $\text{mg}/\text{L}$ ), and  $C_0$  is the initial DO concentration in the aeration tank ( $\approx 0$ ).

### 2.3.2 Inter-phase momentum transfer - drag force

The gas-liquid flow of bubbles is characterised by the relative motion between phases that is affected by an inter-phase drag force (Ishi and Zuber, 1979; Joshi, 2001; Ranade, 2002). Aeration is quantified in terms of the air volume fraction and modelled by the interfacial momentum transfer between the gas bubbles and water. Bubble diameter is an input to the bubble drag coefficient to calculate interfacial momentum transfer (Talvy et al, 2007). Early analytical work on bubble drag (Moore, 1965) expresses the drag coefficient  $C_d$  of spherical bubbles in pure liquids:

$$C_d = (48 - Re_b) \left( 1 - \left( \frac{2.21}{\sqrt{Re_b}} \right) \right) \quad (2.15)$$

where  $Re_b$  is the bubble Reynolds number (dimensionless) (Moore, 1965):

$$Re_b = \rho_l d_b \frac{V_r}{\mu_l} \quad (2.16)$$

where,  $\rho_l$  is liquid water density ( $\text{kg/m}^3$ ),  $d_b$  is bubble diameter (m),  $V_r$  is relative velocity between liquid and gas phases (m/s) and  $\mu_l$  is viscosity of water (kg/ms).

The drag coefficient of spherical bubbles in a CFD model of a gas-liquid air-lift reactor (Talvy et al, 2007) uses this expression of Karamanev and Nikolov, 1992:

for  $Re < 135$

$$C_d = \left( \left( \frac{24}{Re} \right) (1 + 0.15 Re^{0.687}) \right) + \frac{0.413}{(1 + 16.3 Re^{-1.09})} \quad (2.17)$$

for  $Re > 135$

$$C_d = 0.95 \quad (2.18)$$

This is quite similar to the correlation for the low bubble Reynolds number (Schiller and Naumann, 1935):

$$C_d = \left( \frac{24}{Re} \right) (1 + 0.15 Re^{0.687}) \quad (2.19)$$

The Ishii and Zuber drag law uses the concept of a mixture viscosity that can also include bubble shape distortion. It can be used for densely populated bubbles in the oxidation ditch at Potterne WWTP in this project (Ishi and Zuber, 1979). It differs from Schiller and Naumann (equation 2.19) by its expression in the viscous flow regime, and its use of the mixture Reynolds number  $Re_m$  that is based on the mixture viscosity  $\mu_m$ . The mixture Reynolds number  $Re_m$  of spherical bubbles in liquids (Ishi and Zuber, 1979):

$$Re_m = \rho_l d_b \frac{|u_g - u_l|}{\mu_m} \quad (2.20)$$

where,  $\rho_l$  is liquid water density ( $kg/m^3$ ),  $d_b$  is bubble diameter (m),  $u_g$  is velocity of gas phase (m/s),  $u_l$  is velocity of liquid phase (m/s),  $\mu_m$  is mixture viscosity (kg/ms).

The Reynolds bubble number is split into fluid regimes (Ishi and Zuber, 1979):

Stokes (laminar) regime (low  $Re_m$ ):

$$C_d = \frac{24}{Re_m} \quad (2.21)$$

Viscous (transitional) regime (medium  $Re_m$ ):

$$C_d = \left( \frac{24}{Re_m} \right) (1 + 0.1 Re_m^{0.75}) \quad (2.22)$$

Newtons (turbulent) regime (high  $Re_m$ ):

$$C_d = 0.44 \quad (2.23)$$

The gas-liquid CFD model of a channel reactor (Le Moullec et al, 2008b) uses this correlation for the drag coefficient of a spherical bubble (Jamialahmadi et al, 1994):

$$C_d = \frac{4}{3} \frac{\rho_l - \rho_g}{\rho_l} \frac{g d_b}{u_\alpha^2} \quad (2.24)$$

where,  $\rho_l$  is water density ( $kg/m^3$ ),  $\rho_g$  is air bubble density ( $kg/m^3$ ),  $d_b$  is bubble diameter (m),  $u_\alpha$  is the terminal vertical bubble velocity (m/s).

This is the most used drag force equation (Van Baten et al, 2003; Zhang et al, 2012):

$$F_d = \frac{3}{4} \left( \frac{\alpha_g \rho_l C_d}{d_b} \right) |u_g - u_l| (u_g - u_l) \quad (2.25)$$

In the CFD simulation of an aeration tank a three phase (gas, liquid, solid) flow modelling approach can also be considered. The same form of equation (as 2.25) calculates the momentum exchange between the liquid and gas phase in an air-lift reactor (Van Baten et al, 2003) and in an EGSB reactor (Wang et al, 2009):

$$M_{L,G} = \left[ \frac{3}{4} \frac{C_d}{d_b} \rho_L \right] \epsilon_G (u_G - u_L) |u_G - u_L| \quad (2.26)$$

Similarly, momentum exchange between liquid and solid phase (Wang et al, 2009):

$$M_{L,S} = \left[ \frac{3}{4} \frac{C_d}{d_s} \rho_L \right] \epsilon_s (u_s - u_L) |u_s - u_L| \quad (2.27)$$

where,  $M_{L,G}$  is the inter-phase momentum exchange between liquid and gas ( $N/m^3$ ),  $M_{L,S}$  is the inter-phase momentum exchange between liquid and solid phase ( $N/m^3$ ),  $\epsilon_G$  is the gas hold up or gas volume fraction,  $\epsilon_s$  is solid volume fraction,  $d_b$  is bubble diameter (m),  $d_s$  is particle diameter (m).

When considering the solid phase, the drag coefficient that is exerted by the solid phase on the liquid phase  $C_{DLS}$  (Wen and Yu, 1966) in a three phase CFD model of an EGSB reactor (Wang et al, 2009):

$$C_{DLS} = \left( \frac{24}{\lambda_s} \right) \text{Re} [1 + 0.15 (\lambda_s \text{Re}^{0.687})] \lambda_s^{-0.265} \quad (2.28)$$

where  $\lambda_s$  is the solid volume fraction. The Reynolds number between the solid and liquid phases:

$$\text{Re} = \rho_l d_s \frac{|u_s - u_l|}{\mu_l} \quad (2.29)$$

where,  $\rho_l$  is liquid water density ( $kg/m^3$ ),  $d_s$  is particle diameter (m),  $u_s - u_l$  is velocity difference between solid and liquid phases (m/s),  $\mu_l$  is viscosity of water (kg/ms).

CFD modelling of bubbly flow in an aeration tank predominantly assumes there is a spherical bubble shape for modelling simplification. In reality the natural population of bubbles has a variety of distorted bubble shapes (Nopens et al, 2015) that is rarely modelled. The bubble eccentricity assumes that there is an ellipsoidal bubble shape, with a circular horizontal projected area of diameter  $b$ , and a vertical smaller axis  $c$ . The eccentricity is defined as  $E = c/b$ . Bubble shape distortion may therefore be modelled using the eccentricity (Talvy et al, 2007):

$$C_{deq} = C_d - E^{0.67} \quad (2.30)$$

Direct numerical simulation (DNS) is used to predict the distortion of bubble shape and the volume of an individual bubble in a channel reactor (Wang and Zhao, 2009). The characterisation of the bubble diameter is taken from the determined bubble volume of a non-spherical bubble:

$$D_b = \sqrt[3]{\left(\frac{6V_b}{\pi}\right)} \quad (2.31)$$

where  $D_b$  is equivalent non-spherical bubble diameter (m),  $V_b$  is bubble volume ( $m^3$ ).

The Eötvös number correlation ( $E_o$ ) is adapted to the drag coefficient of bubbles in a gas-liquid CFD simulation of an oxidation ditch (Fayolle et al, 2007). It also takes into account an ellipsoidal bubble shape. Therefore, for a bubble size of 4.0 mm the drag coefficient is 0.98 (Clift et al, 1978) or 0.44 (Schiller and Naumann, 1935).  $\gamma$  is the surface tension of the bubble ( $N/m^2$ ) = 0.07  $N/m^2$ .

The bubble drag coefficient when it is dependent only on the Eötvös number,  $E_o$  (Clift et al, 1978):

$$C_d = \frac{2}{3} \sqrt{E_o} \quad (2.32)$$

$$E_o = \frac{g(\rho_l - \rho_g) d_b^2}{\gamma} \quad (2.33)$$

### 2.3.3 Suspended solids particle settling

When the solids phase is also being considered then the settling of the suspended solids is very important. Discrete settling only occurs at very low suspended solids concentrations, when there is negligible inter-particle interaction. The settling velocity of discrete individual particles (Sears et al, 2006) depends on the particle density, porosity, permeability and shape (Ganczarczyk, 1994). Particle settling is derived by equating the gravitational and frictional drag forces:

$$v = \sqrt{\frac{4}{3} \times \frac{g \times d}{C_D} \times \frac{(\rho_p - \rho_w)}{\rho_w}} \quad (2.34)$$

where,  $v$  is the terminal settling velocity of the floc (m/s),  $\rho_w$  is water density ( $\text{kg/m}^3$ ),  $\rho_p$  is primary particle density ( $\text{kg/m}^3$ ),  $d$  is floc diameter (m),  $\mu_w$  is water viscosity (kg/ms). For laminar flow  $C_D$  is drag coefficient =  $24 / \text{Re}$ ;  $\text{Re} = v d \rho_w / \mu_w$ .

In aeration tanks there are usually high particle populations and there is flocculation by the contact between particles to form larger particles. Therefore, as well as discrete settling, there is also flocculent, hindered and compressive settling. This is modelled using relationships (equations 2.35 to 2.37) between the settling velocity and the mixed liquor suspended solids concentration (MLSS) (Vesilind, 1968, Patry and Takacs, 1992). The relative velocity (slip velocity) is the vertical velocity of the sludge phase that is relative to the vertical velocity of the water phase. For a solid-liquid CFD model of a ditch (Xie et al, 2014), a double exponential sedimentation velocity function is used (Takács et al, 1991):

$$V_s = |V_1 - V_2| = V_0 (e^{-k_1 X} - e^{-k_2 X}) \quad (2.35)$$

where,  $V_s$  is solids settling velocity (m/s),  $V_0$  is terminal settling velocity of a discrete particle (m/s),  $V_1$  is velocity of liquid phase (m/s),  $V_2$  is velocity of solid phase (m/s),  $X$  is MLSS concentration (mg/l),  $k_1$  is constant for flocculent settling,  $k_2$  is constant for hindered settling. To calculate the settling constants, experimental settling data is collected for wastewater samples at different suspended solids concentrations (Xie et al, 2014). This model describes discrete, flocculent and hindered settling.

A single exponential solids settling velocity model is used in a solid-liquid CFD model of a channel reactor (Brannock, 2003) to model hindered settling (Vesilind, 1968):

$$V_s = k_1 e^{-(k_2 X)} \quad (2.36)$$

The Vesilind model is used because it has a better fit with experimental data, in comparison to the Takács model for a particular study (Brannock, 2003).

Another type of solids settling velocity model is used (Rasmussen and Larsen, 1996) in the solid-liquid CFD model of an oxidation ditch (Jensen et al, 2006):

$$W_s = W_0 e^{(\beta \cdot C + \gamma \cdot G)} + \lambda \quad (2.37)$$

where  $W_s$  is the settling velocity (m/s),  $W_0$  is the maximum settling velocity (m/s),  $C$  is the suspended solids concentration ( $\text{kg/m}^3$ ),  $G$  is turbulent velocity gradient ( $\text{s}^{-1}$ ),  $\beta$  is empirical constant ( $\text{m}^3/\text{kg}$ ),  $\gamma$  is empirical constant (s),  $\lambda$  is minimum compressive settling velocity (m/s).

Sedimentation in this model is a function of sludge concentration and fluid turbulence (equation 2.37). Settling constants are found by fitting the model to solids settling experiments conducted on the particular wastewater (Rasmussen and Larsen, 1996). The properties of the sludge floc for a three-phase CFD model of a ditch (Lei and Ni, 2014), give a solids density from 1010 to 1060 g/ml (Dammel and Schroeder, 1991), dynamic viscosity from 3.8 to 11.0 mPa.s (Jin et al, 2004) and floc diameter of a spherical particle from 0.05 to 0.5 mm (Grijpspeerdt and Verstraete, 1997).

### 2.3.4 Bubble breakup and coalescence

Bubbles break up and coalesce due to their interactions with turbulent eddies, which produces a bubble size distribution (BSD). These effects are included in some gas-liquid CFD simulations of aeration tanks (Dhanasekharan et al, 2005; Karpinska and Bridgeman, 2017; Climent et al, 2019) by solving a population balance model (PBM). The system is considered two-phase and uses the Euler-Euler multi-fluid model. Mass and momentum balance equations are solved for each phase (equations 4.1 and 4.2). The coupling between the phases is achieved through the inter-phase mass and momentum exchange terms. The gas phase is composed of  $i$  discrete bubble sizes and the discretised PBM equations are solved for the bubble number density, along with the birth and death terms of breakup and coalescence (Figure 2.12). The equation for the  $i$  th bubble class fraction  $f_i$  :

$$\frac{\partial(\alpha_g \rho_g f_i)}{\partial t} + \nabla (\alpha_g \rho_g u_g) f_i = S_i \quad (2.38)$$

$$S_i = B_{br} - D_{br} + B_{co} - D_{co} \quad (2.39)$$

where  $f_i$  is the ratio of the total volume of bubbles of class  $i$  to the total volume of bubbles in all classes,  $B_{br}$  is the birth rate due to breakup,  $D_{br}$  is death rate due to breakup,  $B_{co}$  is birth rate due to coalescence,  $D_{co}$  is death rate due to coalescence.

Turbulent eddies increase the surface energy of the bubbles through deformation. Breakup occurs if the increase in surface energy reaches a critical value. Breakup causes the change from one size to another (Luo and Svendsen, 1996). Bubble coalescence is modelled by the bubble collisions, due to turbulence, buoyancy and laminar shear. Coalescence rate is a product of collision frequency and coalescence probability (Luo and Svendsen, 1996). Coupling between breakup and coalescence and the CFD model is through the bubble drag term, which is based on the Sauter mean bubble diameter. Interfacial bubble-liquid area,  $a$ , is used to calculate the mass transfer coefficient  $K_L$  (Higbie, 1935) and obtained from a bubble size distribution:

$$a = \sum_i 6 \alpha_i d_i \quad (2.40)$$

where,  $\alpha_i$  is the volume fraction of phase  $i$ ,  $d_i$  is the bubble diameter of phase  $i$  (m).

### 2.3.5 Residence time distribution

The residence time distribution (RTD) describes the non-ideal fluid behaviour in the reactor (Danckwerts, 1953; Nauman, 2007; Gresch et al, 2010). It can be found from an experimental tracer test or a numerical equation. A trace is an inert substance introduced at the entrance of the reactor as a pulse or step. The tracer concentration is measured in the effluent and this evolution of concentration in time (graph) can be interpreted by using hydraulic parameters. The RTD from an experimental tracer test (Danckwerts, 1953; Nauman, 2007) can be used to validate an RTD predicted by a CFD simulation. An ideal plug flow tank has an RTD with infinite trace concentration in the effluent, exactly at the mean hydraulic residence time of the tank (equation 2.46). The RTD of a completely mixed tank has an exit age curve that starts at the maximum tracer concentration at time zero and gradually decays over time.

The gas-liquid CFD model of a channel reactor (Le Moullec et al, 2008b) calculates the RTD tracer concentration by using a particle trajectory CFD model (Nauman, 2007). This equation is quite similar to the previous drag force equation (2.25):

$$\frac{\partial u_p}{\partial t} = \frac{3}{4} C_d \left( \frac{\rho_l}{d_p \rho_p} \right) |u_p - u_l| (u_p - u_l) \quad (2.41)$$

where,  $u_p$  is the velocity of the particle (m/s),  $u_l$  is velocity of liquid water (m/s),  $C_d$  is drag coefficient of particle,  $\rho_l$  is density of liquid water ( $\text{kg/m}^3$ ),  $\rho_p$  is density of particle ( $\text{kg/m}^3$ ),  $d_p$  is particle diameter (m).

Another approach to calculate the RTD tracer concentration uses a species transport equation of a passive tracer, which has the same physical properties as the liquid water phase (Le Moullec et al, 2008b). The transport equation for the concentration of a tracer scalar  $C_{tr}$  in turbulent flow:

$$\frac{\partial}{\partial t} (\rho_l C_{tr}) + \nabla \cdot (\rho_l U_l C_{tr}) = \nabla \cdot \left( \left( \rho_l D_m + \frac{\mu_t}{Sc_t} \right) \nabla C_{tr} \right) \quad (2.42)$$

where,  $C_{tr}$  is the concentration of the tracer ( $\text{kg/m}^3$ ),  $U_l$  is statistical average velocity (m/s),  $D_m$  is mass diffusivity ( $\text{m}^2/\text{s}$ ),  $\mu_t$  is turbulent viscosity (kg/ms);  $Sc_t$  is turbulent Schmidt number (dimensionless). On the left side of the equation are the convection terms and on the right side is the molecular and turbulent diffusion.

The RTD graph represents the tracer concentration versus time, in terms of the dimensionless temporal variable  $t' = t/t_0$  on the x-axis, and the dimensionless concentration variable  $C' = C/C_0$  on the y-axis (Brannock, 2003):

$$C' = \frac{C}{C_0} \quad (2.43)$$

where,

$$C_0 = \frac{M_t}{V} = \int_0^\infty C \, dt \quad (2.44)$$

$$t' = \frac{t}{t_0} \quad (2.45)$$

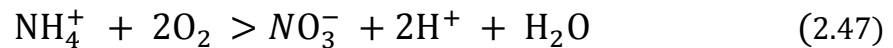
where,

$$t_0 = \frac{V}{Q} \quad (2.46)$$

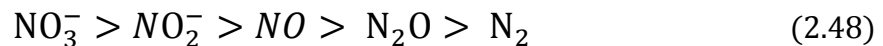
where  $C'$  is the predicted dimensionless concentration of tracer,  $t'$  is the predicted dimensionless time,  $C_0$  is the mean concentration of tracer in the tank ( $\text{kg}/\text{m}^3$ ),  $C$  is the predicted tracer concentration ( $\text{kg}/\text{m}^3$ ),  $M_t$  is mass of tracer injected (kg),  $t_0$  is the hydraulic mean residence time (s),  $V$  is tank fluid volume,  $Q$  is volumetric flow rate ( $\text{m}^3/\text{s}$ ). The mass balance of tracer in the tank is described by equation 2.44. The theoretical or hydraulic (equation 2.46) residence time (HRT) is the mean residence time of a tank, which has volume  $V$  ( $\text{m}^3$ ) and flow rate,  $Q$  ( $\text{m}^3/\text{s}$ ), and is equal to  $V/Q$  (Danckwerts, 1953; Levenspiel, 1998; Nauman, 2007).

### 2.3.6 Biological kinetic models

In wastewater nitrogen is mainly present in organic and ammonia form. Nitrification occurs in aeration tanks that are designed to remove nitrogen. Nitrification is when ammonia nitrogen ( $\text{NH}_4^+$ ) is oxidised into nitrite ( $\text{NO}_2^-$ ) and then into nitrate ( $\text{NO}_3^-$ ) by a chemical oxidation reaction (Degremont, 2007) by oxidising bacteria (autotrophs).



Denitrification occurs when denitrifying bacteria (heterotrophs) reduce the nitrate to a lower oxidation state to form nitrogen. Nitrate ( $\text{NO}_3^-$ ) is reduced to nitrite ( $\text{NO}_2^-$ ), nitrous oxide ( $\text{NO}$ ), di-nitrogen oxide ( $\text{N}_2\text{O}$ ) and nitrogen ( $\text{N}_2$ ) (Degremont, 2007):



The most common biological kinetic models (Henze et al, 2000) - the Activated Sludge Models (ASM) were introduced in 1982 by the International Association of Water Pollution Research and Control (IAWPRC) and developed by the International Water Association (IWA). The ASM models describe the main biological reactor functions of oxygen and energy consumption, biomass production and pollutant removal (Le Moullec et al, 2011). The ASM models can predict the nitrogen, phosphorus, phosphorus accumulating organisms (PAOs), chemical oxygen demand (COD) and biomass (Seco et al, 2020). The first model known as the Activated Sludge Model No. 1 (ASM1) was mainly used for nitrogen removal. In 1995 the group published the Activated Sludge Model No. 2 (ASM2), that is mainly used for nitrogen and phosphorus removal. The ASM2d model was established after ASM2 to be able to incorporate de-nitrification and denitrifying PAOs. In 1998 the group published the ASM3 model that considers chemical oxygen demand and a two-step model for nitrification and de-nitrification (Henze et al, 2000). Another modified ASM1 model is the BNRM-1 model that is used for biomass flocs (Seco et al, 2004).

The ASM1 model (Henze et al, 1987) is used for biochemistry in a channel reactor (Makinia and Wells, 1999; Le Moullec et al, 2011). A one dimensional equation is solved for biomass and carbon oxidation in a ditch (Stamou, 1994). The ASM1 model is extended (Stamou et al, 1999) to include carbon oxidation, nitrification and de-nitrification. The ASM1 model is used to predict dissolved oxygen, nitrogen and COD (Lesage et al, 2003). It is used for dissolved oxygen in a ditch using a compartmental hydraulic model (Alaya et al, 2010). It is used for nitrogen, phosphorus and COD removal in a ditch (Wang et al, 2019). The ASM1 model can be used for gas-liquid (Le Moullec et al, 2010b), solid-liquid (Brannock, 2003) and gas-liquid-solid flow (Lei and Ni, 2014). The benchmark simulation layout (BSM1) model based on ASM1 is an anoxic/aerobic compartmental hydraulic model used for nitrogen removal in a channel reactor (Du et al, 2018). The ASM1 (Le Moullec et al, 2011) and ASM2 models (Littleton et al, 2007b) are summarised in the literature. The activated sludge models are incorporated into simulation software (Table 2.1).

Table 2.1 Activated sludge modelling software

<b>Software</b>	<b>Website reference</b>
BioWin	<a href="http://envirosim.com/products/biowin">http://envirosim.com/products/biowin</a>
GPS-X	<a href="http://www.hydromantis.com">http://www.hydromantis.com</a>
Aquasim	<a href="http://www.eawag.ch/de/abteilung/siam/software">http://www.eawag.ch/de/abteilung/siam/software</a>
Sumo	<a href="http://www.dynamita.com">http://www.dynamita.com</a>
WEST	<a href="https://www.mikepoweredbydhi.com/products/west">https://www.mikepoweredbydhi.com/products/west</a>
DESASS	<a href="http://calagua.webs.upv.es">http://calagua.webs.upv.es</a>
STOAT	<a href="http://www.wrcplc.co.uk/ps-stoat">http://www.wrcplc.co.uk/ps-stoat</a>

These software are not appropriate for computational fluid dynamics. They are used to predict reactor functions of oxygen and energy consumption, biomass production and pollutant removal (Le Moullec et al, 2011). Activated Sludge Digestion model (ASDM) (Batstone et al, 2002) is used for anaerobic digestion and implemented in the software BioWin. The Sumo, Mantis2 and Mantis3 models are incorporated into respective Sumo and GPS-X software. The BNRM (Seco et al, 2004) and BNRM2 models (Barat et al, 2013) are implemented in the software DESASS (Ferrer et al, 2008). Some commercial models such as BioWin (Dorofeev et al, 2017), Sumo or GPS-X have also incorporated recent model extensions. Nitrogen, phosphorus and COD removal in a ditch is modelled using STOAT software (Wang et al, 2019).

## 2.4 CFD modelling

### 2.4.1 Introduction

Computational Fluid Dynamics (CFD) can be used to predict the flow and dissolved oxygen distributions in an aeration tank (Samstag et al, 2016; Wicklein et al, 2016). More work is recommended by investigators in this field (Karpinska and Bridgeman, 2016). For natural bubble and particle size distributions, bubble coalescence and breakup and particle flocculation and breakup models are required (equations 2.38 to 2.40). Population balance models (PBM) are used to predict the bubble size distribution (BSD) or the particle size distribution (PSD). If the biokinetics or the biochemical oxygen demand (BOD) on the dissolved oxygen is modelled there are also source and sink terms in the species transport equation (Wicklein et al, 2016). The change in bubble size can also be caused by the hydrodynamic pressure difference. For particulate flows the suspended solids settling velocity in the direction of gravity is also introduced (equations 2.34 to 2.37).

There are different modelling approaches for gas-liquid (bubbly) and solid-liquid (particulate) flow in an aeration tank. To predict the flow pattern without considering the effects of bubbles or particles, then a single-phase water flow model is sufficient (equations 2.49 and 2.50). When predicting the free water surface in an aeration tank the volume of fluid (VOF) model is used but sparingly. When predicting the dispersion of bubbles or solid particles the Eulerian-Eulerian multi-fluid model is most commonly used (equations 4.1 and 4.2). When predicting the dissolved oxygen distribution, the species transport modelling is the approach (equation 5.1). Dissolved oxygen is dispersed in the tank by the multi-phase flow pattern.

## 2.4.2 Flow and turbulence modelling

The Reynolds Averaged Navier-Stokes (RANS) equations of fluid flow consist of a continuity equation of conservation of mass, three momentum conservation equations and an energy conservation equation (Launder and Spalding, 1974). In the RANS, the flow patterns are obtained from the solution of the nonlinear partial differential equations. The balance of a mass conservation equation may be expressed in general form (Karpinska and Bridgeman, 2016):

$$\frac{\partial \rho \bar{v}_i}{\partial x_i} = 0 \quad (2.49)$$

and momentum conservation equation (Karpinska and Bridgeman, 2016):

$$\rho \left[ \frac{\partial}{\partial x} (\bar{u}^2) + \frac{\partial}{\partial y} (\bar{u}\bar{v}) + \frac{\partial}{\partial z} (\bar{u}\bar{w}) \right] = - \frac{\partial \bar{p}}{\partial x} + \left[ \frac{\partial}{\partial x} \left( \mu \frac{\partial \bar{u}}{\partial x} - \rho \bar{u}'^2 \right) + \frac{\partial}{\partial y} \left( \mu \frac{\partial \bar{u}}{\partial y} - \rho \bar{u}'v' \right) + \frac{\partial}{\partial z} \left( \mu \frac{\partial \bar{u}}{\partial z} - \rho \bar{u}'w' \right) \right] \quad (2.50)$$

Fluid motion is inherently turbulent: irregular, fluctuating, three dimensional, rotational, intermittent, unsteady, disordered and dissipative (Ranade, 2002). There are rotational flow structures known as turbulent eddies with a wide range of length and time scales. The fundamental Reynolds averaged Navier-Stokes (RANS) equations (Launder and Spalding, 1974) model the effects of turbulence on the mean flow properties, for the whole range of turbulent scales (Launder and Spalding, 1974). Turbulent flow is usually decomposed into mean and fluctuating components. However, the governing momentum conservation equation of fluid flow (2.50) does not represent a closed equation system. This is because the Reynolds stresses ( $\bar{u}^2$ ,  $\bar{u}\bar{v}$ ,  $\bar{u}\bar{w}$ ,  $\bar{u}'^2$ ,  $\bar{u}'v'$ ,  $\bar{u}'w'$ ) that are in three dimensions and for the mean and fluctuating components of turbulent flow provide too many variables for the equation to solve. Therefore, it requires a turbulence closure model to be able to solve the Reynolds stresses (Launder and Spalding, 1974). It is not the purpose to assess turbulence models in detail which can be found in the literature (Rodi, 1993; Wilcox, 1998; Pope, 2001).

The principal turbulence models are:

- Two equation eddy viscosity  $k$ - $\epsilon$  ( $k$ -epsilon) models: standard, realizable, renormalized group (RNG).
- Two equation eddy viscosity  $k$ - $\omega$  ( $k$ -omega) models: standard and shear stress transport (SST).
- Six equation Reynolds Stress Model (RSM) and four equation Algebraic Stress Model (ASM).

When turbulence is homogeneous and isotropic then the relationships between the average and fluctuating flow can be deduced. In particular, the kinetic energy that sustains turbulence is extracted from the average flow and dissipated by the viscous motions of the smallest turbulent fluctuations. The features of all two-equation models is they assume isotropic turbulence (Launder and Spalding, 1974; Rodi, 1993). Two equation models (i.e.  $k$ - $\epsilon$  and  $k$ - $\omega$ ) solve two additional transport equations for the turbulence quantities: velocity scale turbulent kinetic energy,  $k$ , turbulence length scale eddy dissipation rate,  $\epsilon$  (epsilon), and specific frequency,  $\omega$  (omega) (Pope, 2001). The turbulent viscosity is a function of these terms. From the two-equation models, the standard  $k$ - $\epsilon$  turbulence model has found the broadest applicability due to its robustness, low computational cost and reasonable accuracy.

The standard two equation  $k$ - $\epsilon$  model is used most often for the CFD models of aeration tanks (equations 2.51 to 2.53). A comprehensive description of the standard  $k$ - $\epsilon$ , Renormalized Group (RNG)  $k$ - $\epsilon$  and realizable  $k$ - $\epsilon$  models are in the literature (Launder and Spalding, 1974; Rodi, 1993; Menter, 1994). The second most widely used two-equation model, introduced by Wilcox, is the  $k$ - $\omega$  model, where turbulent viscosity is a function of  $k$  and  $\omega$  (Wilcox, 1998). The standard  $k$ - $\omega$  model uses enhanced wall treatment to solve the low Reynolds number flows in the viscous near-wall layer. The SST  $k$ - $\omega$  model with a modified turbulent viscosity is considered to be the most accurate two-equation eddy viscosity model. A wider discussion on the standard and SST  $k$ - $\omega$  models is in the literature (Menter, 1994; Wilcox, 1998).

The Reynolds stress model (RSM) (Launder and Spalding, 1974) is a more elaborate and complex turbulence model referred to as second order closure. RANS equations are closed by solving transport equations for Reynolds stresses together with an equation for the dissipation rate, yielding seven additional transport equations. It takes longer to compute than the two equation turbulence models. Another turbulence model with fewer equations in this class is the Algebraic Stress Model (ASM).

The large eddy simulation (LES) is an alternative approach, where large, three-dimensional unsteady scale eddy motions are directly and explicitly solved in a time-dependent simulation, using space-filtered Navier Stokes equations. LES is one of the most computationally expensive models and requires a more refined grid to resolve the eddies in the boundary layer (Pope, 2001). Direct numerical simulation (DNS) is the explicit solution of the whole range of turbulent time and length scales, from the small Kolmogorov scales to the large motion scales that transport most of the kinetic energy (Launder and Spalding, 1974; Ranade, 2002). As a result the computational cost of DNS is high, even at low Reynolds numbers making it impractical for use in industrial aeration tanks. This is illustrated by a study of a deformable bubble shape in a channel reactor. The high computational cost allows for only one bubble to be modelled using DNS in this study (Wang and Zhao, 2009).

The standard two equation  $k-\epsilon$  (k-epsilon) model is the predominant turbulence model for single and multi-phase flow in an oxidation ditch (Cockx et al, 2001; Glover et al, 2006; Jensen et al, 2006; Fayolle et al, 2007; Bhuyar et al, 2009; Yang et al, 2011; Wu et al, 2012; Karpinska, 2013; Lei and Ni, 2014; Samstag and Wicklein, 2014; Norouzi-Firouz, 2018; Zhang et al, 2019), air-lift reactor (Cockx et al, 2001; Mudde and Van den Akker, 2001; Oey et al, 2001; Van Baten et al, 2003; Dhanasekharan et al, 2005; Talvy et al, 2007; Fan et al, 2010; Xu et al, 2010; Zhang et al, 2012) and channel reactor (Kjellstrand, 2006; Le Moullec et al, 2008b; Huang et al, 2009; Hu et al, 2010; Le Moullec et al, 2010a; Le Moullec et al, 2010b; Gresch et al, 2011; Le Moullec et al, 2011; Hu et al, 2013; Terashima et al, 2016; Karpinska and Bridgeman, 2017).

The realizable two equation k-ε turbulence model is used for a ditch (Guo et al, 2013; De Gussem et al, 2014; Liu et al, 2014). The Reynolds normalisation group (RNG) two equation k-ε model is used for a ditch (Wei et al, 2006a; Zhang et al, 2016). The standard k-ω model is used for a ditch (Karpinska, 2013) and channel reactor (Elshaw et al, 2016). The shear stress transport (SST) model is used for a channel reactor (Karpinska and Bridgeman, 2017; Karpinska and Bridgeman, 2018; Hreiz et al, 2019) and a ditch (Climent et al, 2019; Höhne and Mamedov, 2020). RSM is used for ditch (Karpinska, 2013) and channel reactor (Le Moullec et al, 2008b). LES is used for ditch (Karpinska et al, 2015) and DNS for channel (Wang and Zhou, 2009).

For single-phase flow the turbulence models are compared: RANS with the standard k-ε model and unsteady RANS (URANS) with LES. The LES gives better accuracy but much higher computational cost in a ditch (Karpinska et al, 2010; Karpinska et al, 2015). The effect of the turbulence models (standard k-ε, standard k-ω, RSM) on the power requirements of hydrojets in a ditch are assessed. LES yields a slightly higher power than k-ε but lower than k-ω (Karpinska, 2013). Comparison is made between the standard k-ε model and the shear stress transport (SST) k-ω model for bubbly flow in a channel reactor (Karpinska and Bridgeman, 2017). The standard k-ε model has the lowest computational cost and the RSM highest but with better accuracy for single-phase flow in a ditch (Huang et al, 2013). The RSM and standard k-ε model are compared for bubbly flow in a channel. The computational time is only 60% higher for the RSM but it has better accuracy (Le Moullec et al, 2008b).

The standard two-equation k-ε (k-epsilon) turbulence model solves additional transport equations for two turbulence quantities: turbulent kinetic energy, k, and turbulent dissipation rate, ε (Pope, 2000):

$$\frac{\partial(\rho k)}{\partial t} + \frac{\partial(\rho U_i k)}{\partial x_i} = \frac{\partial}{\partial x_i} \left( \left( \mu + \frac{\mu_t}{\sigma_k} \right) \frac{\partial k}{\partial x_i} \right) + G - \rho \epsilon \quad (2.51)$$

$$\frac{\partial(\rho \epsilon)}{\partial t} + \frac{\partial(\rho U_i \epsilon)}{\partial x_i} = \frac{\partial}{\partial x_i} \left( \left( \mu + \frac{\mu_t}{\sigma_\epsilon} \right) \frac{\partial \epsilon}{\partial x_i} \right) + \frac{\epsilon}{k} (C_1 G - C_2 \rho \epsilon) \quad (2.52)$$

where G is the turbulence generation term, C<sub>1</sub> and C<sub>2</sub> are turbulent constants, σ<sub>k</sub> and σ<sub>ε</sub> are the turbulent Schmidt numbers, C<sub>μ</sub> = 0.09.

The eddy or turbulent viscosity,  $\mu_t$  is computed as a function of  $k$  and  $\varepsilon$  in the two equation standard  $k$ - $\varepsilon$  model (Launder and Spalding, 1974):

$$\mu_t = \rho C_\mu \frac{k^2}{\varepsilon} \quad (2.53)$$

In the Boussinesq hypothesis the unknown Reynolds stresses in the momentum equation (equation 2.50) are therefore solved by predicting the turbulent kinetic energy,  $k$ , (equation 2.51), the turbulent dissipation rate,  $\varepsilon$  (equation 2.52) and the turbulent viscosity,  $\mu_t$  (equation 2.53).

### 2.4.3 Computational grid based modelling

In their general form, the Reynolds Averaged Navier-Stokes (RANS) equations (equations 2.49 and 2.50) cannot be solved analytically. For the solution of the RANS equations, the flow domain is discretised by a computational mesh to define the locations where the equations are solved (Launder and Spalding, 1974). This provides hydrodynamic information at a finite number of discrete locations within the flow domain. Most CFD models use the finite volume method, as this allows for an unstructured computational mesh. However the finite difference and finite element methods are also used in wastewater treatment (Wicklein et al, 2016).

The computational mesh is based on the geometry of the flow domain, with a refined mesh near to the boundaries to capture the flow in the boundary layer (Launder and Spalding, 1974; Rodi, 1993; Wilcox, 1998; Pope, 2001; Ranade, 2002). Mesh generation is accomplished using mesh-generating software, that allows for definition of the model geometry, grid cell property variability (size, skewness, aspect ratio, orthogonality) and it provides tools for evaluating grid quality. There are three types of mesh: fully structured (hexahedral cell), unstructured (normally tetrahedral but can be hexahedral) and hybrid (polyhedral). Unstructured and hybrid grids are the most commonly used for complicated geometry, such as for aeration devices in an oxidation ditch. They allow the greatest flexibility in defining the fluid domain geometry and are much faster to construct than structured meshes (Ranade, 2002).

However, structured meshes are numerically more accurate, because the grid lines are better aligned to the boundary surfaces, which better captures boundary layer flow. There is also less numerical diffusion due to lower cell skewness and better grid line orthogonality (Launder and Spalding, 1974; Pope, 2001; Ranade, 2002).

Unstructured tetrahedral meshes are used for oxidation ditches (Jensen et al, 2006; Fayolle et al, 2007; Bhuyar et al, 2009; Fan et al, 2010; Yang et al, 2010; Yang et al, 2011; Lei et al, 2014; Xie et al, 2014; Zhang et al, 2016; Li et al, 2017; Norouzi-Firouz, 2018; Xu et al, 2018; Climent et al, 2019; Zhang et al, 2019) and an air-lift reactor (Zhang et al, 2012). Unstructured hexahedral meshes are used for oxidation ditches (Liu et al, 2014; Karpinska et al, 2015; Wei et al, 2016a; Wei et al, 2016b) and channel reactors (Terashima et al, 2016; Karpinska and Bridgeman, 2017).

Structured hexahedral meshes are used in CFD studies of air-lift reactors (Oey et al, 2001; Dhanasekharan et al, 2005) and channel reactors (Le Moullec et al, 2008b; Le Moullec et al, 2010a; Le Moullec et al, 2010b; Le Moullec et al, 2011; Gresch et al, 2011; Sánchez et al, 2018; Hreiz et al, 2019). Hybrid meshes are used for CFD studies of oxidation ditches (Huang et al, 2013; Karpinska, 2013; Chen and Feng, 2014; Samstag and Wicklein, 2014), channel reactors (Brannock, 2003; Hu et al, 2010; Hu et al, 2013) and a sequencing batch reactor (Samstag et al, 2012).

Mesh independence and convergence analysis is recommended to verify the flow solution is not dependent upon the number or spatial variation of cells. When the flow solution no longer changes significantly there is a grid independent solution. A grid with a fewer numbers of cells and a grid independent solution will save considerable computational cost, when solving the equations of fluid flow (Launder and Spalding, 1974). Mesh independence studies are conducted for oxidation ditches (Huang et al, 2013; Karpinska, 2013; Lei and Ni, 2014; Xie et al, 2014; Karpinska et al, 2015; Zhang et al, 2016; Norouzi-Firouz, 2018; Xu et al, 2018; Climent et al, 2019; Zhang et al, 2019), air-lift reactor (Zhang et al, 2012) and channel reactors (Brannock, 2003; Le Moullec et al, 2008b; Le Moullec et al, 2010b; Terashima et al, 2016; Karpinska and Bridgeman, 2017; Sánchez et al, 2018; Karpinska and Bridgeman, 2018; Hreiz et al, 2019).

The finite difference numerical method (Lauder and Spalding, 1974; Wilcox, 1998; Pope 2000; Ranade, 2002) interpolates the computed cell centre values of the flow variables onto the computational mesh. This is to enable variables to be predicted at discrete locations in the flow domain. Because of the consideration of numerical accuracy in the CFD study in this thesis, the finite difference numerical method, structured hexahedral mesh and second order numerical discretisation are used and a grid convergence study conducted. The residuals of the equations are a measure of how closely each finite difference equation is balanced given the current state of the solution (Figures 3.10, 4.1 and 5.1). The residuals in the program ANSYS-CFX are normalised (Ansys, 2017). The normalised residual is the sum of the imbalance in the equations for all cells in the domain divided by the sum of the quantity at the grid node. A typical hexahedral computational cell surrounding a grid node has four neighbouring nodes in the surrounding cells. The quantity that is interpolated might be any dependent variable (u velocity, turbulent kinetic energy). The finite difference coefficients combine convection and diffusion through the control volume that surrounds the grid node that is of interest (Anderson and Wendt, 1995).

In ANSYS-CFX the conservative first order numerical differencing scheme for all the equations keeps the computation stable (Ansys, 2017). However, it is less accurate than a higher order scheme as it is numerically diffuse (Ranade, 2002). The first order 'upwind' scheme uses the upwind cell centre value and interpolates it to the face centre. A simple approximation to the value at the cell centre is by linear interpolation between the two nearest nodes, which is considered to be first order discretisation. The grid spacing however needs to be small enough to limit the numerical diffusion of a first order numerical scheme (Anderson and Wendt, 1995).

For first-order accuracy, the face quantities are identical to the cell quantities and the face value is equal to the cell centre value in the upstream cell. For second-order accuracy, the higher order accuracy at the cell faces is through a Taylor series expansion that evaluates the value at the cell face from the solution obtained at the cell centre (Ansys, 2017). For second order accuracy three nodal values are used in the interpolation: one downstream and two upstream. For a hybrid scheme that is between first and second order accuracy, the Taylor series truncation error is only first order. Hybrid is thus less accurate than a second order scheme (Ranade, 2002).

## 2.4.4 Boundary conditions

### Inlets and outlets

The inlet of gas from a submerged air sparger is modelled with a velocity inlet boundary in a channel reactor, with a volume fraction of 1 for the gas phase (Le Moullec et al, 2008b). The velocity inlet boundary condition is assigned for the air inlet of a diffuser in a channel reactor (Terashima et al, 2016). The air inlet is modelled by an inlet velocity and a gas fraction in an air-lift reactor (Mudde and Van den Akker, 2001). The velocity inlet boundary condition models the gas inlet from a sparger in an air-lift reactor (Zhang et al, 2016). The inlet is modelled with a flux boundary in a ditch. The outlet is described by an opening boundary at atmospheric pressure and is a free outlet (Jensen et al, 2006). An EGSB reactor inlet is modelled with a velocity inlet boundary condition and outlet is a pressure outlet boundary (Wang et al, 2010). A submerged aerator sparger in a sequencing batch reactor is modelled with an inlet air mass flow rate (Diez et al, 2007). At the inlet boundary of a channel reactor, the velocity distribution is according to velocity measurements and the outflow is defined by an average static pressure. The geometry of grid diffusers is simplified by the diffusers imprinted on the tank floor (Gresch et al, 2011). Grid modules of bubble diffusers in an oxidation ditch are not individually modelled, but the entire grid is simplified by a single boundary surface (Fayolle et al, 2007).

### Water surface

For the water surface that is planar and steady, a rigid lid approximation may be used, with no shear stress applied at the plane. However, if the flow is gradually or rapidly variable, a free water surface model may be required (Wicklein et al, 2016). The water surface is considered flat, horizontal and rigid by many investigators of ditches (Jensen et al, 2006; Fayolle et al, 2007; Bhuyar et al, 2009; Yang et al, 2011; Wu et al, 2012; Guo et al, 2013; Huang et al, 2013; Chen and Feng, 2014; Lei and Ni, 2014; Karpinska et al, 2015; Zhang et al, 2016; Norouzi-Firouz, 2018; Climent et al, 2019), air-lift ditches (Fan et al, 2010; Xu et al, 2010), air-lift reactors (Mudde and Van den Akker, 2001; Oey et al, 2001; Van Baten et al, 2003) and channel reactors (Brannock, 2003; Le Moullec et al, 2008b; Huang et al, 2009; Hu et al, 2010; Gresch et al, 2011; Hu et al, 2013; Terashima et al, 2016; Karpinska and Bridgeman, 2017).

The centrifugal force from a surface aerator causes the water surface to be uneven. However, this is considered negligible compared to the few metres of water depth. This is the reason why a free water surface is often not modelled (Guo et al, 2013). The water surface can be considered fixed and rigid, and uses the “degassing” boundary condition where gas escapes at the interface. The degassing boundary condition eliminates the need of an extra multi-phase model and is therefore more computationally efficient (Talvy et al, 2007). Alternatively, an outlet boundary can be used for the gas phase and a rigid lid symmetry boundary for the liquid phase (Fayolle et al, 2007; Le Moullec et al, 2008b).

Alternatively the water surface may be considered to be deformable. In this case the flow domain includes a region above the water surface that contains gaseous air. A fixed planar water surface is found to have a larger pressure drop in an airlift reactor and a larger liquid velocity when compared to a free surface model (Talvy et al, 2007). To predict the free surface between two fluids (air and water) in a ditch the volume of fluid (VOF) multi-phase flow model is preferred (Liu et al, 2014; Wei et al, 2016a; Wei et al, 2016b; Xu et al, 2018) although used sparingly. Another type of free surface tracking model (Brackbill et al, 1992) used in a ditch predicts the water surface shape for bubbly flow (Climent et al, 2019). Oxygen transfer from the air above the water surface into the water is considered negligible, when compared to the oxygen transfer through the bubble surfaces (Fayolle et al, 2007; Hu et al, 2010).

### **Mixer and surface aerator models**

The simplest mixer model is the momentum source model (MSM), where the thrust force from the mixing impeller produces a momentum source (Brannock, 2003). Next in complexity is the fan boundary condition that predicts the tangential velocity (De Gussem et al, 2014). The moving wall model (MWM) is used for the surface aerators (Xie et al, 2014). The multiple reference frame (MRF) model constructs the impeller geometry which increases the complexity (Brannock, 2003). The propeller resides in one fluid zone and the vessel in another. The most complex is the sliding mesh (SM) model where the propeller is actually rotated. This divides the fluid domain into two zones where the propeller resides and for the rest of the tank. This advanced method is accurate but it is computationally expensive (Brannock, 2003).

### **Momentum source model (MSM)**

The momentum source corresponds to a mixing impeller in a ditch (Fayolle et al, 2007). Momentum sources are assigned to sub domains for mixing impellers in a ditch (Jensen et al, 2006). The hydrojet in a ditch produces a jet stream of water that is saturated with air and this is modelled using a momentum source (Karpinska et al, 2015). Surface disc aerators are modelled with momentum sources (Littleton et al, 2007a). The momentum source is used for flow around a surface aerator in a ditch (Huang et al, 2013) and for mixing propellers in a ditch (Climent et al, 2019).

### **Fan model**

In a fan model a cylindrical moving zone is created for each rotating impeller. The momentum and energy by axial thrust is passed onto the ditch (Wu et al, 2012). The fan model for submerged mixing impellers in a ditch and the pressure difference across the impellers is calculated by the disc area and the flow velocity (Yang et al, 2011). The fan model considers the mixing impellers as cylindrical volumes, with a fixed velocity in the ditch (De Gussem et al, 2014; Lei and Ni, 2014; Xie et al, 2014).

### **Moving wall model (MWM)**

The moving wall model is used for surface disc aerators in a ditch. The moving zone is formed by the sidewalls, outer wall, and surface of the surface aerator. Fluid in each moving zone gets the velocity and momentum from the moving wall (Yang et al, 2011; Wu et al, 2012). Flow in a ditch can be agitated by the rotation of surface blades and the disc surface aerators use the moving wall model (Lei and Ni, 2014). Only the submerged part of the volume of the surface aerator is created with a constant velocity boundary condition (Bhuyar et al, 2009). Due to the large numbers of disc aerators in a ditch, the moving wall model is used instead of the sliding mesh model in order to save computational cost (Chen and Feng, 2014).

### **Multiple reference frame (MRF)**

Ditches with rotating umbrella surface aerators use the MRF model (Fan et al, 2010; Norouzi-Firouz, 2018). A submerged mixing impeller in a ditch uses the MRF model to initialise the flow field and a sliding mesh model for flow computation (Wei et al, 2016a; Wei et al, 2016b). A submerged mixing impeller in a ditch uses the rotating

frame of reference (RFR) model (Samstag and Wicklein, 2014). Mixing impellers in a channel reactor use the MRF model (Karpinska and Bridgeman, 2017).

### **Sliding mesh model (SMM)**

For a sliding mesh model the fluid domain is divided into two parts: the inner-rotating part, and the outer-stationary part that is defined by an interface (Zhang et al, 2016). Different approaches for modelling a surface impeller in a ditch are compared: the momentum source (MSM), moving reference frame (MRF) and sliding mesh (SM). The accuracy of the momentum source is better than MRF and near to SM. Moreover, momentum source is easier to use than MRF and SM (Huang et al, 2013).

### **2.4.5 Single-phase flow modelling**

The main aim of single-phase flow simulation is to predict the flow pattern of the liquid water in an aeration tank. The modelling assumptions of single-phase flow are:

- Inter-phase drag forces of bubbles and particles are negligible.
- Density effects of suspended solids are negligible.
- There is no inter-phase oxygen mass transfer.

CFD simulation of an oxidation ditch can be computationally expensive (Karpinska et al, 2010) due to complex hydrodynamics, interactions between phases (activated sludge flocks and air bubbles) and oxygen mass transfer. For a single phase flow simulation there are fewer equations to solve (RANS and turbulence - equations 2.49 to 2.53). The pure liquid water enables easier setup of an experimental laboratory (Littleton et al, 2007a; Karpinska, 2013; Karpinska, 2015). Using real wastewater in a laboratory means that the fluid contains suspended solids. Laboratory data from clean water can be used to validate water velocity distributions from single-phase CFD simulations (Karpinska, 2013). Moreover, it can be used to evaluate the energy costs of design systems, for example hydrojets (Karpinska et al, 2010). Single-phase flow modelling can also be the first step towards a more comprehensive multi-phase flow modelling study (Karpinska, 2015). Moreover, solid-liquid flow modelling of an aeration tank may be conducted after a single-phase flow modelling study (Kjellstrand, 2006; Samstag et al, 2012; Zhang et al, 2016).

Single-phase CFD simulations can predict the water velocity distributions in ditches (Littleton et al, 2007a; Littleton et al, 2007b; Bhuyar et al, 2009; Karpinska et al, 2010, Yang et al, 2010; Yang et al, 2011; Wu et al, 2012; Guo et al, 2013; Huang et al, 2013; Karpinska, 2013; De Gussem et al, 2014; Karpinska et al, 2015; Zhang et al, 2016) and in channel reactors (Kjellstrand, 2006; Huang et al, 2009; Elshaw et al, 2016). In an oxidation ditch the mixed liquor suspended solids concentration (MLSS) ranges from 3,000 - 5,000 mg/l, the density of activated sludge from 1000 - 1200 kg/m<sup>3</sup> (Dammel & Schroeder, 1991; Sears et al, 2006; Fan et al, 2010). Pure liquid water is therefore not considered to be an accurate fluid for real dirty wastewater.

#### **2.4.6 Multi-phase flow modelling**

Momentum exchange between phases is significant in gas-liquid and solid-liquid flow. Gas-liquid flow around bubbles is characterized by the relative motion between phases that produces local pressure and shear stress gradients (Joshi, 2001). The surface tension coefficient models the interface behaviour between the phases. Knowledge of the rise velocity of bubbles in water can accurately predict the gas-liquid inter-phase drag force (Moore, 1965; Wallis, 1974; Ishi and Zuber, 1979; Karamanev, 1994). For suspended solids concentrations there is particle flocculation and density driven flow (Samstag et al, 2016). Knowledge of the settling velocity of particles can accurately predict the solid-liquid inter-phase drag force (Schiller and Nauman, 1935; Vesilind, 1968, Takacs and Patry, 1991).

The second Eulerian approach in wastewater multi-phase flow modelling is the Eulerian-algebraic (slip mixture or algebraic slip) model for two or more phases, that are treated as interpenetrating continua. The phases are treated as a single continuous phase. Single differential equation is solved for the continuity and momentum of the mixture and the model tracks the motion of each phase. This single fluid approach can model phases at different velocities by the concept of the slip or drift velocity (Ranade, 2002; Karpinska and Bridgeman, 2016). It is computationally more efficient than the Euler-Euler multi-fluid model due to fewer equations to solve, which is one of the main reasons for its use. For phases that are moving with the same velocity the mixture approach models homogeneous

multiphase flow (Manninen et al, 1996; Wicklein and Samstag, 2009). Similar type of model is the 'drift flux' model, which also utilises the inter-phase slip velocity. In gas-liquid flow the slip velocity is equal to the relative rise velocity of the bubbles in the water (Ishi and Zuber, 1979). In solid-liquid flow the slip velocity is equal to the relative settling velocity of particles in the water (Takacs and Patry, 1991). The mixture model relies upon the input of bubble and particle sizes. Additional empirical functions for the relationship between the settling velocity and the mixed liquor suspended solids concentration (MLSS) can be used to model hindered and compressive settling in wastewater treatment (Wicklein et al, 2016).

The third Eulerian approach is the full Eulerian-Eulerian or multi-fluid model. Phases are treated as separate and interpenetrating continuum, hence the phasic volume fractions. The sum of the volume fractions in each phase is equal to unity. Each phase is governed by a separate set of continuity and momentum conservation equations (Simonin, 1990; Joshi, 2001; Ranade, 2002) - equations 4.1 and 4.2. The multi-fluid model is thought to be preferable for wastewater bubbly flow due to its considerable use in the literature for aeration tanks. The multi-fluid model is used where there are a large number of bubbles in an aeration tank (Talvy et al, 2007). It can also incorporate a range of bubble properties by linking it to coalescence and break-up models, through the inter-phase momentum drag term (equations 2.38 to 2.40), unlike the algebraic slip mixture model. There is an increased computational cost due to the number of equations in the multi-fluid model (Simonin, 1990).

The alternative is the Eulerian-Lagrangian multi-phase model (Sokolichin et al, 1997). The governing phase (fluid) is treated as a continuum (Eulerian) and solved by the RANS equations. It tracks a large number of particles, using random-walk Lagrangian trajectory calculations, for the disperse phase through the continuous flow field. Particles or bubbles exchange momentum, mass, and energy with the fluid phase. Trajectories of bubbles (equation 2.41) are solved by integrating the force balance on a single component (Ranade, 2002). One limitation for aeration is that the large number of bubbles tracked have a high computational cost (Ranade, 2002) making this model less popular (Karpinska and Bridgeman, 2016). For example, in an aeration tank of  $1\text{m}^3$  and global gas hold-up of 1% there are about 700,000

bubbles (Fayolle et al, 2007). Its other limitation is its poor accuracy in predicting the air volume fraction distribution (Karpinska and Bridgeman, 2016).

The Euler-Euler multi-fluid model is the most common multi-phase model for bubbly flow (Karpinska and Bridgeman, 2016). It is used for gas-liquid flow in ditches (Glover et al, 2006; Fayolle et al, 2007; Climent et al, 2019; Höhne and Mamedov, 2020), air-lift reactors (Cockx et al, 1997; Do-Quang et al, 1998; Mudde and Van den Akker, 2001; Oey et al, 2001; Van Baten et al, 2003; Dhanasekharan et al, 2005; Talvy et al, 2007; Zhang et al, 2012) and channel reactors (Hu et al, 2010; Le Moullec et al, 2010a; Le Moullec et al, 2010b; Gresch et al, 2011; Le Moullec et al, 2011; Terashima et al, 2016; Karpinska and Bridgeman, 2017; Sánchez et al, 2018; Karpinska and Bridgeman, 2018; Hreiz et al, 2019), expanded granular sludge bed (EGSB) reactor (Wang et al, 2009; Wang et al, 2010) and sequencing batch reactor (SBR) (Diez et al, 2007). The multi fluid model is the most common multi-phase flow model for solid-liquid flow in a ditch (Jensen et al, 2006; Fan et al, 2010; Norouzi-Firouz, 2018) and EGSB (Wang et al, 2009; Wang et al, 2010). The ASMM and drift flux models are used for solid-liquid flow in a ditch (Chen and Feng, 2014; Xie et al, 2014; Zhang et al, 2019), air-lift reactor (Oey et al, 2001; Talvy et al, 2005) and channel reactor (Brannock, 2003). They have also been used for bubbly flow in a ditch (Xu et al, 2010; Chen and Feng, 2014) and air-lift reactor (Talvy et al, 2005).

## **Bubble size**

The bubble size is an important parameter in inter-phase oxygen mass transfer (equation 2.5), as it influences the interfacial gas-liquid area (equation 2.7). In the drag coefficient the ellipsoidal bubble shape may also be considered using the Eötvös number (Fayolle et al, 2007) or eccentricity (Talvy et al, 2007). The effect of hydrostatic pressure may be considered by measurement of bubble size and water depth (Fayolle et al, 2006). The fixed mean bubble size is often used in CFD models, mostly from measurements; in oxidation ditches (Lei and Ni, 2014 (2.6 mm); Höhne and Mamedov, 2020 (3 mm)), air-lift reactors (Do Quang et al, 1998 (3.5 mm); Mudde and Van den Akker, 2001 (3 mm); Van Baten et al, 2003 (5 mm); Talvy et al,

2005 (2.7 to 4.3 mm); Talvy et al, 2007 (3.4 mm); Zhang et al, 2012 (5 mm)) and channel reactors (Le Moullec et al, 2010b (4 mm); Gresch et al, 2011 (3.5 mm); Hreiz et al, 2019 (1 and 4 mm)). Bubble size is also calculated from measurements of mass transfer coefficients for membrane, fine-pore and coarse bubble diffusers to give respective sizes of 3 mm, 5 - 6 mm and 7 - 8 mm (Terashima et al, 2016).

Multiphase flow models which incorporate bubble size distribution (BSD) or particle size distribution (PSD) require population balance modelling (PBM) (Bridgeman, 2009). These models predict particle-particle (agglomeration/flocculation) and bubble-bubble (coalescence) interaction. PBM with bubble breakup and coalescence models (Prince and Blanch, 1990) are coupled to the multi-fluid model in an air-lift reactor (Dhanasekharan et al, 2005) and ditch (Climent et al, 2019). Other coalescence and breakage models (Ishii and Kim, 2001) are used for a channel reactor (Karpinska and Bridgeman, 2017; Karpinska and Bridgeman, 2018). Air bubbles are modelled as a polydisperse phase using the multiple size group (MUSIG) model (Lo, 1998). Discretisation of the full bubble size range is in distinct classes. A free surface tracking model (Brackbill et al, 1992) is used in a ditch for predicting the three dimensional shape of a bubble plume (Climent et al, 2019). Numerous studies model bubbly flow in aeration tanks but mostly without suspended solids and with a simplified fixed mean bubble diameter (Cockx et al, 2001). It is suggested that the influence of BSD and oxygen mass diffusivity on the oxygen transfer in an aeration tank should be investigated further (Le Moullec et al, 2010b).

## **Water surface**

The Volume of Fluid (VOF) model is a single-fluid approach based on surface tracking, that solves the momentum equation of the continuous phase, while the disperse phase follows closure conditions for the volume fraction (Ranade, 2002). The VOF model is used to predict the water surface shape in a ditch (Lui et al, 2014) for determining the impeller depth (Wei et al, 2016a; Xu et al, 2018) and for baffle design (Wei et al, 2016b). It is computationally more expensive and its accuracy evaluation requires comparison with measurement of water levels. Another free surface tracking model (Brackbill et al, 1992) is used in a ditch to predict the water

surface shape (Climent et al, 2019). An alternative is the Level Set method where two fluids can be treated as a single fluid and the properties of phases are distinguished by the level set function. The level set method is able to simulate surface bubble deformation (Wang and Zhao, 2009). However, the water surface is often still considered to be flat, rigid and planar in many CFD studies. Investigators state that surface aerators and submerged jet aerators and air diffusers cause water surface deformation but this is negligible compared to the overall ditch depth (Fan et al, 2010; Guo et al, 2013). However, expansion in an air-lift reactor means that a rigid boundary condition predicts larger water velocities than when using a free boundary condition (Talvy et al, 2007). An uneven water surface may also exist in an air-lift oxidation ditch (Fan et al, 2010; Xu et al, 2010).

### **Suspended solids**

The suspended solids distribution is modelled in a ditch by using the algebraic slip mixture model (Chen and Feng, 2014). The multi-fluid model is used for solid-liquid flow in an ALOD (Ishi and Zuber, 1979). It is assumed the solid particles are rigid spheres and the interactions between particles are negligible. The simulated density of activated sludge in this model is  $1150 \text{ kg/m}^3$  (Fan et al, 2010). Sludge in an aeration tank is considered two-phase using the multi-fluid model (Xie et al, 2014; Norouzi-Firouz, 2018). The slip velocity is defined as the velocity of the sludge phase that is relative to the velocity of the water phase, where both are in the vertical direction. A double exponential settling velocity relationship with respect to the MLSS concentration (Takacs et al, 1991) can represent the slip velocity distribution (equation 2.35). Settling velocity column experiments on the wastewater are conducted. The settling velocity is also modelled (equation 2.37) as a function of MLSS and turbulence (Rasmussen and Larsen, 1996). This model is calibrated with settling velocity column experiments (Jensen et al, 2006). The drift flux mixture model is used for solid-liquid flow in a channel reactor (Brannock, 2003). An expression for hindered settling (Vesilind, 1968) is fitted with settling velocity experimental data on real wastewater (equation 2.36). The two-phase suspended solids distribution in an oxidation ditch is simulated using the algebraic slip mixture model (Zhang et al, 2019). The density of the activated sludge is modelled as  $1050 \text{ kg/m}^3$ . The double exponential settling velocity relationship is used (Xie et al, 2014).

### Three phase flow (gas-liquid-solid)

A three phase flow model (Le Moullec et al, 2010b) considers the oxygen transfer from the gas to the liquid phase (equation 2.5), the oxygen transfer from the liquid to the flocs, and the biological reactions. Two fluid phases can have activated sludge as the continuous phase and air as the disperse phase with a bubble diameter. Activated sludge has also been simplified with a uniform viscosity (Bokil and Bewtra, 1972) and uniform suspended solids concentration, while only predicting the bubble distribution (Gresch et al, 2011; Terashima et al, 2016). Pseudo three-phase modelling of a ditch considers the sewage water, activated sludge, and air as respective liquid, pseudo-solid, and gas phases (Lei and Ni, 2014). The density of activated sludge ranges from 1010 to 1060 kg/m<sup>3</sup> (Dammel and Schroeder, 1991). Activated sludge floc is a separate pseudo-solid phase (Lei and Ni, 2014), with the oxygen mass transfer between the gas and liquid phases (equation 2.10), modified in terms of the suspended solids concentration (Mena et al, 2011). Wastewater, activated sludge and gas in a ditch may represent the activated sludge as a pseudo-solid phase (Li et al, 2017). Full three phase flow simulation of a channel reactor (Hu et al, 2013) considers the main phase as liquid. Bubbles and solid particles are treated as separate dilute disperse phases. There are separate drag forces modelled between the liquid and gas and between the liquid and solid (Schiller and Naumann, 1935) - equation 2.19. The multi-fluid three-phase flow model of an EGSB reactor treats the wastewater as a primary phase with the same properties as water and the gas and sludge granules as the secondary phases. Sludge granules have a diameter of 1 mm with a density of 1460 kg/m<sup>3</sup> (Wang et al, 2009). Three phase flow in an air-lift reactor uses the drift flux model of Zuber and Findlay, 1965 (Talvy et al, 2005) and in an SGBR uses the multi-fluid model (Diez et al, 2007). There is a continuous liquid phase and there are two disperse phases modelled (bubbles and particles). Activated sludge may be considered as spherical particles with a uniform density of 1050 kg/m<sup>3</sup>, diameter of 2 mm and viscosity of 0.00102 kg/ms (Talvy et al, 2005).

#### 2.4.7 Species transport modelling

Wastewater is liquid water that contains dissolved species. Species are different materials that share a common phase (liquid, gas, solid). The first Eulerian approach is the species transport model. The governing equations of fluid motion of the primary phase are solved and the other species follow the convective flow and are modelled as species or scalars. The mass transport equation predicts the local mass fraction concentration of a species. It accounts for the advection and diffusion of the species (Ranade, 2002) - equation 5.1. Transported species may be treated as a scalar (e.g. density, viscosity, temperature, dissolved oxygen, BOD). A species can either be coupled to the momentum equation as an equation of state or treated as a passive property that is transported by the fluid (Ranade et al, 2002). It may even include a chemical reaction. Wastewater flows are mostly turbulent, so turbulent diffusion dominates molecular (mass) diffusion. Species transport can be computationally efficient, when there is a limited number of additional equations for different chemicals in the system (Ranade, 2002).

The spatial distribution of oxygen in an aeration tank considers the mass transport of oxygen in the air phase, the interfacial mass transfer of oxygen from the air to water phase, the mass transport of oxygen in the water phase, and the dissolution of oxygen into the water, which produces the dissolved oxygen in the water phase (Karpinska et al, 2016). Species transport simulation can predict the oxygen mass transport in an aeration tank (Karpinska et al, 2016). To predict the dissolved oxygen (DO) distribution in an oxidation ditch (Littleton et al, 2007a; Yang et al, 2011; Guo et al, 2013; Karpinska et al, 2016), the oxygen transport equation includes oxygen sources for aeration devices and an oxygen sink for the oxygen consumption by biochemical oxygen demand (BOD). Oxygen consumption by BOD may be assumed to be homogeneous throughout the ditch (Littleton et al, 2007a). Therefore, the effect of BOD on the DO is usually modelled in the literature by a uniform BOD. However, in real WWTPs there is usually found to be a BOD distribution in an aeration tank, which is not accounted for in the CFD models in the literature - equations 5.1 to 5.9. Therefore, it is recommended by investigators that the effect of the BOD distribution on the DO distribution in the aeration tank should be investigated (Ghawi, 2014; Karpinska et al, 2016; Karpinska and Bridgeman, 2018).

#### 2.4.8 CFD Software

Commercial CFD software uses the latest advances in turbulence and multi-phase flow modelling. They have sophisticated software for grid generation and for the graphical visualisation of results. There are built-in mechanical mixer tools. With user-defined functions experimental data can be used to calibrate the models. The most commonly used CFD software is ANSYS™, which includes FLUENT™ and CFX™ and the latter is used in this study. ANSYS™ can be used for structures, electronics, automotive, turbo-machinery, chemical, oil and gas, food, drink, built environment, sports, renewable energy, water and the natural environment (<https://www.ansys.com/>)

Commercial CFD programs are also used for wastewater aeration tanks (Wicklein and Samstag, 2009). ANSYS™ is used for single phase, gas-liquid and solid-liquid flow in an aeration tank (Brannock, 2003; Van Baten et al, 2003; Dhanasekharan et al, 2005; Jensen et al, 2006; Diez et al, 2007; Fayolle et al, 2007; Littleton et al, 2007a; Littleton et al, 2007b; Talvy et al, 2007; Le Moullec et al, 2008b; Bhuyar et al, 2009; Huang et al, 2009; Wang et al, 2009; Fan et al, 2010; Karpinska et al, 2010; Le Moullec et al, 2010a; Le Moullec et al, 2010b; Wang et al, 2010; Yang et al, 2010; Gresch et al, 2011; Le Moullec et al, 2011; Yang et al, 2011; Samstag et al, 2012; Wu et al, 2012; Zhang et al, 2012; Guo et al, 2013; Karpinska et al, 2013; Chen and Feng, 2014; De Gussem et al, 2014; Lei and Ni, 2014; Liu et al, 2014; Samstag et al, 2014; Xie et al, 2014; Karpinska et al 2015; Elshaw et al, 2016; Terashima et al, 2016; Wei et al, 2016a; Wei et al, 2016b; Zhang et al, 2016; Li et al, 2017; Karpinska and Bridgeman, 2018; Xu et al, 2018). ASTRID™ software is used for gas-liquid flow in an aeration tank (Cockx et al, 1997; Do Quang et al, 1998; Cockx et al, 2001). DISSIM™ software is used for gas-liquid and solid-liquid flow in an aeration tank (Oey et al, 2001). COMSOL™ software is used for single-phase in an aeration tank (Kjellstrand, 2006).

## 2.5 Experimental validation

### 2.5.1 Residence time distribution

Tracer experiments consist of an inert substance introduced at the influent (inlet) of a reactor as a pulse. The tracer concentration is measured in the effluent (outlet) and this evolution of concentration in time is the residence time distribution (RTD) of the fluid in the reactor. It measures a key feature of hydraulic performance of a reactor. Comparison between an RTD graph from a tracer test (Danckwerts, 1953; Nauman, 2007) and a numerical RTD may be used to validate a CFD simulation.

The most commonly used tracer for experiments in aeration tanks is a chemical salt, where its concentration is detected by a conductivity probe or by sample measurements (De Clerq et al, 1999; Brannock, 2003; Olivet et al, 2005; Potier et al, 2005; Kjellstrand, 2006; Talvy et al, 2007; Le Moullec et al, 2008a; Gresch et al, 2010; Karpinska et al; 2010; Karpinska, 2013; Climent et al, 2019). Other commonly used tracers in aeration tanks are fluorescent dyes (e.g. Rhodamine), that are detected by an ultra-violet fluorometer (Burrows et al, 1999; Burrows et al, 2001; Makinia and Wells, 2005; Zima et al, 2008; Zima et al, 2009; Samstag and Wicklein, 2014). An example of a tracer test is to inject a pulse of salt solution at the inlet, and monitor its concentration with a conductivity probe at the outlet (Potier et al, 2005) or to measure samples by a fluorescent spectrophotometer (Climent et al, 2019).

Numerical RTDs can be calculated using these mathematical models:

- Euler-Lagrangian particle tracking equation models the particle concentration of a passive particle that does not affect the hydrodynamics (equation 2.41).
- Species transport equation models the scalar concentration of a passive chemical tracer that does not affect the hydrodynamics (equation 2.42).

Model parameters for numerical RTDs can be adjusted for their calibration with experimental RTD data. Species transport is sensitive to the mass diffusivity of the species tracer and the numerical diffusion of grid discretisation (Ranade, 2002).

Euler-Lagrangian particle tracking is used to calculate the numerical RTD to validate a CFD simulation (Le Moullec et al, 2008b). An accurate statistical RTD is deduced from a sufficient number of injected particles. Particles are approximate perfect tracers of the background fluid. Their diameter is very small ( $10^{-6}$  m) and they have the same properties as water (Le Moullec et al, 2008b; Karpinska et al; 2010).

Tracer experiments provide RTD data to validate CFD studies of ditches (Jensen et al, 2006; Karpinska, 2013), air-lift reactor (Talvy et al, 2007), channel reactors (Brannock, 2003; Kjellstrand, 2006; Ghawi, 2014; Karpinska and Bridgeman, 2018) and SBR (Samstag and Wicklein, 2014), by injecting a low concentration of passive chemical tracer that does not affect the hydrodynamics. Numerical RTDs using species transport are used to validate CFD simulation of an air-lift reactor (Talvy et al, 2007) and channel reactors (Brannock, 2003; Le Moullec et al, 2008b; Ghawi, 2014; Karpinska and Bridgeman, 2018; Hreiz et al, 2019). Numerical RTDs using the particle tracking method are used to validate CFD simulations of ditches (Karpinska et al, 2010; Karpinska, 2013) and a channel reactor (Le Moullec et al, 2008b).

### **2.5.2 Single-phase flow**

In a single-phase CFD study (Karpinska et al, 2013) the water velocity in a pilot scale ditch is measured using Acoustic Doppler Velocimetry (ADV). Dissolved oxygen concentrations are measured with a DO probe; COD using a COD Cell Test and spectrophotometric method;  $\text{NH}_4\text{-N}$  using an Ammonium Cell Test and  $\text{NO}_3\text{-N}$  measured using a Nitrate Cell Test. Velocities in another full-scale Carrousel ditch are measured by a portable propeller current meter (Yang et al, 2010). Laser Doppler Velocimetry (LDV) and ADV are proposed for better accuracy. In another study, a current velocity meter measures the velocities in a pilot-scale Orbal ditch. Velocity and DO in a full-scale Orbal ditch are measured using a portable velocity meter and a portable DO meter. Single-phase flow velocities in both tanks agree with the measurements (Littleton et al, 2007a).

Velocities in a Carrousel ditch are measured using a propeller current meter (Zhang et al, 2016) and are in agreement with a single-phase CFD simulation. Water velocity is measured with a Doppler velocimeter in another Carrousel ditch and is in good agreement with a single-phase CFD simulation (De Gussem et al, 2014). Single-phase simulation of a full-scale surface aerated channel reactor is validated (Huang et al, 2009). The flow rate of spray water from a surface aerator is measured with a flow meter and measurements of DO with a meter. The mass transfer coefficient of surface aeration is measured using the unsteady-state oxygen absorption method. In another study surface aeration is modelled using a single-phase flow model (Huang et al, 2013). Velocity measurements using an ultrasonic Doppler instrument are in agreement. Measurements of DO with a meter are taken in a ditch and compared to the predictions of a compartmental hydraulic model (Alaya et al, 2010).

Velocity measurements use a probe in a full-scale channel reactor (Elshaw et al, 2016). There is agreement with single phase simulation. Velocities are measured using Particle Image Velocimetry (PIV) in another channel reactor (Ghawi, 2014). Comparison of power and flow number indicate that the single-phase simulation is accurate. Single-phase simulation of a full-scale ditch shows good agreement between the oxygen mass transfer coefficient of a surface aerator and experimental measurements (Bhuyar et al, 2009). The deoxygenating procedure is a non-steady-state re-aeration test (Thakre et al, 2009).

### **2.5.3 Gas-liquid flow**

LDV measurements of velocities in a bench-scale channel reactor with clear water are in agreement with a gas-liquid flow simulation. Modelled void fractions show good agreement with optical probe measurements. A double optical probe measures the bubble size for input to a CFD model (Le Moullec et al, 2008b). Gas-liquid flow simulation agrees with measured DO in another bench-scale channel reactor (Le Moullec et al, 2010b). Nitrate is measured using ionic chromatography; ammonium and soluble CODs by standard HACH protocols and DO with a probe. The mass transfer coefficient is determined by an experimental method of Le Bonté et al, 2005.

Gas-liquid simulation is validated with a measured mass transfer coefficient in a laboratory airlift reactor (Cockx et al, 2001). Bubble size is measured and is uniform in the CFD model. CFD simulation is also validated with velocity (PIV) and gas fraction measurements (Cockx et al, 1997). In another study the effect of hydrostatic pressure on bubble size is considered by measurements of the bubble size and water depth. Moreover, bubble sizes are measured from camera images obtained by an immersed camera within a bubble plume. The diameter of spherical bubbles has the same volume as ellipsoidal bubble shapes observed by a camera within a plume (Fayolle et al, 2006). In another study, gas-liquid simulation of a ditch is validated with measurements of velocity, bubble size, gas hold-up and oxygen transfer coefficient. Velocities are measured with a flow meter and is well predicted by the CFD simulation. There is good agreement with experimental gas hold-up profiles in a pilot scale tank (Fayolle et al, 2007). In another study, gas-liquid simulation of an airlift reactor is validated with experimental data of the velocity and gas volume fraction. The bubble size is visualised by a video camera. The velocity field is measured using PIV (Talvy et al, 2007). In another study, a mean numerical bubble size is compared to a bubble size distribution for gas-liquid flow simulation of a laboratory channel reactor. It is validated with velocity measurements using PIV (Karpinka and Bridgeman, 2017). Gas-liquid flow simulation is validated with measurements of water velocity in a ditch by using Acoustic Doppler Velocimetry (Climent et al, 2019).

Gas-liquid flow simulates velocities and gas hold up profiles in an air-lift oxidation ditch (ALOD) and is compared to experimental data (Xu et al, 2010). Particle Doppler Anemometry (PDA) measures velocities in a lab-scale ALOD. DO is measured by a probe; COD by a COD reactor; BOD<sub>5</sub> by a BOD meter and animal and vegetable oils (AVO) and mineral oils (MO) by infrared spectrophotometer. Total phosphorus (TP) is determined by a phosphate analyser; ammonia-nitrogen (NH<sub>4</sub>-N) and nitrite-nitrogen (NO<sub>2</sub>-N) is by using a UV spectrophotometer. Nitrate-nitrogen (NO<sub>3</sub>-N) and total nitrogen (TN) are measured by an UV spectrophotometer.

Gas-liquid flow simulates a channel reactor (Terashima et al, 2016). The oxygen mass transfer coefficient is compared with measurements and uses a calibrated modelled bubble size. Gas-liquid simulation agrees with lab-scale PIV

measurements in another channel reactor (Hu et al, 2010). There is good agreement between CFD and lab-scale experiments in another air-lift reactor (Van Baten et al, 2003). Gas-liquid simulation of another airlift reactor is compared to experimental data for the overall gas fraction and confirmed by LDA velocity data (Mudde and Van den Akker, 2001). The computationally expensive DNS method studies the shape of a single bubble in a channel reactor (Wang and Zhao, 2009). High-speed camera bubble images are in agreement with the DNS simulation. In another study a key factor that influences oxygen mass transfer (Dhanasekharan et al, 2005) is the bubble size distribution (BSD). The gas holdup and mass transfer coefficients are compared to experimental data in an air lift reactor. In another study there is good agreement between the numerical and measured velocities (ADV) in a channel reactor, using a gas-liquid simulation that incorporates BSD (Karpinska and Bridgeman, 2018). The numerical and measured velocity profiles and the average gas hold up in an oxidation ditch, when using a gas-liquid volume of fluid (VOF) model are in good agreement (Xu et al, 2018).

#### **2.5.4 Solid-liquid flow**

Velocities are measured using a propeller flow-meter in a Carrousel ditch. Solids concentrations are measured using a portable suspended solids analyser. The solid-liquid flow simulation is found to be more accurate than a single-phase simulation. Measurements from settling cylinder experiments model the actual settling behaviour of the suspended solids of the wastewater (Xie et al, 2014). PDA measures the velocities in an ALOD. The particle diameter distribution is measured using a laser particle analyser. Solid-liquid simulation is consistent with velocity measurements that are made by PDA (Fan et al, 2010). Solid-liquid simulation of a channel reactor is validated with measurements of flow velocities by using ADV (Brannock, 2003). Suspended solids modelling incorporates solids settling that is calibrated to solids profile field data (Samstag et al, 2012). The evaluation of mixing devices in a SBR and a ditch use field testing to calibrate solid-liquid simulation. Grab samples are measured for the total suspended solids (TSS) (Samstag and Wicklein, 2014).

### **2.5.5 Three phase flow (gas-liquid-solid)**

Pseudo three-phase flow simulation of a ditch is experimentally validated (Lei and Ni, 2014). Measurements of MLSS, DO, COD, ammonia nitrogen, and nitrate are obtained from a pilot-scale Carrousel ditch. ADV is used to measure the flow velocities. Ammonia, nitrogen and nitrate concentrations are measured using spectrophotometry. DO is measured using an oxygen probe. Agreement with measured data suggests there is accuracy for pseudo three-phase flow modelling, carbon oxidation, nitrification and de-nitrification (Lei and Ni, 2014). For a pseudo three-phase flow simulation of a ditch, there is good agreement with measured velocities and suspended solids concentrations. Moreover, an artificial neural network (ANN) that is trained on the results of a pseudo three-phase flow model agrees with the measurements of ammonia, nitrogen, nitrate, DO and COD (Li et al, 2017). Three phase flow simulation of a channel reactor agrees with velocity measurements obtained by PIV (Hu et al, 2013). Solid-liquid and gas-liquid flow simulation of a ditch are in agreement with velocity measurements made by ADV (Chen and Feng, 2014). Three phase flow simulation of a EGSB reactor is validated experimentally. Comparison between measurements by PIV and simulated velocities are in good agreement (Wang et al, 2009). Three-phase flow simulation of an airlift reactor uses input measurements of bubble diameter. Solids volume fractions are in agreement with measurements (Talvy et al, 2005). For an SBR reactor three phase flow simulation is validated with measured velocities by using PIV (Diez et al, 2007).

## 2.6 CFD application to aeration design

CFD simulations are used in the development and optimisation of the design of aeration tanks, aeration devices and mixing impellers (Karpinska and Bridgeman, 2016). The criteria for improved design is the uniformity of the flow pattern, dissolved oxygen and suspended solids distribution, increasing DO concentration, increasing the residence time of the tank and reducing the energy consumption of aeration.

A ditch experiences short-circuiting of the influent towards the effluent which reduces the residence time. The inlet and outlets are positioned at opposite ends of the ditch and this increases residence time. Positioning the inlet and outlet centrally splits the flow equally by the central wall and increases residence time (Jensen et al, 2006).

In a channel reactor, corrective measures are studied to deal with the high velocity of the inlet flow: inlet damper wall, mixer, baffles. To quantify the improvement of the hydraulics there is a comparison of residence times. The hydraulics of the baffles is verified with an experimental RTD tracer test (Kjellstrand, 2006).

In a channel reactor modifications are made to baffles and mixers. When the flow is closer to plug flow (uniform flow) there is a greater removal of the pollutants. An even distribution of mixers and baffles along the length of the reactor induces several small well mixed zones in series (Brannock, 2003).

The mixing impellers with optimal impeller radius in a ditch make the flow distribution more uniform, maximise the velocity greater than 0.3 m/s and reduce return flow (Liu et al, 2014). Guiding baffles downwards at an angle and just downstream of the surface aerators increase the bottom tank velocity, make the vertical velocity distribution more uniform, which helps prevent sludge deposits and increases residence time. Baffles guide DO into the ditch bottom, which increases the mixture time between oxygen and water and the oxygen mass transfer (Wei et al, 2016a). The optimum submergence depth of impellers maximises the velocities greater than 0.3 m/s and makes the vertical velocity distribution more uniform (Wei et al, 2016b). An optimal depth of a submerged impeller is beneficial for minimising sludge deposition in an oxidation ditch by maintaining sufficient velocity (Xu et al, 2018).

By adjusting the position, rotating speed and number of submerged propellers, the problems of sludge deposits and low velocity in the bend of a ditch are improved. With three propellers operating simultaneously the flow distribution is homogeneous, and velocities in almost every section are higher than 0.15 m/s (Zhang et al, 2016).

A ditch consists of surface aerators and submerged impellers. The uniformity of the flow field and DO distribution has a relationship with the energy consumption and process efficiency. Changes to operation involve turning on and off selected surface aerators and impellers (Yang et al, 2011). In a further study, the distribution of suspended solids is made more uniform by the same strategy (Xie et al, 2014).

An oxidation ditch has vertical axis surface aerators at the ends of the central wall. Suspended solids are dispersed more evenly with a higher surface aerator speed. The effect of aerator speed on velocity is more significant in the middle depth of the ditch. Propellers at the bottom prevent sludge settling (Fan et al, 2010).

Six different configurations of mechanical surface aerators are evaluated in an oxidation ditch. The curved blade rotor type is the best with an oxygen transfer coefficient ( $K_La$ ) of  $11.50 \text{ h}^{-1}$ , at a rotational speed of 60 rpm. In order of effectiveness, cage fin rotor is  $4.33 \text{ h}^{-1}$ , cage rope wound rotor is  $3.78 \text{ h}^{-1}$ , and the Kessener brush rotor is the worst at  $2.94 \text{ h}^{-1}$  (Thakre et al, 2008; Bhuyer et al, 2009).

An oxidation ditch consists of two treatment lanes in parallel, similar to an orbal ditch. There is a gap in the channel, so flow can pass between the inner inlet channel and outer outlet channel. The best design to reduce this flow stream is by considering the optimum location of the mixing propellers (Climent et al, 2019).

A new type of aeration tank design called an air lift oxidation ditch (ALOD) with aerators at the bottom is designed. The idea comes from combining an airlift reactor with a fluidised bed. The new design allows the depth of a ditch to be increased. The influence of the location of the clapboards, distance between the clapboards and surface and the aerator array are considered (Xu et al, 2010).

Development of a new aeration method for oxidation ditches, consists of an external unit, and a pressurized aeration chamber (PAC) with slot jet agitators (hydrojets). When compared to conventional membrane diffusers that are agitated with slow speed mixers, the new aeration system provides higher oxygen transfer efficiencies (OTE) and a significant reduction in energy consumption (Karpinska, 2013).

Different diffuser types are studied in a channel reactor. The oxygen mass transfer coefficients are measured and fitted using a calibrated mean bubble size in the CFD model. Coarse-bubble, fine-pore, and slitted membrane diffusers have respective bubble sizes of 7-8 mm, 5-6 mm, and 3 mm (Terashima et al, 2016). In a channel reactor the spatial distribution of diffusers determines the flow field (Gresch et al, 2011). In an orbal ditch there are grids of fine bubble diffusers in a circular pattern. When diffusers are spaced out, increasing the air flow rate reduces the oxygen transfer efficiency and there is vertical movement of liquid caused by the bubble plume. Including a horizontal velocity neutralises this spiral flow (Gillot and Hedit, 2000). This evidences the superiority of total floor coverage over diffusers placed on separate grids. Configurations which induce spiral flow (separate grids, small aerated areas) result in lower oxygenation performance (Gillot et al, 2005). In a channel reactor by arranging the membrane aerators in a 'full floor coverage' configuration, it provides better homogeneity of flow and gas fraction distribution and higher average gas fraction. This is when compared to the same membrane diffusers located on one side, two sides and centrally in the channel (Hreiz et al, 2019). Fixed floor fine bubble diffusers have a significant energy saving when compared to mechanical surface aerators in an oxidation ditch (Höhne and Mamedov, 2020).

The energy consumption of surface aerators in an orbal ditch is determined. The efficiency of the aerators is determined by the oxygen transfer efficiency (OTE) (oxygen transfer rate (OTR) divided by mechanical power). Process monitoring is conducted of the oxygen uptake rate, DO, velocity and shaft power (Qiu et al, 2018).

The aeration performance caused by inorganic scaling of different types of fine-pore membrane diffusers are studied in a pilot scale aeration tank. To increase the anti-scaling performance, the surface potential and roughness of the material and the optimum thickness of the membrane are found to be important (Wang et al, 2020).

## 2.7 Summary

CFD modelling can be used to predict the multi-phase flow pattern and multi-component distribution of dissolved oxygen in an aeration tank (Karpinska et al, 2010; Le Moullec et al, 2011). It can investigate how aeration design affects the hydrodynamics and aeration performance (Brannock, 2003). CFD is a more powerful modelling tool than hydraulic modelling (Karpinska and Bridgeman, 2016). It is used for disinfection, dissolved air flotation, primary and secondary sedimentation, aeration and anaerobic digestion (Wicklein et al, 2016). CFD models of aeration tanks are still in need of further improvement (Karpinska and Bridgeman, 2016).

Single-phase flow models can be an initial step before multi-phase flow because the interactions between phases (flocks and bubbles) can be complex and computationally expensive (Karpinska, 2015). Water as a model fluid also enables the easier setup of an experimental laboratory to validate a CFD simulation (Karpinska, 2015). The standard two equation  $k$ - $\epsilon$  ( $k$ -epsilon) turbulence model is the predominant turbulence model used for flow in an aeration tank. The residence time distribution (RTD) describes the non-ideal fluid behaviour in an aeration tank, which is between ideal plug flow and fully mixed (Gresch et al, 2010). The RTD can be found from an experimental tracer test or a numerical equation. The RTD can be interpreted by hydraulic parameters to determine the hydraulic efficiency of the tank.

The Euler-Euler (E-E) multi-fluid model is the most common multi-phase model used for the large numbers of bubbles and particles in an aeration tank (Talvy et al, 2007). The multi-fluid model can also be used to predict the bubble size distribution (BSD) and particle size distribution (PSD), by coupling its drag term to coalescence and flocculation models (Simonin, 1990). The simpler Euler-algebraic slip mixture model is more computationally efficient, but it is limited to a single bubble and particle size. The Euler-Lagrangian multi-phase model is not used for an aeration tank, because of its expense in tracking a large number of bubbles or particles and its poor accuracy in predicting multi-phase component distributions (Wicklein and Samstag, 2009). To model the shape of the water surface the volume of fluid (VOF) surface tracking method is preferred but used sparingly (Xu et al, 2018).

Bubble size is an important parameter as it influences the interfacial gas-liquid surface area. In the bubble drag coefficient the ellipsoidal bubble shape may be taken into account (Fayolle et al, 2007). Another factor that influences the bubble size is the hydrostatic water pressure (Fayolle et al, 2007). Another factor is the increase in fluid viscosity from the solid particles, which promotes bubble coalescence (Nopens et al, 2015). Bubble size is spatially distributed by coalescence and particle size is spatially distributed by flocculation (Nopens et al, 2015).

Numerous CFD studies simulate bubbly flow, but often without any suspended solids and ignoring bubble coalescence (Cockx et al, 2001). A uniform mean bubble size, in the range of 2 to 5 mm, is often modelled and may be taken from experimental measurements (Lei and Ni, 2014). Multiphase flow models that incorporate BSD or PSD require a population balance model (PBM) to describe the population changes (Bridgeman, 2009). PBM with bubble coalescence may be coupled to the multi-fluid model (Dhanasekharan et al, 2005; Karpinska and Bridgeman, 2018; Climent et al, 2019). Polydisperse air bubbles are modelled (Climent et al, 2019) using the multiple size group (MUSIG) Model (Lo, 1998). Alternatively, a free surface tracking model (Brackbill et al, 1992) is used to predict the three dimensional shape of a bubble plume (Climent et al, 2019). It is important to progress even further than these studies and consider the influence of BSD on the inter-phase oxygen mass transfer and dissolved oxygen (DO) distribution in the tank (Karpinska and Bridgeman, 2016).

When predicting the suspended solids distribution, a two-phase solid-liquid flow model may be used (Xie et al, 2014). Discrete, flocculent, hindered and compressive settling occur because of a high particle concentration (Takács et al, 1991). The settling velocity relationship with respect to the mixed liquor suspended solids (MLSS) concentration models the slip (settling) velocity between the liquid and solid phases (Xie et al, 2014). Three phase flow is able to consider the oxygen transfer from the gas to liquid phase, transfer from the liquid to flocs and biological reactions (Le Moullec et al, 2010b). The "pseudo" three phase approach simplifies two of the phases (solid-liquid) as activated sludge in a single continuous phase and the bubbles as a disperse phase (Terashima et al, 2016). Full three phase flow models have the main phase as liquid and the bubbles and particles as disperse phases (Hu et al, 2013). Wastewater can be modelled as pure water and the sludge flocs as spherical particles with uniform diameter, density and viscosity (Wang et al, 2009).

Species transport modelling is able to predict the dissolved oxygen (DO) concentration and the inter-phase oxygen mass transfer (Karpinska et al, 2016). Oxygen transfer from atmospheric air through the water surface is considered negligible, in comparison to the total transfer through the bubble surfaces (Hu et al, 2010). The oxygen species equation can predict the oxygen mass transfer for mechanical surface aeration (Huang et al, 2009). Aeration and oxygen consumption by biochemical oxygen demand (BOD) are modelled respectively by using source and sink terms in the oxygen species transport equation (Yang et al, 2011; Wicklein et al, 2016). The oxygen consumption by BOD in an aeration tank is often simplified as being homogeneous (Littleton et al, 2007a). However, there is normally a BOD distribution in an aeration tank, which the current CFD models fail to address. It is therefore recommended that the BOD distribution is not ignored. BOD distribution should be modelled as a heterogeneous sink term in the oxygen transport equation in order to predict the DO distribution (Ghawi, 2014; Karpinska and Bridgeman, 2018).

*The gaps in research* are with regards to the gas-liquid flow simulation of the bubble size distribution (BSD), species transport simulation of the biochemical oxygen demand (BOD) distribution, gas-liquid flow simulation of the free water surface and three phase (gas-liquid-solid) flow simulation. The main benefits are to improve the accuracy of the DO distribution and to improve the understanding of CFD modelling. This can also help reveal new knowledge about factors that affect DO distribution.

The *bubble size distribution (BSD)* can be predicted using the multi-fluid model and coupled to population balance modelling (PBM). Bubble coalescence and breakup models in the multiple size group (MUSIG) model may be used. The BSD can be helpful in determining the real physical bubble size range and comparing this to measurements. It can also be helpful in understanding how aeration devices produce different bubble sizes. The bubble size distribution in an aeration tank has rarely been modelled in the literature. The *biochemical oxygen demand (BOD) distribution* can be predicted by species transport modelling. The BOD distribution can then be used to determine the DO distribution by modelling it as a heterogeneous oxygen sink term. This approach considers how the distribution of oxygen demand from the biomass affects the distribution of dissolved oxygen in an aeration tank. The BOD distribution in an aeration tank has not been modelled in the literature.

*Disturbance of the water surface* can be due to the fluid dynamic effects of different types of aerators. However, the unevenness of the surface is often considered negligible, in comparison to the few metres of water depth, and therefore the free water surface is often neglected. To predict the free water surface between two fluids (air and water), the single fluid surface tracking volume of fluid (VOF) model may be used. *Three phase flow modelling is the most challenging issue.* Bubbly and particulate flow can utilise the multi-fluid model, which is best suited for the large numbers of bubbles and particles. The main phase is the liquid to represent the wastewater and the bubbles and particles are disperse phases. Bubbles and particles can be simplified with uniform properties and considered to be spherical. Particle settling should considers discrete, flocculent, hindered and compressive settling. Bubble coalescence and particle flocculation should also be considered.

Comparison between the numerical RTD and experimental tracer test may be used to validate a CFD simulation. Velocity measurement can utilise a portable current meter or use advanced velocimetry. Measurements can be taken of in-tank concentrations of dissolved oxygen (DO), chemical oxygen demand (COD), mixed liquor suspended solids (MLSS), biochemical oxygen demand (BOD), ammonia, nitrite, total nitrogen, total phosphorus and phosphate. Measurements can also be taken of the gas-liquid mass transfer coefficient and the bubble size. These two parameters are intrinsically related. Measurements can be taken in a full-scale aeration tank in a WWTP or in a physical laboratory scale model of an aeration tank.

CFD simulation is used in the development and design optimisation of the aeration devices. The criteria for improving the design of an aeration device is to improve the uniformity of the flow pattern, DO distribution and suspended solids distribution, increase the residence time of the tank and reduce the energy consumption. Some of the design recommendations found in the literature are with regards to the location of the influent and effluent weir, the design of the inlet damper wall, location and design of baffling, design of mixing impeller in terms of radius, submergence depth, position, number and rotating speed; operation of surface aerator and mixing impeller, oxygen transfer rate of surface aerator, diffuser design that produces different bubble sizes, grid diffuser spacing and some novel designs such as the air-lift oxidation ditch and the submerged hydro-jet aerator.

### **3. Numerical model of single-phase flow**

#### **3.1 Introduction**

CFD simulation of an oxidation ditch can be computationally expensive due to the multiple phases and oxygen mass transfer (Karpinska et al, 2010). In an oxidation ditch the mixed liquor suspended solids (MLSS) concentration ranges from 3,000 - 5,000 mg/l (Dammel & Schroeder, 1991; Sears et al, 2006; Fan et al, 2010). Single-phase flow modelling is therefore not accurate enough to predict real fluid behaviour. However, it can be useful for understanding major flow characteristics and a first step towards more complex multi-phase and multi-component flow modelling (Karpinska, 2015). There are fewer equations to solve for single-phase flow (RANS and turbulence) and it is more computationally efficient (equations 2.49 to 2.53).

Single-phase flow simulations can predict water velocity distributions in ditches (Littleton et al, 2007a; Littleton et al, 2007b; Bhuyar et al, 2009; Karpinska et al, 2010, Yang et al, 2010; Yang et al, 2011; Wu et al, 2012; Guo et al, 2013; Huang et al, 2013; Karpinska, 2013; De Gussem et al, 2014; Karpinska et al, 2015; Zhang et al, 2016). The standard two equation k- $\epsilon$  model is the predominant turbulence model for single-phase flow in ditches (Bhuyar et al, 2009; Karpinska et al, 2010; Yang et al, 2011; Wu et al, 2012; Huang et al, 2013; Karpinska, 2013; Karpinska et al, 2015).

In this chapter a single-phase flow model and standard two equation k- $\epsilon$  turbulence model are used to predict water velocity distributions in two full-scale operational oxidation ditches (OD1 and OD2) at Potterne WWTP. This chapter considers geometric modelling, computational meshing and single-phase flow modelling.

## 3.2 Theory

### 3.2.1 Flow and turbulence equations

The Reynolds Averaged Navier-Stokes (RANS) equations consist of a continuity equation for conservation of mass, three momentum conservation equations and an energy conservation equation (Launder and Spalding, 1974). The mass and momentum conservation equations are given in equations 2.49 and 2.50 (Karpinska and Bridgeman, 2016). The standard two-equation k- $\epsilon$  (k-epsilon) turbulence model is used to solve additional transport equations for two turbulence quantities that are given in equations 2.51 and 2.52: the turbulent kinetic energy, k, and the turbulent eddy dissipation rate,  $\epsilon$  (Pope, 2000). The equation for the turbulent viscosity is given in equation 2.53.

For the multiple reference frame (MRF) model of the rotating surface aerators, the MRF model is a rotating reference frame model. Therefore, the Navier Stokes equations in the sub domain that represents the rotating aerator is represented in relative velocity form. Consider a coordinate system which is rotating steadily with angular velocity  $\overline{\omega}$  relative to a stationary (inertial) reference frame. The rotating system is located by a position vector  $\overline{r}$ . The fluid velocities can be transformed from the stationary frame to the rotating frame:

$$\overline{v}_r = \overline{v} - \overline{u}_r \quad (3.1)$$

$$\overline{u}_r = \overline{\omega} \times \overline{r} \quad (3.2)$$

In the above equations,  $\overline{v}_r$  is the relative velocity (viewed from the rotating frame),  $\overline{v}$  is the absolute velocity (viewed from the stationary frame), and  $\overline{u}_r$  is the "whirl" velocity (due to the moving frame).

### 3.2.2 Boundary conditions

The equations to solve the inlet conditions for  $k$  and  $\varepsilon$  in the standard two equation  $k$ - $\varepsilon$  (k-epsilon) model are as follows (Launder and Spalding, 1974; Rodi, 1993) :

$$k_{inl} = C_{p1} u_{inl}^2 \quad (3.3)$$

$$\varepsilon_{inl} = \frac{k_{inl}^{1.5}}{C_{p2} D} \quad (3.4)$$

where  $C_{p1} = 0.002$ ,  $C_{p2} = 0.3$ ,  $u_{inl}$  is inlet velocity (m/s),  $D$  is hydraulic diameter (m).

On the wall boundaries, conditions relate to dependent variables in the viscous sub layer by a logarithmic wall function. The tangential velocity at the grid node  $p$ ,  $u_p$  next to the wall, follows the log law of the wall

$$\frac{u_p}{u^*} = \frac{1}{K} \ln y_p^+ \quad (3.5)$$

where the dimensionless wall distance:

$$y_p^+ = \frac{y_p u^*}{\nu} \quad (3.6)$$

where  $K$  is the von Karman constant,  $y_p$  is distance to wall (m),  $u^*$  is friction velocity (m/s),  $\nu$  is kinematic fluid viscosity ( $m^2/s$ ).

The rate of production of turbulence near the wall is equal to its rate of dissipation, which gives a single boundary condition (Launder and Spalding, 1974; Rodi, 1993):

$$\varepsilon = \frac{C_{\mu}^{3/4} k^{3/2}}{K(d-y)} \quad (3.7)$$

### 3.2.3 Surface aerators

The multiple reference frame (MRF) model of a solid rotor determines the solid-liquid interaction between the rotating drum and the water fluid. The model predicts the tangential velocity of the fluid near the drum of the surface aerators. To calculate the tangential velocity,  $V_t$  of the rotating drums of the surface aerators:

$$V_a = \frac{2\pi}{60} D_{\text{rotsp}} \quad (3.8)$$

$$V_t = V_a D_{\text{radius}} \quad (3.9)$$

where,  $V_t$  is tangential velocity (m/s) = 2.20 m/s,  $V_a$  is angular velocity (rad/s),  $D_{\text{radius}}$  is drum radius = 0.3 m,  $D_{\text{rotsp}}$  is drum rotational speed = 70 rpm.

### 3.2.4 Flow booster

The momentum source model (MSM) predicts the average velocity that is produced by the rotating mixing impeller in the flow booster. For the propeller in the flow booster,  $V_p$  is the fluid velocity = 2.66 m/s (equation 3.12), and  $S_p$  is the fluid momentum source = 28405 kg/m<sup>2</sup>s<sup>2</sup> (equation 3.14):

$$Pr_t = \int \rho U \Delta U dA \equiv \rho V_p^2 Pr_a \quad (3.10)$$

$$Pr_a = \pi Pr_r^2 \quad (3.11)$$

$$V_p = \sqrt{\frac{Pr_t}{\rho Pr_a}} \quad (3.12)$$

$$S_m = \frac{\rho V_p Pr_a}{Pr_v} \quad (3.13)$$

$$S_p = S_m V_p \quad (3.14)$$

where  $Pr_t$  is the propeller reaction thrust = 1680 N (kg m/s<sup>2</sup>),  $\rho$  is water density (kg/m<sup>3</sup>),  $Pr_r$  is propeller radius = 0.275 m,  $Pr_a$  is propeller area = 0.237 m<sup>2</sup>,  $Pr_v$  is propeller volume = 0.059 m<sup>3</sup>,  $S_m$  is fluid mass source (kg/m<sup>3</sup>s).

### 3.3 Numerical methods

#### 3.3.1 Geometric modelling

##### Maguire jet aerator in OD1

The Maguire jet aerator in OD1 is shown in Figure 3.1, with two horizontal orientated outflow water jet nozzles near the tank bottom. Water is pre-aerated until it is saturated with air and then pumped into the aerator. The submerged flow stream of aerated water through the nozzles enables the aeration of the water.



Figure 3.1 Maguire jet aerator in OD1

##### Brush surface aerators in OD1

The four surface aerators in OD1 are designed upon the Kessener brush aerators which have a cylinder with bristles. They are located in two sets of pairs across the width of the channel, as shown in Figure 3.2. The semi-submerged bristles attached to the rapidly rotating cylinder make contact with the top layer of the water to create flow circulation around the ditch. They enable aeration through the water surface.



Figure 3.2 Surface brush aerators in OD1

### Grid membrane diffuser aerators in OD1 and OD2

The grid diffusion aeration system in both ditches (Figure 3.3) injects air under pressure into the water through multiple membrane porous surfaces. The diffusers are tubular membrane porous surfaces located near the bottom of the tank. In each grid diffuser there are 32 tubular membrane surfaces, where smaller air bubbles are released into the water. The rising bubble plume enables aeration of the water.

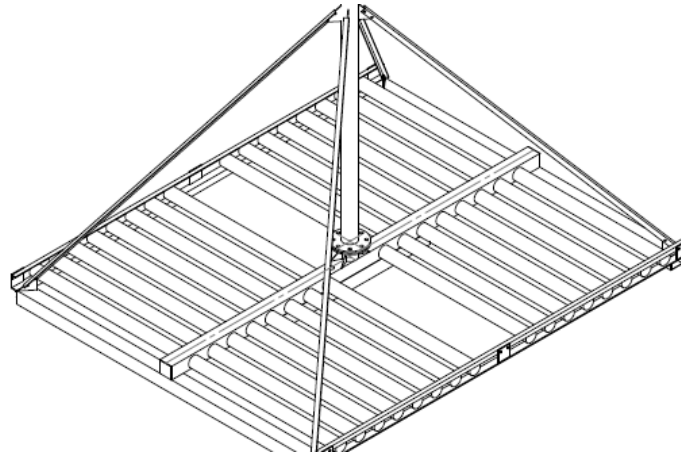


Figure 3.3 Grid membrane diffusers in OD1 and OD2

### Fuch jet aerators in OD2

The three operational Fuch jet aerators in OD2 are categorised as fine bubble depth aeration devices, with an air jet coming from the downward angled direction of flow. There is intake of air through a hollow shaft, and a high velocity jet of pure air. The jet enters the water at mid depth and enables the aeration of the water (Figure 3.4).

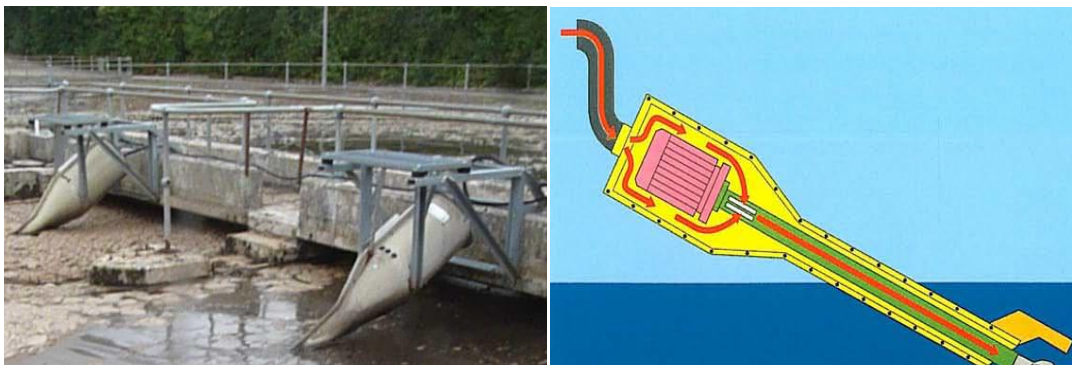


Figure 3.4 Fuch jet aerators in OD2

## Flow booster in OD2

The aim of the flow booster in OD2 is to provide a fluid momentum source that provides an additional local flow stream without any additional fluid mass. Fluid enters the volume surrounding the rotating propeller (Figure 3.5). This creates a momentum source and a horizontal flow stream at the mid depth of the ditch. The flow booster does not aerate the water.



Figure 3.5 Propeller in flow booster in OD2

The geometries of the two oxidation ditches are the same including the influent and effluent weirs. However, the geometries of the aeration devices in each ditch differ due to their designs and locations. Three dimensional geometries of OD1 and OD2 are modelled using Computer Aided Design (CAD) software Rhino CAD. To mesh the whole geometry using a structured hexahedral mesh, the geometry of each ditch is divided into multiple fluid volumes using poly-surfaces (multi-block geometry method). Grid diffusion aerators, jet aerators, brush aerators and the flow booster are each modelled by individual fully enclosed poly-surfaces. The geometry of OD1 and its devices is composed of 24 poly-surfaces and shown in Figure 3.6. The geometry of OD2 and its devices is composed of 19 poly-surfaces and shown in Figure 3.7.

In Figure 3.6 of OD1 the influent is on an outer curved segment edge at the top right, and effluent is on the right end on an outer curved segment edge. The Maguire jet aerator is modelled as two narrow cuboids (flow nozzles) on the left of Figure 3.6 (inlet is horizontal and left oriented). The grid structure of the diffusion aerator is greatly simplified by a single geometric cuboid and a single inlet. The grid diffuser aerator is shown on the left as a square geometry and the inlet is oriented upwards. The inlet area of the grid diffuser aerator is equal to the total surface area of all the open pores in the tubular porous membrane surfaces in Figure 3.3. Four rotating brush surface aerators are each partial cylinders with their top surface flush with the water surface. Only the volume of the brush aerator that is submerged is modelled. The water depth of the ditch is 1.8 m, its full length is 65 m, and its width is 21 m. The geometric co-ordinate directions are x, along the ditch length, y along the ditch width and z, along the ditch depth.

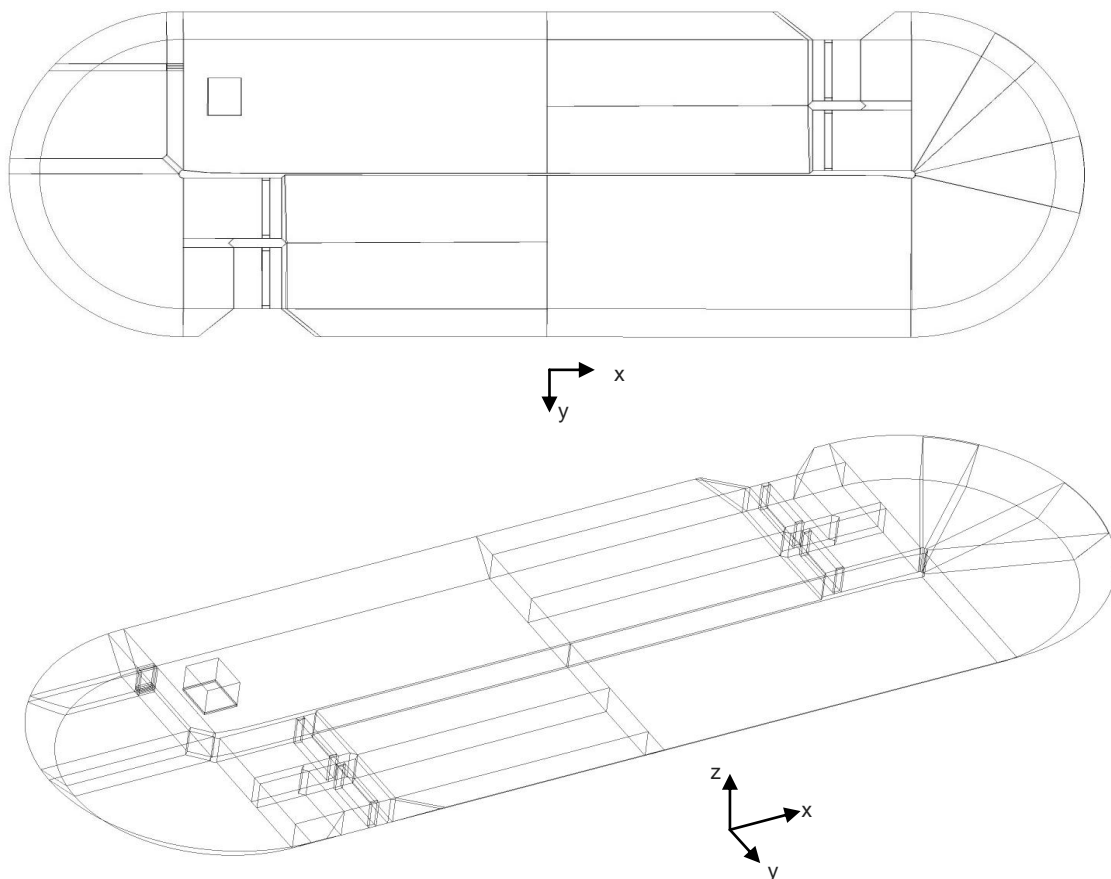


Figure 3.6 Geometry of oxidation ditch 1

In Figure 3.7 of OD2 the influent is on an outer curved segment at the bottom right, and the effluent is at the right end on an outer curved segment. The submerged inlets from the Fuch jet aerators are oriented diagonally down, along the major axis of the ditch and aligned with the straight sided walls. Grid diffuser aerators are each greatly simplified by a single inlet oriented upwards. The inlet of the flow booster is oriented horizontal towards the left and aligned with the straight sided wall. Three Fuch jet aerators, three diffuser aerators and one flow booster are each modelled with geometric cuboids. In both ditches the entire top surface is considered to be the water surface, the outer surfaces are the solid outer walls and the solid floor, and the central wall has a curved section at both ends.

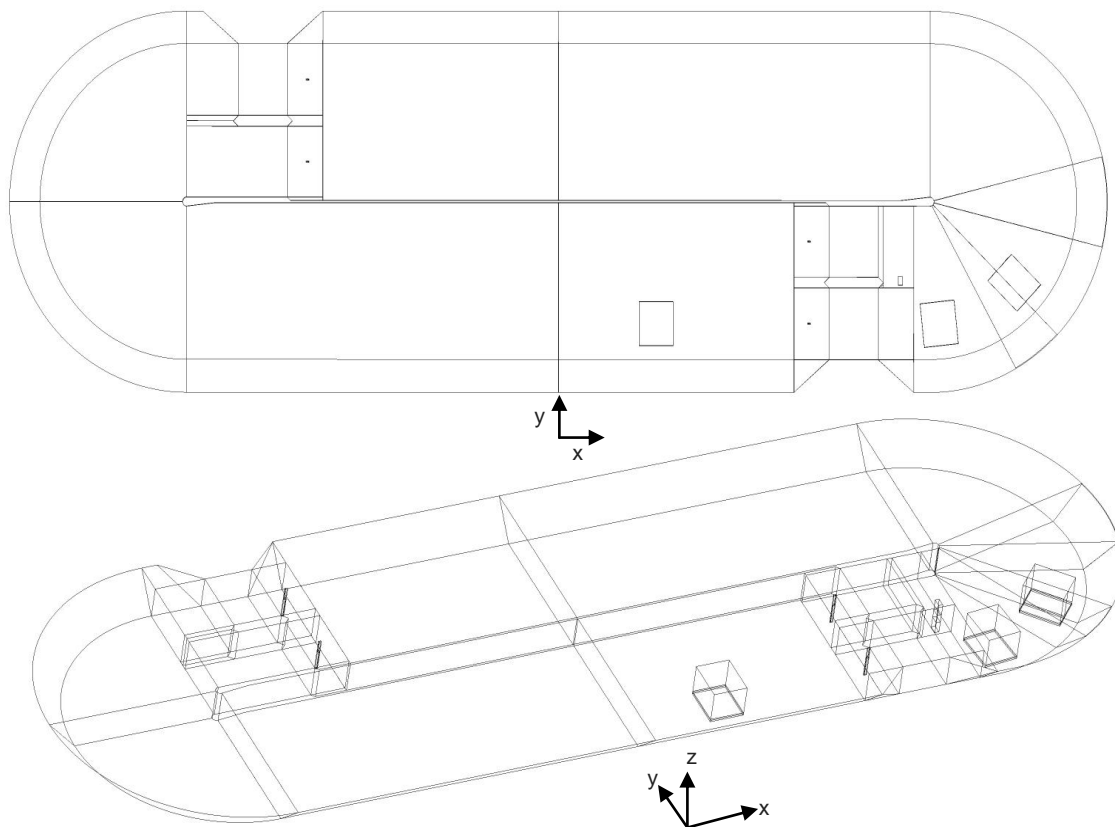


Figure 3.7 Geometry of oxidation ditch 2

### 3.3.2 Computational meshing

The finite difference numerical method (Lauder and Spalding, 1974; Wilcox, 1998; Pope 2000; Ranade, 2002) is used to interpolate the computed cell centre values of the flow variables onto the computational mesh. This is to enable variables to be predicted at discrete locations in the ditch. The meshing strategy is to use a fully structured hexahedral mesh rather than an unstructured mesh. A second order numerical grid discretisation scheme is used to improve the spatial accuracy (section 2.4.3). Structured meshes are more numerically accurate because grid lines are better aligned to boundary surfaces, which better capture the flow in the boundary layer. There is also less numerical diffusion due to lower cell skewness and better orthogonality of grid lines. The cells with highest skewness are near the sharp bends and curved surfaces of the oxidation ditch. The structured hexahedral mesh has fewer computational cells than an unstructured mesh and is therefore faster to solve. But it requires a longer development time, as the mesh is composed of multiple small meshes. Smaller meshes are each a single fluid volume that surround a single aeration device. Grid interfaces between smaller meshes are fluid-fluid boundaries. In the moving reference frame (MRF) model of the rotating surface aerators in OD1, the computational nodes between the brush aerators and surrounding fluid need to be matching. There are 13 mesh blocks in OD1 and 12 in OD2.

The total number of cells in OD1 and OD2 are 396268 and 452239 and are shown in Figures 3.8 and 3.9. All cells in OD1 are hexahedrons. Only 0.3% of the cells in OD2 are tetrahedrons, prisms and pyramids. In the mesh independency and convergence study in the next chapter, in OD1 the meshes range from 206 to 698 thousand cells, and in OD2 from 235 to 648 thousand cells. A mesh independency study has also been conducted for single-phase flow simulation but it is not presented in the thesis.

The mesh surrounding each of the four surface aerators (top left) and the grid diffuser aerator (middle left) in OD1 are shown in Figure 3.8. The mesh surrounding the Maguire jet aerator in OD1 is shown in the bottom left of Figure 3.8. The triangular section of OD1 is shown in the right of Figure 3.8. The mesh surrounding the Fuch jet aerators in OD2 is shown in two locations in Figure 3.9. The mesh surrounding one of the grid diffuser aerators in OD2 is shown in the top right, and flow booster is shown in the middle right of Figure 3.9.

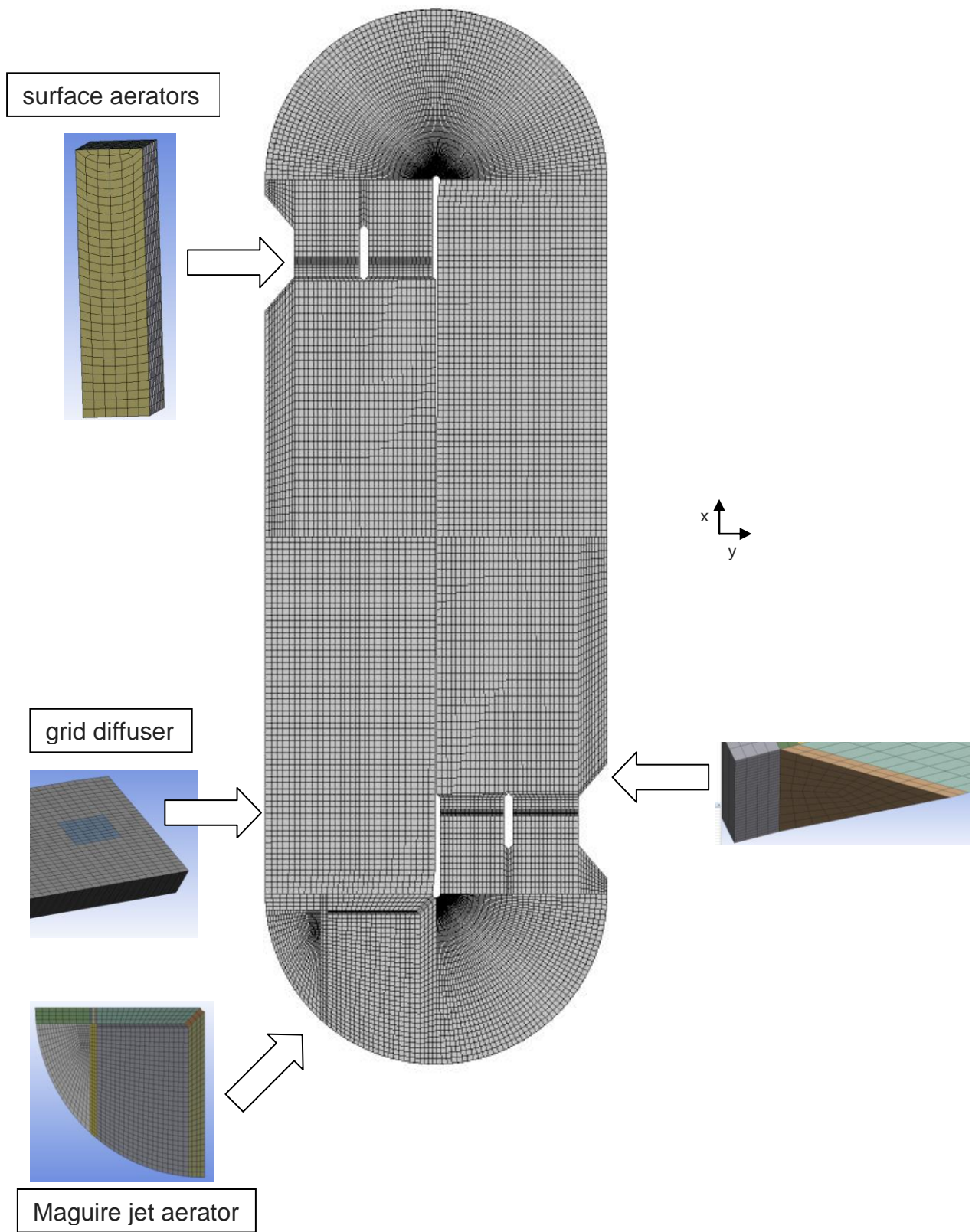


Figure 3.8 Computational mesh of oxidation ditch 1

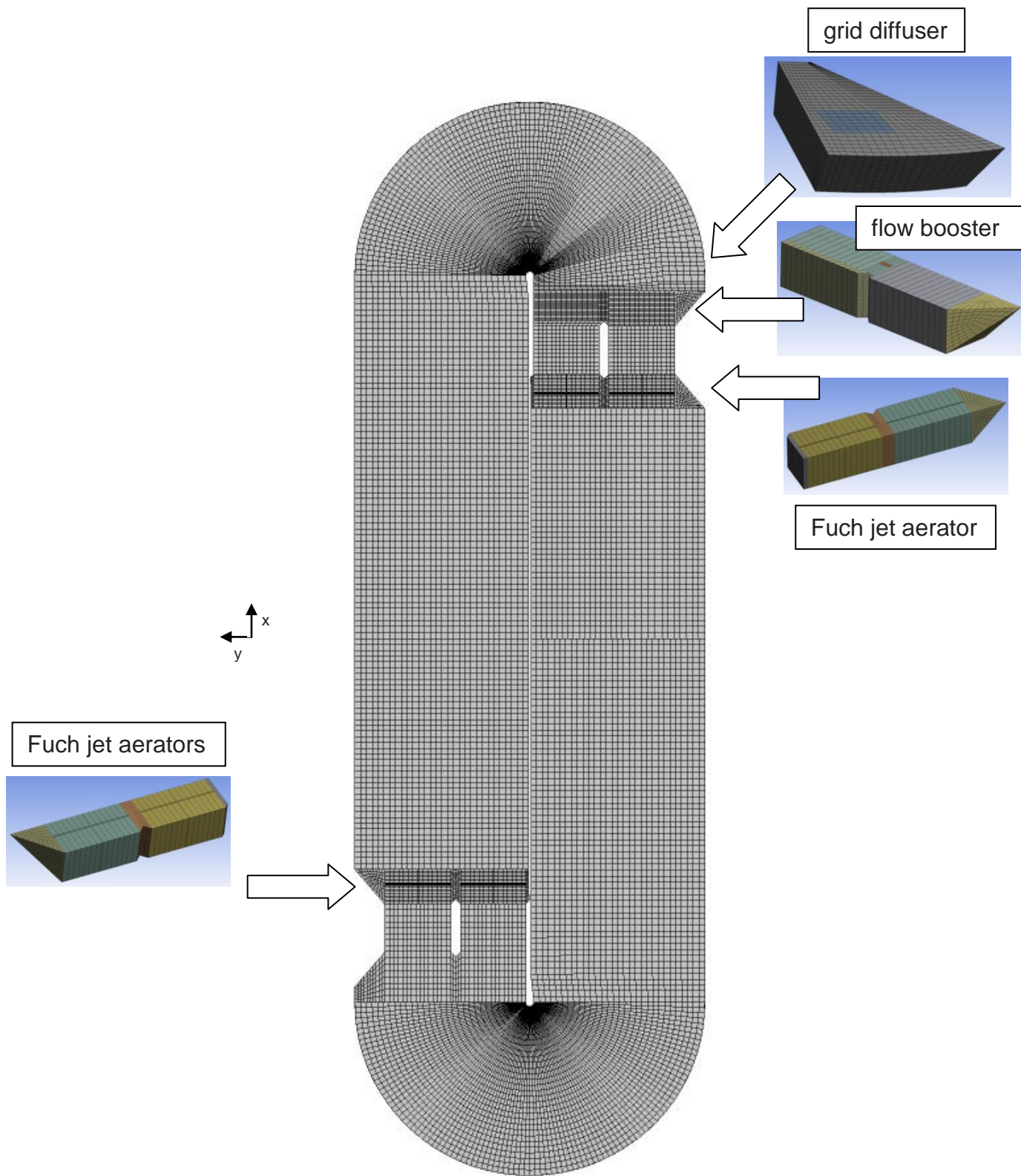


Figure 3.9 Computational mesh of oxidation ditch 2

### 3.3.3 Single-phase flow boundary conditions

The flow domain is bounded by the inlet flow over the influent weir, exit flow over the effluent weir, the entire top surface represents the water surface, and solid boundaries represent outer walls, solid floor and central wall. Boundary conditions of the ditches differ only in terms of aeration systems. The Maguire jet aerator produces an additional stream of water and the surface aerators and flow booster only create additional flow circulation. These can be simulated using single-phase flow equations (2.49 and 2.50). However, the diffuser aerator and Fuch jet aerator produce a stream of pure air and are therefore simulated by multi-phase flow equations (4.1 and 4.2).

The water surface covers the entire top surface area of the ditches. Disturbance can be caused by shear wind forces, variable influent flow rate, centrifugal force of a rotating mechanical surface aerator, rising bubble plume and flow re-circulation from the submerged diffuser, jet aerator and flow booster (Wicklein et al, 2016). This unevenness is considered negligible by investigators, compared to the few metres of water depth, and therefore the free water surface is often neglected (Guo et al, 2013). In this study it is similarly modelled using a rigid lid 'symmetry' boundary condition, fixed at a water depth of 1.8 m, with no shear stress applied at the plane.

The influent flow stream to both ditches is a velocity inlet boundary condition, with inlet depth equal to the measured height of water over the influent weir. An inlet velocity of 0.247 m/s is modelled at the influent weir. The effluent flow stream from both ditches is an outlet pressure boundary condition, with outlet depth also equal to the measured height of water. The Maguire jet aerator in OD1 is modelled with an inlet velocity boundary condition with an inlet velocity of 3.5 m/s. This creates fluid mass and the flow rate over the effluent weir in OD1 is greater than in OD2. The variation of influent flow to the ditches at Potterne WWTP is both diurnal (24 hours) and annual (365 days). For all CFD simulation in this study the mean annual inlet flow rate is used. To determine if there is any effect of the inlet flow rate, the single-phase flow pattern is also simulated at 10% and 300 % of the mean annual flow rate.

The multiple reference frame (MRF) mixer model (rotor-stator) in ANSYS has the rotating surface aerator residing in one fluid zone and the ditch volume residing in

another (Brannock, 2003). MRF calculates the solid-liquid interaction force between the surface aerator and the water. This produces a directional momentum source without a fluid mass source. The rotational speed of the surface aerator is 70 rpm. The maximum tangential velocity from the rotational drum of the aerator is predicted by MRF to be 2.20 m/s (equations 3.8 and 3.9). This is the correct velocity based on a cylindrical drum with diameter and rotational speed. The momentum source model (MSM) in ANSYS of the rotating impeller in the booster in OD2 calculates the impeller area and flow velocity from its reaction thrust (equations 3.10 to 3.14). This produces a horizontal directional momentum source without a fluid mass source. The correct average velocity from the booster is predicted by MSM to be 2.66 m/s. There is no air from the booster and therefore it can be simulated by single-phase flow.

### 3.3.4 Numerical convergence

To decrease the duration of a simulation it is assumed there is no heat transfer. The water surface is also simplified by a rigid lid symmetry boundary plane. Simulations are also solved iteratively to steady-state. Second order grid discretisation is undertaken for better accuracy. Convergence is achieved when all equations have reached a convergence criteria of  $10^{-6}$ . The rate of convergence is fast and achieved between 1500 and 5000 iterations. The duration of simulations is between 4 and 12 hours for 396268 and 452239 mesh cells in OD1 and OD2. Computer hardware is a 2.50 GHz processor (8 CPUs) with 16 GB RAM. Simulations are speeded up by parallel processing. Convergence residuals are in Figure 3.10 (case S4 in OD1).

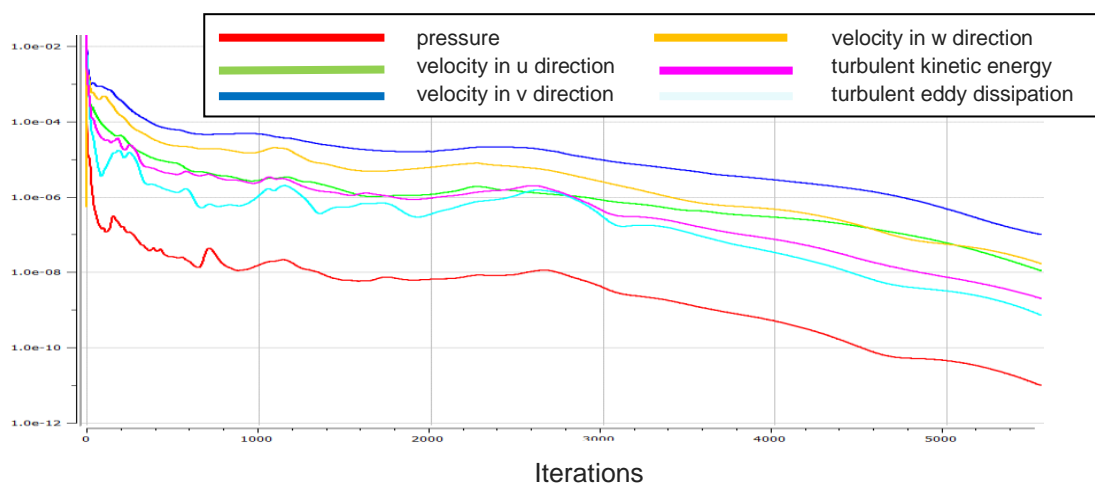


Figure 3.10 Numerical residuals of case S4

### 3.4 Results and discussion

The simulation cases for single-phase flow in each oxidation ditch at Potterne are shown in Table 3.1. The Potterne wastewater treatment plant is near Devizes, Wiltshire in the South West of England and the treatment plant is operated by Wessex Water. The mean annual temperature at Potterne WWTP is 13 °C. Therefore for ambient conditions at 13 °C and 1 atm pressure, the mean annual density of water is 999.4 kg/m<sup>3</sup> and mean annual viscosity of water is 0.0012 kg/ms.

Table 3.1 Single-phase flow simulations

Case	Ditch	Devices	No	Description	Model
S1	1&2	none	0	-	-
S2 & S4	1	Maguire jet aerator	1	hydro-jet	-
S3 & S4	1	surface aerator	4	rotating drum	MRF
S5	2	flow booster	1	propeller	MSM

Case S1 simulates OD1 and OD2 with no aeration devices. Case S2 simulates OD1 with a Maguire jet aerator only. Case S3 simulates OD1 with brush surface aerators only. Case S4 simulates OD1 with Maguire jet aerator and surface aerators. Case S5 simulates the other ditch OD2 with a submerged flow booster. Note that the full operational conditions at Potterne WWTP includes all of the devices operating (i.e. Maguire, surface, diffuser, booster, Fuch). Operational conditions require the use of multi-phase flow simulation to account for aeration conditions and this is undertaken in the next chapter. Results are shown on a horizontal plane near to the water surface unless otherwise specified. The geometric co-ordinate directions are x, along the ditch length, y along the ditch width and z, along the ditch depth. Note the naming convention for the different case simulations in the next few chapters (S1 to S5 - single phase flow, M1 to M9 - multi-phase flow, O1 to O9 - dissolved oxygen).

### Case S1 No devices in OD1 and OD2

The first case is single-phase flow in OD1 and OD2 when there are no devices. There is an inlet velocity of 0.247 m/s at the influent weir.

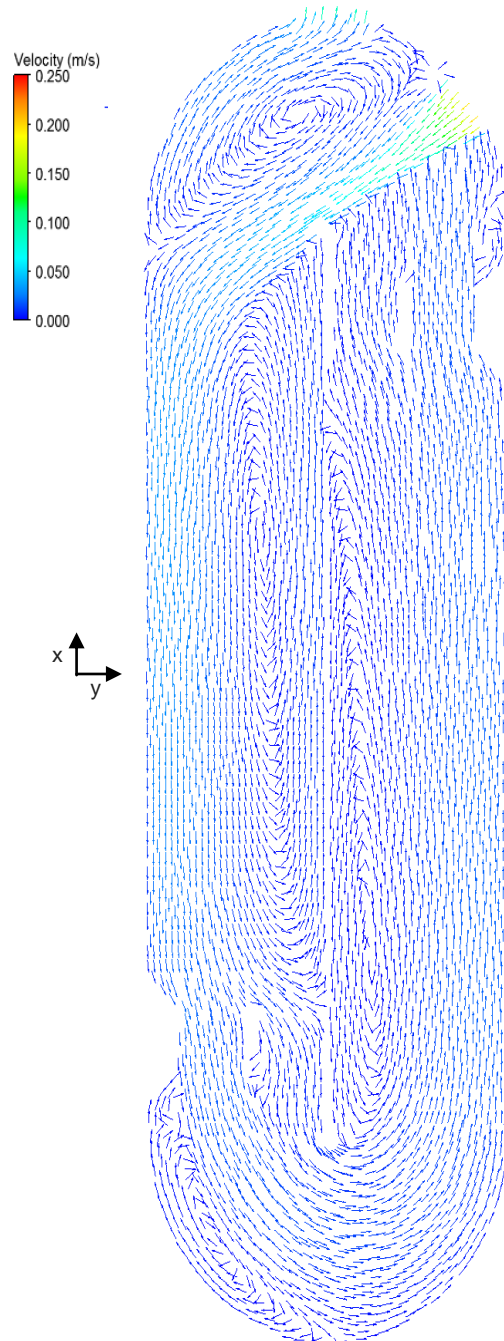


Figure 3.11 Water velocity in OD2 with no devices

Figure 3.11 shows the velocity vectors in OD2 without any devices and near the water surface (5 mm below). The influent over the weir (top right) comes in at an angle to the major longitudinal axis of OD2. Flow from the influent reaches the opposing wall of OD2 and there is a large zone of flow recirculation. Flow circulates in a clockwise direction around OD1 and in an anti-clockwise direction around OD2 in an almost plug flow regime (Figure 3.11). There is a second zone of recirculation at the far end of the ditch from the influent. There is longitudinal recirculation further downstream in the ditch. Direct flow short circuiting from the influent to effluent weir reduces the residence time of fluid in the ditch. In Figure 3.12 the velocity contours are shown in OD1 near to the water surface, and in OD2 at high, mid and low water depths. The flow patterns in OD1 and OD2 are the same when there are no devices in the ditch (Figure 3.12).

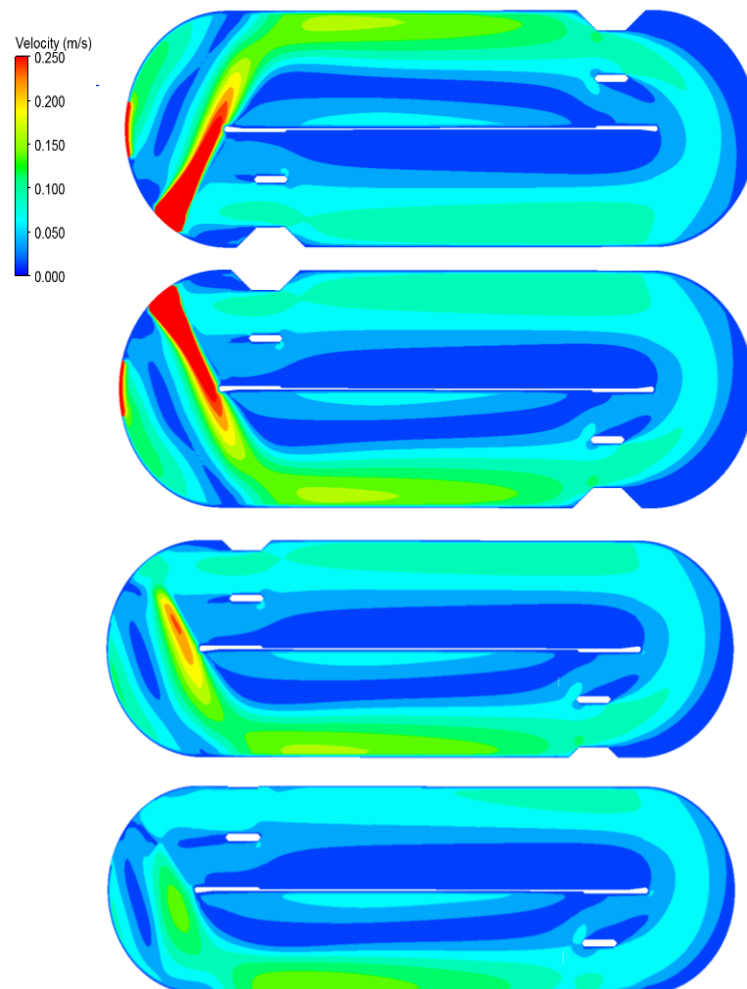


Figure 3.12 Water velocity in both ditches with no devices  
(from top to bottom) OD1: surface; OD2: surface, mid depth, bottom

## Case S2 Maguire jet aerator only in OD1

The second case is single-phase flow in OD1 with only a Maguire jet aerator. There is an inlet velocity of 3.5 m/s from two horizontal water jet nozzles in the aerator.

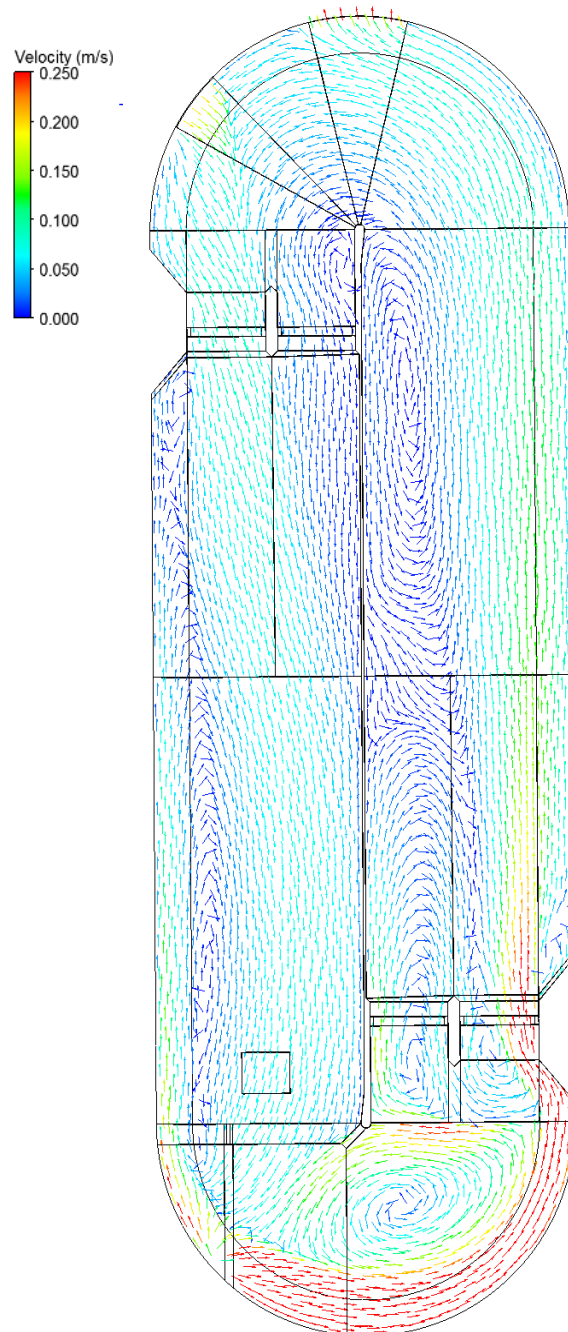


Figure 3.13 Water velocity in OD1 with Maguire jet aerator

Figure 3.13 shows the velocity vectors near to the water surface in OD1. The water jet from the Maguire aerator reverses the flow direction in the ditch to anti-clockwise. Flow reversal is an intention of design of the jet aerator to mitigate against short-circuiting of the influent towards the effluent weir. There is significant return flow that is aligned with the walls and caused by the jet in Figure 3.13. There is flow recirculation at the far end of the ditch from the influent weir and in the downstream section of the ditch. The Maguire jet aerator increases the total flow throughput in the ditch and therefore increases the average flow velocities. Figure 3.14 shows there is some vertical flow recirculation that is caused by the jet aerator.

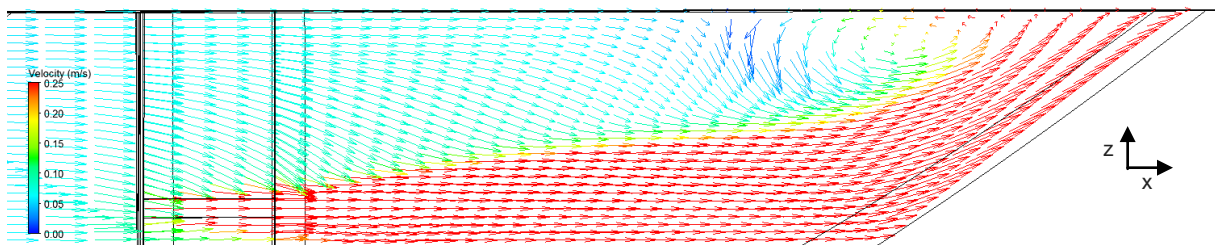


Figure 3.14 Water velocity in OD1 caused by Maguire jet aerator

### Case S3 Rotating surface aerators only in OD1

The third case is the single-phase flow in OD1, when there is only rotation of the brush surface aerators in the ditch. The brush aerators are rotating at 70 rpm, and the MRF mixer model correctly predicts a tangential velocity of 2.20 m/s at the outside edge of the rotating drums of the aerators (equations 3.8 and 3.9).

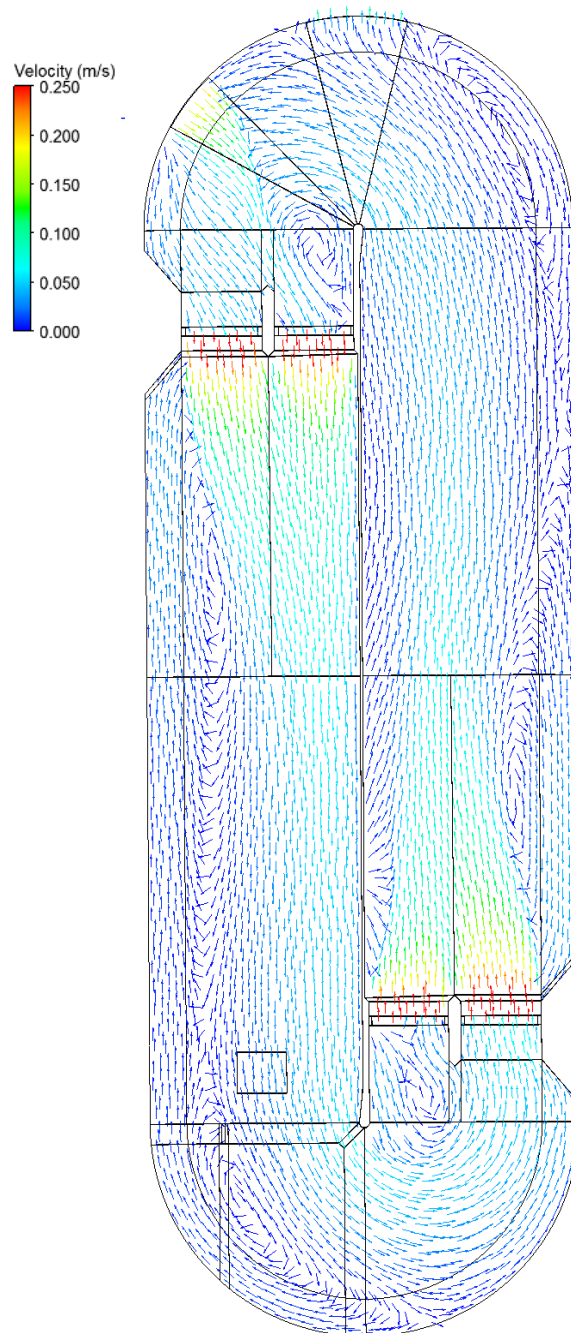


Figure 3.15 Water velocity in OD1 with surface aerators only

Figure 3.15 shows that the main effects of surface aeration are to reverse the flow direction in the ditch to anti-clockwise and to increase the average flow velocities. Reversal of flow is an intention of design to mitigate against short-circuiting of the influent towards the effluent. The rotating aerators create two velocity plumes near the water surface which are asymmetrical, due to the flow recirculation near the ditch walls in Figure 3.15. Just downstream of the rotating aerators the flow pattern is fairly uniform. Figure 3.16 shows the curved velocity profiles from the rotating aerators that are correctly simulated by the MRF mixer model. Figure 3.16 shows there to be higher velocities near the water surface and some return flow near the tank floor.

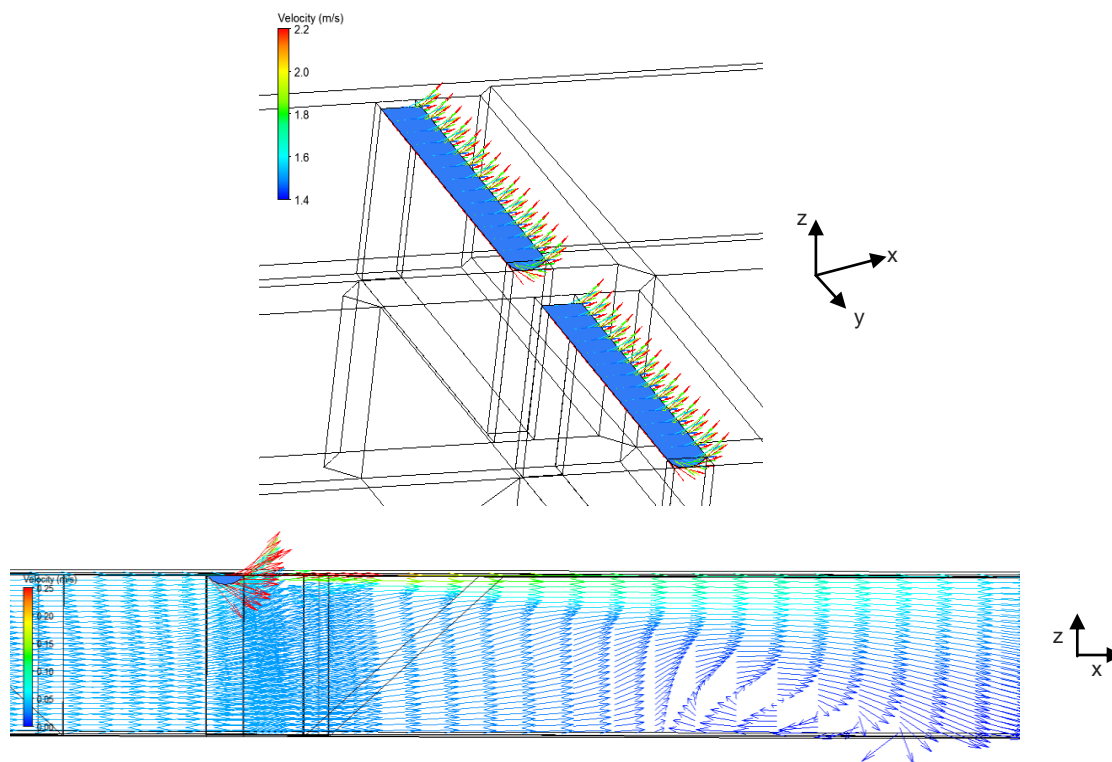


Figure 3.16 Water velocity in OD1 caused by surface aerators  
 - (top) isometric; (bottom) side view

## Case S4 Jet aeration and surface aeration in OD1

The fourth case is single-phase flow in OD1, with the combination of the rotation of the brush surface aerators and the water jet (hydro-jet) from the Maguire aerator.

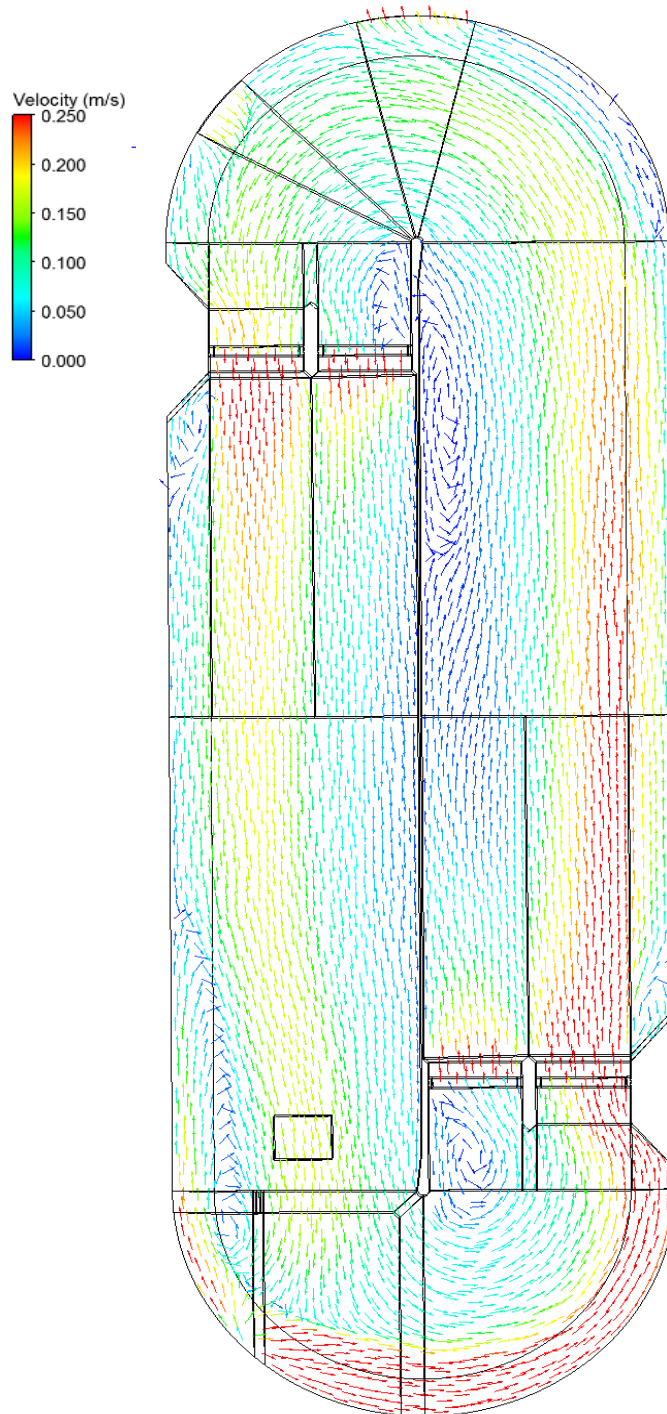


Figure 3.17 Water velocity vectors in OD1 with surface and jet aeration

The hydro-jet from the Maguire aerator and the surface rotation of the drums in the brush surface aerator reverse the flow direction in the ditch to anti-clockwise in Figure 3.17, which is an intention of design to mitigate against flow short-circuiting. Combination of the two types of aerators causes even stronger flow nearer to and aligned to the curved wall at the far end from the influent. This is because the induced flow from the surface aerators is in the same direction as the jet aerator in Figure 3.18. The flow plumes from the surface aerators are now much more asymmetrical (elongated nearer the outside wall of the ditch), which is caused by the pull of the strong flow stream of the Maguire jet aerator.

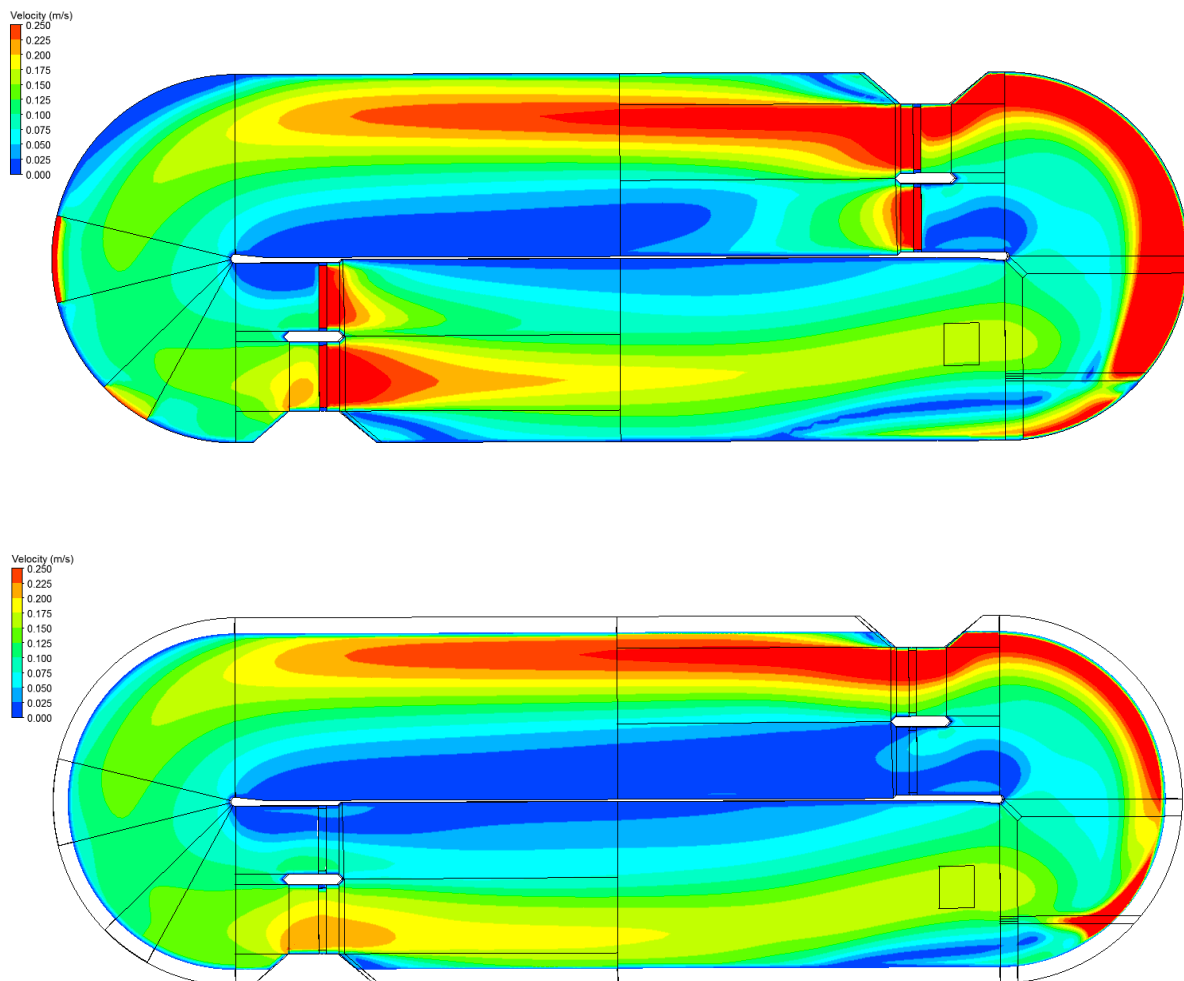


Figure 3.18 Water velocity contours in OD1 with surface and jet aeration  
 - (top) surface, (bottom) mid depth

## Case S5 Flow booster in OD2

The fifth case is single-phase flow in the other oxidation ditch, OD2, with a flow booster located at the mid water depth. The booster is modelled with a directional horizontal momentum source. The booster is composed of a rotating impeller that provides extra flow circulation, but does not provide more flow rate, as intended.

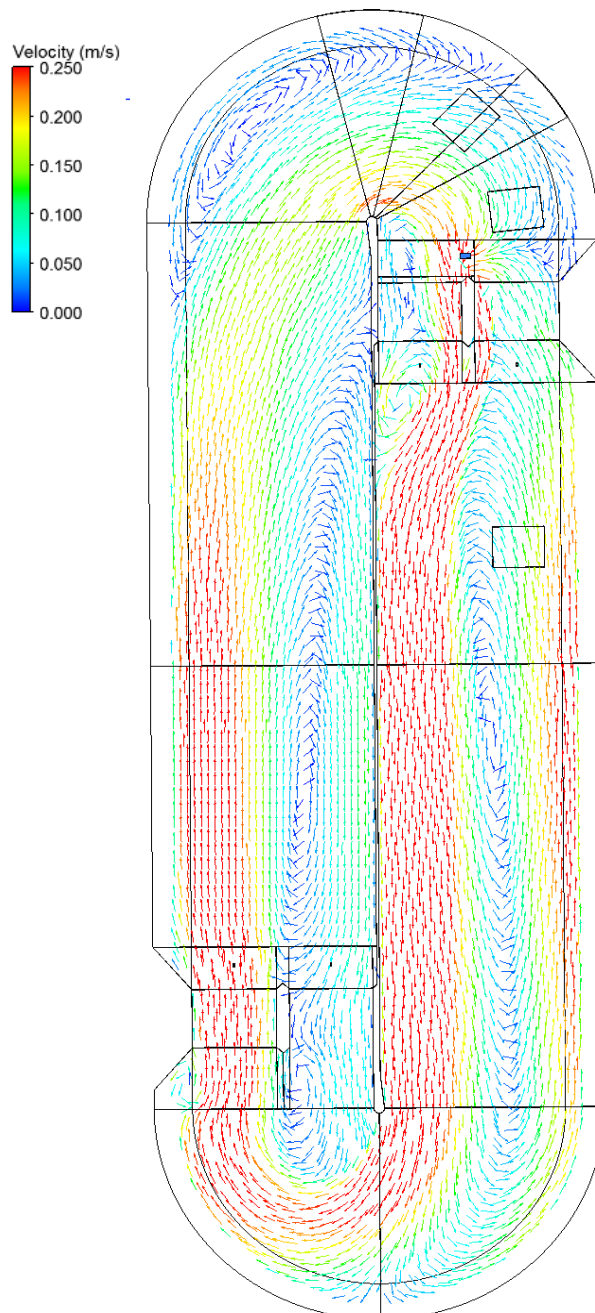


Figure 3.19 Water velocity in OD2 with flow booster - mid depth

Figure 3.19 shows there is a significant fluid plume in OD2 caused by the flow booster. Fluid momentum from the booster is significant in maintaining the velocity magnitude for a considerable distance downstream in the ditch. The overall flow direction in OD2 is reversed by the booster to clockwise, an intention of design, to mitigate against the flow short-circuiting between the influent and effluent weir flows. There is considerable undesirable flow recirculation that is caused by the flow stream from the booster. Spatial expansion of the flow plume is shown more clearly in Figure 3.20. The flow plume is hindered by the boosters ineffective position upstream of a solid blockage, shown in the top of Figure 3.20. The increase in flow velocities in OD2 is significant in Figure 3.21 with a booster. Figure 3.21 also shows the overall differences in flow patterns for each of the cases simulated in ditch OD1.

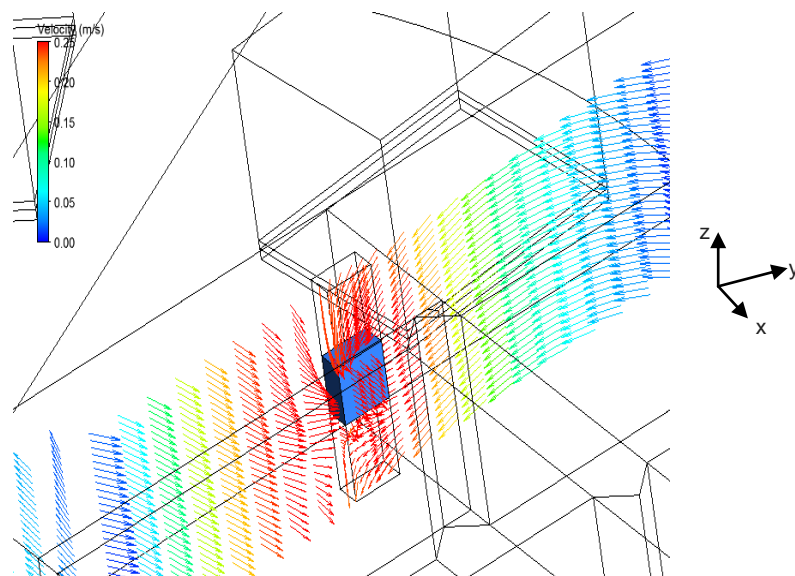
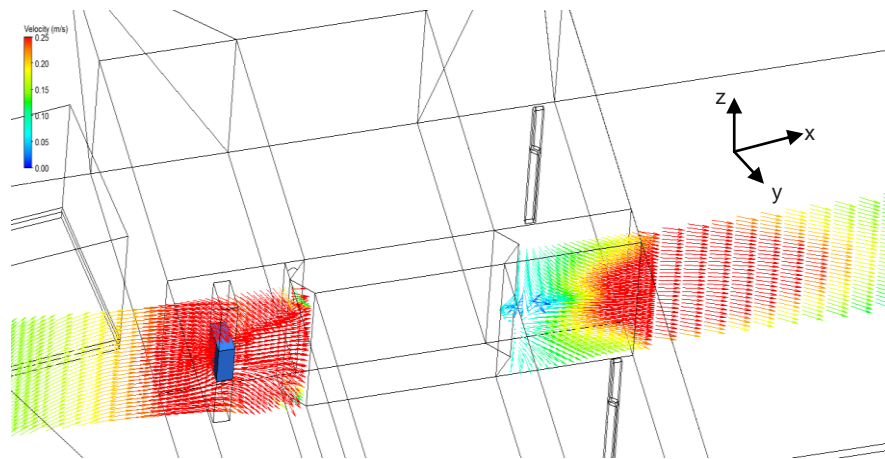


Figure 3.20 Water velocity in OD2 caused by flow booster

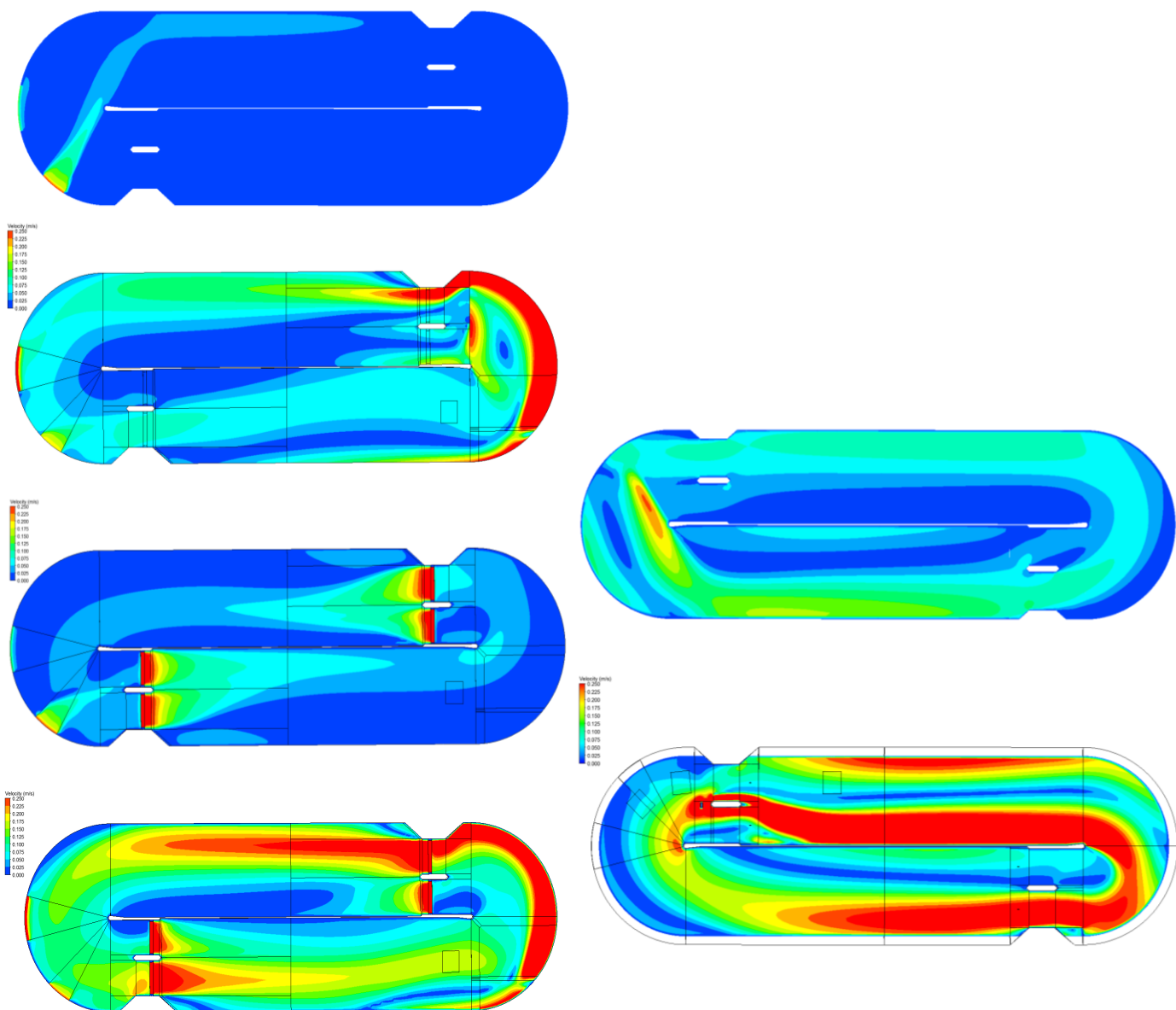


Figure 3.21 Water velocity in OD1 and OD2 - different cases

OD1 - surface (top left down): no aerators, jet, surface, jet and surface;

OD2 - mid depth (top right down) no booster, with booster

Table 3.2 Mean water velocity for single-phase flow

Case	Ditch	Devices	Effluent flow (m <sup>3</sup> /s)	Mean ditch velocity (m/s)
<b>S1</b>	1&2	none	0.0429	0.0114
<b>S2</b>	1	Maguire jet aerator only	0.1835	0.0663
<b>S3</b>	1	surface aerators only	0.0429	0.0268
<b>S4</b>	1	jet + surface	0.1835	0.1147
<b>S5</b>	2	flow booster	0.0429	0.1613

Table 3.2 shows the mean water flow velocities in ditches OD1 and OD2 for single-phase flow simulation with the inclusion of different devices. The rotating surface aerators in OD1, Maguire jet aerator in OD1 and flow booster in OD2 provide extra flow circulation. Therefore there is an increase in the average water velocity in the ditch for each of the devices (Table 3.2). The largest increase in mean water velocity is with the flow booster in OD2 (14:1). The rotating surface aerators increase the mean water velocity in OD1, with a factor of about 2:1, which is not as high as adding a fluid mass source from the Maguire jet aerator, with a factor of about 6:1.

For the analysis of the effect of the inlet flow rate over the weir, in Case S1 (no devices), there is no significant difference in flow pattern for 10% of the mean influent flow, mean flow and 300 % of mean flow. At 300%, there is a slightly more direct flow path between the influent and effluent weirs. At 300 %, the influent plume extends slightly past the central wall. For Case S4 (Maguire jet aerator and surface aerators in OD1), at 10%, the surface aerator closest to the influent has slightly higher velocities near the outlet wall, but this does not affect the downstream flow pattern. At 300%, the influent plume is no longer suppressed and this influences the flow pattern of the nearest surface aerator, but further downstream it has little effect. For Case S5 (flow booster in OD2), there is no significant difference between flow patterns. At 300 %, there is a slightly more direct flow path between the influent and flow booster. Therefore, the flow streams of the booster, Fuch jet aerator and Maguire jet aerator have a much more significant impact on the flow pattern than the flow stream of the influent flow over the weir.

### 3.5 Summary

For single-phase flow simulation when there are no aeration devices or flow booster, the flow patterns are the same in the two ditches at Potterne WWTP. Without any devices, the flow circulates around OD1 in a clockwise direction and in OD2 in an anticlockwise direction due to the influent stream coming over the weir. Without any devices the flow in both ditches is mostly in the plug flow regime. With a Maguire jet aerator in OD1 there is an additional mass flow rate from the aerator which increases the average velocities in the ditch. The Maguire jet aerator also reverses the flow direction in OD1 to anticlockwise. The jet of water from the Maguire aerator causes increased localised flow in the ditch and return flow that is aligned with the walls.

The brush surface aerators reverse the flow direction in OD1 to anti-clockwise and increase average flow velocities. Surface aerators create velocity plumes near the water surface, which are asymmetrical due to flow recirculation. Surface aerators increase the average flow velocity in OD1 by about 2:1. This is less than the Maguire jet aerator with about a 6:1 increase, due to the increase in mass flow rate in OD1. The combination of the Maguire jet aerator and surface aerators in OD1 cause even stronger flow that is aligned with the curved wall, due to the flow circulation from the surface aerator in the same direction as the jet aerator. The flow plumes from the surface aerators are asymmetric caused by the jet stream of the Maguire jet aerator.

The overall flow direction in OD2 is reversed by the flow booster to clockwise. The booster creates a significant flow stream that is maintained for a considerable distance downstream, which causes considerable flow recirculation. This stream is however hindered by the boosters ineffective position upstream of a solid blockage. There is a significant increase in average flow velocities in OD2 caused by the booster by 14:1. Flow streams of the booster, Fuch jet aerator and Maguire jet aerator have a much greater effect on flow pattern than the influent weir flow stream.

*The benefits from the single-phase flow study for ditch design are as follows.* The mixing efficiency of an oxidation ditch depends on the hydraulics and operation of the devices. The Maguire jet aerator, surface aerators and flow booster each produce a dominant flow direction in the ditch, which reduces the flow short circuiting of the influent to the effluent weir. For each of the devices, this is confirmed by an increase in residence time (Chapter 4) and therefore improvement in the hydraulic efficiency of the ditch. Each of the devices also increase the velocity in the ditch. When the water velocity is too low activated sludge can deposit to the bottom, which decreases the working volume and causes flow short circuiting, that can lead to higher energy consumption. Moreover, when the water velocity is too low it is not able to sufficiently transport dissolved oxygen around the ditch. The benefit of the surface aerators is to uniformly disperse the flow near the water surface.

*The drawbacks from the single-phase flow study for ditch design are as follows.* The aeration performance of a ditch depends on the homogenisation of the flow pattern, because this will improve the homogenisation of the dissolved oxygen (DO) distribution. The ditches have a bend geometry and relative shallow depth and therefore their velocity distribution is heterogeneous. The surface aerators are more effective near the water surface and therefore produce a heterogeneous vertical flow distribution. The Maguire jet aerator produces zones of undesirable flow recirculation. It also produces flow disturbance that causes the flow plumes of the surface aerators to be asymmetric. The booster has a strong flow stream that produces zones of undesirable flow recirculation. The ineffective position of the booster upstream of a blockage also produces undesirable fluid turbulence.

## **4. Numerical model of multi-phase flow**

### **4.1 Introduction**

The momentum exchange between the gas and liquid phases is significant in an aeration tank (Karpinska and Bridgeman, 2016). Bubble size is an important parameter in inter-phase momentum exchange, as it influences the interfacial gas-liquid area (Fayolle et al, 2007). A fixed mean bubble size is often used in CFD models (Xu et al, 2010; Gresch et al, 2011; Zhang et al, 2012; Lei and Ni, 2014; Terashima et al, 2016). Factors that influence bubble size and shape are hydrostatic pressure and bubble breakup and coalescence (Fayolle et al, 2007). These factors are ignored in the gas-liquid flow modelling in this chapter. Suspended solids are also ignored due to the increased complexity of modelling three phase flow.

The Euler-Euler (E-E) multi-fluid model is the most accurate multi-phase flow model for the large numbers of bubbles in aeration tanks (Talvy et al, 2007). It is the most commonly used multi-phase flow model for an aeration tank (Karpinska and Bridgeman, 2016), and specifically for ditches (Do-Quang et al, 1998; Glover et al, 2006; Fayolle et al, 2007). The standard two equation  $k-\epsilon$  ( $k$ -epsilon) model is the predominant turbulence model for gas-liquid flow in a ditch (Cockx et al, 2001; Glover et al, 2006; Fayolle et al, 2007; Xu et al, 2010; Lei and Ni, 2014). Efficiency of a ditch also depends on the liquid residence time distribution (RTD) (Potier et al, 2005). Numerical RTDs of aeration tanks can be predicted by using models for particle tracking (Karpinska et al, 2010; Karpinska, 2013) or species transport (Brannock, 2003; Talvy et al, 2007; Le Moullec et al, 2008b; Ghawi, 2014; Karpinska and Bridgeman, 2018).

In this chapter the multi-fluid model predicts water and air velocity distributions and volume fractions of air in two oxidation ditches (OD1 and OD2). A fixed mean bubble size of 4 mm is used as an averaged value from the literature. A mesh independence study is undertaken. Species transport modelling is used to predict numerical RTDs.

## 4.2 Theory

### 4.2.1 Multi-phase flow equations

The Euler-Euler (E-E) multi-fluid model is a multi-phase flow model, where mass continuity and momentum equations (4.1 and 4.2) are solved separately for each phase (Simonin, 1990; Ranade, 2002). Each phase is governed by a set of continuity and momentum conservation equations, which have similar structures for all phases. Thus considering an n-phase system, the mass conservation equation for phase q, in a simplified partial differential form is as follows (Joshi, 2001; Ratkovich, 2010):

$$\frac{\partial}{\partial t} (\alpha_q \rho_q) + \nabla \cdot (\alpha_q \rho_q \overline{\mathbf{v}}_q) - \sum_{p=1}^n (m_{pq} - m_{qp}) = 0 \quad (4.1)$$

where  $\rho_q$  is density, the term  $\alpha_q \rho_q$  is the effective density of phase q,  $\overline{\mathbf{v}}_q$  denotes its velocity,  $m_{pq}$  and  $m_{qp}$  are the mass transfer mechanisms from phase p to q and from q to p. Generalised momentum conservation equation for phase q (Ratkovich, 2010):

$$\frac{\partial}{\partial t} (\alpha_q \rho_q \overline{\mathbf{v}}_q) + \nabla \cdot (\alpha_q \rho_q \overline{\mathbf{v}}_q \overline{\mathbf{v}}_q) = -\alpha_q \Delta p + \nabla \cdot \mu_q (\nabla \alpha_q \overline{\mathbf{v}}_q + \nabla \alpha_q \overline{\mathbf{v}}_q T) + \rho_q \overline{\mathbf{g}} + \overline{\mathbf{F}}_q \quad (4.2)$$

where p is the pressure shared by all phases,  $\mu_q$  denotes shear viscosity of phase q, and  $\overline{\mathbf{F}}_q$  is the sum of interfacial forces between the continuous and disperse phases.

### 4.2.2 Bubble drag force

The gas-liquid flow around bubbles is characterised by the relative motion between phases, which is affected by the inter-phase drag force (Ishi and Zuber, 1979; Joshi, 2001; Ranade, 2002). Bubble diameter is an input to the bubble drag force (Talvy et al, 2007). The Ishii and Zuber drag law uses the concept of mixture viscosity, that can include bubble shape distortion (Ishi and Zuber, 1979). Densely distributed fluid particles (high numbers of bubbles) are modelled using the Ishii-Zuber drag model (equation 2.22). It differs from the Schiller-Naumann (Schiller and Naumann, 1935) drag model (equation 2.19) by its expression in the viscous flow regime, and its use of the mixture Reynolds number,  $Re_m$  that is based on the mixture viscosity,  $\mu_m$ .

### 4.2.3 Turbulent dispersion force

Consider the turbulent continuous phase that is interacting with the disperse phase. Bubbles get carried by turbulent eddies from regions of high to low bubble concentrations (Burns et al, 2004). For non-uniform bubble motion, the interfacial forces may need to account for drag and non-drag forces (if significant) such as the virtual mass force, lateral lift force and wall lubrication force. These forces may be neglected in our study (Karpinska and Bridgeman, 2016). However, the turbulent dispersion force (equation 4.3) does take into account the dispersion of bubbles that is caused by the turbulent eddies. Inhomogeneous turbulence is modelled using the two equation k- $\epsilon$  (k-epsilon) model for the water phase and the disperse phase zero equation model for the bubble phase. For turbulence transfer between the phases, the enhanced eddy viscosity model (Sato et al, 1981) uses a simple algebraic relationship between the disperse phase and the continuous phase kinematic eddy viscosities ( $\frac{\nu_{tl}}{\sigma_{\alpha l}}$  in equation 4.3). The Favre averaged drag model is tested in this study for turbulent dispersion (Burns et al, 2004). The turbulent dispersion force by the time averaging of the fluctuating component of the inter-phase drag force:

$$\overline{M_L^{td}} = C_d C_{td} \frac{\nu_{tl}}{\sigma_{\alpha l}} \left( \frac{\nabla \alpha_g}{\alpha_g} - \frac{\nabla \alpha_l}{\alpha_l} \right) \quad (4.3)$$

where  $C_d$  is drag force coefficient,  $C_{td}$  is turbulent dispersion force coefficient and taken to be 1.  $\nu_{tl}$  is kinematic eddy viscosity of liquid phase ( $m^2/s$ ),  $\sigma_{\alpha l}$  is the turbulent Schmidt number for the liquid phase volume fraction and taken to be 1.

### 4.2.4 Oxygen transfer rate of surface aerators

To calculate the oxygen transfer rate ( $OTR_{sp}$ ) of the spray water in air from the brush surface aerators (McWhirter et al, 1995; Huang et al, 2009):

$$OTR_{sp} = K_L a V (C_{DS} - C_o) \approx Q E C_{DS} \quad (4.4)$$

$$0.000833 \frac{1}{s} \times 2000 m^3 \times 0.0105 \frac{kg}{m^3} = 0.0175 \frac{kg}{s} \quad (4.5)$$

where  $OTR_{sp}$  is the oxygen transfer rate of spray water (mg/h),  $K_L a$  is overall mass transfer coefficient ( $h^{-1}$ ) of oxygen transfer from gas (air) to liquid (water),  $V$  is tank volume =  $2000 m^3$ ,  $Q$  = spray water flow rate (l/h),  $E$  is aeration efficiency of spray water in air,  $C_{DS}$  is saturation concentration of dissolved oxygen (DO) at the wet-bulb temperature of air (mg/l) and  $C_o$  is the initial DO concentration in the aeration tank.

The saturation concentration ( $C_{DS}$ ) of dissolved oxygen in water (Degremont, 2007) at the mean annual temperature of 13 °C is 10.5 mg/l (0.0105 kg/m<sup>3</sup>). Physical measurements of DO at the influent to the ditches using a portable DO meter are 0.08 mg/l in OD1 and 0.04 mg/l in OD2. To simplify one can assume that the initial DO in the aeration tank is  $\approx 0$  mg/l. However, no physical measurement is taken of the overall mass transfer coefficient,  $K_La$  of the surface aerators at Potterne WWTP.

In the literature, measurements are taken of a horizontal shaft rotating aerator with curved blades (CBR) at a range of rotational speeds 42 - 60 rpm (Bhuyer et al, 2009). Comparison between literature  $K_La$  values of different types of surface aerators at 70 rpm (brush rotor = 3 h<sup>-1</sup>, cage rope wound rotor (CRWR) = 4 h<sup>-1</sup>, cage fin rotor (CFR) = 4.5 h<sup>-1</sup>, CBR = 14 h<sup>-1</sup>; Thakre et al, 2008, Bhuyer et al, 2009). Therefore, a value of 3 h<sup>-1</sup> is used for the brush surface aerators in OD1.

The total air mass flux value of 0.0175 kg/s is used for  $OTR_{sp}$  in the whole of ditch OD1 (equation 4.5). Mass inlets representing surface aerators may be set to a source of DO (Yang et al, 2011). The oxygen mass flux (kg O<sub>2</sub>/s) may be equal to the aeration capacity of a brush surface aerator (Stamou et al, 1999). Therefore, for each of the four brush surface aerators in OD1 a source of 0.0044 kg/s of air is used for the boundary, where the rotating drum makes contact with the water.

## **4.3 Numerical methods**

### **4.3.1 Multi-phase flow boundary conditions**

The water surface is considered fixed and planar and uses the “degassing” boundary condition. This allows air to be released from the water surface from rising bubbles and is therefore an air sink for the bubbles departing the ditch. It does not allow water to exit through the surface by agitation, diffusion or evaporation. It eliminates the need of a multi-phase model for a free water surface and is computationally efficient (Talvy et al, 2007). Air coming in from the atmospheric air is considered negligible in comparison to the air coming in through the bubble surfaces (Fayolle et al, 2007; Hu et al, 2010). In a multi-phase flow model, air is modelled at the boundaries of the air sources: influent weir, surface aeration, Maguire jet aerator,

diffuser aerator and Fuch jet aerator. The Maguire jet aerator has a horizontal jet flow stream of saturated aerated water. The diffuser aerator has a vertical stream of pure air. The Fuch jet aerator has a downward angled jet flow stream of pure air.

The influent stream over the weir has a velocity inlet boundary condition (0.247 m/s). Air content in the influent is defined by a very low volume fraction of air in water equivalent to the DO measurements of 0.08 mg/l in OD1 and 0.04 mg/l in OD2. The Maguire jet aerator has an inlet velocity boundary condition (3.5 m/s). The assumption is that the water in the Maguire jet stream is fully saturated with air. The saturation DO concentration at 13 °C is 10.5 mg/l (Degremont, 2007). An equivalent volume fraction of air of 0.036 is at the inlet of the Maguire jet aerator. Grid diffusers are modelled as a single surface, equivalent to the total surface area of all the pores on the porous membrane tubes in a single grid. An inlet velocity boundary condition (0.01 m/s) of air is modelled. The flow stream from the diffuser is pure air and has a volume fraction of air of 1. The Fuch jet aerators have an inlet velocity boundary condition of air of 21 m/s. The flow stream from the Fuch jet aerator is pure air and has a volume fraction of air of 1. The air source from the surface aerators is through the rotating drum surface that in contact with the water. The mass source of air (0.0044 kg/s from each surface aerator) is calculated from the mass transfer coefficient ( $3 \text{ h}^{-1}$ ) of a brush surface aerator (equation 4.5). There is no air from the booster, but it does produce a directional momentum source of water, without producing an additional mass of water in the ditch.

#### **4.3.2 Residence time distribution (RTD)**

When predicting the RTD, the flow equations of mass, momentum, turbulence and volume fraction are not solved further, so that the already solved multi-phase flow pattern is kept at steady-state throughout the RTD calculation. The RTD is calculated by a species transport model of a tracer (scalar defined as an additive variable) - equation 2.42. Physical properties of the tracer are the same as the background fluid (water). The mass diffusivity and the turbulent Schmidt number of the tracer in the water phase are defined. The tracer is an inert substance that is introduced at the entrance of the tank as a pulse or step. A uniform value of 1 for the tracer variable at the influent weir represents a uniform dose pulse for a short period (10 s). Transient

simulation with physical time stepping is used for the species simulation. It is solved for a duration that is equal to 4 times the theoretical hydraulic mean residence time (HRT) of the ditch - equation 2.46. The concentration of the tracer is measured in the effluent. This evolution of concentration in time is plotted as an RTD graph and is further interpreted in terms of the hydraulic performance of the ditch. The theory of the RTD and the species transport equation of the tracer are given in section 2.3.5.

### 4.3.3 Numerical convergence

For the multi-phase fluid solver the initial volume fraction weighted smoothing algorithm is used. The volume fraction solver is segregated which solves the water and air phase equations consecutively. To decrease the computational duration, the water surface is simplified by a degassing boundary condition, mesh independency study is conducted and the equations are solved iteratively to steady-state. Second order numerical grid discretisation is used. Convergence is achieved when all equations reach a convergence criteria of  $10^{-6}$ . Rate of convergence is fast and achieved between 4000 and 7000 iterations. Duration of multi-phase flow simulations is between 16 to 36 hours (396268 cells in OD1 and 452239 in OD2). Convergence residuals during a multi-phase flow simulation are shown in Figure 4.1 (case M5).

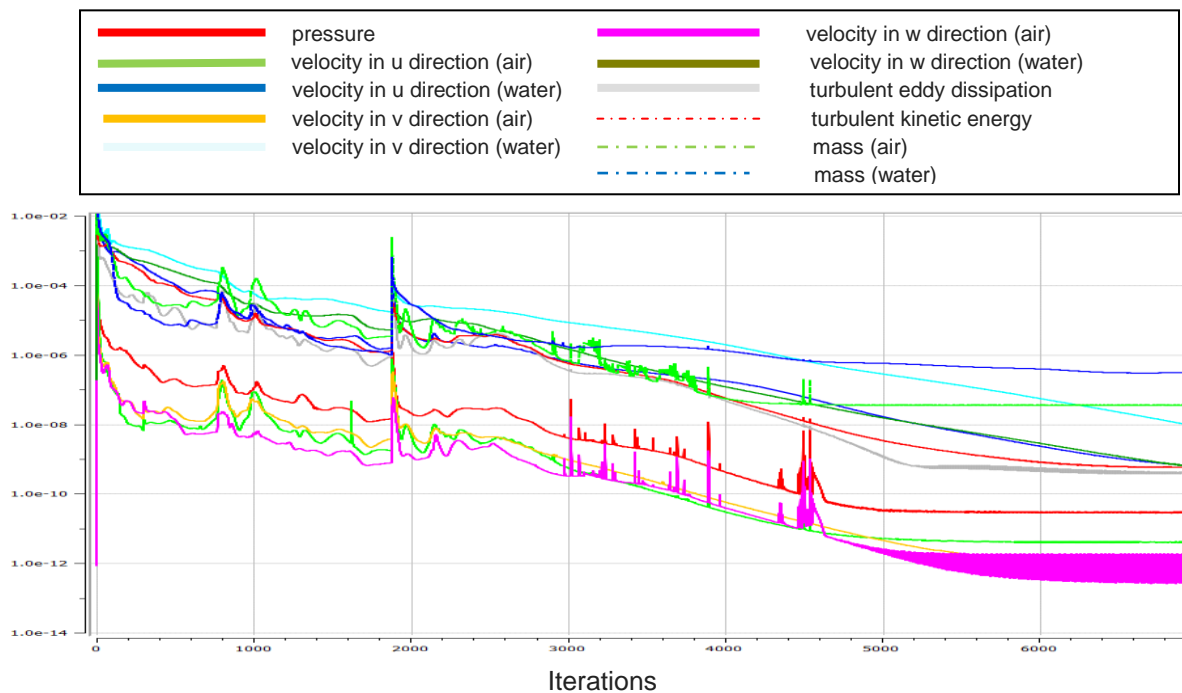


Figure 4.1 Numerical residuals of case M5

## 4.4 Results and discussion

### 4.4.1 Gas-liquid flow simulation

Cases for the multi-phase flow simulations in each ditch at Potterne WWTP are shown in Table 4.1. The mean annual temperature at Potterne WWTP is 13 °C. Therefore the mean annual density of water at 13 °C and 1 atm of pressure is 999.4 kg/m<sup>3</sup> and mean annual viscosity of water is 0.0012 kg/ms. The mean annual density of air is 1.233 kg/m<sup>3</sup> and mean annual viscosity of air is 0.000179 kg/ms. From the literature the average bubble size in oxidation ditches is around 4 mm. The effluent flow rates and mean velocities in the ditches are in Table 4.1 for each simulation.

Table 4.1 Gas-liquid flow simulations

Case	OD	Devices	No	Description	Effluent (m <sup>3</sup> /s)	Mean velocity (m/s)
M1	1&2	none	0	-	0.0429	0.0079
M2	1	Maguire jet aerator	1	aerated hydro-jet	0.1785	0.0731
M3	1	surface aerator	4	rotating drum	0.0429	0.0316
M4	1	diffuser aerator	1	air diffusion	0.0429	0.0120
<b>M5</b>	<b>1</b>	<b>operating (OD1)</b>	<b>6</b>	<b>All</b>	<b>0.1785</b>	<b>0.1195</b>
M6	2	flow booster	1	propeller	0.0429	0.1582
M7	2	Fuch jet aerator	3	air jet	0.0429	0.0279
M8	2	diffuser aerator	3	air diffusion	0.0429	0.0219
<b>M9</b>	<b>2</b>	<b>operating (OD2)</b>	<b>7</b>	<b>All</b>	<b>0.0429</b>	<b>0.1157</b>

Case *M1* simulates OD1 and OD2 with no devices. Case *M2* simulates OD1 with a Maguire jet aerator only. Case *M3* simulates OD1 with surface aerators only. Case *M4* simulates OD1 with a diffuser aerator only. Case *M5* simulates OD1 with Maguire jet aerator, surface aerators and diffuser aerator. Case *M6* simulates the other ditch, OD2 with flow booster only. Case *M7* simulates OD2 with Fuch jet aerators only. Case *M8* simulates OD2 with diffuser aerators only. Case *M9* simulates OD2 with booster, Fuch jet aerators and diffuser aerators. Cases *M5* and *M9* are the gas-liquid flow simulations that represent the operating conditions at the WWTP for the ditches.

## Case M1 No devices in OD1 and OD2

The results are shown on a horizontal plane near to the water surface, unless otherwise specified. The geometric co-ordinate directions are x, along the ditch length, y along the ditch width and z, along the ditch depth. Figure 3.11 shows the water flow patterns in OD2 near the water surface without any devices for single-phase flow. The influent to OD2 has a low DO concentration of 0.04 mg/l. Air quickly reaches the water surface and dissipates out of the ditch, and there is no air in the rest of the ditch (Figure 4.2). The influent over the weir (top right) comes in at an angle to the longitudinal direction of the ditch. The influent flow stream reaches the opposite wall and there is a large zone of recirculation. Flow circulates in an anti-clockwise direction in an almost plug flow regime (Figure 3.11). Direct flow short circuiting from the influent to effluent weir is evident. The flow patterns in OD1 and OD2 are the same when there are no devices.

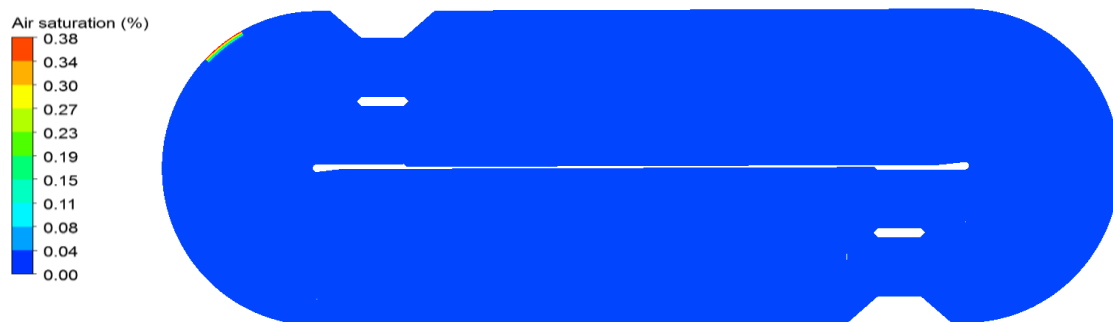


Figure 4.2 Volume fraction of air in OD2 with no aerators  
(scale: % air saturation)

**Case M2    Maguire jet aerator only in OD1**

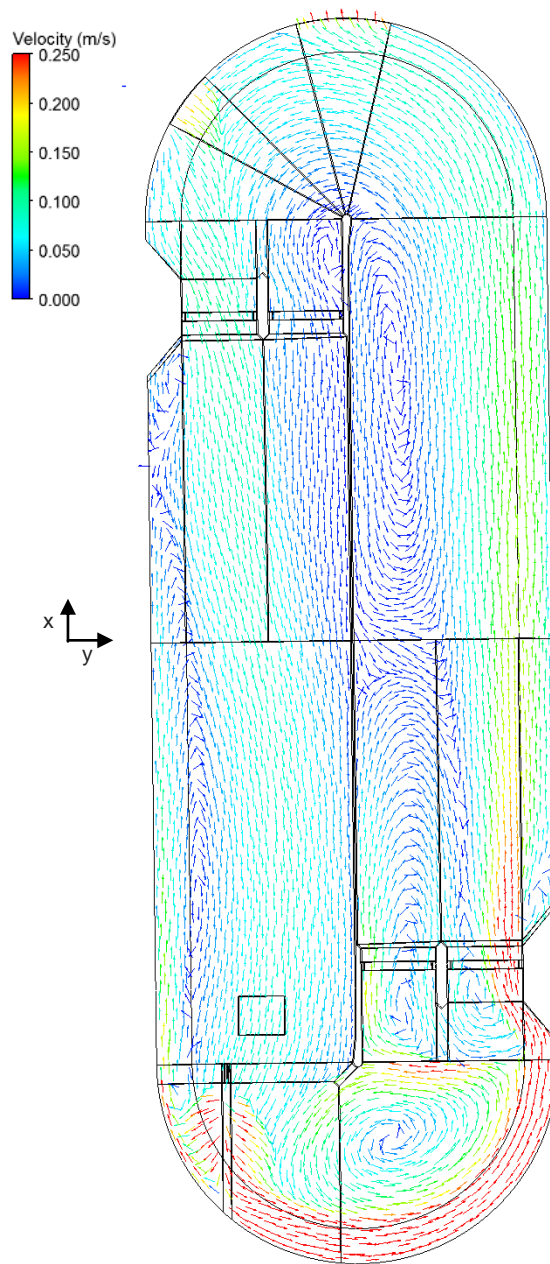


Figure 4.3    Water velocity in OD1 with Maguire jet aerator

Figure 4.3 shows the water velocity vectors for multi-phase flow near the water surface in OD1. The jet from the Maguire aerator reverses the flow direction in the ditch to anti-clockwise, as intended to mitigate against the flow short-circuiting of the influent stream, and it also increases the flow velocities in the ditch. There is significant return flow along the walls that is caused by the jet. There is strong recirculation at the opposite end of the ditch to the influent, and in the downstream section of the ditch. Figure 4.4 shows in a vertical plane the jet flow behaviour from the aerator in a multi-phase flow. The air content in the inlet water of the Maguire jet aerator is fully saturated (volume fraction of 0.036). Figure 4.5 shows the air plume from the Maguire jet aerator and how the air rises to the water surface.

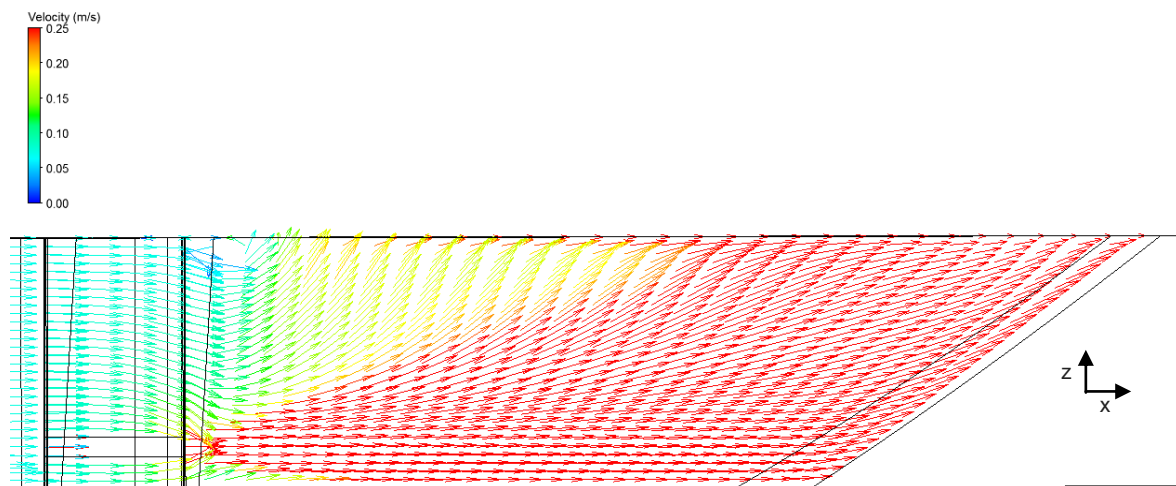


Figure 4.4 Water velocity in OD1 caused by Maguire jet aerator

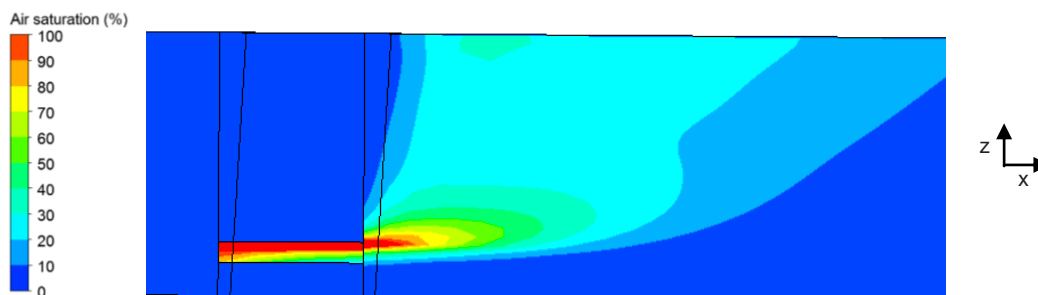


Figure 4.5 Volume fraction of air in OD1 caused by Maguire jet aerator  
(scale: % air saturation)

**Case M3    Rotating surface aerators only in OD1**

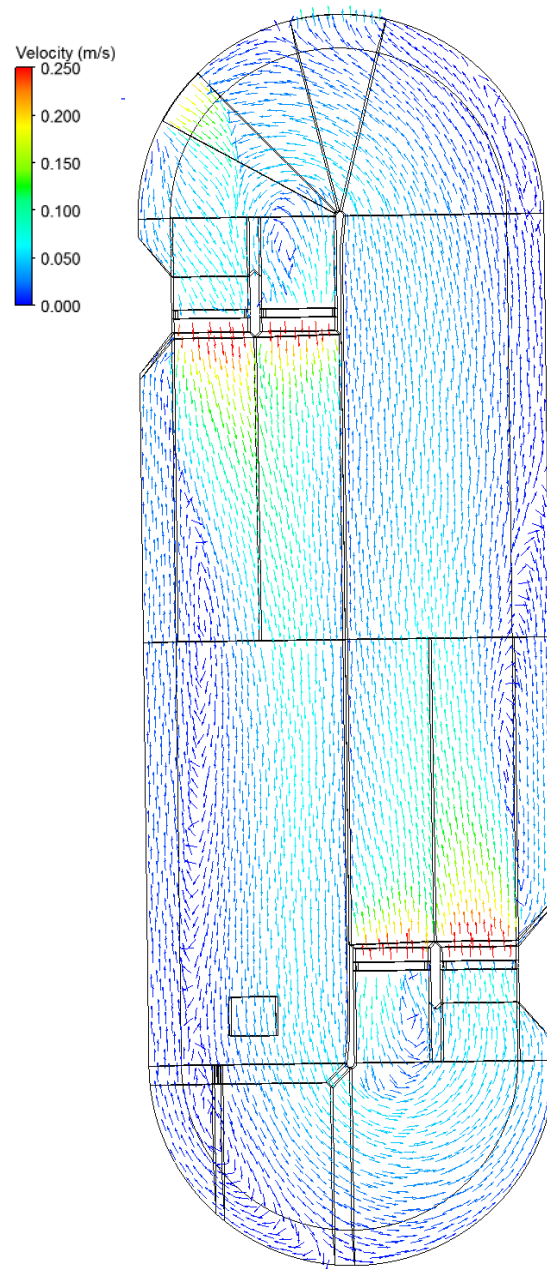


Figure 4.6    Water velocity in OD1 with surface aerators only

Figure 4.6 shows that for multi-phase flow the rotating brush aerators reverse the flow direction to anti-clockwise, as intended, and increase the flow velocities. The four rotating brush aerators create two large velocity plumes. Brush aerators near the influent cause the plume to be non-symmetrical, and there is significant return flow along the outside wall of the ditch. Further downstream from the influent flow the flow becomes more uniform. There are two small regions of recirculation just upstream of the brush aerators and close to the inner wall of the ditch. The air distributions are near the brush aerators and water surface (Figure 4.7). Air volume fractions reach saturation (shown by red in the bottom of Figure 4.7), where the drum makes contact with the water. Note the difference in scale is to highlight these features.

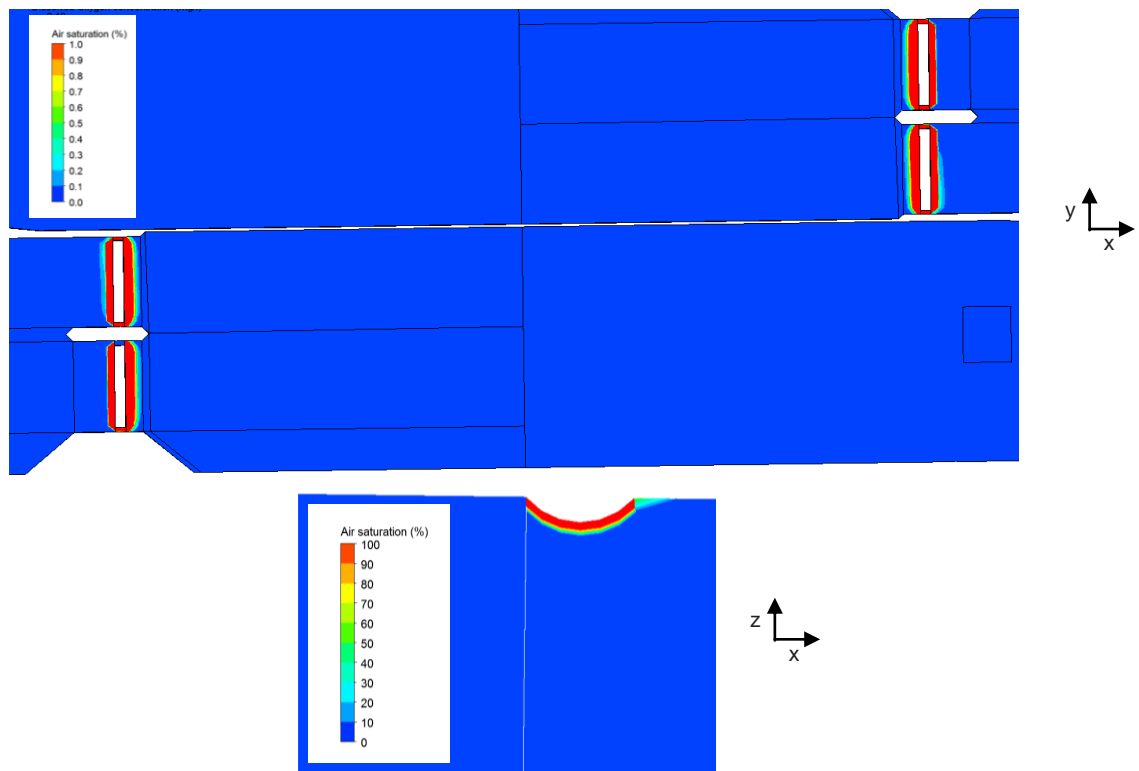


Figure 4.7 Volume fraction of air in OD1 caused by surface aerators  
(scale: % air saturation)

**Case M4 Grid diffusion aerator only in OD1**

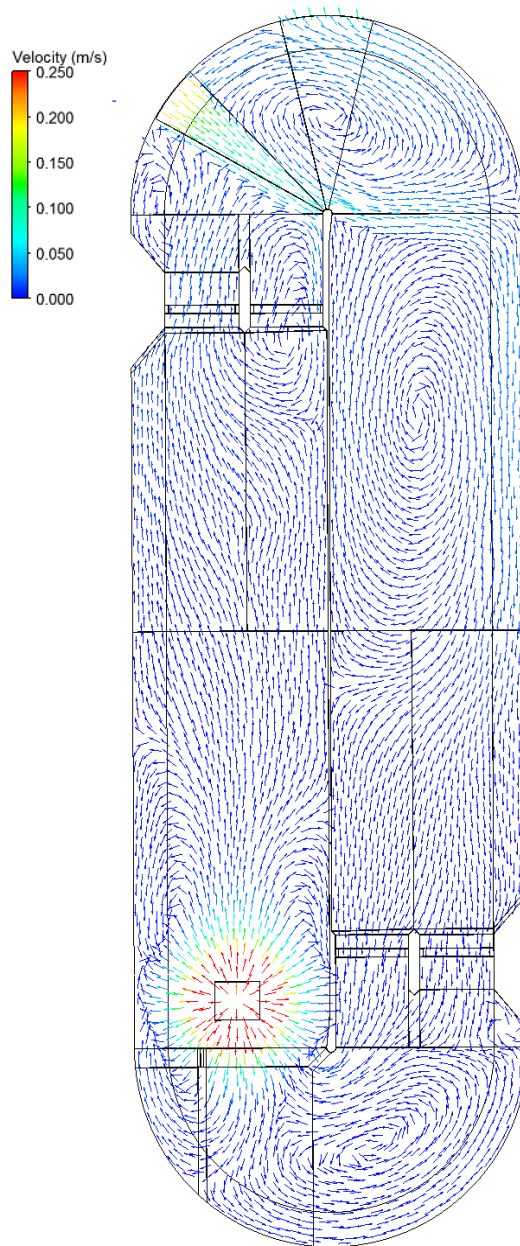


Figure 4.8 Water velocity in OD1 with diffuser only

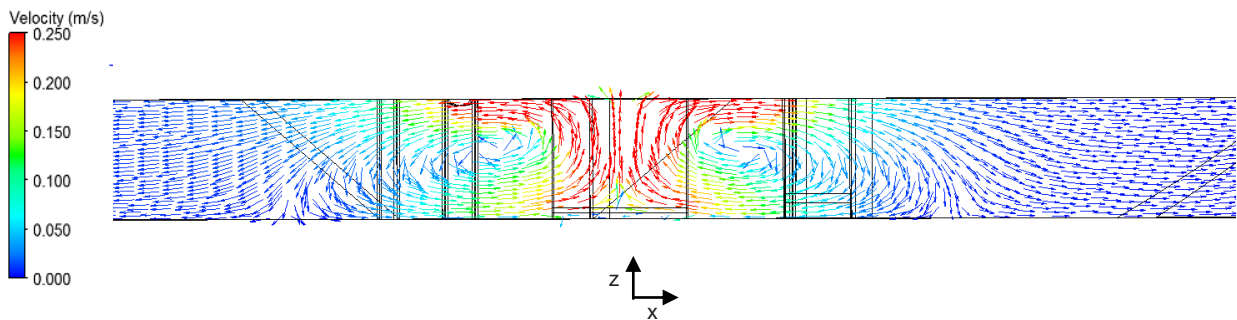


Figure 4.9 Water velocity in OD1 caused by diffuser

Figure 4.8 shows that for multi-phase flow the diffuser in OD1 creates a complex flow pattern. Flow velocities in the ditch are increased to a maximum value of 0.54 m/s near to the water surface directly above the diffuser. Figure 4.9 shows strong upward flow above the diffuser and recirculation on either side of the diffuser. The upward flow from the diffuser reaches the water surface and there is local radial dispersion (Figure 4.8). There are two small regions of recirculation on the outside wall near to the diffuser. Recirculation is at the opposite end of the ditch to the influent. Unlike the surface aerators and the Maguire jet aerator, the diffuser aerator does not provide a strong flow direction in the ditch. Therefore, the horizontal velocities dissipate quickly in the ditch and in most of the ditch there are low flow velocities (Figure 4.8).

The air volume fractions in OD1 with the diffuser show that there is a distinct circular region of high air concentration directly above the diffuser (left part of Figure 4.10). The air volume fraction above the grid diffuser forms a vertical concave shape (right part of Figure 4.10). The water shown by red in the right part of Figure 4.10 is at the saturation concentration of air. Note the difference in scale is to highlight these features.

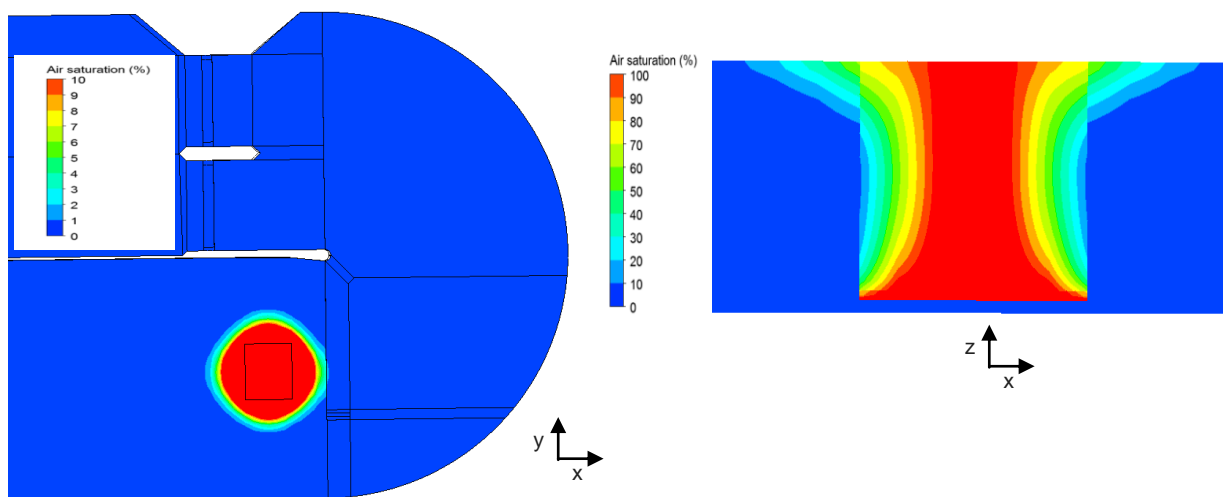


Figure 4.10 Volume fraction of air in OD1 caused by diffuser  
 - top and side views (scale: % air saturation)

### Case M5    Operating conditions with all aerators in OD1

This is the most important predicted flow pattern in OD1, as it simulates the actual operational conditions at Potterne WWTP when using a multi-phase flow model.

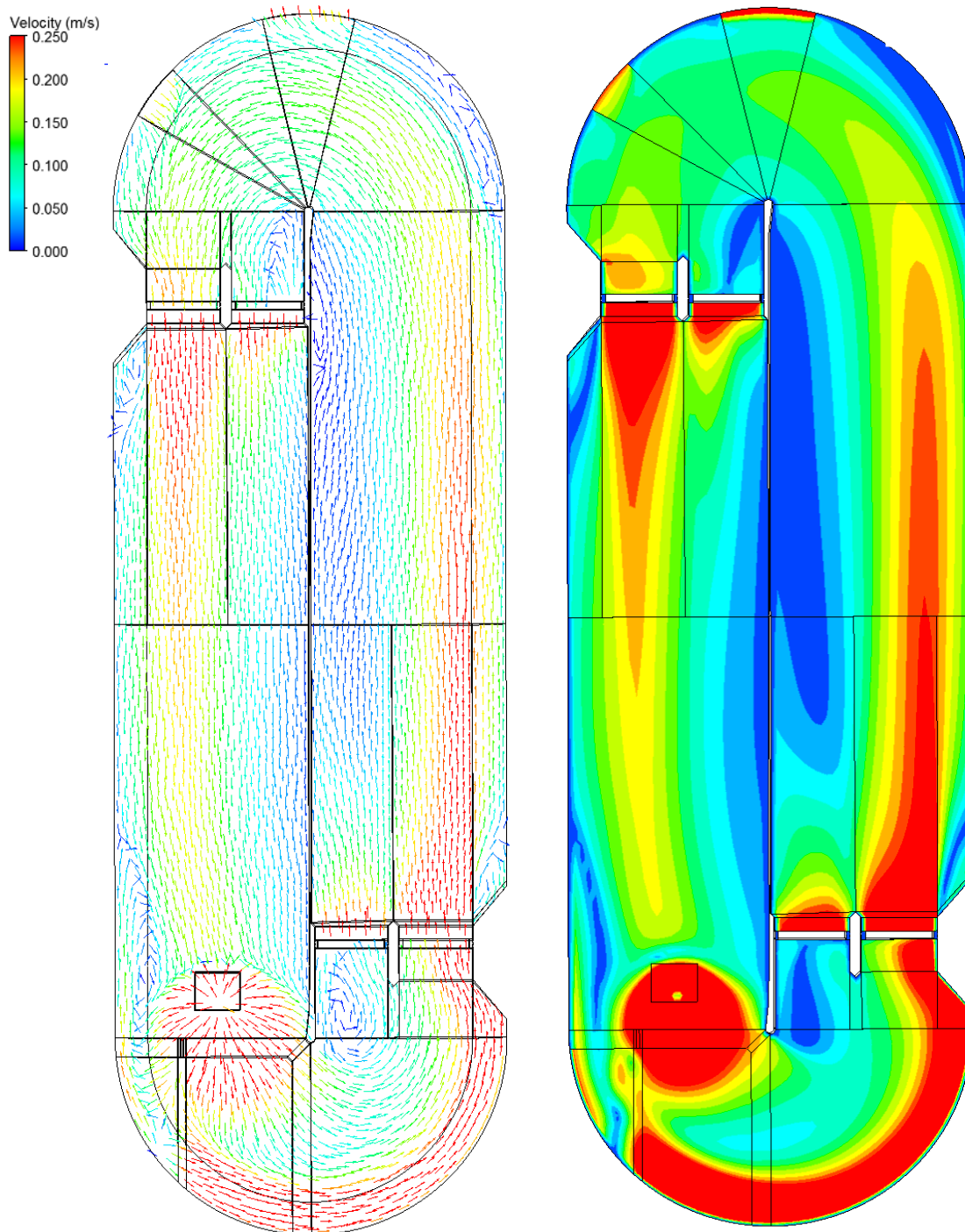


Figure 4.11 Water flow patterns in OD1 - operating conditions at WWTP

The flow stream from the Maguire jet aerator collides with the curved wall and there is strong flow parallel to this wall (Figure 4.11). This creates return flow in the opposite direction that is adjacent to this wall. The jet aerator and surface aerators combine to form a strong flow current. The main cause of heterogeneous flow distribution in the ditch is the Maguire jet aerator, with stronger flow on the outside wall and weaker flow nearer the inner wall. The surface aerators nearer the outside of the ditch produce stronger flow plumes. The main reason for this is the local effect of the strong flow stream of the jet aerator. The strong upward flow from the diffuser pushes out local surrounding fluid in a radial pattern (Figure 4.11). Flow coming from the surface aerators pushes the upward flow from the diffuser in the direction of the jet aerator. There are four small regions of recirculation in OD1, but generally the flow circulates in one direction around the ditch, due to the jet aerator and surface aerators. The maximum water velocities are near the water surface: 0.34 m/s (surface aerators), 0.47 m/s (jet aerator) and 0.64 m/s (diffuser). The air volume fractions at the water surface in OD1 show that there are small air patches above the diffuser, jet aerator and surrounding the surface aerators (Figure 4.12). There is a plume of air rising from the jet aerator (middle of Figure 4.12). Above the diffuser there is a stack of rising air, with some saturated air concentrations (red shape - bottom of Figure 4.12). Note the difference in scale is to highlight these features.

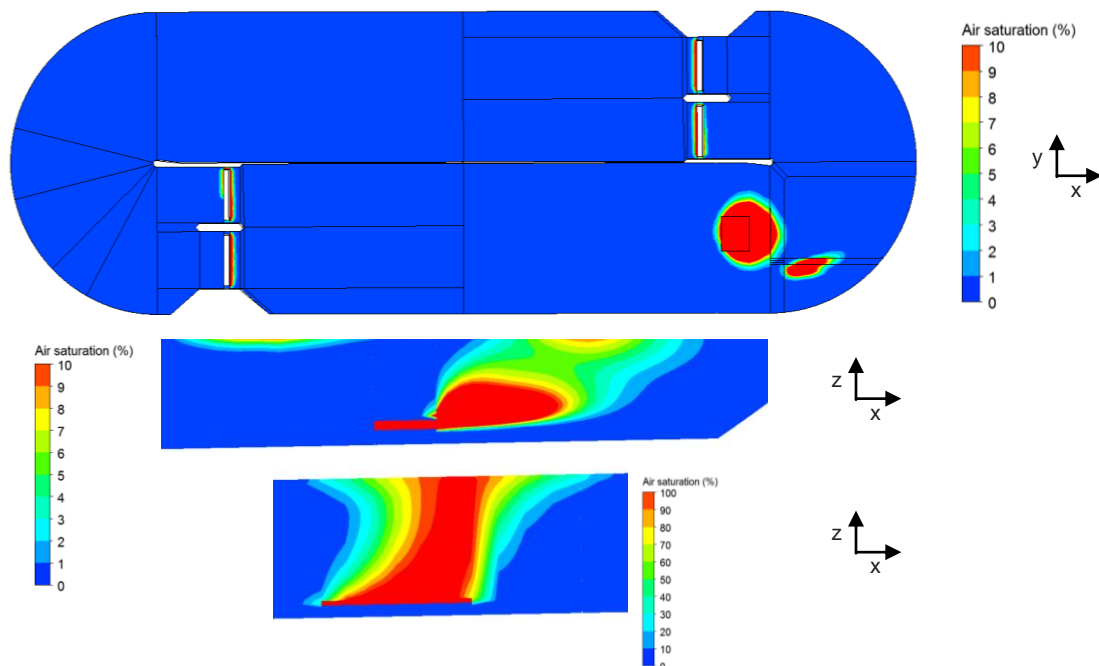


Figure 4.12 Volume fraction of air in OD1 - operating conditions  
(scale: % air saturation)

## Case M6 Flow booster only in OD2

Figure 4.13 shows a significant water plume in OD2 that is produced by the booster that reverses the flow direction to clockwise, as desired. There is significant heterogeneous flow distribution due to higher velocities. The flow stream exiting from the booster is hindered by its ineffective position upstream of a solid object. There is significant return flow on the same side of the ditch as the influent. The air content of the influent in OD2 is low (DO is 0.04 mg/l) and there is no air content in the booster. Air from the influent quickly reaches the water surface and dissipates out of the ditch.

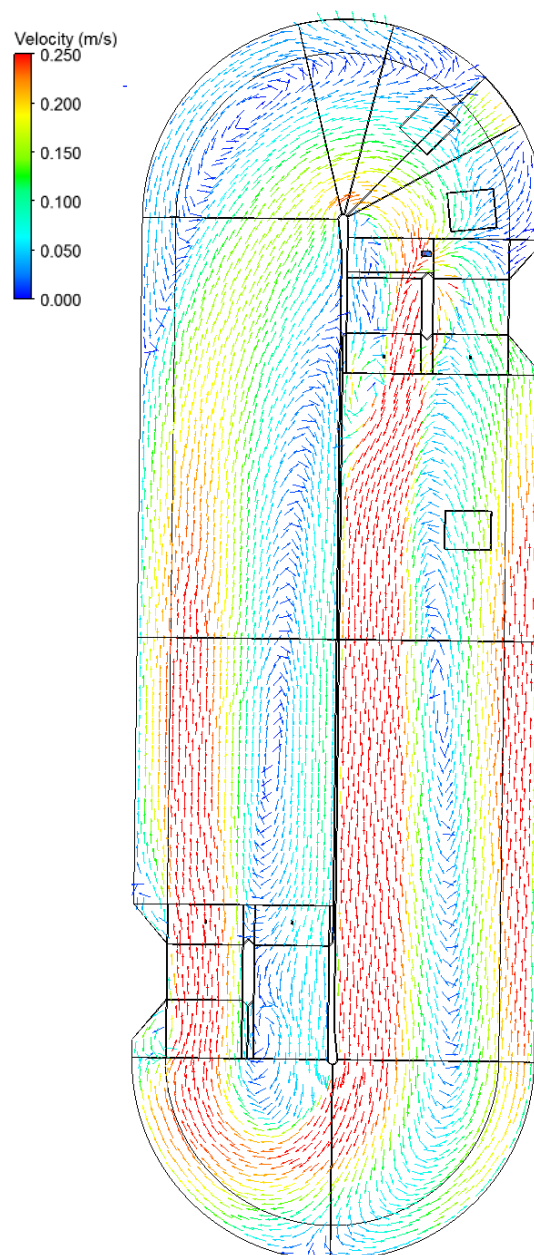


Figure 4.13 Water velocity in OD2 with flow booster

**Case M7 Fuch jet aerators only in OD2**

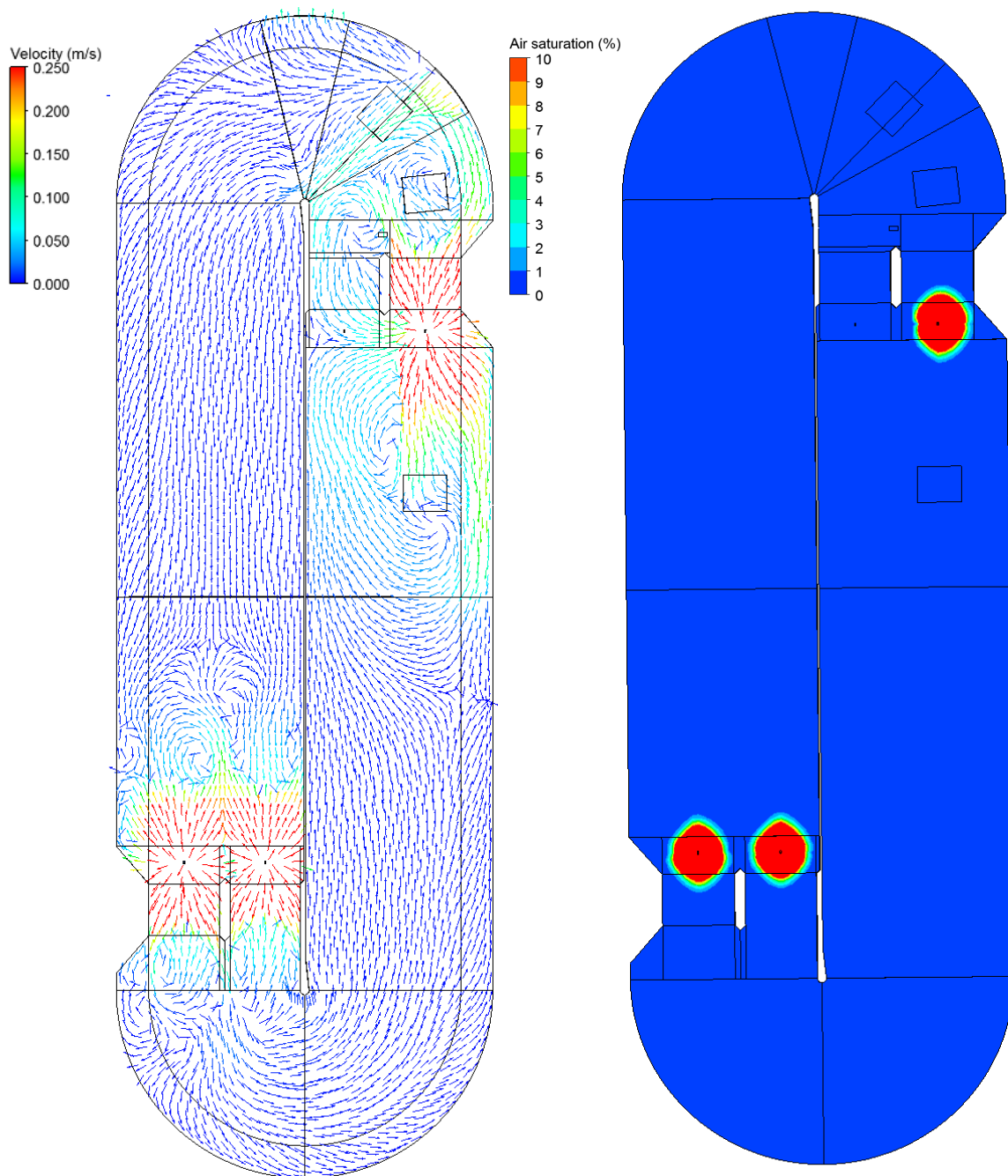


Figure 4.14 Water velocity and air volume fraction in OD2 with Fuch aerators

The flow pattern in OD2 with the three Fuch jet aerators is complex (Figure 4.14). Surrounding the Fuch aerators the water flows upwards because of the local effects of the air stream from the aerator. This creates higher velocities just underneath the water surface and recirculation surrounding the jet aerators (Figure 4.14). The highest velocity near the water surface is around 1.5 m/s (Figure 4.14). The jet aerator nearest to the influent weir produces local flow recirculation patterns (Figure 4.14). The influent stream to the ditch produces an anti-clockwise flow direction in the ditch. The other two jet aerators block this flow direction, because they produce localised upward flow, which spread out bi-directionally just beneath the water surface (Figure 4.14). The air volume fractions in OD2 around the Fuch jet aerator that is nearest to the influent shows saturated concentrations of air (red), that form a vertical plume that spreads underneath the water surface (Figure 4.15). Viewed from above (Figure 4.14) each jet aerator forms an elliptic patch of air above it. Note the difference in scale to highlight these features.

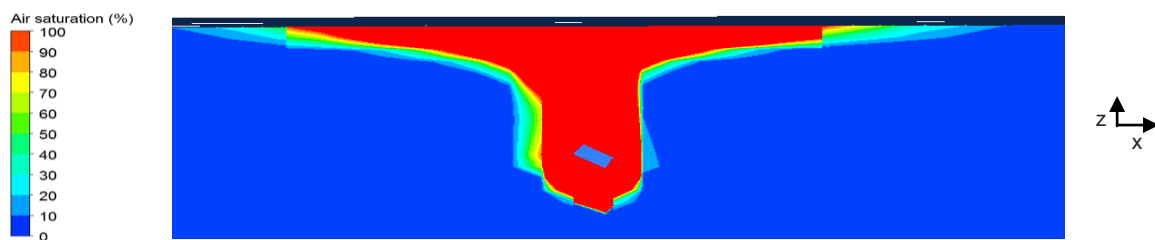


Figure 4.15 Volume fraction of air in OD2 caused by Fuch jet aerator  
(scale: % air saturation)

**Case M8 Grid diffusion aerators only in OD2**

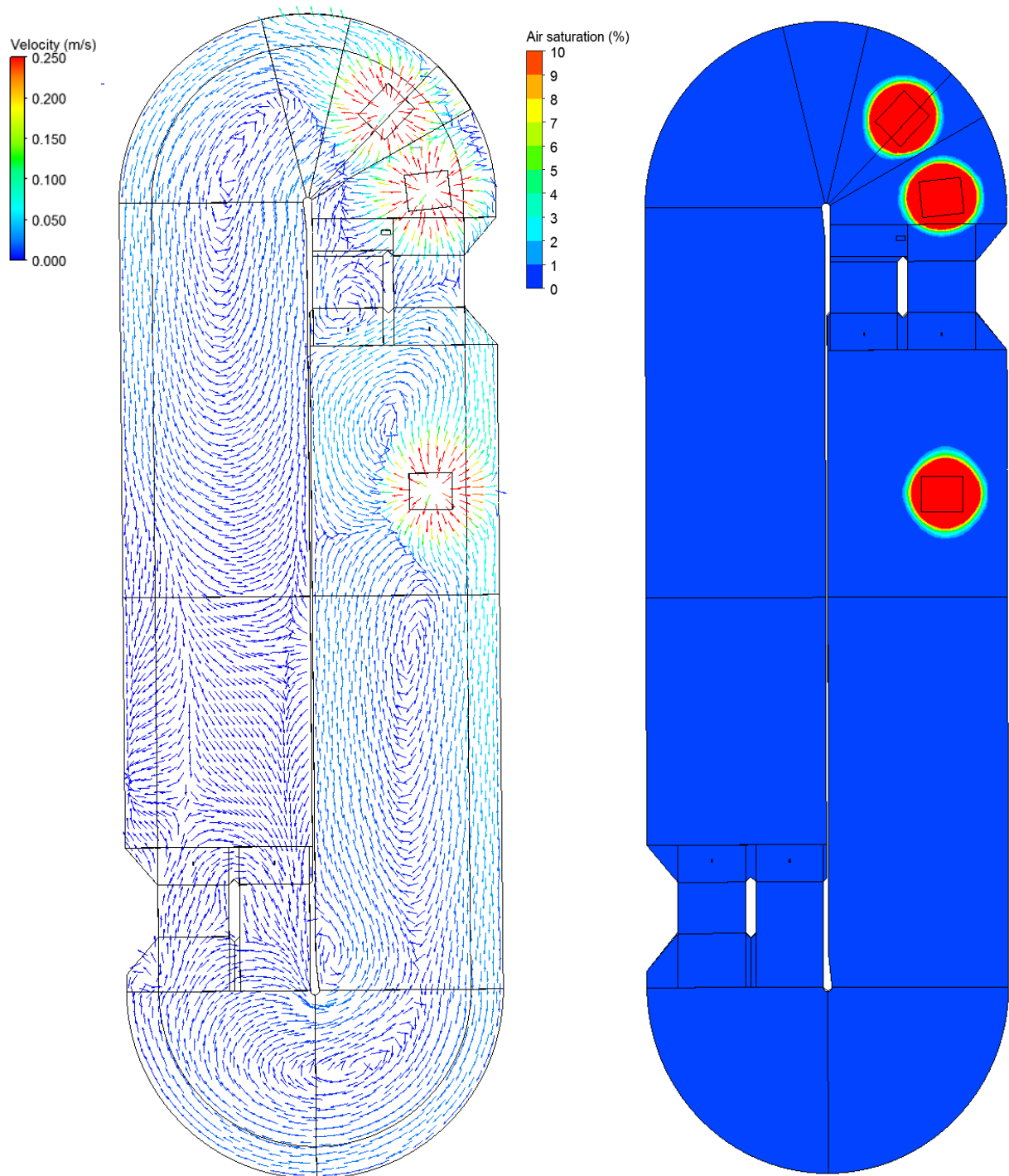


Figure 4.16 Water velocity and air volume fraction in OD2 with diffusers

The flow pattern in OD2 with the three diffusers is complex (Figure 4.16). Air rising from each diffuser causes local water to flow upwards. This can be seen more clearly in Figure 4.17 for just one diffuser. Higher velocities are just underneath the water surface and there is local recirculation surrounding the diffuser (Figure 4.17). In OD2 this is shown by red velocity vectors (Figure 4.16) just above the three diffusers. The highest velocities are near the water surface and are around 0.5 m/s (Figure 4.16). The influent to the ditch creates an anti-clockwise flow direction. The diffusers disturb this flow direction, even more so than with the Fuch jet aerators. Unlike the flow booster the diffusers do not create a dominant flow direction in the ditch. The upward flow from the diffuser reaches the water surface and forms a radial flow pattern. Horizontal velocities in the ditch dissipate quickly, therefore in most of the ditch there are relatively low flow velocities (Figure 4.16). Viewed from above (Figure 4.16) each diffuser forms a circular patch of air near the water surface.

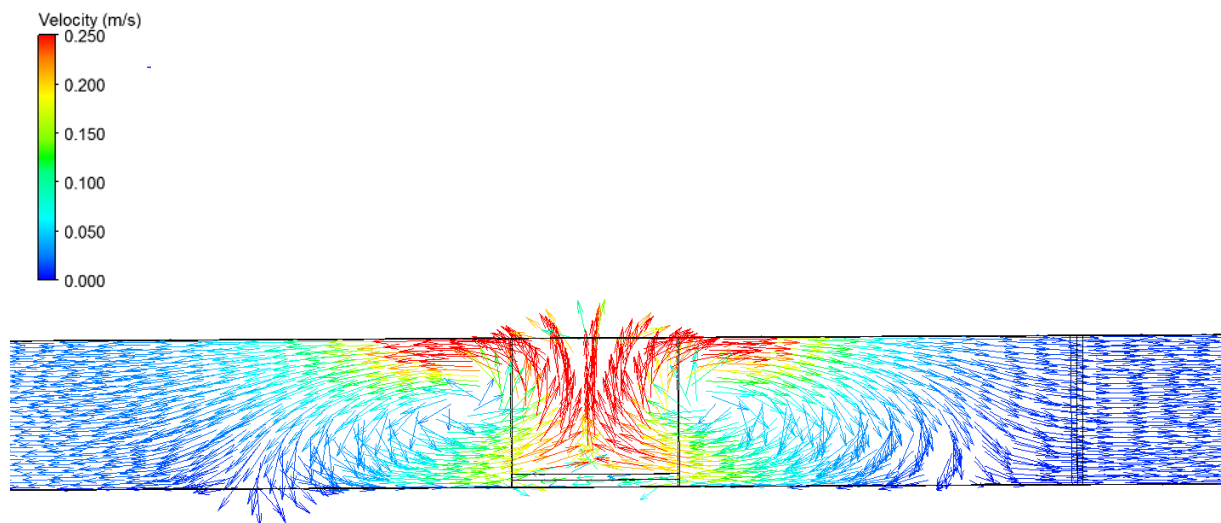


Figure 4.17 Water velocity in OD2 caused by diffuser

## Case M9 Operating conditions with all aerators in OD2

This is the most important predicted flow pattern in OD2, as it simulates the actual operational conditions at Potterne WWTP when using a multi-phase flow model.

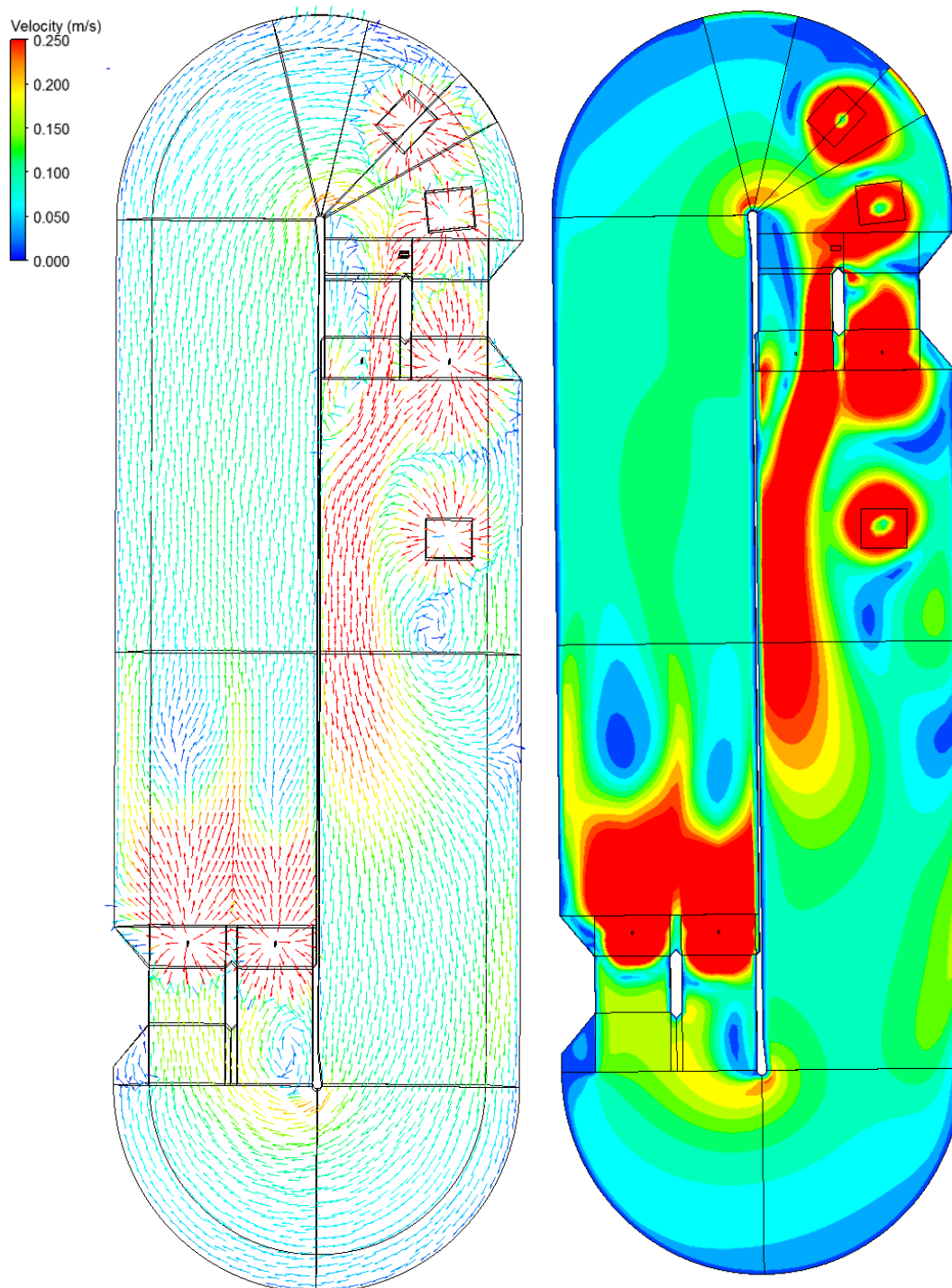


Figure 4.18 Water flow pattern in OD2 - operating conditions at WWTP

The water flow pattern in OD2 for multi-phase flow (Figure 4.18) shows that the flow direction in the ditch by the influent stream is anti-clockwise. The booster causes a reversal in flow direction to clockwise, which is intended to mitigate against short-circuiting of the influent towards the effluent. Most of the ditch has fairly low uniform flow (green in Figure 4.18) in the velocity range from 0.1 - 0.2 m/s. There is flow stagnation near the outside curved wall near to the influent weir, at the opposite end of the ditch and at the ends of the central wall. The flow in a clockwise direction near the influent weir is blocked by upward flow from the two diffusers (Figure 4.18). The flow stream from the booster is diverted towards the central wall by the upward flow from the third diffuser (Figure 4.18). Flow is accelerated by the two jet aerators that are in parallel. Downstream of them there are two small stagnation flow zones as the flow dissipates. Further downstream the flow is even more uniform and dissipates to create a large stagnation fluid zone near the effluent weir.

Near the diffusers the flow pushes upwards and at the water surface it flows out radially. This creates vertical flow recirculation near to each of the diffusers (Figure 4.19). There are small horizontal recirculation zones also near to each diffuser (Figure 4.18). Around the Fuch jet aerators the air flow from the jet pushes the water upwards and causes recirculation (Figure 4.20). The flow direction near the Fuch jet aerators is in the same direction as the air jet pointing longitudinally along the ditch, but there is some return flow near the water surface (Figure 4.20). The booster forms a strong current plume which is suppressed by collision with a wall. Further downstream of the booster there is more homogeneous flow. The booster increases flow velocities in the ditch as intended. Unlike the booster the diffusers do not create a dominant flow direction in the ditch (Figure 4.18). The maximum water velocities near the water surface are 1.5 m/s (jet aerators) and 0.5 m/s (diffusers). The air volume fractions at the water surface in OD2 show that there are small circular air patches above the diffusers and small elliptic air patches above the jet aerators (Figure 4.21). There are air plumes that rise from the diffusers and jet aerators (Figure 4.22). Note the difference in scale is to highlight these features.

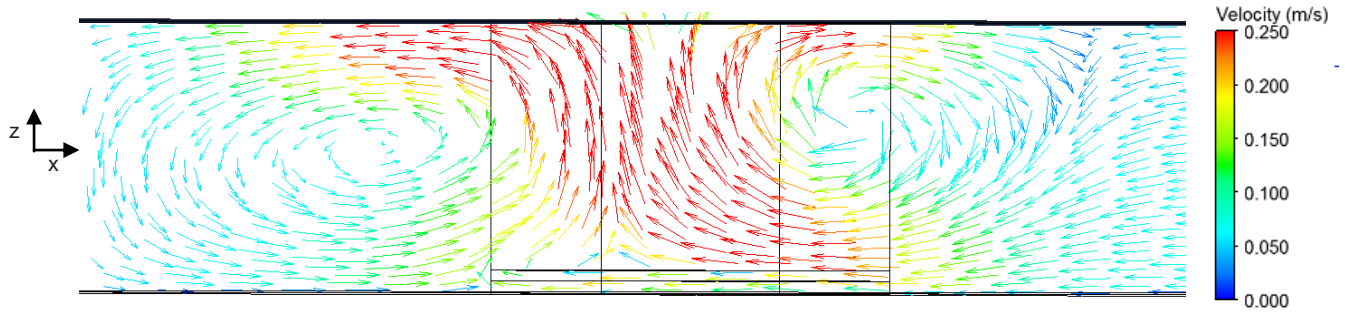


Figure 4.19 Water velocity in OD2 near diffuser - ditch length

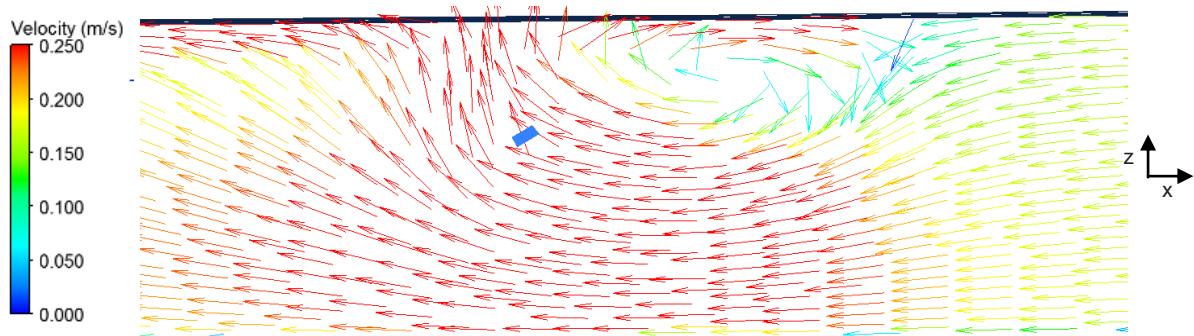


Figure 4.20 Water velocity in OD2 near Fuch jet aerators in parallel

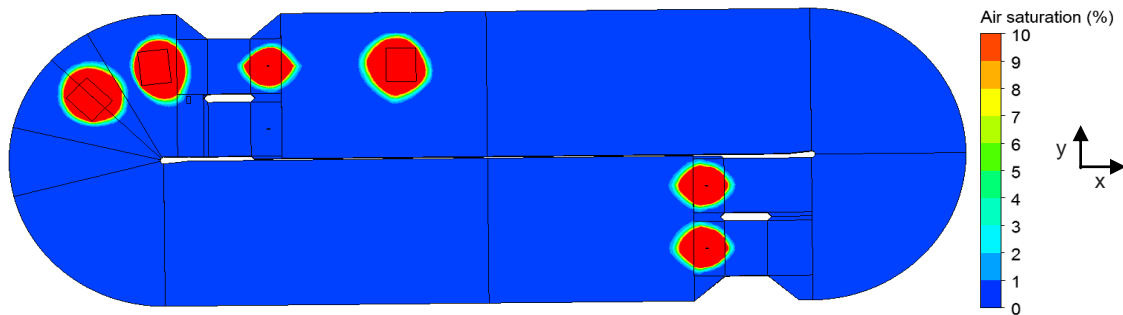


Figure 4.21 Volume fraction of air in OD2  
(scale: % air saturation)

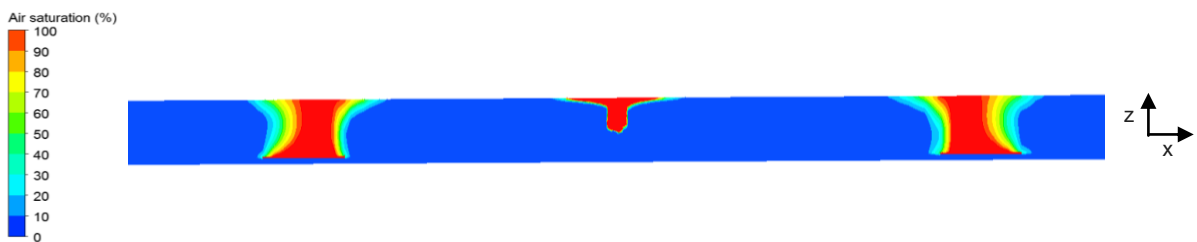


Figure 4.22 Volume fraction of air in OD2 near diffusers and Fuch jet aerator  
(scale: % air saturation)

## Turbulent dispersion force

The turbulent dispersion force (section 4.2.3) is neglected in the multi-phase flow modelling, because it causes poor numerical convergence (equation 4.3). Even smaller time steps in a transient simulation or the multi-phase coupled flow solver does not converge the solution. The non-converged solution is presented to show that the force does have a dispersive effect on the air distribution in OD1 (case M5). With a converged solution it is expected to increase the dispersion of gas phase in the ditch. Without this force (Figure 4.23), the two air patches near the water surface are distinctly separate. The rising air plume from the Maguire jet aerator has a reduction in the volume fraction of air and then increases again when reaching the water surface (Figure 4.23). With the turbulent dispersion force the two air patches on the water surface are joined together and the air plume from the jet aerator shows more contiguous air dispersion behaviour (Figure 4.24).

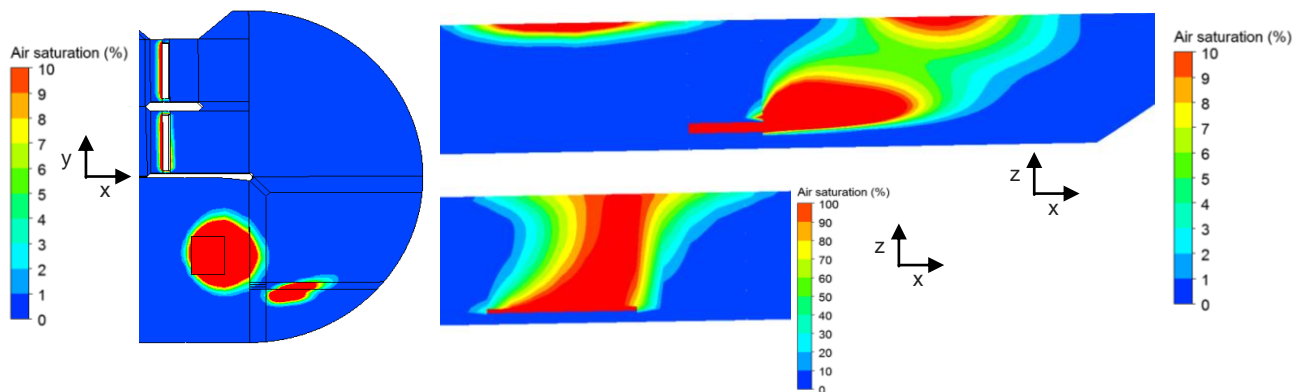


Figure 4.23 Volume fraction of air in OD1 (case M5 - without TDF)  
(scale: % air saturation)

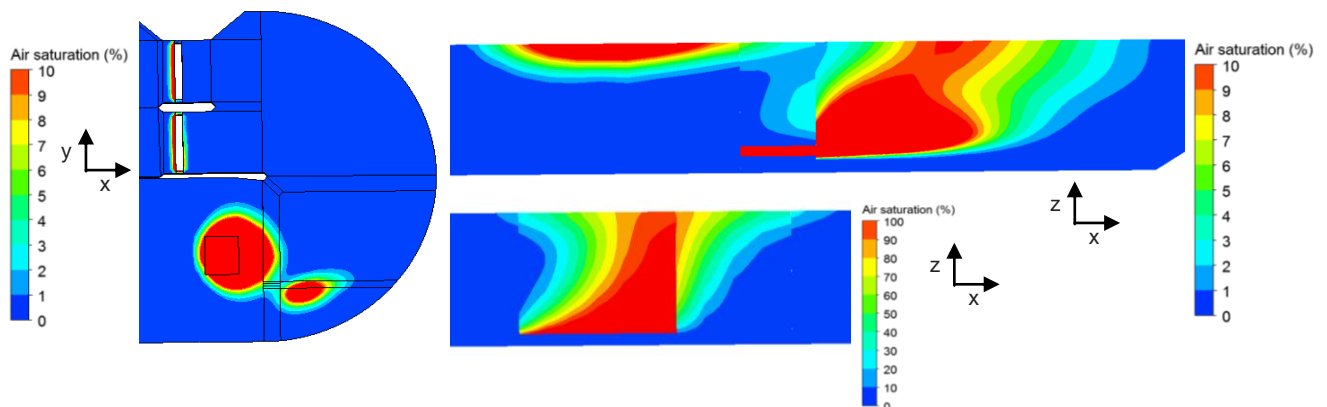


Figure 4.24 Volume fraction of air in OD1 (case M5 - with TDF)

#### 4.4.2 Mesh independency

*Mesh independency has also been undertaken for single-phase flow, but it is not presented in the thesis, because multi-phase flow is more critical in this study.* Description of the meshing strategy and mesh design are in Chapter 3. In a mesh independency study the number of cells and cell resolution is changed until the flow solution no longer changes significantly. Then the flow solution is deemed to be independent of the mesh. The mesh is then considered to be sufficiently refined. The benefit is to use the optimum number of cells to be able to improve computational efficiency. This is undertaken for multi-phase flow in the ditches (OD1 and OD2) at their operating conditions (cases M5 and M9). In OD1 the meshes tested range from 206 to 698 thousand cells and are structured hexahedral cells. In OD2 the meshes range from 235 to 648 thousand cells and are 97 % structured hexahedral cells.

In OD1 there is no significant difference between the flow patterns of water for all of the meshes (Figure 4.25). For a lower mesh resolution (206 and 298) there are slightly higher velocities near the Maguire jet aerator and an increase in flow plume length. When comparing the mesh used in this study (396) with a finer mesh (491) there is no difference in the flow pattern. With more refinement (698) there are slightly lower velocities near the jet aerator. There is a reduction in plume length of a surface aerator near the influent weir. The mesh used (396) is sufficiently accurate. The structured hexahedral mesh design is able to optimise the mesh in OD1.

In OD2 there is also no significant difference between the flow patterns for all of the meshes (Figure 4.26). For a lower mesh resolution (235 and 331) there are slightly higher velocities near a Fuch jet aerator (bottom right) and a slight change to the plume. There are lower velocities near a diffuser (top middle) and a slightly different flow plume location. There are slightly lower velocities around the middle diffuser. The plume from the booster has some flow separation for the lowest mesh resolution (235). When comparing the mesh that is used (452) with the most refined mesh (648) there is no significant difference in flow pattern. The mesh used (452) is sufficiently accurate. There is however more effect of mesh refinement in OD2 than in OD1. The structured hexahedral mesh is also able to optimise the mesh in OD2.

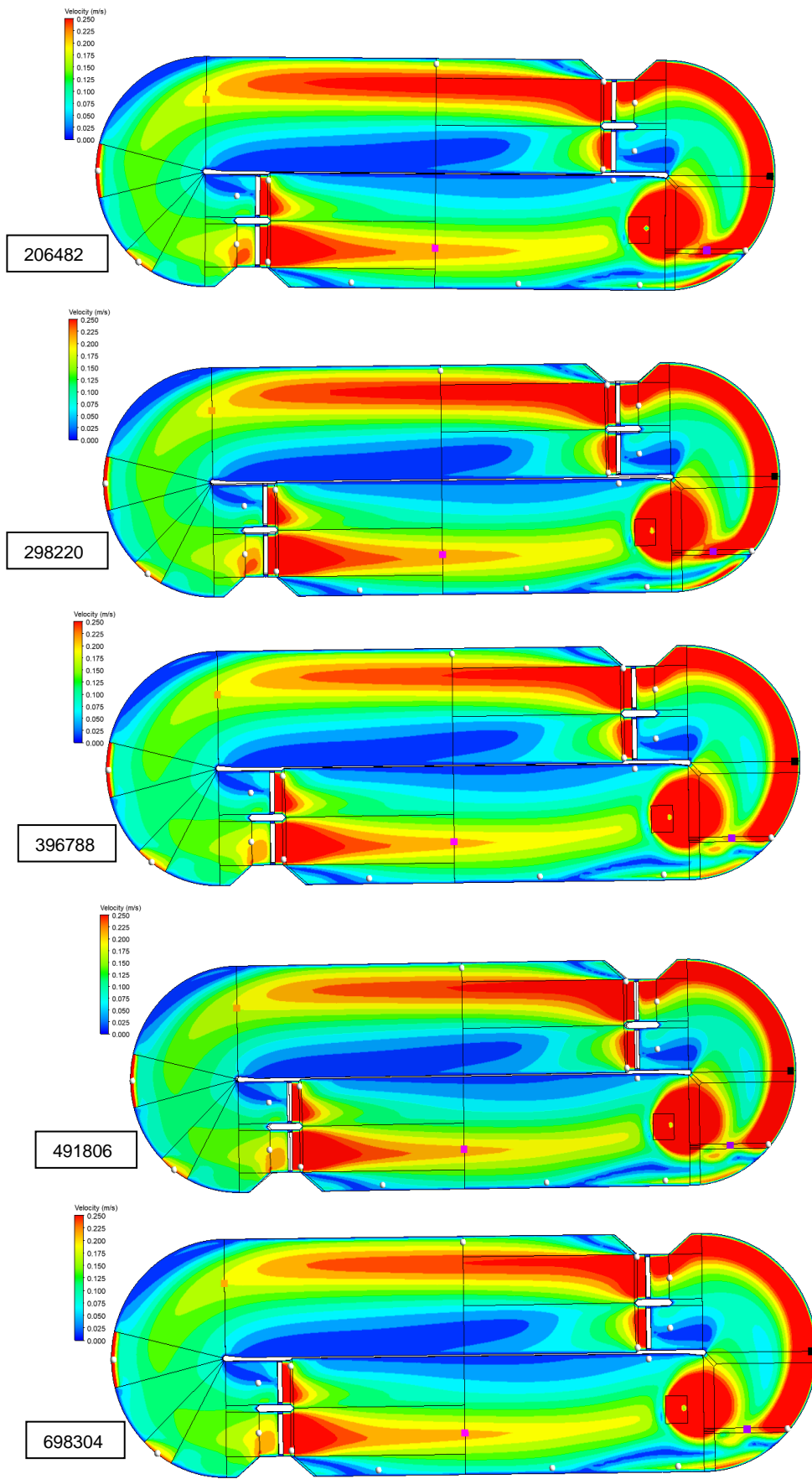


Figure 4.25 Multi-phase water flow pattern in OD1 with mesh refinement

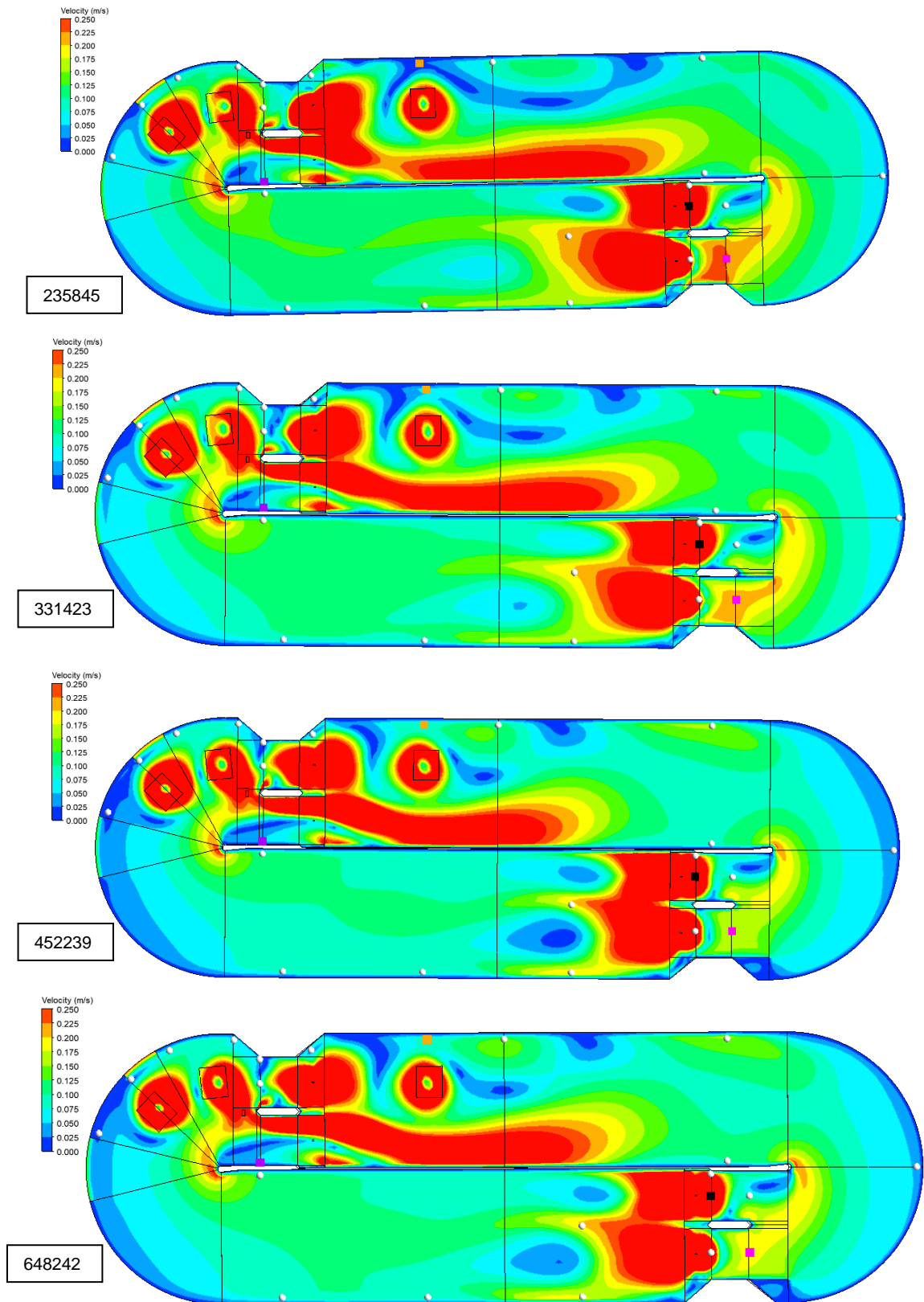


Figure 4.26 Multi-phase water flow pattern in OD2 with mesh refinement

Table 4.2 Mesh convergence study

Ditch	Cells	Ditch velocity (m/s)				 (mean)	 (max)
1	206482	0.122	0.307	0.186	0.211	0.186	0.489
1	298220	0.120	0.322	0.184	0.211	0.182	0.481
<b>1</b>	<b>396788</b>	<b>0.115</b>	<b>0.209</b>	<b>0.174</b>	<b>0.206</b>	<b>0.192</b>	<b>0.438</b>
1	491806	0.116	0.209	0.175	0.208	0.189	0.437
1	698304	0.115	0.197	0.175	0.206	0.187	0.426
2	235845	0.128	0.059	0.018	0.226	0.131	0.472
2	331423	0.124	0.045	0.053	0.214	0.127	0.500
<b>2</b>	<b>452239</b>	<b>0.116</b>	<b>0.047</b>	<b>0.087</b>	<b>0.162</b>	<b>0.122</b>	<b>0.441</b>
2	648242	0.119	0.048	0.081	0.180	0.123	0.447

The quantification of mesh independency is undertaken by a mesh convergence study. For the different meshes (OD1 and OD2) the velocities are shown in Table 4.2 for multiple locations near the water surface. The locations of the circles and boxes are shown in Figures 4.25 and 4.26. The velocities for the mean value in the ditch, mean value at the DO measurement locations in Chapter 7 (white circles), maximum value at the DO measurement locations (black box) and values at three specific locations in the ditch (purple, orange and pink boxes) are shown in Table 4.2.

In ditch OD1 as the mesh is refined, for almost all the columns in Table 4.2, the velocity values become uniform for the more refined meshes from 396 to 698 thousand cells. This suggests that the mesh with 396 thousand cells is sufficiently accurate and no further refinement is required. In ditch OD2 as the mesh is refined, for almost all the columns of Table 4.2, the velocity values become uniform for the more refined meshes from 452 to 648 thousand cells. This suggests that the mesh with 452 thousand cells is sufficiently accurate and no further refinement is required. Therefore, the meshes that are chosen for the single-phase, multi-phase and multi-component flow simulation have 396788 cells for ditch OD1 and 452239 cells for ditch OD2 respectively.

#### 4.4.3 Numerical residence time distribution (RTD)

The tracer is an inert substance that is injected at the influent weir of the ditch. A uniform step value of 1 for the tracer variable at the influent weir represents a uniform dose pulse for a very short period (10 s). The molecular (mass) diffusivity of tracer in water ( $1.35 \times 10^{-9} \text{ m}^2/\text{s}$  for a chloride salt solution) is low enough to have no diffusive effect on the RTD. It is found that only much higher values (0.1 and 0.01) have an effect on the RTD. The turbulent Schmidt number of 0.7 does however have an effect on RTD. The transient simulation is run for a lengthy period to allow as much tracer to pass from the influent to effluent. A large time step of 10 s reduces the duration of the simulation. The multi-phase flow simulations for cases M5 (OD1) and M9 (OD2) best represent the operational conditions at Potterne WWTP.

The RTD graph shows the tracer concentration over the effluent weir versus time, in terms of the dimensionless temporal variable on the x-axis (equation 2.45) and the dimensionless concentration variable on the y-axis (equation 2.43). The theoretical hydraulic residence time (HRT - equation 2.46) is the tank volume divided by the mean influent flow rate. For all single and multi-phase RTDs they are run for a duration of 4 theoretical HRTs. The partial RTD graphs (Figures 4.27 to 4.33) show only up to 1 theoretical residence time to show more clearly the peak time and peak concentration. Figures 4.32 and 4.33 show the complete RTD for multi-phase flow simulation. The numerical simulation time is therefore 140000 s (39 hours) for cases S1, S3, S5 and M9 and 33000 s (9 hours) for cases S2, S4 and M5.

The most important parameter in Table 4.3 is the dimensionless mean HRT when it is compared to the theoretical HRT. Moreover, the dimensionless time at the peak tracer concentration in the RTD determines how much flow short circuiting there is in the ditch. The percentage of residual tracer in the ditch after 4 theoretical HRTs is calculated, which measures a small error (i.e. longer duration->lower error). To calculate the mean HRT (Table 4.3), the area under the complete RTD graph is determined after 4 theoretical HRTs. The mean HRT is the dimensionless time on the graph at the point where half of the cumulative graph area has elapsed. In practical terms, this is the residence time when half of the mass of tracer has travelled from the influent weir to the effluent weir in the ditch.

## Single-phase flow RTD graphs

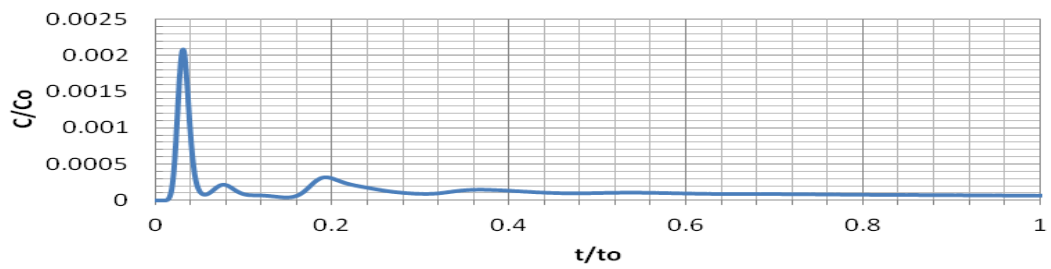


Figure 4.27 RTD of OD1 and OD2 without aerators (case S1)

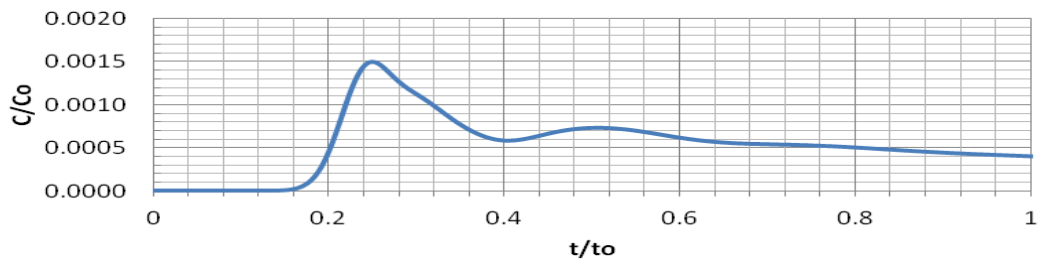


Figure 4.28 RTD of OD1 with Maguire jet aerator only (case S2)

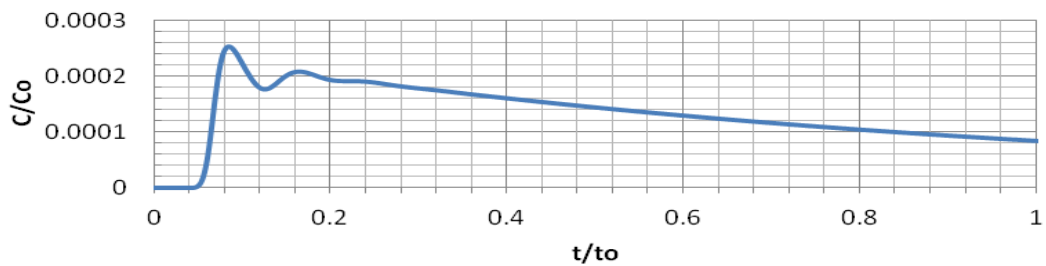


Figure 4.29 RTD of OD1 with surface aerators only (case S3)

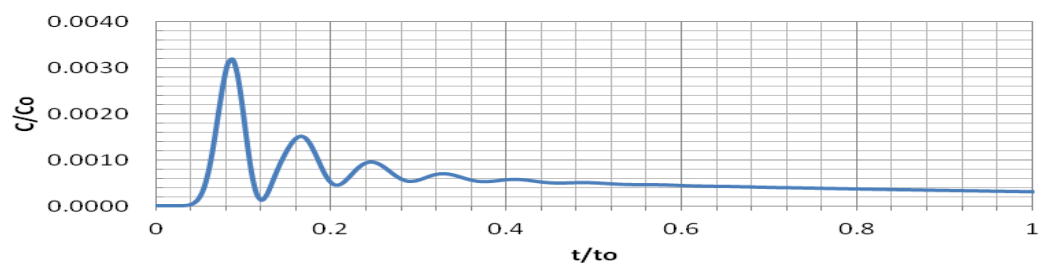


Figure 4.30 RTD of OD1 with Maguire jet and surface aerators (case S4)

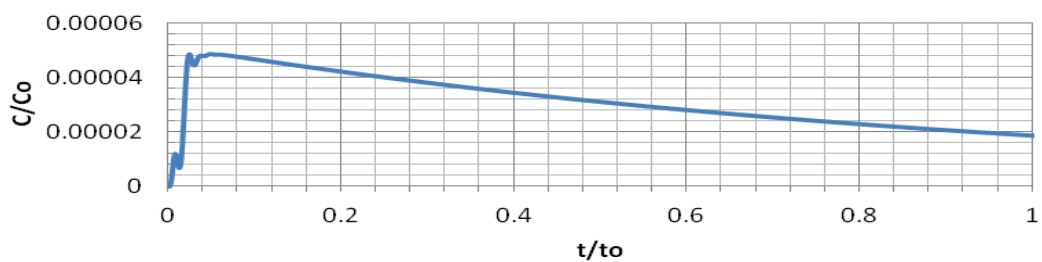


Figure 4.31 RTD of OD2 with flow booster (case S5)

### Multi-phase flow RTD graphs for operating conditions at WWTP

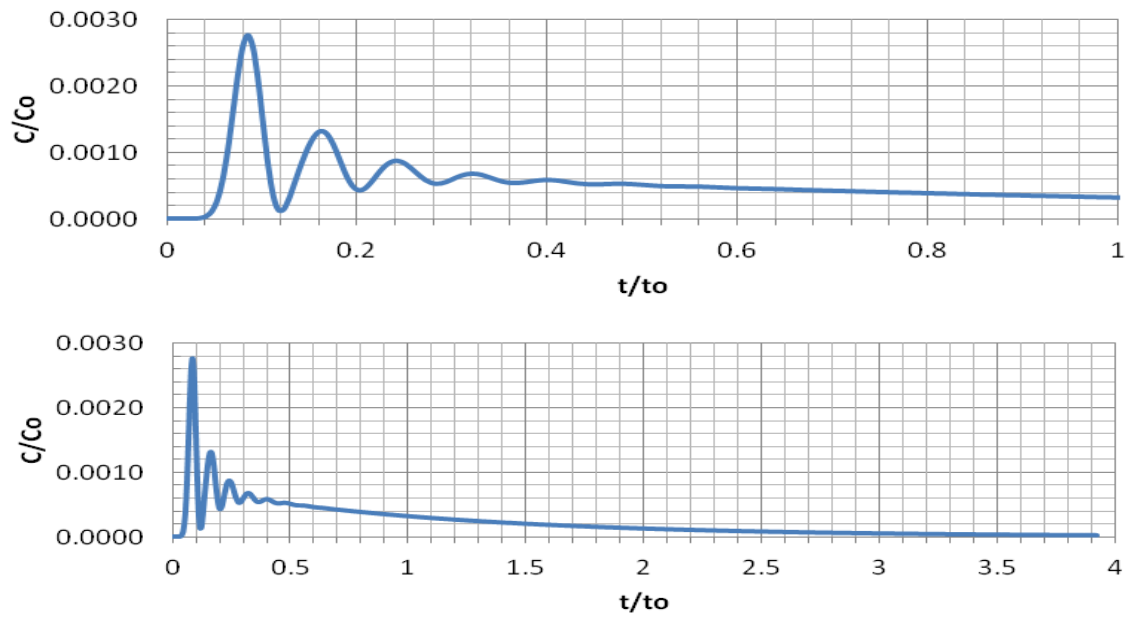


Figure 4.32 RTD of OD1 - operating conditions (case M5)

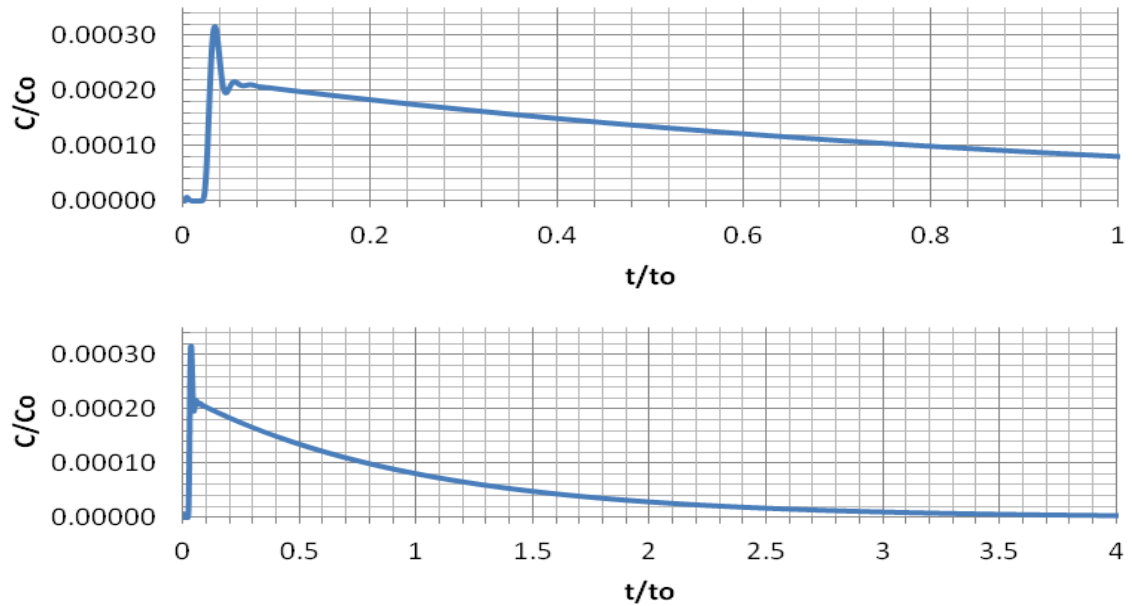


Figure 4.33 RTD of OD2 - operating conditions (case M9)

Table 4.3 Hydraulic parameters of residence time distribution

Case	OD	Devices	Theory HRT (s)	Predicted HRT (t/t <sub>0</sub> )	Time at peak conc (t/t <sub>0</sub> )	Peak conc (C/C <sub>0</sub> )	Residual tracer (%)
S1	1&2	none	46776	<b>0.570</b>	0.0321	0.00208	0.52
S2	1	Maguire jet aerator	10932	<b>0.768</b>	0.2470	0.00149	0.47
S3	1	surface aerator	46776	<b>0.683</b>	0.0846	0.00025	0.34
S4	1	jet + surface	10932	<b>0.615</b>	0.0880	0.00319	0.63
S5	2	flow booster	46776	<b>0.661</b>	0.0487	0.00005	0.56
<b>M5</b>	<b>1</b>	<b>All devices (OD1)</b>	10932	<b>0.695</b>	0.0855	0.00276	0.28
<b>M9</b>	<b>2</b>	<b>All devices (OD2)</b>	46776	<b>0.684</b>	0.0332	0.000315	0.12

For single-phase flow simulation the predicted mean HRT of the ditches is between 0.57 and 0.77 of the theoretical HRT (Table 4.3). Without any aeration the actual HRT is only 0.570. The inclusion of Maguire jet aeration improves (i.e. increases residence time) plug flow behaviour considerably from 0.570 to 0.768 in OD1. The inclusion of surface aeration improves it from 0.570 to 0.683 in OD1. The combination of the Maguire jet and surface aeration improves it from 0.570 to 0.615 in OD1. The flow booster in OD2 improves it from 0.570 to 0.661. In OD1 the time for the initial effluent breakthrough is improved (lengthened) by the Maguire jet and surface aeration, from 0.0321 to 0.0880. The flow booster in OD2 improves this from 0.0321 to 0.0487. The overall effect is that there is an increase in residence time of fluid in the ditches by using each of the aeration devices. There is a small fraction (0.12 - 0.63 %) of tracer that does not pass through the ditch (within 4 theoretical residence times), which is a small enough error to accept.

For multi-phase flow simulation at the operating conditions (Table 4.3), the predicted mean HRT improves from 0.615 to 0.695 for case M5 (OD1) and from 0.661 to 0.684 for case M9 (OD2), when compared to single-phase flow of the individual devices in the ditches (S4 and S5). Multi-phase flow simulation provides more accuracy than single-phase flow. Multi-phase flow simulation therefore predicts a hydraulic performance of almost 70 % of the theoretical residence time in the two ditches at the operating conditions at Potterne WWTP.

## 4.5 Summary

For multi-phase flow simulation of OD1, with no devices, the low air content in the influent produces little air. There is a plume of air from the Maguire jet aerator that rises to the water surface where there is a small patch of air. The surface aerators near the influent have a non-symmetrical plume. There are air patches near the surface aerators. For the membrane diffuser, there is upward flow, recirculation, and radial dispersion near the water surface. The diffuser does not provide a strong flow direction in the ditch. The air stack above the diffuser has a vertical concave shape which forms a circular region of air. For operating conditions in OD1, the Maguire jet aerator and surface aerators form a strong fluid stream that drives the flow direction.

For multi-phase flow simulation of OD2, the flow booster does not supply any air. Near the Fuch aerators the water flows upwards because of the effect of the air stream. This creates higher water velocities near the water surface in opposing directions. A vertical plume of rising air spreads upwards from each Fuch jet aerator with an elliptic patch of air above. The upward flow from the diffusers produces radial dispersion near the water surface. Diffusers do not provide a strong flow direction in the ditch. The air rising from the diffusers forms a vertical concave shape and a distinct circular region of air above. For operating conditions in OD2, the flow stream from the booster is diverted towards the central wall, by obstruction with an internal wall and upward flow from a diffuser. The booster drives the flow direction in OD2.

For multi-phase flow the Maguire jet aerator increases the mean water velocity in OD1 by 9 because of a fluid mass source, surface aerators increase it by 4, and the diffuser increases it by 1.5. For operating conditions in OD1 it increases by 15. The booster increases the mean water velocity in OD2 by 20, Fuch jet aerators increase it by 3.5 and diffusers increase it by 2.8. For operating conditions in OD2 it is increased by 20. The mean water velocity in both ditches is similar (0.11 m/s) at the operating conditions in Potterne WWTP. The effect of the turbulent dispersion force is to disperse air slightly further and produce a more contiguous air distribution, as expected. The multi-phase flow pattern is considered to be independent of the mesh refinement for the ditches, for meshes with 396 and 452 thousand cells respectively. The meshes used in the study are therefore considered to be suitable for use.

In the numerical RTDs for single-phase flow, the predicted hydraulic residence times (HRT) are between 0.57 and 0.77 of the theoretical HRT. The Maguire jet aerator improves plug flow behaviour from 0.570 to 0.768. The surface aerators improve it from 0.570 to 0.683. The combination of Maguire jet and surface aerators improve it from 0.570 to 0.615 in OD1. In OD2 the flow booster improves it from 0.570 to 0.661. The initial effluent breakthrough is improved by Maguire jet and surface aeration in OD1 from 0.0321 to 0.0881 and by the flow booster in OD2 from 0.0321 to 0.0487. For multi-phase flow simulation the predicted HRT is almost 70 % of the theoretical HRT in both of the ditches at the operating conditions in Potterne WWTP.

*The benefits from the multi-phase flow study for ditch design are as follows.* The Maguire jet aerator, surface aerators and booster produce a dominant flow direction that reduces flow short circuiting in the ditch. For all devices there is an increase in residence time and an improvement in the hydraulic efficiency of the ditches. For all devices there is an increase in water velocity, which can mitigate against sludge deposition that causes flow short circuiting and can also increase the transport of dissolved oxygen (DO) around the ditch. The highest air concentrations in OD1 are above the diffuser and Maguire jet aerator and near the surface aerators.

*The drawbacks from the multi-phase flow study for ditch design are as follows.* The surface aerators are more effective near the water surface and therefore they produce a heterogeneous vertical flow distribution. The oxygen transfer rate (OTR) of a surface aerator is difficult to quantify unless it is physically measured. The main cause of heterogeneous distribution in OD1 is the strong flow stream of the Maguire jet aerator. It makes the velocity plumes from the surface aerators asymmetric. The air jet from the Fuch aerator causes the water to flow bi-directionally. The diffusers produce local flow recirculation. The diffusers and Fuch jet aerators block the general flow direction in the ditch. The flow booster has a strong flow stream that produces undesirable recirculation in OD2. Its ineffective position upstream of a blockage also produces undesirable fluid turbulence.

## 5. Numerical model of dissolved oxygen

### 5.1 Introduction

Wastewater requires enough dissolved oxygen (DO) for bacteria to be sufficiently aerobic to be able to reduce the biochemical oxygen demand (BOD). There is however insufficient natural oxygen in wastewater for this to occur and therefore an aeration system is required (Metcalf et al, 2003). While aeration increases the dissolved oxygen the biomass reduces it through bacterial oxygen demand. Aeration depends on the oxygen mass transfer (equation 2.5) between the air and water phases (Potier et al, 2005; Lei and Ni, 2014). This can be improved by increasing the interfacial area (equation 2.7) between the liquid water and the gaseous air, where the bubble size is an important parameter (Fayolle et al, 2007). Oxygen mass transfer also depends on the aeration system design (Degremont, 2007).

The species transport equation is the most commonly used CFD model for the dissolved oxygen distribution (Guo et al, 2013) and oxygen mass transfer. The oxygen scalar equation that includes de-aeration of oxygen by BOD is able to predict the DO distribution in a ditch (Yang et al, 2011). It includes an oxygen source term for aeration and usually a uniform oxygen sink term for the BOD effect (Littleton et al, 2007a). In real ditches however there is a BOD distribution, which is ignored in CFD models (Karpinska et al, 2016). Therefore to make further progress in research the effect of the BOD distribution is considered and modelled in this study.

In this chapter multi-phase and multi-component flow simulation of two oxidation ditches with different aeration systems is conducted. The species transport model (equation 5.1) predicts the BOD and DO distribution based on the multi-phase flow pattern. The dissolved oxygen sink is modelled with both a uniform and a distributed BOD (equation 5.7). There are two mutually exclusive ways of modelling the BOD distribution. The local BOD concentration may be a function solely of the local residence time (equation 5.3) or the local DO concentration (equation 5.4). There is close agreement between the BOD distribution when using both models. There is a two-way coupled relationship between the DO and BOD in this study.

## **5.2 Theory**

### **5.2.1 Oxygen mass balance**

The mechanisms of oxygen transfer will determine the dissolved oxygen (DO) concentration. The multi-phase flow simulation solves for the local velocities of air and water which transport air around the ditch. The mass balance equation for oxygen includes the oxygen mass sources, inter-phase oxygen mass transfer from the air to water phase and the oxygen mass sinks. Oxygen concentration in the water phase is equivalent to the DO concentration. On one side of the oxygen mass balance are the oxygen sources and on the other side are the oxygen sinks. The oxygen sources in the water phase are in the influent and the Maguire jet aeration. The oxygen sources in the air phase are the atmospheric diffusion through the water surface (assumed negligible), mechanical surface aeration, membrane diffusion aeration and Fuch jet aeration. The oxygen sinks in the water phase are in the effluent and the de-aeration of oxygen by BOD. An oxygen sink in the air phase is the bubbles exiting the water surface (degassing boundary condition).

There is a two way coupled relationship between the DO and BOD. Biodegradation of BOD in the activated sludge consumes oxygen and therefore decreases the DO concentration. DO determines the activity of the microorganisms in the sludge. Higher DO in the ditch is more likely to increase the BOD degradation and therefore result in local lower BOD levels.

### **5.2.2 Species transport equation**

The governing equations of fluid motion of the primary phase are solved and the species are transported by the flow and treated as a scalar. The species transport equation predicts the local mass fraction concentration (Ranade et al, 2002). The concentration scalar can be coupled to the momentum equation as an equation of state (oxygen in air and water phases, BOD in water phase). Another use is a passive tracer (residence time), which has the same properties as the continuous liquid water phase and is transported by the water (Le Moullec et al, 2008b).

The mathematical model to predict the oxygen concentration (air and water phase), BOD concentration (water phase) and residence time (water phase) uses the species transport equation for scalar concentration in turbulent flow (equation 5.1):

$$\frac{\partial}{\partial t} (\rho_l C_{tr}) + \nabla \cdot (\rho_l U_l C_{tr}) = \nabla \cdot \left( \left( \rho_l D_m + \frac{\mu_t}{Sc_t} \right) \nabla C_{tr} \right) \quad (5.1)$$

where,  $C_{tr}$  is the concentration of the tracer ( $\text{kg/m}^3$ );  $U_l$  is statistical average velocity ( $\text{m/s}$ );  $D_m$  is mass diffusivity ( $\text{m}^2/\text{s}$ );  $\mu_t$  is turbulent viscosity ( $\text{kg/ms}$ );  $Sc_t$  is turbulent Schmidt number (dimensionless). On the left side of the equation are the convection terms and on the right side is molecular and turbulent diffusion.

### 5.2.3 Interfacial (inter-phase) bubble drag law

The bubble drag law in this study (equation 2.22) uses the concept of mixture viscosity for bubbly flow (Ishi and Zuber, 1979), which can include shape distortion, although spherical bubbles are modelled in this study.

### 5.2.4 Interfacial (inter-phase) oxygen mass transfer

Inter-phase oxygen mass transfer is an essential part of the DO distribution. The oxygen mass transfer coefficient ( $K_L a$ ) is used to quantify the interfacial (inter-phase) mass transfer between the gas and liquid phases (units of  $\text{s}^{-1}$ ). The oxygen mass transfer coefficient is modelled (equation 2.6) using Higbie's film penetration theory (Higbie, 1935). It is also used (equation 2.14) in this study to determine how much oxygen is transferred to the water from the surface aerators (units of  $\text{h}^{-1}$ ). The local mass transfer coefficient  $K_L$  depends on the local distributed quantities predicted by the multi-phase flow pattern (equation 2.6). These are the local air and water velocity, volume fraction of air (gas holdup) and bubble diameter. In this chapter a uniform mean bubble size is modelled throughout the ditch, while in the next chapter a bubble size distribution is modelled.

### 5.2.5 BOD distribution in water phase

Two approaches are used for predicting the BOD concentration distribution.

- (1) The decay of local BOD concentration in the water phase from influent to effluent in the ditch is dependent on local residence time in the water phase.

This is modelled using a first order exponential decay of the BOD concentration (equation 5.3) from the influent to effluent in terms of the local mean age of the fluid (LMA) to give the BOD distribution. This first approach does not consider the dissolved oxygen distribution and therefore the DO is assumed to be uniform in the ditch. LMA is a method used in the CFD modelling of ventilation systems in the built environment, to determine the age of air anywhere in and around a building (Ramponi et al, 2015). LMA can also be applied to a settling tank and an aeration tank in wastewater treatment (Karches and Buzas, 2013) and in a mixing reactor (Li et al, 2011). LMA can also be applied to determine the decay of BOD in a channel aeration tank (Ghawi, 2014; Karpinska and Bridgeman, 2018) and in lagoons (Salter et al, 2000; Wu, 2010; Wu and Chen, 2011). It can also determine the chlorine decay in contact tanks (Rauen et al, 2012) and in service reservoirs (Zhang et al, 2011).

The distribution of LMA in the water phase in a ditch is determined by the species transport equation (5.1). LMA is defined as a passive tracer that does not affect the flow pattern of the water and the DO and BOD concentrations. The decay of local BOD in the water is then subsequently calculated by using first-order kinetics, that depends only on the predicted LMA in the water phase (Metcalf and Eddy, 2003), which is based on Chick-Watson law (Haas and Karra, 1984; Butler et al, 2017):

$$\frac{\partial C}{\partial t} = -k C \quad (5.2)$$

$$C_t = C_o e^{-kt} \quad (5.3)$$

where,  $C_t$  is the local BOD concentration in the water phase (mg/l),  $C_o$  is the BOD concentration (mg/l) in the influent ( $t = 0$ ),  $k$  is the temperature dependent rate constant ( $\text{day}^{-1}$ ) and  $t$  is the LMA in the water phase (day).

- (2) The dissolved oxygen determines the activity of the microorganisms in the sludge. Higher dissolved oxygen in the ditch is more likely to increase the BOD degradation and therefore result in lower local BOD concentrations.

The BOD distribution in the water phase is determined by the species transport equation (5.1). The reduction of local BOD is subsequently modelled as a 'sink term' ( $BOD_{\text{sink}}$  - equation 5.4) throughout the ditch, that is only dependent on the local predicted mass fraction of DO. The resulting solution is the BOD distribution.

$$BOD_{\text{sink}} = DO \times \frac{BOD_{\text{load}}}{BOD_{\text{inf}}} \quad (5.4)$$

$$BOD_{\text{load}} = Q_{\text{inf}} \times BOD_{\text{inf}} \quad (5.5)$$

$$DO = DO_{\text{sat}} \times \frac{DO_{\text{mf}}}{DO_{\text{smf}}} \quad (5.6)$$

where  $BOD_{\text{sink}}$  is the local sink term of BOD (kg/s), DO is the local dissolved oxygen concentration (mg/l),  $BOD_{\text{load}}$  is influent mass flow rate of BOD (kg/s),  $Q_{\text{inf}}$  is influent flow rate (l/s),  $BOD_{\text{inf}}$  is influent BOD concentration (mg/l),  $DO_{\text{sat}}$  is saturation DO concentration (mg/l),  $DO_{\text{mf}}$  is local predicted mass fraction of DO,  $DO_{\text{smf}}$  is saturation mass fraction of DO. The input constants are  $BOD_{\text{load}}$ ,  $Q_{\text{inf}}$ ,  $BOD_{\text{inf}}$ ,  $DO_{\text{sat}}$ ,  $DO_{\text{smf}}$ .

### 5.2.6 Dissolved oxygen in water phase that is affected by BOD

The de-aeration of local DO that is caused by the BOD depends only on the local BOD concentration. Using the previously predicted BOD distribution, the reduction of local DO concentration is subsequently modelled as a 'sink term' ( $DO_{\text{sink}}$  - equation 5.7) throughout the ditch, that is only dependent on the local predicted BOD concentration. The resulting solution is the DO distribution.

$$DO_{\text{sink}} = BOD \times \frac{DO_{\text{load}}}{BOD_{\text{inf}}} \quad (5.7)$$

$$DO_{\text{load}} = Q_{\text{inf}} \times DO_{\text{inf}} \quad (5.8)$$

where  $DO_{\text{sink}}$  is the local sink term of DO (kg/s), BOD is the local predicted BOD concentration (mg/l),  $DO_{\text{load}}$  is influent weir mass flow rate of DO (kg/s),  $Q_{\text{inf}}$  is influent flow rate (l/s),  $BOD_{\text{inf}}$  is influent BOD concentration (mg/l),  $DO_{\text{inf}}$  is influent DO concentration (mg/l). The input constants are  $DO_{\text{load}}$ ,  $Q_{\text{inf}}$ ,  $BOD_{\text{inf}}$ ,  $DO_{\text{inf}}$

### 5.2.7 Interfacial (inter-phase) equilibrium model - Henry's law

In physical chemistry, Henry's law states that the dissolved gas in a liquid is proportional to its partial pressure above the liquid (equation 5.9). The proportionality factor is called Henry's law constant. Consider two phases, which are gas and liquid, which both contain component A. Consider the situation where component A is in dynamic equilibrium between the phases. For absorption / dissolution of the gas into a dissolved liquid, Henry's Law describes this equilibrium. It states there is a linear relationship between the mole fraction of component A that is dissolved in the liquid and the partial pressure of component A in the gas:

$$P_{Ag} = H^x X_{Al} \quad (5.9)$$

where  $P_{Ag}$  is the partial pressure of component A in the gas phase (Pa),  $X_{Al}$  is the mole fraction of component A in the liquid phase,  $H^x$  is the molar fraction Henry coefficient (Pa).

## 5.3 Numerical methods

### 5.3.1 Species transport modelling

The multi-phase flow pattern and volume fraction of water and air is firstly predicted. Then the multi-phase flow equations are no longer solved and the multi-phase solution is used further. The assumption is that the flow patterns has an effect on the oxygen species concentration, but the reverse is negligible (one way coupled). Two scalars (or species) represent the oxygen concentration in each phase. The equations of the mass fraction of oxygen in the air phase and the mass fraction of oxygen in the water phase are solved using the species transport model. The latter quantity is converted into the DO concentration. The inter-phase mass transfer of oxygen is also solved. The species transport equation (5.1) solves the spatial distributions of variables in the water phase: DO, BOD and residence time.

The DO-BOD model is a two way coupled relationship between the dissolved oxygen and the biochemical oxygen demand. Wastewater is aerated by the aeration devices and this increases DO. The oxygen demand from the biomass decreases the DO by the biodegradation of BOD. The DO determines the activity of microorganisms in the sludge. Higher DO in the ditch is more likely to increase BOD degradation and result in lower local BOD levels. The predicted BOD distribution is adjusted in the BOD sink term by a factor to predict a minimum BOD concentration of 0 mg/l in the ditch.

The first approach is to use a mean uniform BOD concentration in the ditch. The second approach is a BOD distribution by decay, that depends only on the local fluid residence time (equation 5.3). The third approach is a BOD distribution that depends only on the local DO concentration. The first and third approaches are used further. This study models the third approach which is the reduction of the local BOD by the local DO (Wicklein et al, 2016) - equation 5.4. This study also models the reduction of local DO by the local BOD - equation 5.7. An oxygen species transport equation includes a sink term for the oxygen that is removed by BOD. There are two approaches in determining the DO distribution: (1) uniform BOD concentration and homogeneous oxygen sink in ditch; (2) BOD distribution and heterogeneous oxygen sink in ditch. The uniform BOD concentration is the mean of the BOD distribution.

The local mean age (LMA) or local residence time is defined as a scalar and solved as a distribution using the species transport equation (5.1). The BOD concentration is also defined as a scalar and solved as a distribution using the species transport equation. The arbitrary mass diffusivity of the residence time scalar is  $1.35 \times 10^{-9} \text{ m}^2/\text{s}$ . This is intentionally the same value that is used for the tracer in the RTD calculation. These are considered to be passive scalars that do not affect the water fluid. For the BOD scalar its mass diffusivity is  $3.5 \times 10^{-9} \text{ m}^2/\text{s}$ . The turbulent Schmidt number of the residence time and BOD concentration scalars are 0.7. There is a distributed BOD sink in the whole ditch that depends solely on the local DO concentration. In the species transport equation (5.1), the scalar for residence time in the water phase has units of time. The residence time is defined as zero at the influent to the ditch. A source term of 1 unit for the residence time scalar is applied to the whole flow domain in the ditch. For species transport the scalars for dissolved oxygen in the water and air phases and the BOD in the water phase have units of concentration.

### 5.3.2 Species boundary conditions

The boundary conditions for the influent and effluent weir flows, water surface (degassing boundary condition), solid surfaces, influents of aeration systems and flow booster are the same as in the multi-phase flow model in the previous chapter. The oxygen transfer from atmospheric air into the bulk liquid through the water surface is considered negligible, in comparison to the oxygen transfer through the surface areas of the bubbles (Fayolle et al, 2007; Hu et al, 2010). The Maguire jet aerator has a flow stream of saturated aerated water. The membrane diffusion aerators and Fuch jet aerators have flow streams of pure air. The influent BOD concentration is defined at the influent weir and is taken from measured data. From measured data at Potterne WWTP in the two ditches, the mean annual influent BOD is around 300 mg/l and the mean annual effluent BOD is around 5 mg/l.

Two scalars represent the oxygen concentration in the air and water phases. In an oxygen species transport model the boundary conditions for oxygen are modelled for the air sources: influent weir (water), brush surface aeration (air), Maguire jet aerator (water), diffusion aerator (air) and Fuch jet aerator (air). There is an oxygen sink boundary condition at the water surface from the rising bubbles (degassing boundary condition) and in the effluent (water). The oxygen concentrations at the inlet boundaries are defined for the influent weir, Maguire jet aerator, surface aerators, diffusers and Fuch jet aerators, using the same mass fraction of oxygen in the air phase. The standard mass fraction of dry oxygen in dry air is 0.229 at 1 atm pressure and 20 °C (Çengel and Boles, 2008). The oxygen concentrations in the influent weir streams are defined by the mass fraction of oxygen in the water phase. These are equivalent to the influent DO measurements of 0.08 mg/l in OD1 and 0.04 mg/l in OD2 (mass fractions are  $8.7 \times 10^{-8}$  and  $4.35 \times 10^{-8}$ ).

### 5.3.3 Numerical convergence

To decrease the duration of the species transport simulations, the flow equations of mass, momentum, turbulence and volume fraction are not solved any further. This is to ensure that the multi-phase flow pattern is kept at steady-state throughout the species computation. Therefore only the equations of mass fractions of the local DO, BOD and residence time components in the ditch are solved. The species transport equations are solved iteratively to steady-state. An under relaxation factor of 0.3 is used for the scalar equations. Lowering the under relaxation factor for an equation can make the convergence more stable. When solving the next iteration a lower under relaxation factor uses relatively more of the solution of the previous iteration in order to maintain stability. Second order numerical grid discretisation is undertaken for better accuracy. The convergence is achieved when all scalar equations reach a convergence criteria of  $10^{-6}$ . The rate of convergence is fast and convergence is achieved between 3000 and 10000 iterations. The duration of the simulations is between 15 and 30 hours. The convergence residuals of the oxygen and residence time scalars are shown at the operating conditions in OD1 in Figure 5.1.

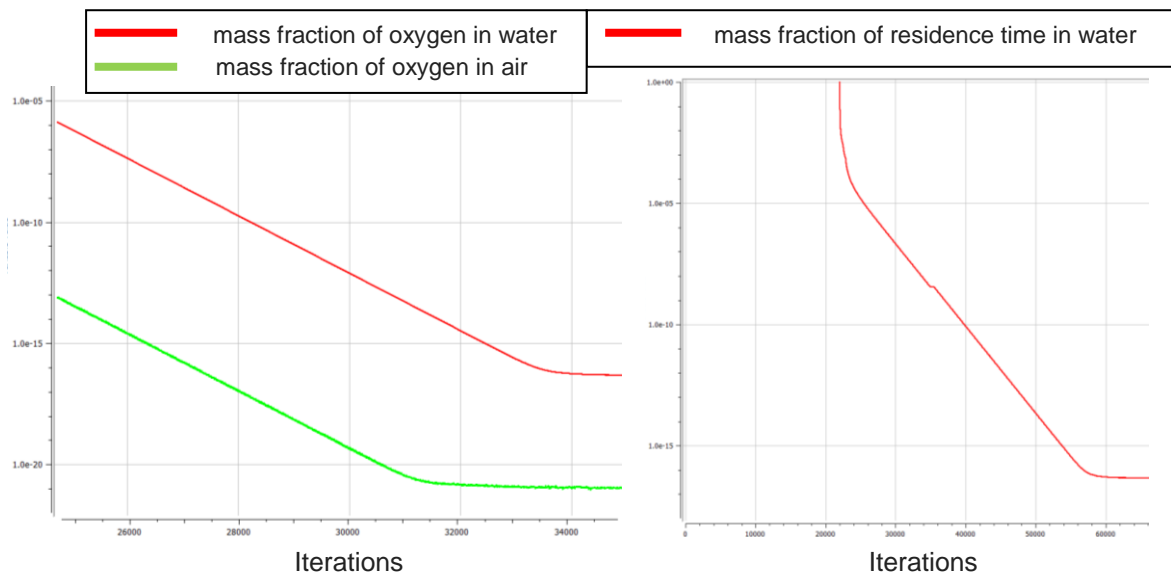


Figure 5.1 Numerical residuals of scalar equations  
oxygen (left), residence time (right)

## 5.4 Results and discussion

The physical properties in Table 5.1 of the water, air and oxygen at the mean annual temperature at Potterne WWTP at 13 °C, include the density, viscosity, mass diffusivity and Henry law coefficients. The scalar component of oxygen in the dry air gas phase is the oxygen gas. The scalar component of oxygen in the water phase is the dissolved oxygen (DO). Dry oxygen approximately occupies 21% by volume of dry air. It has a higher density and viscosity than air (Çengel and Boles, 2008). The saturation DO concentration in water is 10.5 mg/l at the mean annual temperature at Potterne WWTP of 13 °C (Degremont, 2007). This is the upper limit of the DO concentration in the ditch. The standard mass fraction of the oxygen in dry air is about 0.229 at 1 atm pressure and 20 °C (Degremont, 2007). The mass diffusivity of dry oxygen in dry air is  $1.26 \times 10^{-5} \text{ m}^2/\text{s}$ . The mass diffusivity of DO in water is much lower at  $1.2 \times 10^{-9} \text{ m}^2/\text{s}$  (Çengel and Boles, 2008). From the literature the average bubble size used in the CFD models is around 4 mm.

Table 5.1 Physical properties of dissolved oxygen modelling

Physical Property	Value	Units
temperature	13	°C
density of water	999.4	kg/m <sup>3</sup>
density of air	1.233	kg/m <sup>3</sup>
density of oxygen	1.370	kg/m <sup>3</sup>
viscosity of water	0.0012	kg/ms
viscosity of air	0.0000179	kg/ms
viscosity of oxygen	0.0000201	kg/ms
bubble diameter	4	mm
mass fraction of oxygen in air	0.233	-
saturation of air in water (volume fraction)	0.036	-
saturation of dissolved oxygen in water	10.5	mg/l
mass diffusivity of oxygen in air	$1.26 \times 10^{-5}$	m <sup>2</sup> /s
mass diffusivity of oxygen in water	$1.2 \times 10^{-9}$	m <sup>2</sup> /s
turbulent Schmidt number of oxygen in air	0.7	-
turbulent Schmidt number of oxygen in water	0.7	-
molar concentration Henry coefficient	61636	Pa.m <sup>3</sup> /mol
molar fraction Henry coefficient	$3.4 \times 10^9$	Pa
mass transfer coefficient of surface aeration	3	h <sup>-1</sup>

The results of the dissolved oxygen distributions in this chapter are shown firstly, without the effect of de-oxidation due to the biochemical oxygen demand (BOD). This is to study the individual effects of the different aeration systems, and therefore better understand the aeration performance of aerators in terms of dissolved oxygen. Secondly the BOD distribution is simulated in the ditch. Thirdly the effect of the BOD on the DO distribution is then simulated for operating conditions at Potterne WWTP. These final set of results can be compared to experimental data in a later chapter.

#### 5.4.1 Dissolved oxygen distribution without BOD for different aerators

Case O1 simulates OD1 with no devices. Case O2 simulates dissolved oxygen distribution in OD1 with the surface aerators. Case O3 simulates OD1 with one diffusion aerator. Case O4 simulates OD1 with one Maguire jet aerator. Case O5 simulates OD1 with surface aerators, diffusion aerator and Maguire jet aerator. Case O6 simulates the other ditch OD2 with the flow booster. Case O7 simulates OD2 with three diffusion aerators. Case O8 simulates OD2 with three Fuch jet aerators. Case O9 simulates OD2 with the flow booster, diffusion aerators and Fuch jet aerators. Cases O5 and O9 represent the current operating conditions at Potterne WWTP. Table 5.2 shows the predicted mean and maximum DO concentration and the percentage of saturation DO in ditches OD1 and OD2 without any effect of BOD.

Table 5.2 Dissolved oxygen concentrations without BOD

Case	OD	Devices	No	Oxygen supply (kg/s)	Max DO (mg/l)	Mean DO (mg/l)	Max DO (% sat)	Mean DO (% sat)
O1	1	none	0	$3.7 \times 10^{-6}$	0.087	0.087	1	1
O2	1	surface aeration	4	0.01632	3.07	2.48	29	24
O3	1	diffusion aeration	1	0.01386	7.91	5.44	75	52
O4	1	Maguire jet aeration	1	0.00139	0.68	0.44	7	4
<b>O5</b>	<b>1</b>	<b>operating condition</b>	<b>6</b>	0.0311	<b>4.12</b>	<b>3.46</b>	<b>39</b>	<b>33</b>
O6	2	flow booster	1	$1.8 \times 10^{-6}$	0.0435	0.0435	0.4	0.4
O7	2	diffusion aeration	3	0.0413	9.60	8.74	91	83
O8	2	Fuch jet aeration	3	0.0747	10.22	5.97	97	57
<b>O9</b>	<b>2</b>	<b>operating condition</b>	<b>7</b>	0.1165	<b>10.23</b>	<b>8.74</b>	<b>97</b>	<b>83</b>

Table 5.2 shows in OD1 that the Maguire jet aerator provides a low level of mean DO in the ditch (4 % of saturation) compared to surface aeration (24 %) and diffusion aeration (52 %). Diffusion is the most efficient aeration system in OD1, as it produces a higher DO from a lower oxygen supply than surface aeration. Table 5.2 shows that in OD2 the Fuch jet aeration provides a considerable mean DO in the ditch (57 %). Again the diffusion aeration is the most efficient aeration system in OD2, as it produces a high mean DO (83 %) from a lower oxygen supply.

The water flow patterns in the ditches are predicted by the Euler-Euler multi-fluid multi-phase flow model, which is described in the previous chapter. The measured influent DO concentration in OD1 is 0.08 mg/l and in OD2 is 0.04 mg/l. These values are used for the influent boundary condition (oxygen mass fraction in water phase). The results are shown on a horizontal plane near to the water surface.

With no aeration from the devices (cases O1 and O6 in Table 5.2), there are low velocities throughout the ditch (Figure 5.2), and low uniformly distributed DO concentrations. In OD1, there are flow plumes that are dispersed from the surface brush aerators (Figure 5.3). The highest DO concentrations are near the brush aerators due to surface aeration (Figure 5.4). The DO concentrations are dispersed by the velocity plumes from the surface aerators. Near the influent there is a stream of very low DO concentrations (Figure 5.4). The flow pattern just above the diffuser is radially dispersed (Figure 5.5). The DO concentrations are evenly spread by a diffuser (Figure 5.6). The overall effect is a zonal DO pattern in OD1 due to the better aeration efficiency of the diffuser (Figure 5.6). There is a sudden drop in DO concentration, where flow circulates around the ditch in opposing directions, and meets where there is recirculation and mixing of water at different DO concentrations (top right of Figure 5.6). The Maguire jet aerator in OD1 creates a strong flow stream around the outside of the ditch (Figure 5.7). The DO concentrations are highest near the Maguire jet aerator, but then they dissipate quickly and are much more evenly spread (Figure 5.8). However, the DO concentrations are generally low in the ditch suggesting that the Maguire jet aerator is an ineffective aeration system.

For the operating conditions in OD1, there are flow plumes from the surface aerators, strong flow stream from the Maguire jet aerator and radial dispersed flow from the diffuser (Figure 5.9). The greatest difference between the water and air

velocities (Figure 5.10) is above the Maguire jet aerator, where air enters the ditch as an aerated water stream. There are local air hotspots near the aerators (Figure 5.11). The oxygen concentration in the air has oxygen hotspots near the aerators (Figure 5.12). The convection and diffusion of the oxygen in the air predicts that the oxygen is spread quite evenly around the ditch (Figure 5.12). The interfacial oxygen mass transfer from the air to water phase (Figure 5.13) is highest near the aeration sources (influent, surface, diffuser, jet aeration). The spatial distribution of mass fraction of oxygen in the water phase (Figure 5.14) is equivalent to DO concentration (mg/l) in water (Figure 5.15) and the percentage of DO saturation concentration (%) in water (Figure 5.16). The DO concentration (mg/l) is calculated from the predicted mass fraction of oxygen in water (equation 5.1). The DO concentration as a percentage of saturation is calculated from the DO concentration in mg/l. The highest DO concentrations are near the surface aerators and directly above the diffuser (Figure 5.15). There are higher DO concentrations near the internal wall (Figure 5.15). Near the influent there is a stream of very low DO concentrations.

In OD2, the flow booster creates a strong flow stream, especially near the internal and outside walls (Figure 5.17). There is no air supplied by the booster. The DO concentrations are very low, because there is only a low air supply from the influent stream. The flow pattern that is caused by the diffusers in OD2 includes radial flow directly above each diffuser and local flow recirculation (Figure 5.18). The DO distribution in OD2 is zonal with the highest concentrations close to each diffuser (Figure 5.19). The flow pattern is quite complicated with several small zones of recirculation. There is a sudden drop in DO concentration, where flow circulates around the ditch in opposing directions, and meets where there is mixing of water at different DO concentrations (lower right of Figure 5.19). The Fuch jet aerators have a very complex local flow pattern, because the jets are composed of pure air that causes the water to flow in opposing directions near the water surface (Figure 5.20). The DO is dispersed in opposing directions with an overall zonal DO pattern (Figure 5.21). For the operating conditions in OD2 the flow pattern is the most complex near each diffuser and Fuch jet aerator (Figure 5.22). This creates high DO local hot spots near the aerators, while further away DO is more evenly spread (Figure 5.23). The influent flow stream has a low air concentration that lowers the DO concentrations around two of the diffusers (Figure 5.23).

**Case O1: no devices**

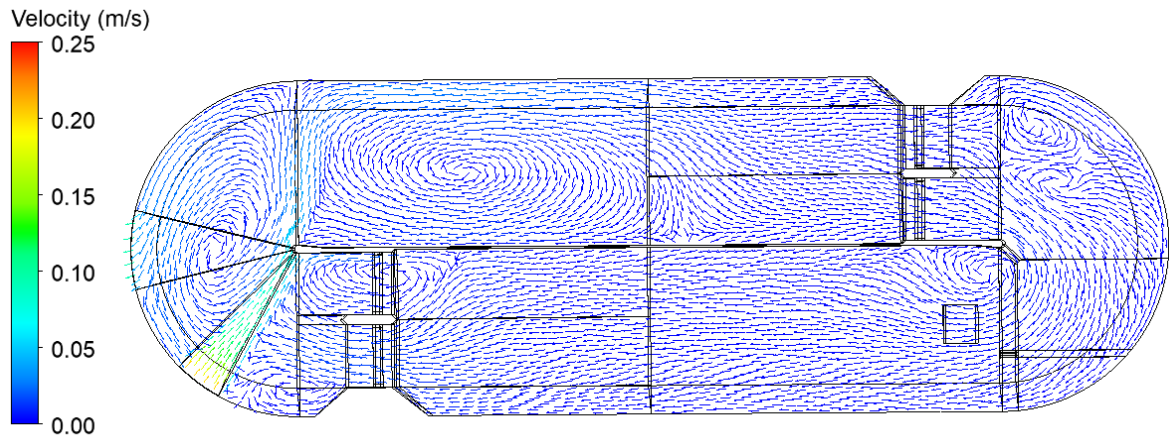


Figure 5.2 Water velocity in OD1 without devices

**Case O2: surface aerators only in OD1**

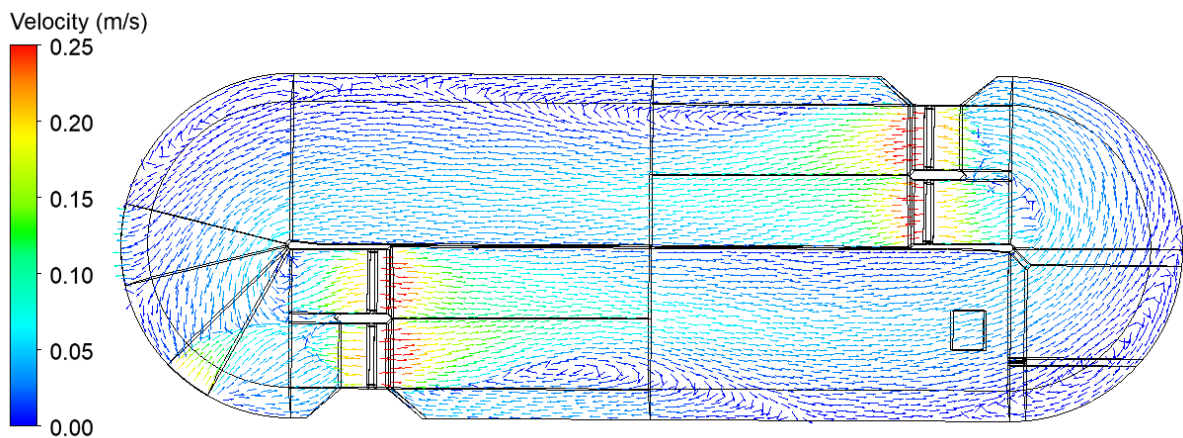


Figure 5.3 Water velocity in OD1 with surface aerators only

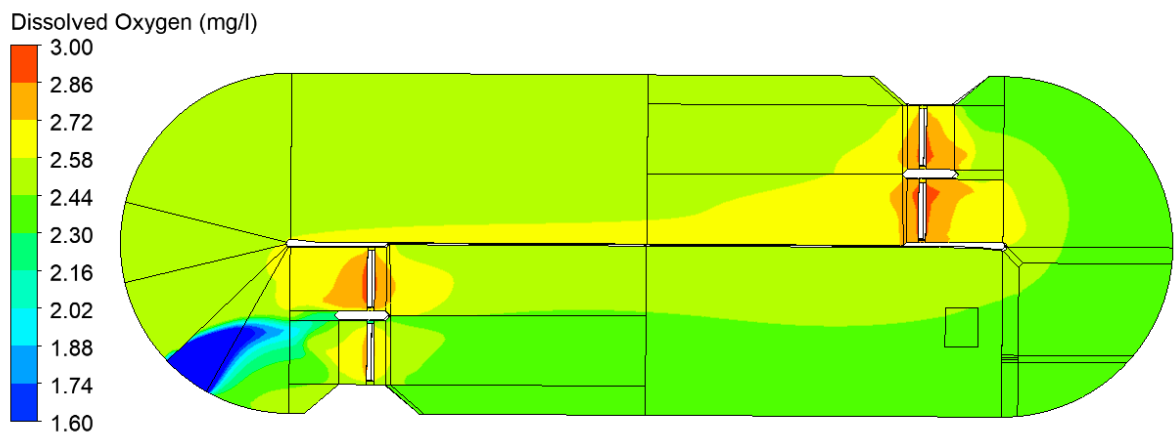


Figure 5.4 DO concentration in OD1 with surface aerators only

(max = 3.07 mg/l, mean = 2.48 mg/l)

**Case O3 Grid diffusion aerator only in OD1**

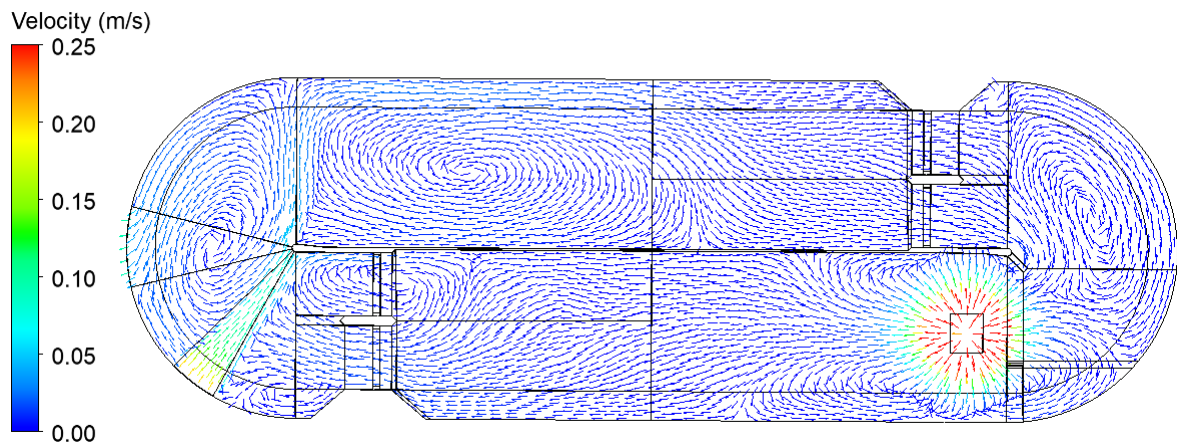


Figure 5.5 Water velocity in OD1 with diffuser only

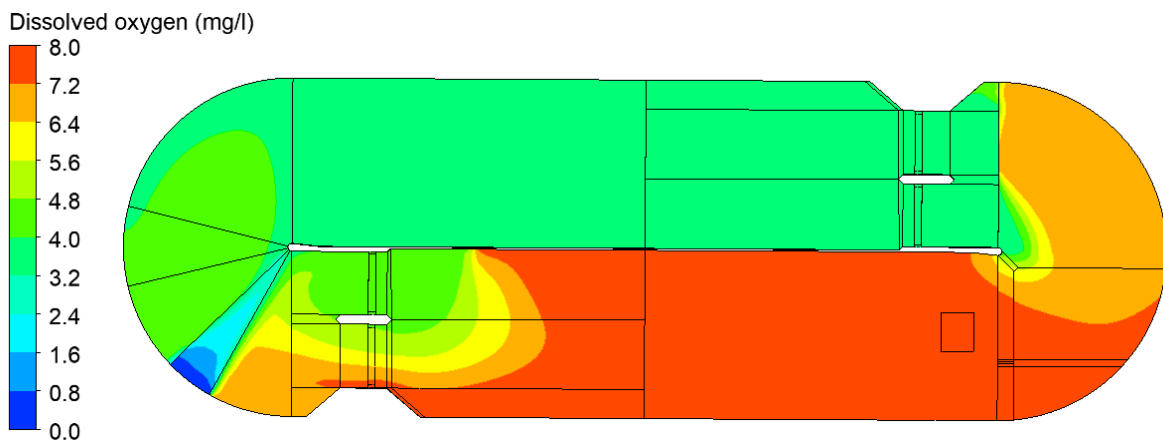


Figure 5.6 DO concentration in OD1 with diffuser only  
(max = 7.91 mg/l, mean = 5.44 mg/l)

**Case O4 Maguire jet aerator only in OD1**

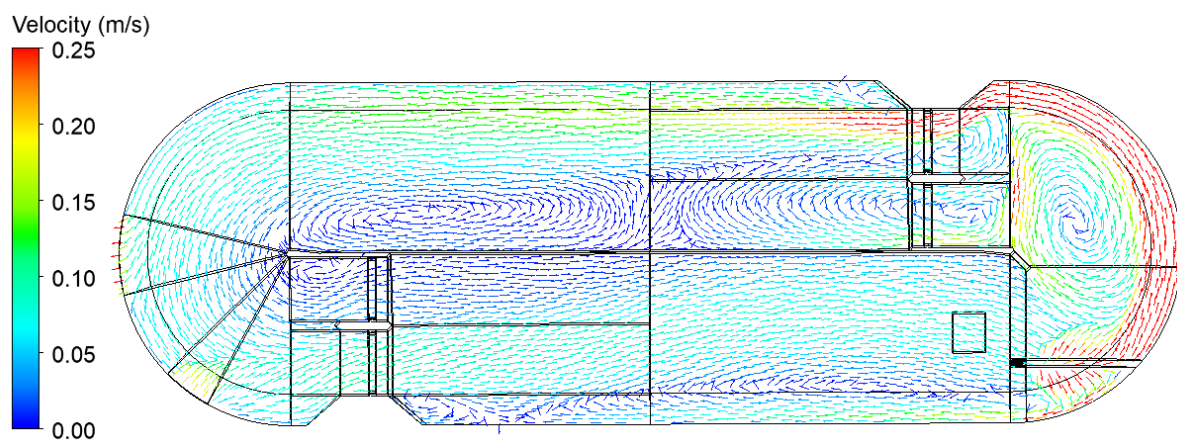


Figure 5.7 Water velocity in OD1 with Maguire jet aerator only

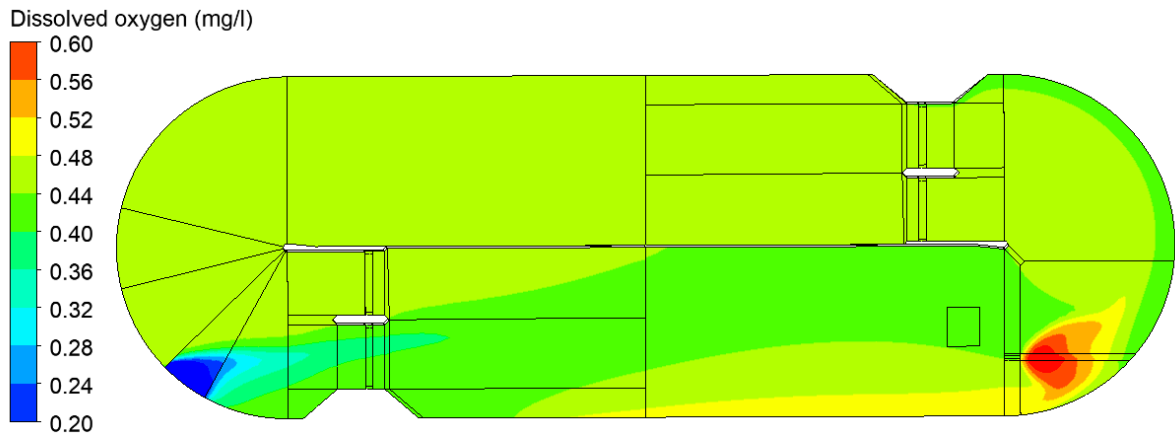


Figure 5.8 DO concentration in OD1 with Maguire jet aerator only  
(max = 0.68 mg/l, mean = 0.44 mg/l)

### Case O5 Operating conditions with all aerators in OD1

This is the most important DO concentration distribution in OD1, as it simulates the operational conditions at WWTP. *Note that it neglects the effect of the BOD.*

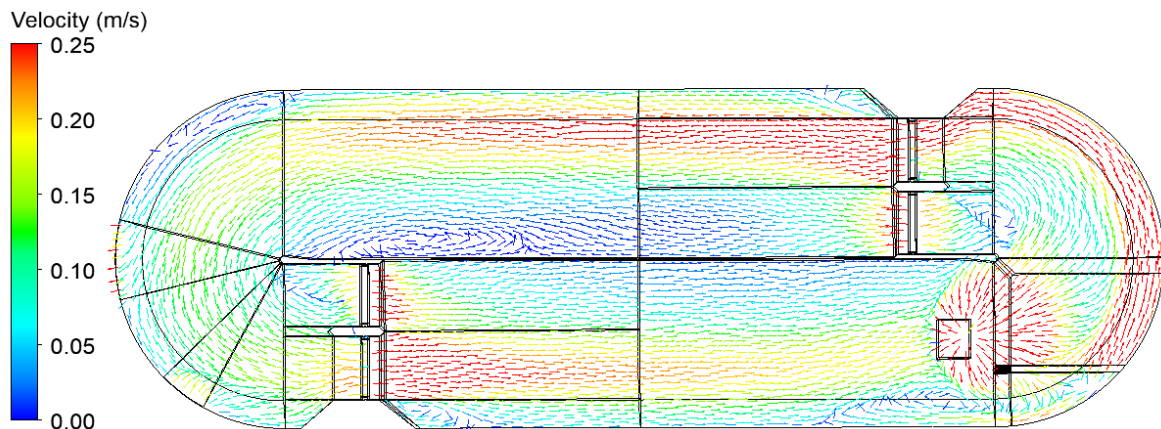


Figure 5.9 Water velocity in OD1 - operating conditions at WWTP

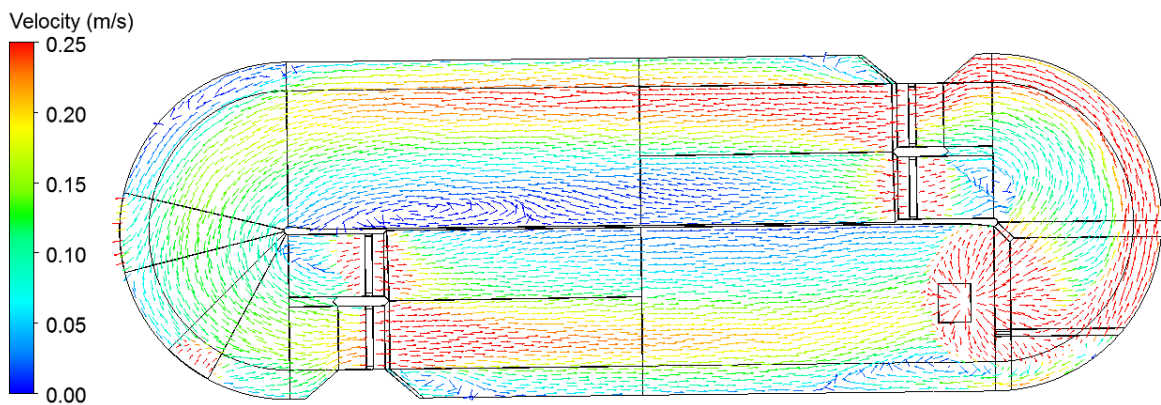


Figure 5.10 Air velocity in OD1 - operating

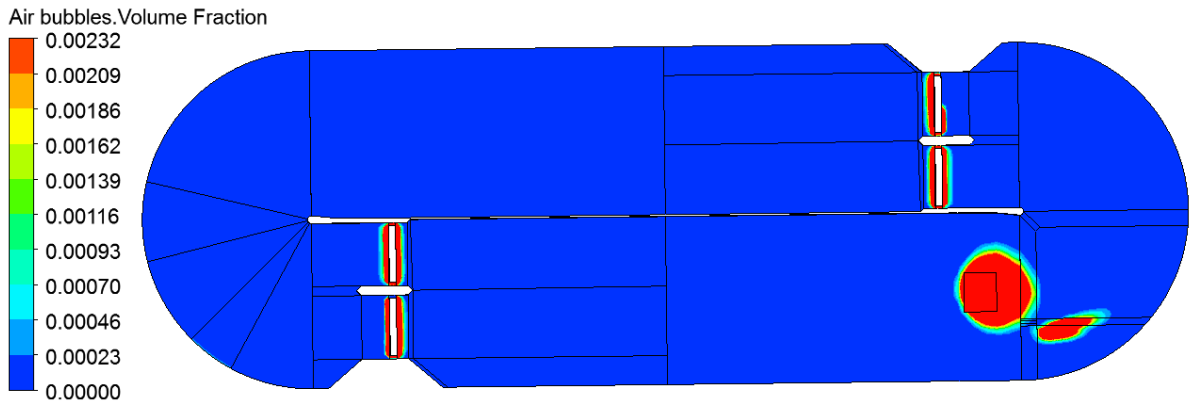


Figure 5.11 Volume fraction of air in OD1 - operating

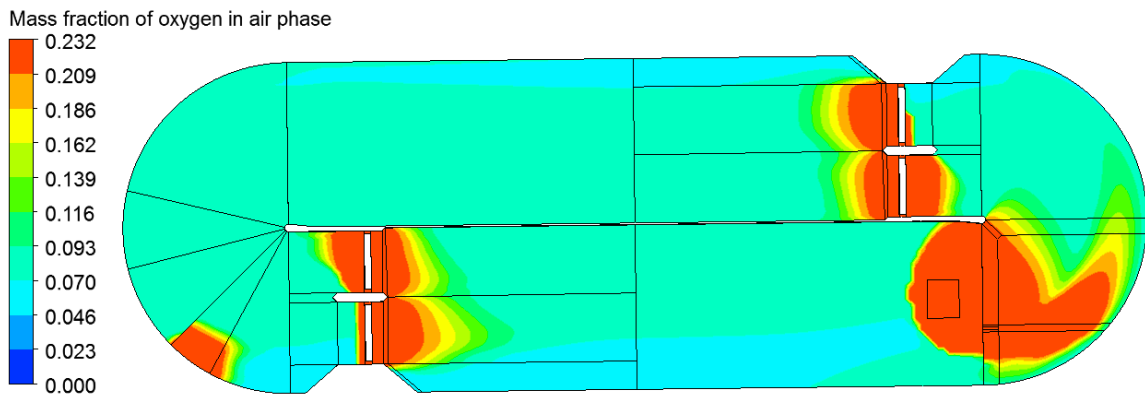


Figure 5.12 Mass fraction of oxygen in air phase in OD1 - operating  
(max = 0.233, mean = 0.078)

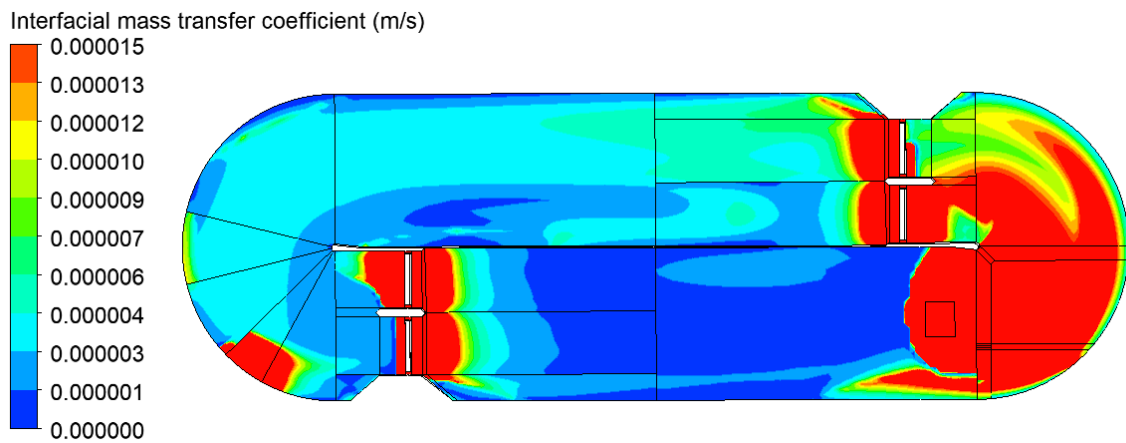


Figure 5.13 Mass transfer coefficient in OD1 - operating  
(max =  $9.4 \times 10^{-4}$ , mean =  $1.1 \times 10^{-5}$  m/s)

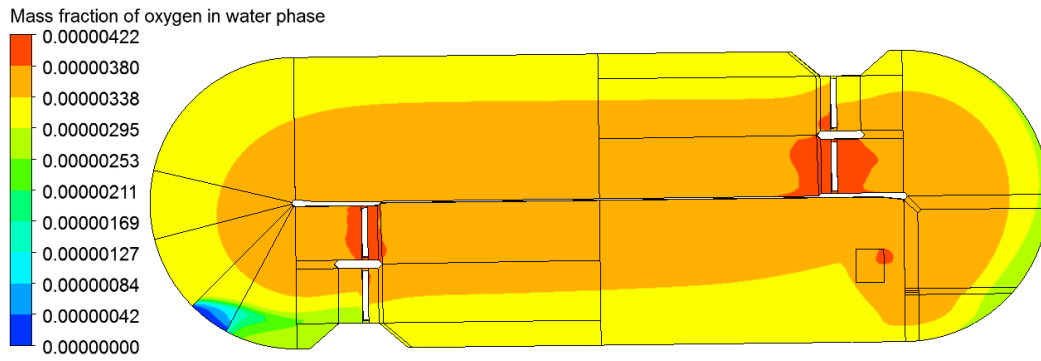


Figure 5.14 Mass fraction of oxygen in water phase in OD1 - operating  
(max =  $4.12 \times 10^{-6}$ , mean =  $3.45 \times 10^{-6}$ )

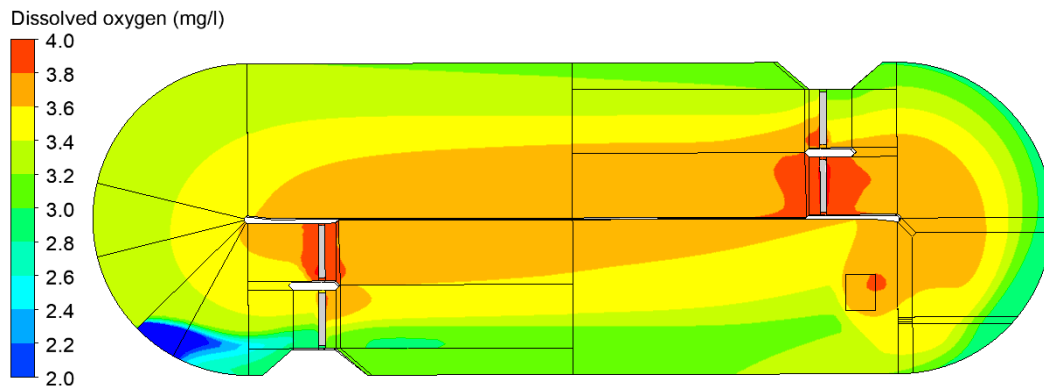


Figure 5.15 DO concentration in OD1 - operating  
(max = 4.12 mg/l, mean = 3.46 mg/l)

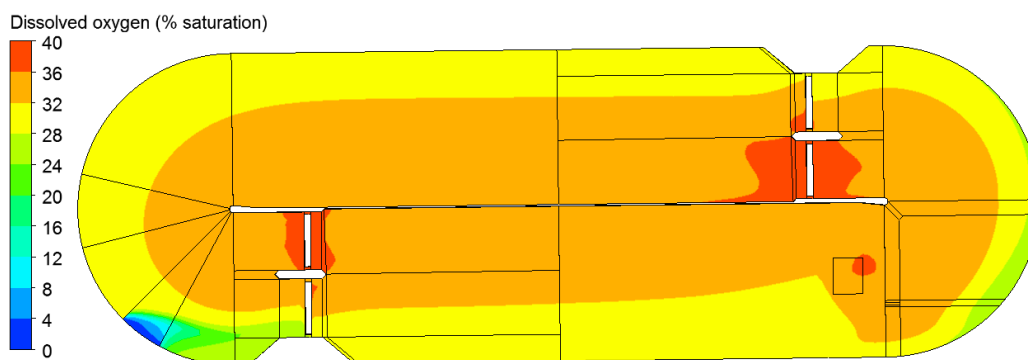


Figure 5.16 DO percentage saturation in OD1 - operating  
(max = 39 %, mean = 33 %)

**Case O6 Flow booster**

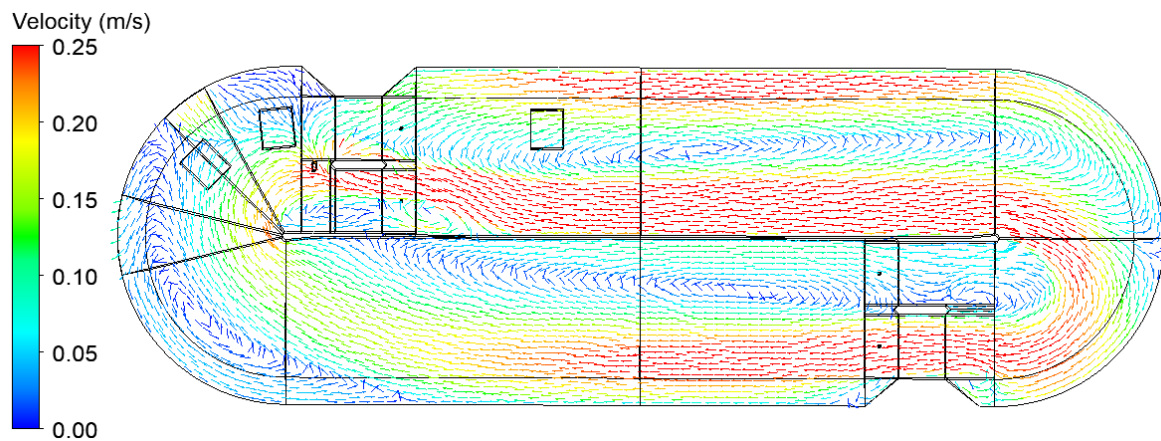


Figure 5.17 Water velocity in OD2 with flow booster

**Case O7 Grid diffusion aerators in OD2**

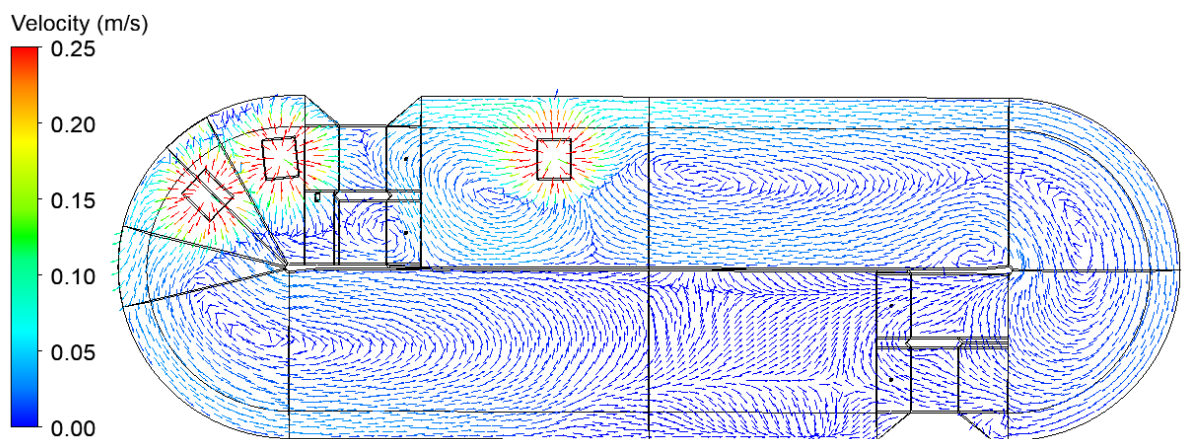


Figure 5.18 Water velocity in OD2 with diffusers only

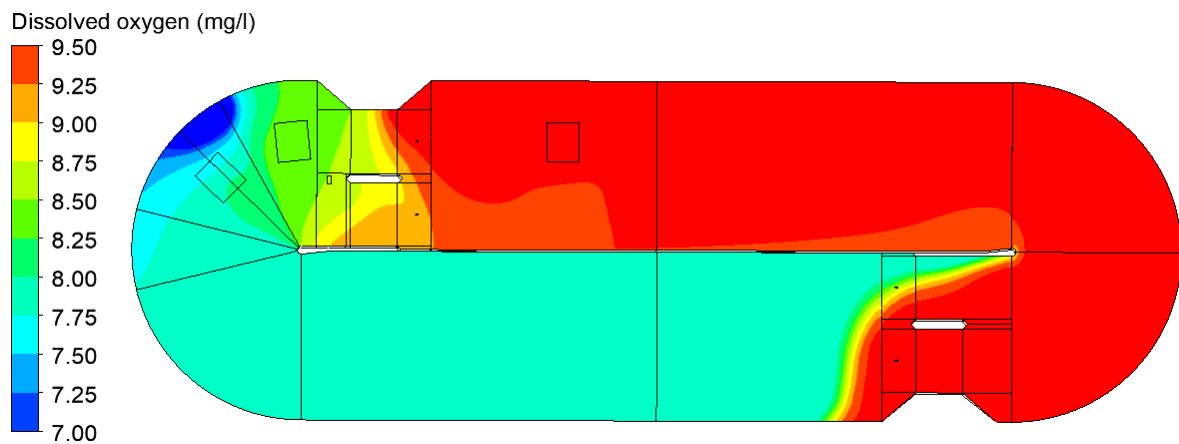


Figure 5.19 DO concentration in OD2 with diffusers only

(max = 9.60 mg/l, mean = 8.74 mg/l)

**Case O8 Fuch jet aerators only in OD2**

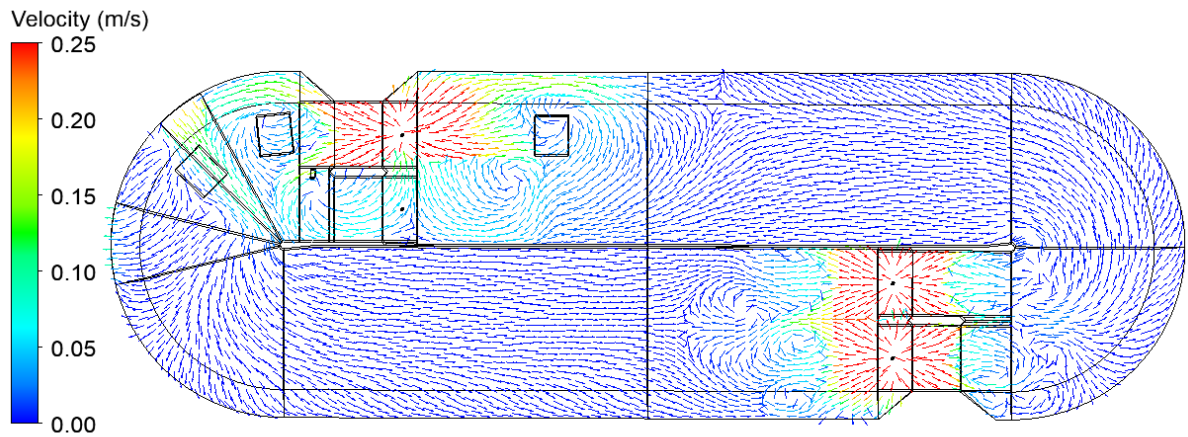


Figure 5.20 Water velocity in OD2 with Fuch jet aerators only

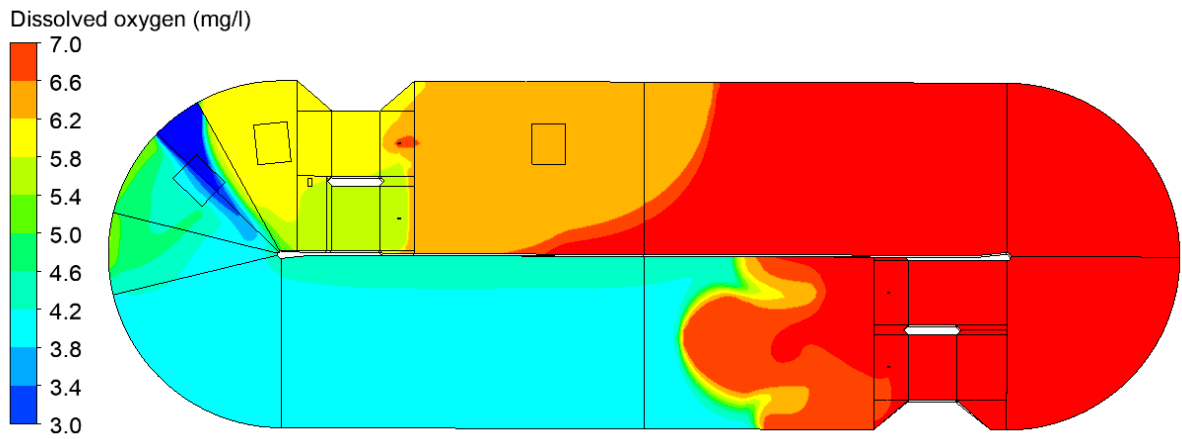


Figure 5.21 DO concentration in OD2 with Fuch jet aerators only  
(max = 10.22 mg/l, mean = 5.97 mg/l)

## Case O9 Operating conditions with all aerators in OD2

This is the most important DO concentration distribution in OD2, as it simulates the operational conditions at WWTP. *Note that it neglects the effect of the BOD.*

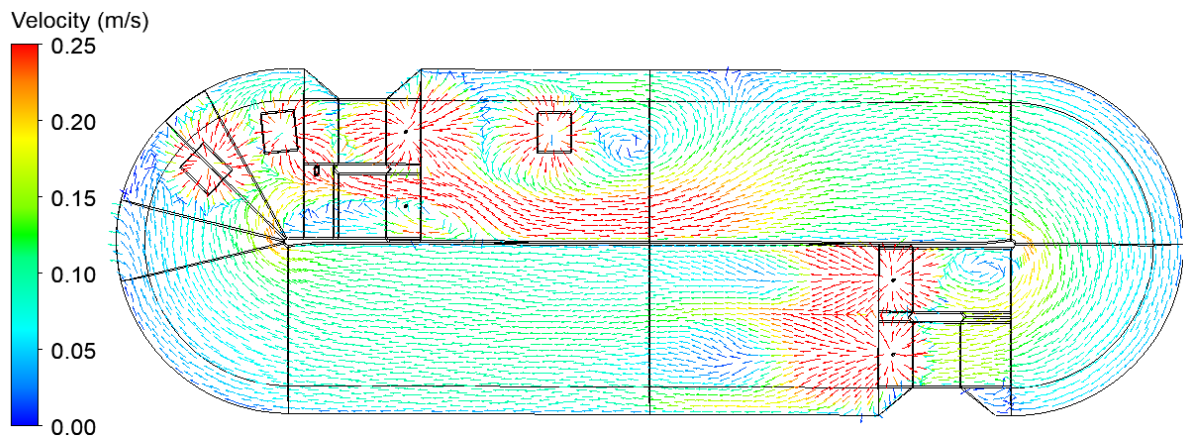


Figure 5.22 Water velocity in OD2 - operating conditions

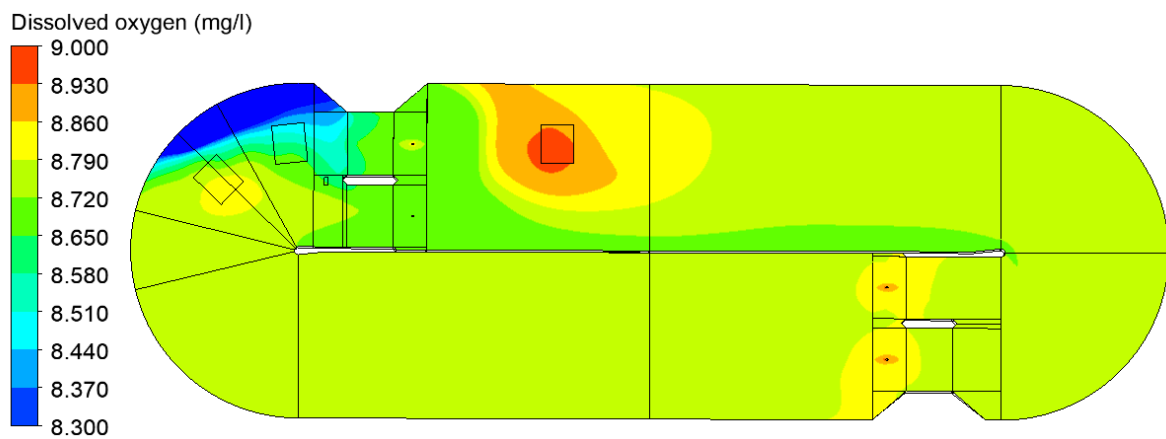


Figure 5.23 DO concentration in OD2 - operating conditions

(max = 10.23 mg/l, mean = 8.73 mg/l)

### 5.4.2 Biochemical oxygen demand distribution

From the measured data at Potterne WWTP in the two ditches, the mean annual influent BOD is around 300 mg/l and the mean annual effluent BOD is around 5 mg/l.

#### Local residence time model

The local BOD concentration in the water depends solely on the local residence time in the water by a decay term for the BOD (equation 5.3). The BOD distribution is adjusted to give a minimum BOD concentration of 0 mg/l in the ditch (maximum BOD is in the influent). The adjusted parameter is the decay rate constant (equation 5.3), with a value of  $0.23 \text{ day}^{-1}$  (Butler et al, 2017). This gives a mean BOD concentration in OD1 of 13 mg/l and an effluent BOD concentration of 14 mg/l.

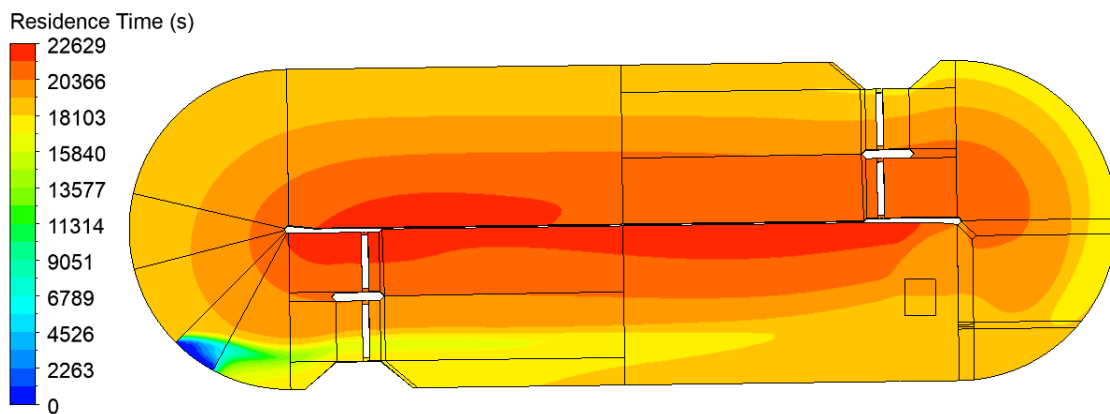


Figure 5.24 Residence time in OD1 - operating conditions

(max = 22629 s, mean = 19902 s, effluent = 18843 s, inlet = 0 s)

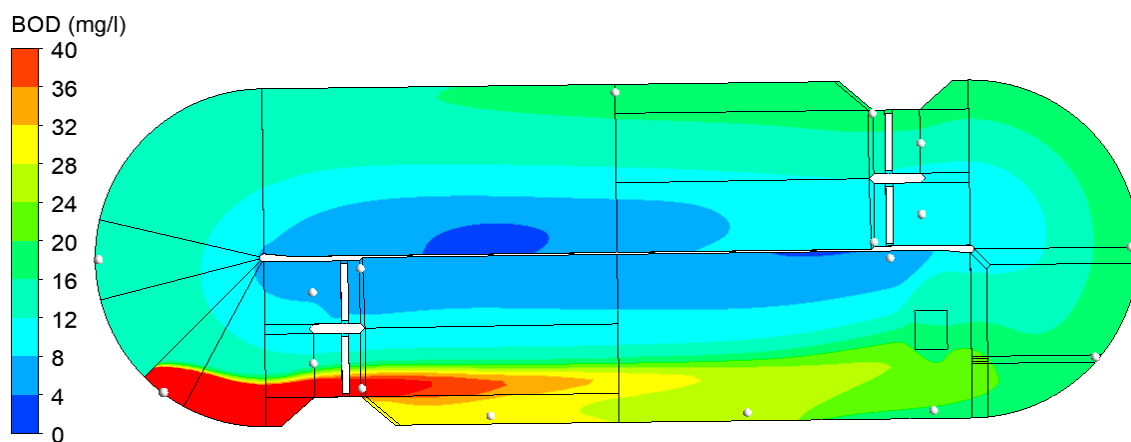


Figure 5.25 BOD concentration in OD1 depends on residence time

(inlet = 300 mg/l, mean = 13 mg/l, effluent = 14 mg/l, min = 0 mg/l)

## Local dissolved oxygen model

The local sink term of BOD in the water depends solely on the local DO concentration in the water phase (equation 5.4). The BOD distribution is adjusted in the BOD sink term equation by an adjustment factor, to give a minimum BOD concentration of 0 mg/l in the ditch (maximum BOD is in influent). This gives a mean BOD concentration in OD1 of 15 mg/l and an effluent BOD concentration of 18 mg/l.

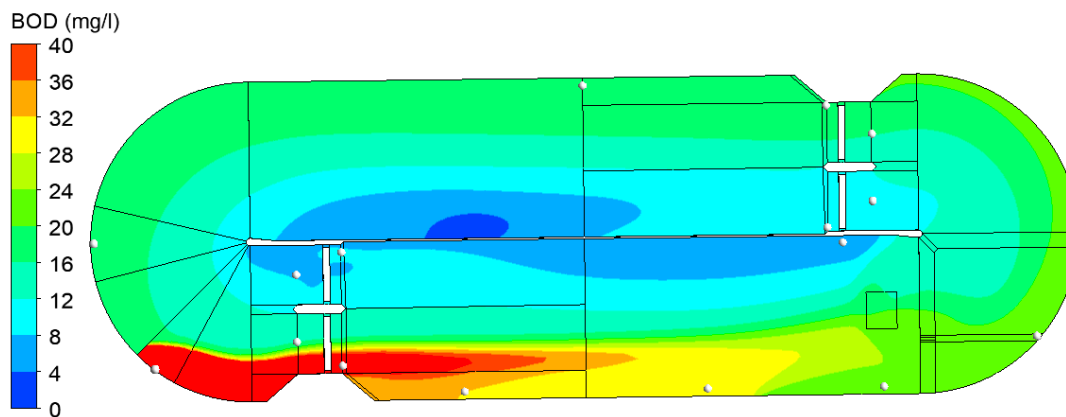


Figure 5.26 BOD concentration in OD1 depends on DO  
(inlet = 300 mg/l, mean = 15 mg/l, effluent = 18 mg/l, min = 0 mg/l)

The local residence time shows an increase near the inner wall, which is furthest away from the influent weir (Figure 5.24). Comparing the BOD distributions in OD1 for the two methods there is close agreement (Figures 5.25 and 5.26). Therefore it would be reasonable to use either method. However, in the literature there is a recognised two way coupled relationship between DO and BOD ('DO-BOD' model). Therefore, the two-way coupled DO-BOD relationship is used to determine the BOD distribution, that subsequently has an effect on the DO distribution.

### 5.4.3 Dissolved oxygen distribution with BOD for operating conditions

There is a two way coupled relationship between the DO and BOD. The biodegradation of BOD in the activated sludge consumes oxygen and therefore decreases the DO concentration. The DO determines the activity of the microorganisms in the sludge. Higher DO concentrations are more likely to increase the BOD degradation and therefore result in lower local BOD concentrations. The predicted BOD distribution is calculated by the local dissolved oxygen method (Figure 5.26). Reduction of the DO concentration is modelled by a 'sink term', that is dependent only on the local BOD concentration (equation 5.7). There are two methods to predict the de-aeration of DO by BOD, either by a uniform or a distributed BOD. The uniform BOD concentration is the mean value of the BOD distribution which is 15 mg/l. In OD1 both uniform and distributed BOD models are compared to predict the DO distribution at the operating conditions at Potterne WWTP. In OD2 only a uniform BOD model is used to predict the DO distribution at the operating conditions.

The flow pattern of water in OD1 is shown in Figure 5.27. It is shown beside the DO concentrations to see more clearly how DO is dispersed around the ditch. Comparison between the DO distributions for uniform and distributed BOD (Figures 5.28 and 5.29) show that the mean (0.41 and 0.42 mg/l) and maximum (1.26 and 1.24 mg/l) DO concentrations in the ditch are very similar. The main difference is the variation of DO (Figures 5.28 and 5.29). For a uniform BOD the lowest DO concentrations are near the central wall (Figure 5.28). For a distributed BOD the lowest DO concentrations are downstream of the influent and near the outside wall (Figure 5.29). In the predicted BOD distribution (Figure 5.26) the highest BOD is also downstream of the influent, while the lowest is also near the inside wall.

The flow pattern of water in OD2 is shown in Figure 5.30. It is shown beside the DO concentrations to see more clearly how DO is dispersed around the ditch. The flow pattern of air which is very similar is shown in Figure 5.31. The distribution of the volume fraction of air predicted by the multi-phase flow model shows there are high air concentrations near the diffusers and Fuch jet aerators and some radial spreading of air (Figure 5.32). The interfacial mass transfer of oxygen from the air to

the water phase (Figure 5.33) is localised around the aerators in OD2, which is a similar phenomena that is found in OD1. The distributions of mass fraction of oxygen in water, DO concentrations (Figure 5.34) and DO saturation concentrations have the same distributions due to their mathematical equivalence.

The difference between the DO distribution in OD1 (Figure 5.28) and OD2 (Figure 5.34) - for a uniform BOD - is mostly due to the aeration systems. The range of DO concentrations is the main difference: 0 -> 1.26 mg/l (OD1) and 0 -> 3.07 mg/l (OD2). The maximum DO concentration in OD1, with a uniform BOD (Figure 5.28) is near the surface, diffuser and Maguire jet aerators. In OD2 there are no surface aerators but instead there are diffusers and air jet aerators. The maximum DO in OD2 with a uniform BOD is near the Fuch jet aerators and diffusers (Figure 5.34). The effect of surface aeration in OD1 is to spread DO in a plume like pattern (Figure 5.28). Away from the surface aerators the DO concentrations are more homogeneous and better mixed (Figure 5.28). In OD2 there is gradual diffusion of DO in the direction of flow (Figure 5.34). In OD2 there are local high concentrations of DO (Figure 5.34) caused by the submerged air jets. However, in quite a lot of OD2 there are very low DO concentrations (Figure 5.34). The highest DO concentrations in OD2 are near the diffusers and Fuch jet aerators. In OD1, the mean saturation concentration of DO in the ditch is 4 % and it reaches a maximum of 12 % of saturation (near the aerators) when there is a uniform BOD (Figure 5.28). In OD2, the mean saturation concentration of DO in the ditch is 5 % and reaches a maximum of 29 % of saturation (near Fuch air jet aerators) for uniform BOD (Figure 5.34).

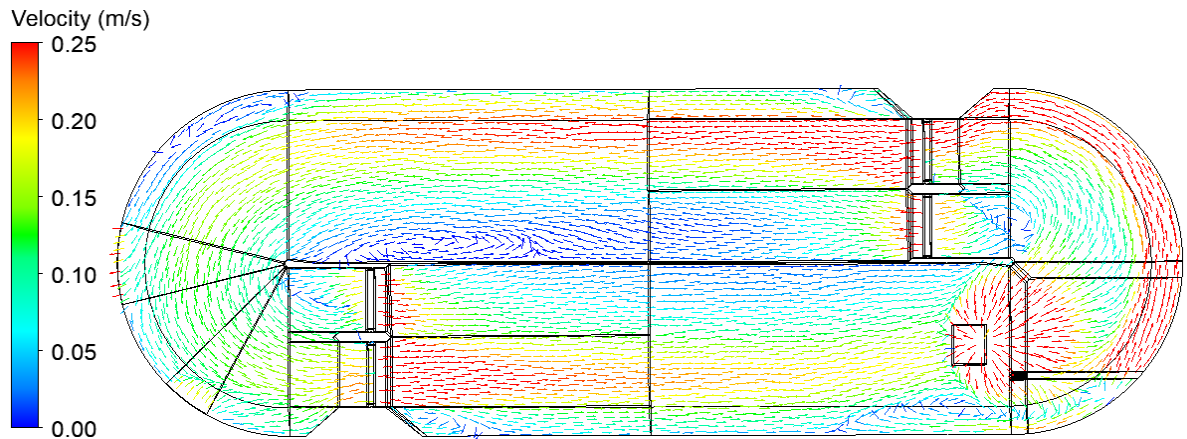


Figure 5.27 Water velocity in OD1 - operating conditions

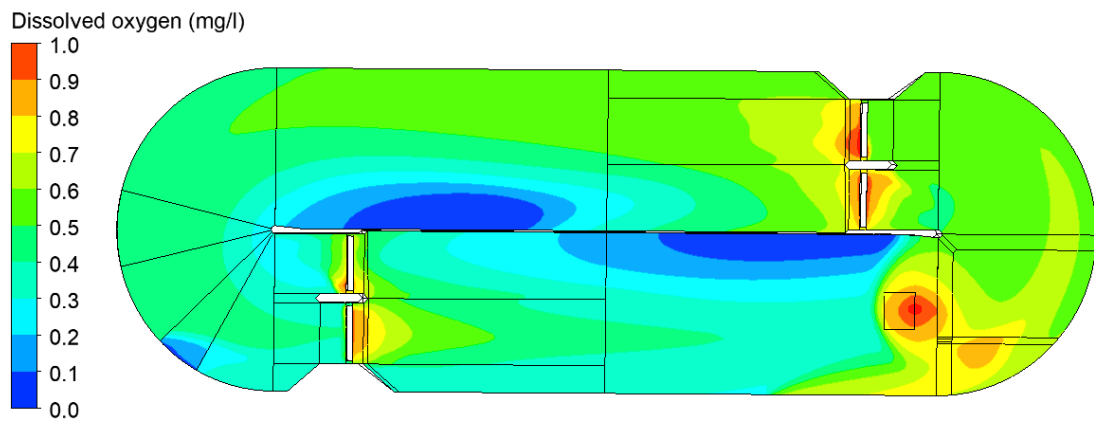


Figure 5.28 DO concentration in OD1 - operating - uniform BOD (15 mg/l)  
(max = 1.26 mg/l, mean = 0.41 mg/l)

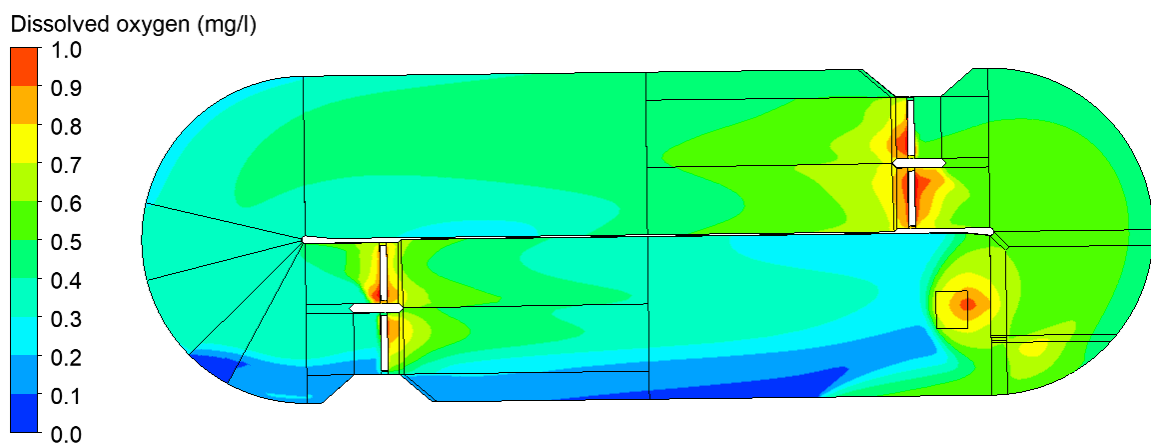


Figure 5.29 DO concentration in OD1 - operating - distributed BOD  
(max = 1.24 mg/l, mean = 0.42 mg/l)

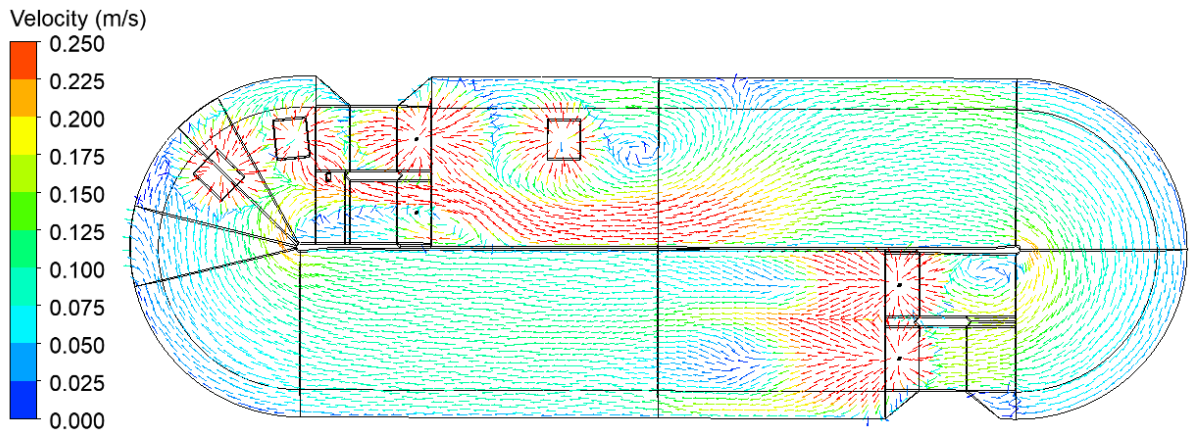


Figure 5.30 Water velocity in OD2 - operating conditions

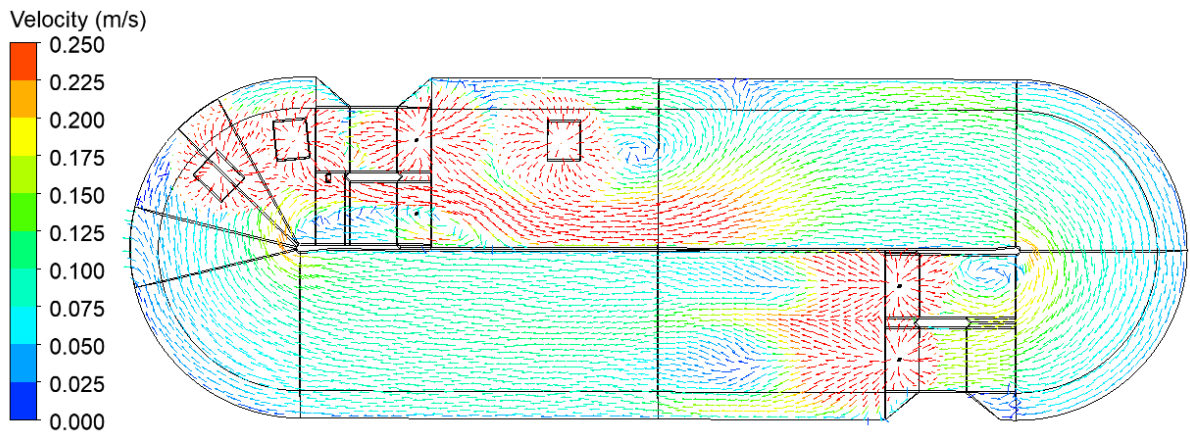


Figure 5.31 Air velocity in OD2 - operating

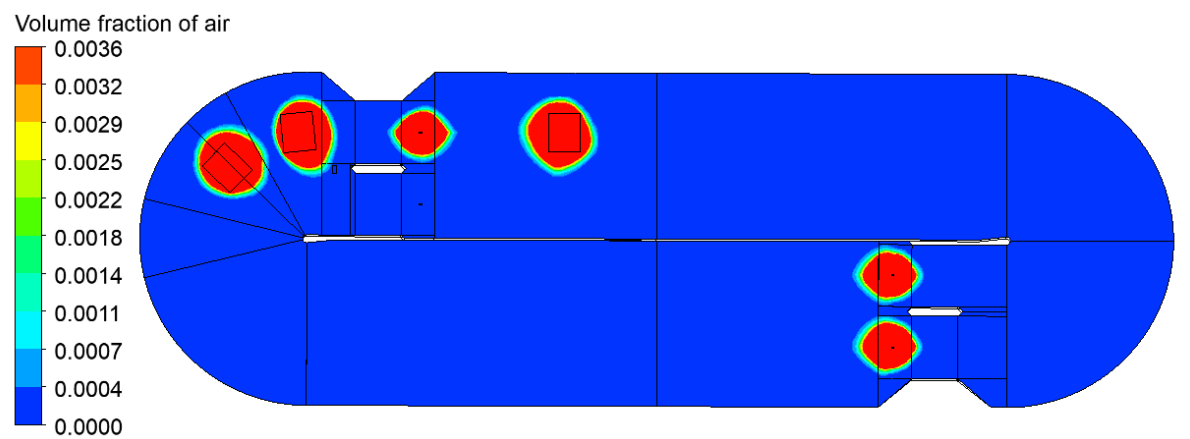


Figure 5.32 Volume fraction of air in OD2 - operating

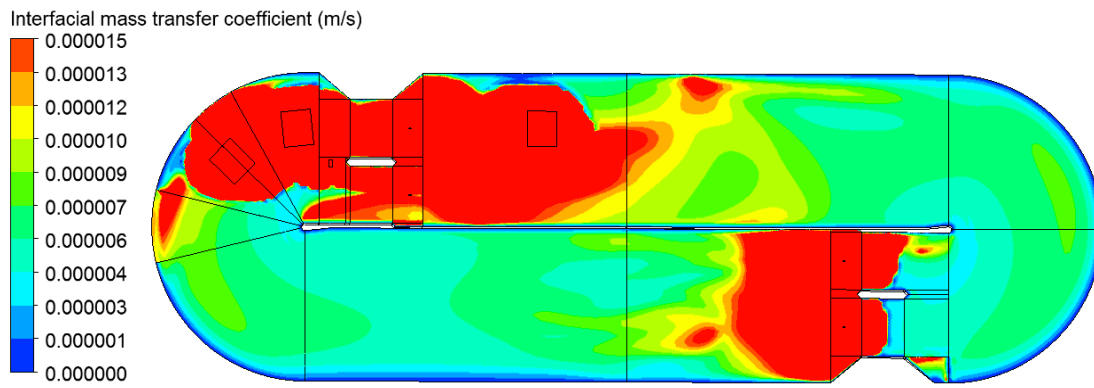


Figure 5.33 Mass transfer coefficient in OD2 - operating

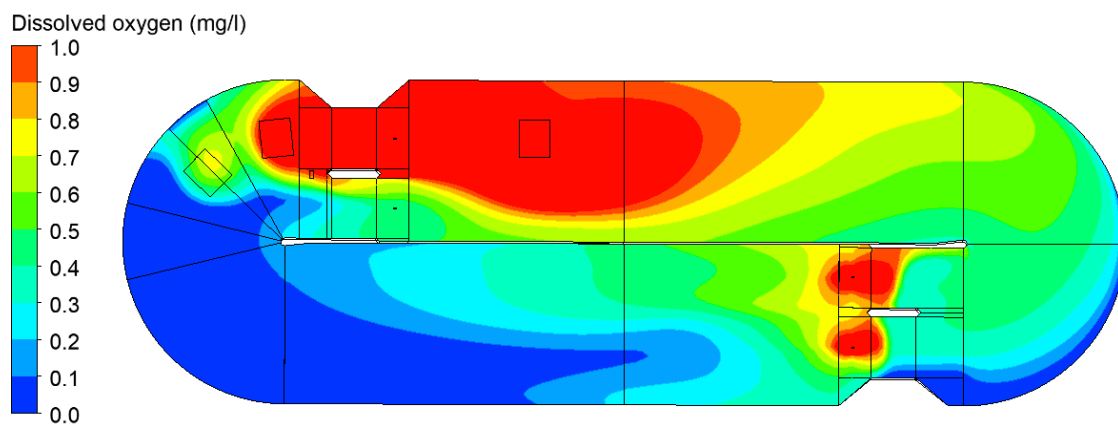


Figure 5.34 DO concentration in OD2 - operating - uniform BOD (15 mg/l)  
(max = 3.07 mg/l, mean = 0.52 mg/l)

## 5.5 Summary

In this chapter firstly is the DO distribution without the effect of BOD to illustrate how each aerator affects the dissolved oxygen. Moreover, the effect of BOD on the DO distribution is predicted to represent the process conditions at Potterne WWTP. Local BOD can depend on either local DO or local residence time. The reduction of DO is modelled by an oxygen sink term throughout the ditch that depends solely on the local BOD. This is modelled with both a uniform and distributed BOD in the ditch.

*The overall benefits for oxidation ditch design are as follows.* In OD1, the DO is dispersed quite evenly around the ditch by the surface aerators, diffuser and Maguire jet aerator. There is a desirable zonal DO pattern with the diffuser. In OD1, the highest DO is near the surface aerators and above the Maguire jet aerator and diffuser. In OD1, the diffuser provides a higher mean DO (52 % of saturation), with a lower oxygen supply than the surface aerators (24 %) and a much higher DO than the Maguire jet aerator (4 %). In OD2, the DO distribution from the diffusers is zonal which is desirable. The diffusers provide a high mean DO in OD2 (83 %), with a lower oxygen supply than the Fuch jet aerators. The Fuch aerators bi-directionally spread DO which creates a desirable zonal DO pattern. Fuch aerators still provide a considerable mean DO in OD2 (57 %) by having a pure air source. In OD2, the DO is highest near the aerators, while in most of the ditch it is quite homogeneous which is desirable. There is improved homogenisation of DO by the fluid mixing of the surface aerators, Maguire aerator and booster. The difference between the DO distribution in the ditches is due to the aeration systems. With a uniform BOD modelled in OD1, the mean DO is 4 % of saturation and maximum DO is 12 %. With a uniform BOD in OD2, the mean DO is 5 % of saturation and maximum DO is 29 %.

*The overall drawbacks for oxidation ditch design are as follows.* The DO is low in most of OD1 when using the Maguire jet aerator suggesting it is an ineffective aerator, with a low oxygen supply from an aerated water stream. Fuch jet aerators in OD2 form a complex flow pattern, as the air jets cause water to flow bi-directionally. Near to each diffuser there is considerable flow recirculation. The influent flow stream lowers DO near two of the diffusers in OD2. There is a sudden drop of DO in OD2 by the mixing of opposing water streams with different DO concentrations.

## **6. Parameter study**

### **6.1 Introduction**

The bubble size has an effect on the flow pattern by the inter-phase momentum transfer of the drag force of the bubble (Karpinska et al, 2016). The bubble size has an effect on the dissolved oxygen distribution by the inter-phase mass transfer through the air/water interface of the surfaces of the bubbles (Karpinska et al, 2016). Bubbles break up and coalesce due to their interactions with turbulent eddies which result in a bubble size distribution (BSD), which is a key parameter for oxygen mass transfer (Potier et al, 2005; Lei and Ni, 2014). The oxygen mass transfer can be increased by increasing the interface area between the water and air by reducing the bubble size (Fayolle et al, 2007). It can also be increased by increasing the oxygen transfer rate (OTR) of the surface aerators (Degremont, 2007).

Numerous studies simulate bubbly flow in an aeration tank, but only with a fixed mean bubble diameter (Cockx et al, 2001). It is proposed that the effects of BSD and mass diffusivity on oxygen transfer should be investigated (Le Moullec et al, 2010b). The multiphase flow modelling that incorporates BSD requires a population balance model (PBM) (Bridgeman, 2009). PBM with bubble breakage and coalescence models are coupled to the multi-phase multi-fluid model in order to predict the BSD in the ditch (Dhanasekharan et al, 2005). The species transport equation is the most commonly used model for predicting the DO distribution (Littleton et al, 2007a; Yang et al, 2011; Guo et al, 2013) and the oxygen mass transfer (Karpinska et al, 2016).

In this chapter the species transport model predicts the DO and BOD distribution that is based on the multi-phase flow pattern. This is undertaken in only one oxidation ditch (OD1) and only for the operating conditions in Potterne WWTP. There is a two way coupled relationship between BOD and DO. The de-aeration of DO is modelled with both a uniform BOD and a distributed BOD. The effect on the DO concentration by the mean bubble size, BSD, seasonal temperature, surface aeration, mass diffusivity, turbulent Schmidt number and Henrys law coefficient are studied.

## 6.2 Theory

To simulate the oxygen concentration in the air and water phases and the BOD concentration in the water phase, the species transport equation is used (5.1). The bubble drag law uses the concept of the mixture Reynolds number (equation 2.20) for spherical bubbles (Ishi and Zuber, 1979). Interfacial oxygen mass transfer uses Higbie's film penetration theory (Higbie, 1935; Terashima et al, 2016). The local mass transfer coefficient is spatially distributed (equation 2.6). It depends on the local distributed quantities predicted by the multi-phase flow simulation: air velocity, water velocity, air volume fraction and bubble diameter. In this chapter both uniform and distributed bubble sizes are simulated. Bubble size distribution has an effect on the oxygen mass transfer distribution. The oxygen transfer rate (OTR) of spray water in air is the main oxygen transfer process for high-speed surface aerators (McWhirter et al, 1995; Huang et al, 2009) - equation 2.14. For dissolution/absorption of oxygen gas into liquid water, Henry's Law describes the equilibrium condition between the two phases (equation 5.9).

*Equations for interfacial oxygen mass transfer, oxygen transfer rate of surface aeration, bubble drag, bubble size distribution, species transport and dissolution of oxygen are in sections 2.3.1, 2.3.2, 2.3.4, 5.2.2 and 5.2.7 respectively.*

## 6.3 Numerical methods

### 6.3.1 Species transport modelling and boundary conditions

The multi-phase flow pattern and the volume fraction distribution of water and air are predicted in Chapter 4. The multi-phase flow equations are not solved further in order to maintain a steady-state flow pattern. The mass fractions of the scalars of the oxygen in the air phase, oxygen in the water phase and BOD in the water phase are simulated by the species transport model. Inter-phase oxygen mass transfer from the air to water phase is also simulated using species transport. The dissolution of oxygen into water that provides the dissolved oxygen uses Henry's law.

To calculate the BOD distribution the BOD species transport equation includes a sink term in order to model the reduction of BOD by DO (equation 5.4). The BOD sink term (negative kg/s of BOD) is applied to the whole of the ditch. The BOD sink term is adjusted to give a BOD distribution that has a minimum BOD concentration of 0 mg/l in the ditch. To calculate the DO distribution the oxygen species transport equation includes a sink term in order to model the reduction of DO by BOD (equation 5.7). The DO sink term (negative kg/s of DO) is applied to the whole of the ditch. There are two methods to predict the DO distribution that includes the effect of the biochemical oxygen demand: (1) uniform BOD and homogeneous oxygen sink in ditch; (2) BOD distribution and heterogeneous oxygen sink in ditch. The uniform BOD concentration is the mean value of the BOD distribution. The *boundary conditions for multi-phase and multi-component flow modelling are the same as in the previous chapter on dissolved oxygen modelling.*

### **6.3.2 Bubble size distribution (BSD)**

This study investigates the effect of bubble size distribution on the DO distribution in OD1. The poly-disperse homogeneous multiple size group model (Lo, 1998) predicts the BSD. The MUSIG model (Lo, 1998) is used considerably in industrial bubbly flow. It solves the continuity and momentum equations in an Euler-Euler framework for the continuous phase (liquid) and for one single disperse phase (gas). Continuity equations for different bubble size groups are solved. The bubble coalescence and break-up are based on the population balance method. Bubble coalescence and break-up uses the models of Prince & Blanch, 1990 and Luo and Svendsen, 1996. The performance of the homogeneous MUSIG model is limited to convective bubbly flow (for example in stirred vessels) and a homogeneous velocity field in all bubble size classes (Frank et al, 2005). The homogeneous MUSIG model is not suitable, for example, for the multiple fluid regimes in gas-liquid pipe flow (bubbly, slug, churn turbulent, annular, droplet). It is however sufficient for the flow in large tank volumes such as in aeration tanks, where the fluid regime is mainly bubbly flow, and non-drag forces are not as important, such as the lateral lift force (Frank et al, 2005). In this study there is subdivision of the full range of bubbles sizes in the ditch into distinct classes. In most cases 3 or 4 groups is sufficient (Frank et al, 2005). The full range is

0 - 8 mm with 4 subdivisions (0-2, 2-4, 4-6, 6-8 mm), that is based on a mean bubble size of 4 mm in the standard model. The lower and upper boundaries of the bubble diameter intervals for the size classes is controlled by either equal bubble diameter discretisation or equal bubble mass discretisation (Lo, 1998).

### **6.3.3 Parameter study**

Different parameters are studied to see what effect they have on the DO distribution. The 'standard' CFD model (Table 6.1) has a mean bubble size of 4 mm, physical properties at the mean annual temperature of 13 °C at Potterne WWTP and mass transfer coefficient of surface aeration is 3 h<sup>-1</sup>. Summer conditions at 20 °C are also simulated that affect the physical properties (density, viscosity, saturation DO, mass diffusivity, turbulent Schmidt number, Henrys law coefficients). No physical measurement is taken of mass transfer coefficient of the surface aerators at Potterne WWTP. The K<sub>L</sub>a value for the brush aerators at 70 rpm is 3 h<sup>-1</sup>, which is taken from the literature (Thakre et al, 2008). A further boundary condition modelled is a fourfold increase in K<sub>L</sub>a to 12 h<sup>-1</sup> for surface aeration. Different mean bubble sizes (3, 2, 1 mm) and a BSD are modelled. Different values of mass diffusivity and turbulent Schmidt numbers of the BOD scalar in the water phase, oxygen scalar in the air phase and oxygen scalar in the water phase are modelled. Different values of molar concentration Henry coefficient and molar fraction Henry coefficient are modelled.

### **6.3.4 Numerical convergence**

To decrease the computational duration of the species simulation, only mass fraction equations of DO and BOD scalars are solved and not the flow equations of mass, momentum, turbulence and volume fraction, so that the multi-phase flow pattern is kept at steady-state. The species transport equations are solved iteratively to steady-state. The convergence rate is improved further by using an under relaxation factor (0.3) for the scalar equations. The convergence is achieved when all the scalar equations reach a convergence criteria of 10<sup>-6</sup>. The rate of convergence is fast and convergence is achieved between 3000 and 10000 iterations. Computer hardware is a 2.50 GHz processor (8 CPUs) with 16 GB RAM. Simulations are speeded up by parallel processing. Duration of all species simulations is between 15 and 30 hours.

## 6.4 Results and discussion

Table 6.1 gives the physical properties at the mean annual temperature of 13 °C (blue) and mean summer temperature of 20 °C (purple). Dry oxygen occupies about 21% by volume of dry air. Oxygen has a higher density and viscosity than air (Çengel and Boles, 2008). At the mean annual temperature of 13 °C at Potterne WWTP, the saturation DO concentration is 10.5 mg/l and at 20 °C it is 9.1 mg/l (Degremont, 2007). This is the upper limit of the DO concentration. The standard mass fraction of oxygen in dry air is 0.229 at 1 atm pressure and 20 °C (Çengel and Boles, 2008). The mass diffusivity of DO in water is much lower than it is for dry oxygen in air (Çengel and Boles, 2008). In the literature the mean bubble size in an oxidation ditch in the CFD models is around 4 mm. The physical properties are dependent on the temperature (purple). Some parameters can be changed independently (orange). These are the mean bubble diameter, bubble size distribution and the OTR of surface aeration. Other parameters (green) depend on each other: mass diffusivity, turbulent Schmidt number and Henry law coefficient. Different parameters are studied to see what effect they have on the DO distribution.

Table 6.1 Physical properties of parameter study in OD1

Physical Property	Annual	Change	Summer	Units
temperature	13	13	20	°C
density of water	999.4	999.4	998.2	kg/m <sup>3</sup>
density of air	1.233	1.233	1.204	kg/m <sup>3</sup>
density of oxygen	1.370	1.370	1.314	kg/m <sup>3</sup>
viscosity of water	0.0012	0.0012	0.0010	kg/ms
viscosity of air	1.79x10 <sup>-5</sup>	1.79x10 <sup>-5</sup>	1.81x10 <sup>-5</sup>	kg/ms
viscosity of oxygen	2.01x10 <sup>-5</sup>	2.01x10 <sup>-5</sup>	2.03x10 <sup>-5</sup>	kg/ms
bubble diameter	4	3, 2, 1; BSD	4	mm
mass transfer of surface aeration	3	12	3	h <sup>-1</sup>
mass fraction of oxygen in air	0.233	0.233	0.229	-
saturation of air in water (volume fraction)	0.036	0.036	0.032	-
saturation of DO in water	10.5	10.5	9.1	mg/l
mass diffusivity of oxygen in air	1.26x10 <sup>-5</sup>	2.52x10 <sup>-5</sup> , 0.63x10 <sup>-5</sup>	1.58x10 <sup>-5</sup>	m <sup>2</sup> /s
mass diffusivity of oxygen in water	1.2x10 <sup>-9</sup>	2.4x10 <sup>-9</sup> , 0.6x10 <sup>-9</sup>	1.9x10 <sup>-9</sup>	m <sup>2</sup> /s
mass diffusivity of BOD in water	3.5x10 <sup>-9</sup>	7x10 <sup>-9</sup> , 1.75x10 <sup>-9</sup>	5.5x10 <sup>-9</sup>	m <sup>2</sup> /s
turbulent Schmidt number of oxygen in air	0.7	1.4, 0.35	0.7	-
turbulent Schmidt number of oxygen in water	0.7	1.4, 0.35	0.7	-
turbulent Schmidt number of BOD in water	0.7	1.4, 0.35	0.7	-
molar concentration Henry coefficient	61636	123272, 30818	70998	Pa.m <sup>3</sup> /mol
molar fraction Henry coefficient	3.4x10 <sup>9</sup>	6.8x10 <sup>9</sup> , 1.7x10 <sup>9</sup>	3.9x10 <sup>9</sup>	Pa

#### 6.4.1 Dissolved oxygen distribution without BOD for model parameters

Table 6.2 shows for different model parameters, the predicted mean and maximum DO in ditch OD1 at the operating conditions in Potterne WWTP, without any effect of the BOD. The 'standard' model has a mean bubble size of 4 mm, mean annual temperature of 13 °C (Table 6.1) and mass transfer coefficient of surface aeration of 3 h<sup>-1</sup>. Summer conditions are at 20 °C (Table 6.1), surface aeration is at 12 h<sup>-1</sup>, mean bubble sizes (3, 2, 1 mm) and BSD are simulated. Other parameters simulated are the mass diffusivity, turbulent Schmidt number and Henry law coefficients. In the results in Table 6.2 the parameters shown in red are found to have a significant effect on the mean dissolved oxygen in the ditch.

Table 6.2 Effect of parameters on dissolved oxygen - without BOD in OD1

Parameter	Value	Unit	Mean mass transfer, $K_L \times 10^{-5}$ (m/s)	Mean DO (mg/l)	Max DO (% sat)	Mean DO (% sat)	$\Delta$ Mean DO (% sat)
standard (13 °C)	Table 6.1	-	1.119	3.46	39	33	-
summer (20 °C)	Table 6.1	-	1.084	3.43	45	38	+5
surface aeration	12	h <sup>-1</sup>	1.125	3.90	46	37	+4
bubble diameter	3	mm	1.274	4.44	50	42	+9
bubble diameter	2	mm	1.476	5.72	64	55	+22
bubble diameter	1	mm	1.783	7.23	78	69	+36
bubble size distribution (BSD)	1 → 6.3 (mean = 1.9)	mm	1.387	3.15	37	30	-3
molar fraction Henry coefficient	6.8x10 <sup>9</sup> / 1.7x10 <sup>9</sup>	Pa	-	1.74 / 6.81	20 / 78	17 / 65	-16 / +32
mass diffusivity of oxygen in water	2.4x10 <sup>-9</sup> / 0.6x10 <sup>-9</sup>	m <sup>2</sup> /s	-	4.23 / 2.75	48 / 31	40 / 26	+7 / -7
turbulent Schmidt of oxygen in water	1.4 / 0.35	-	-	3.54 / 3.31	41 / 37	34 / 32	+1 / -1
mass diffusivity of oxygen in air	2.52x10 <sup>-5</sup> / 0.63x10 <sup>-5</sup>	m <sup>2</sup> /s	-	3.46	39	33	0
mass diffusivity of BOD in water	7x10 <sup>-9</sup> / 1.75x10 <sup>-9</sup>	m <sup>2</sup> /s	-	3.46	39	33	0
turbulent Schmidt of oxygen in air	1.4 / 0.35	-	-	3.46	39	33	0
turbulent Schmidt of BOD in water	1.4 / 0.35	-	-	3.46	39	33	0
molar concentration Henry coefficient	123272 / 30818	Pa.m <sup>3</sup> /mol	-	3.46	39	33	0

Parameters that have a significant effect on the dissolved oxygen (Table 6.2) are temperature, mean bubble size, BSD, OTR of surface aeration, molar fraction Henry coefficient, mass diffusivity of oxygen in water and turbulent Schmidt number of oxygen in water. There is an inverse linear relationship between the molar fraction Henry coefficient and the DO and the gradient of this relationship is 1. There is a direct linear relationship between the mass diffusivity of oxygen in water and the DO. When there is no oxygen demand from BOD, the 'standard' model predicts a mean DO in ditch OD1 of 33 % of saturation (Table 6.2). By decreasing bubble size, the total interfacial surface area of the bubbles increases significantly and the oxygen mass transfer increases. For a mean bubble size of 3 mm, mean DO in ditch OD1 increases to 42 % of saturation; for 2 mm bubble size it increases to 54 % of saturation; and for 1 mm bubble size it increases to 69 % of saturation.

The bubble size distribution (BSD) predicts a mean bubble size of 1.9 mm. The mean interfacial oxygen mass transfer in the ditch increases by 24 % (compared to the 'standard' model). This is comparable to the mass transfer of a bubble between 2 and 3 mm. The maximum mass transfer in the ditch is also increased and is comparable to a bubble between 1 and 2 mm. However, with a BSD the mean DO in the ditch is reduced only slightly to 30 % of saturation. When the OTR of surface aeration is increased fourfold, the mean DO increases from 33 to 37 % of saturation. For an increase in temperature from 13 to 20 °C, the DO saturation concentration drops from 10.5 to 9.1 mg/l and mean saturation DO actually rises from 33 to 38 %.

For the 'standard' model, the flow pattern in OD1 predicts flow plumes from the surface aerators, strong flow stream from the Maguire jet aerator and radial flow from the diffuser (Figure 6.1). Inter-phase oxygen mass transfer (Figure 6.2) is highest near the aeration sources (surface, diffuser, jet, influent). There is little oxygen mass transfer in the rest of the ditch. The highest DO concentrations are near the surface aerators and the diffuser (Figure 6.3). There is a drop in DO from the internal wall to the outside wall of the ditch. Near the influent there are lower DO concentrations.

For an increase in temperature to 20 °C, there is little difference to the water flow pattern. The DO distribution is also hardly affected, except magnitudes are lower near the surface aerators (Figure 6.4). When the surface aeration is increased, there

is stronger bi-directional flow from the aerators (Figure 6.5). There is also a significant increase in DO within the plumes of the surface aerators (Figure 6.6).

When mean bubble size decreases from 4 to 3 mm the water flow pattern changes only slightly. However, the DO concentrations increase by about 1 mg/l and the DO distribution is affected (Figure 6.7). The DO distribution is quite similar to the case with increased surface aeration (Figure 6.6). When mean bubble size decreases from 4 to 2 mm the water flow pattern changes very slightly. However, DO concentrations increase by about 2 mg/l. The DO distribution for a 2 mm mean bubble size (Figure 6.8) is quite similar to a 3 mm size (Figure 6.7), but with higher magnitudes of DO. When mean bubble size decreases from 4 to 1 mm, the water flow pattern only changes slightly. However, DO concentrations increase by about 4 mg/l. Moreover, the DO distribution for a 1 mm bubble size is different to the other bubble sizes (Figure 6.9). The DO distribution for 4, 3 and 2 mm bubble sizes appear similar, but with different magnitudes of DO concentration. The air flow pattern for the 1 mm bubble size is different near the Maguire jet aerator (Figure 6.10) and this might explain the effect it has on the DO distribution.

When BSD is predicted for equal diameter discretisation the range of bubble sizes is from 0.99 to 6.32 mm with a mean bubble size of 1.94 mm in the ditch (Figure 6.11). For equal mass discretisation the range is from 1.02 to 6.74 mm with a mean bubble size of 3.36 mm (Figure 6.12). The BSD has a small effect on the DO concentration (Table 6.2). The predicted mean bubble size of 1.94 mm, for equal diameter discretisation, is near to the best value of 2 mm that is determined by comparison to experimental data in the next chapter. The largest bubbles predicted by the BSD are near the surface, diffuser and Maguire jet aerators and the central wall (Figure 6.11).

BSD does not have a significant effect on flow pattern (Figure 6.13). However, it does increase interfacial mass transfer using equal diameter discretisation (Figure 6.14). There is no significant increase in mass transfer with equal mass discretisation (Figure 6.15). The DO distribution is quite similar for the BSD (Figure 6.16) when compared to a mean bubble size of 4 mm (Figure 6.3). The DO distribution does not change significantly with molar fraction Henry coefficient, however its magnitude does change significantly (Figure 6.17). The DO distribution and magnitudes of DO change significantly with the mass diffusivity of oxygen in water (Figure 6.18).

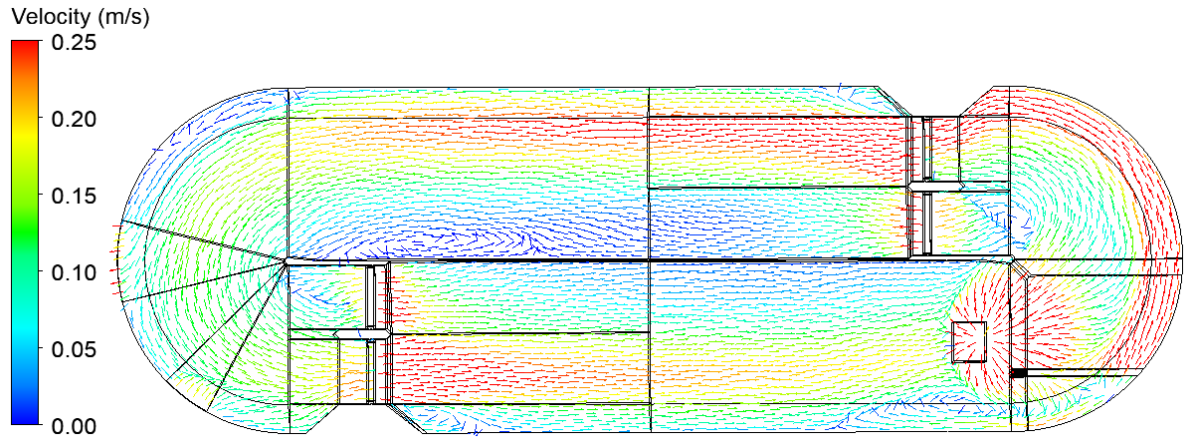


Figure 6.1 Water velocity in OD1 - standard model

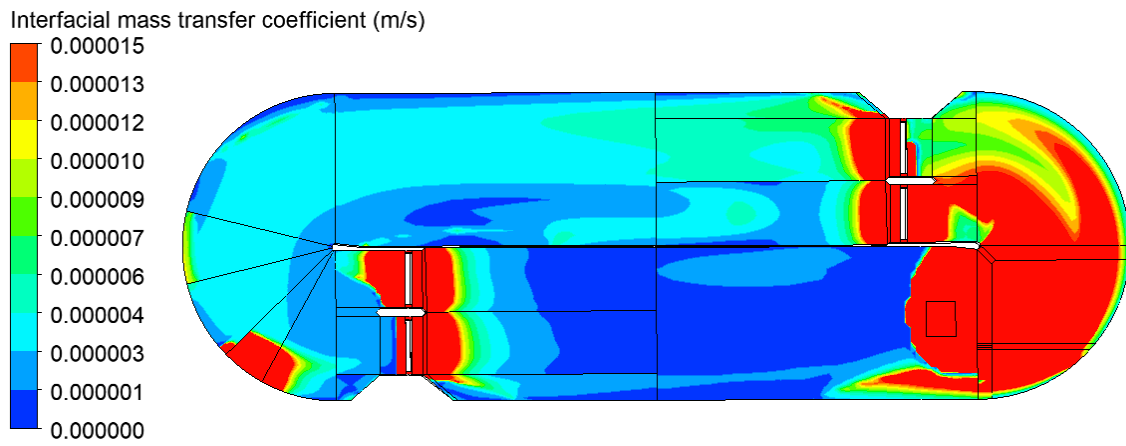


Figure 6.2 Mass transfer coefficient in OD1 without BOD - standard  
(max =  $9.4 \times 10^{-4}$ , mean =  $1.1 \times 10^{-5}$  m/s)

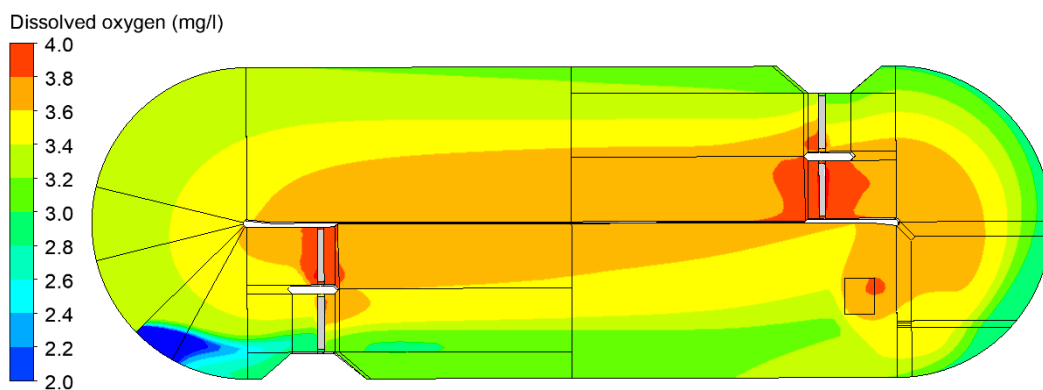


Figure 6.3 DO concentration in OD1 without BOD - standard  
(max = 4.12 mg/l, mean = 3.46 mg/l)

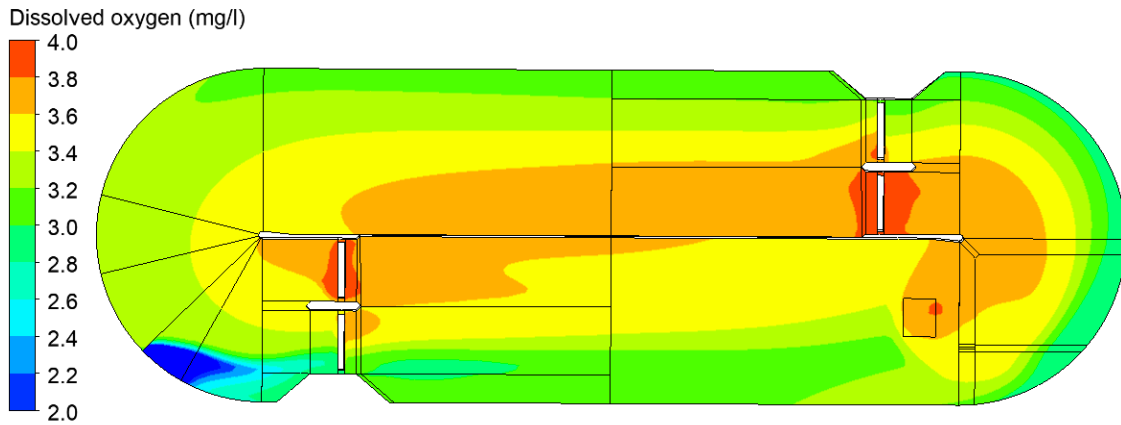


Figure 6.4 DO concentration without BOD - summer (20 °C)  
(max = 4.08 mg/l, mean = 3.43 mg/l)

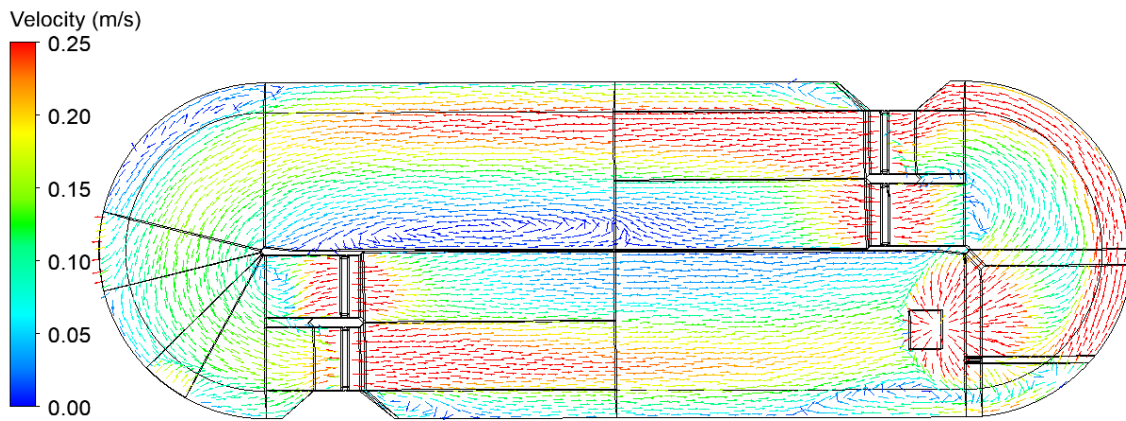


Figure 6.5 Water velocity - surface aeration (12 h<sup>-1</sup>)

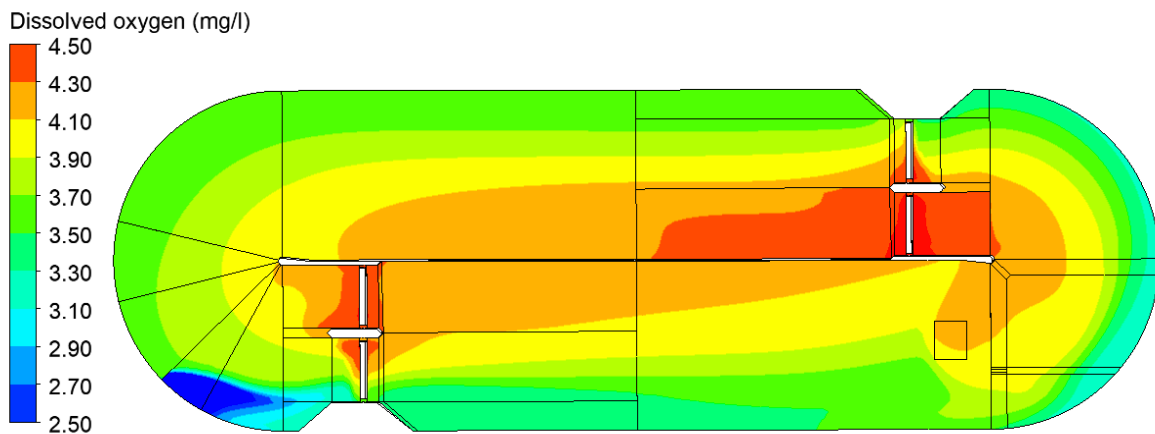


Figure 6.6 DO concentration without BOD - surface aeration (12 h<sup>-1</sup>)  
(max = 4.88 mg/l, mean = 3.90 mg/l)

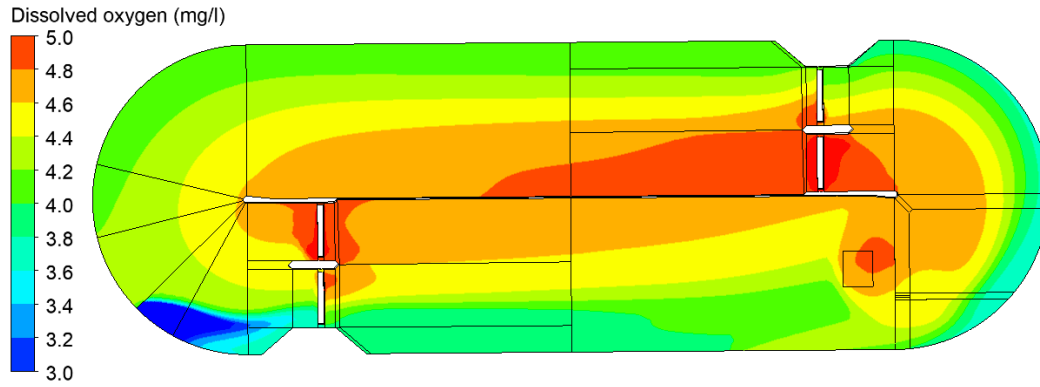


Figure 6.7 DO without BOD - bubble diameter (3 mm)  
 (max = 5.27 mg/l, mean = 4.44 mg/l)

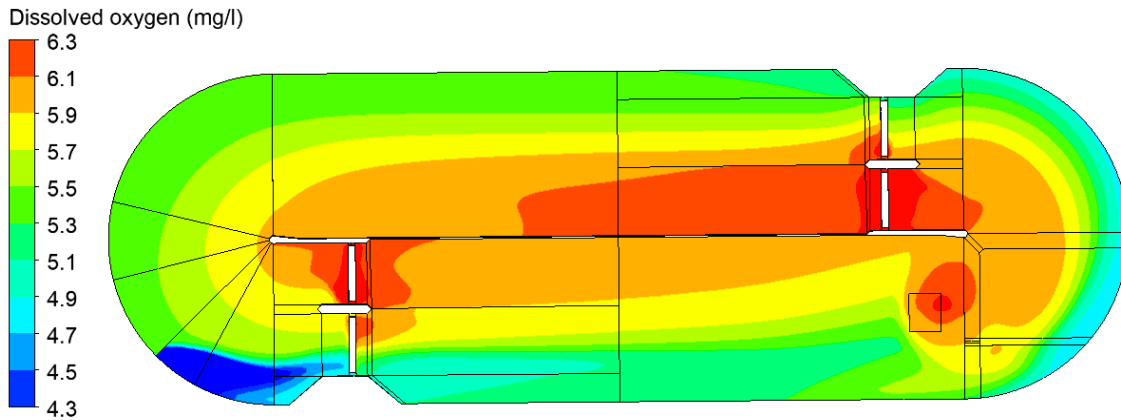


Figure 6.8 DO without BOD - bubble diameter (2 mm)  
 (max = 6.69 mg/l, mean = 5.72 mg/l)

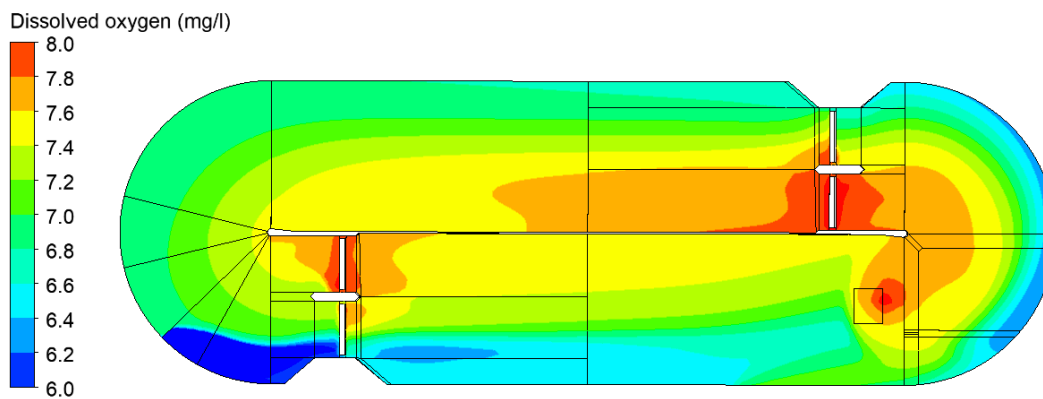


Figure 6.9 DO without BOD - bubble diameter (1 mm)  
 (max = 8.22 mg/l, mean = 7.23 mg/l)

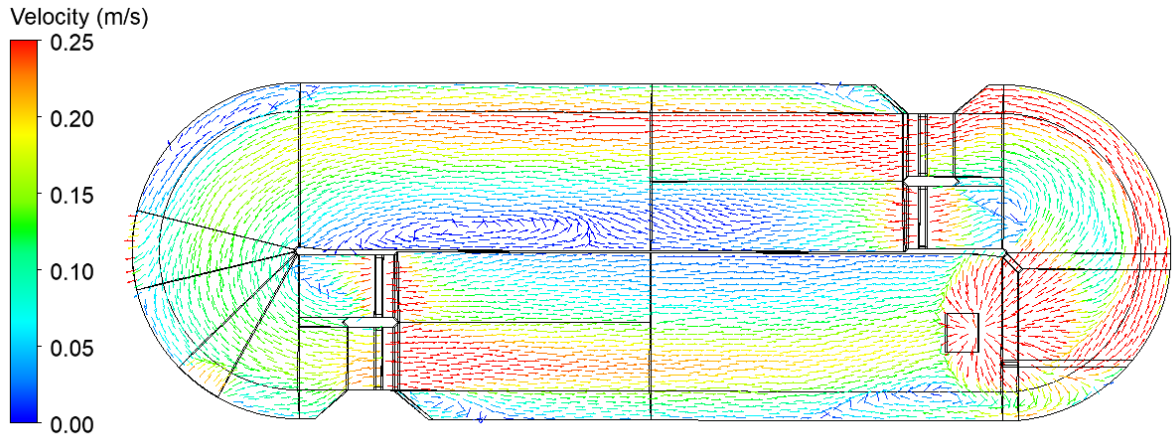


Figure 6.10 Air velocity - bubble diameter (1 mm)

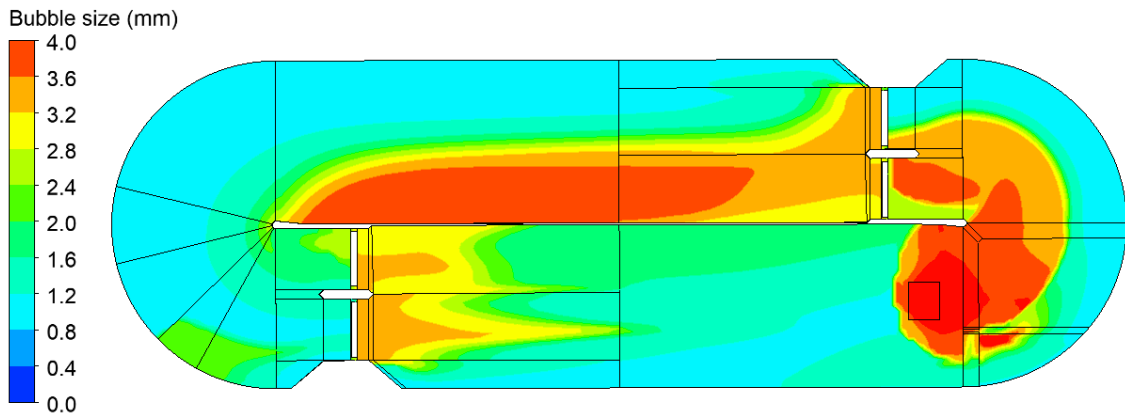


Figure 6.11 BSD without BOD - equal diameter discretisation  
(max = 6.32 mm, mean = 1.94 mm, min = 0.99 mm)

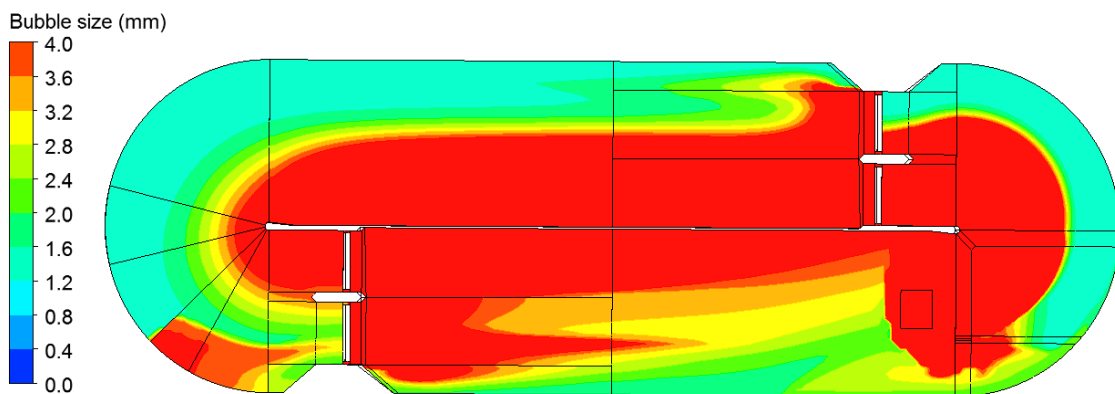


Figure 6.12 BSD without BOD - equal mass discretisation  
(max = 6.74 mm, mean = 3.36 mm, min = 1.02 mm)

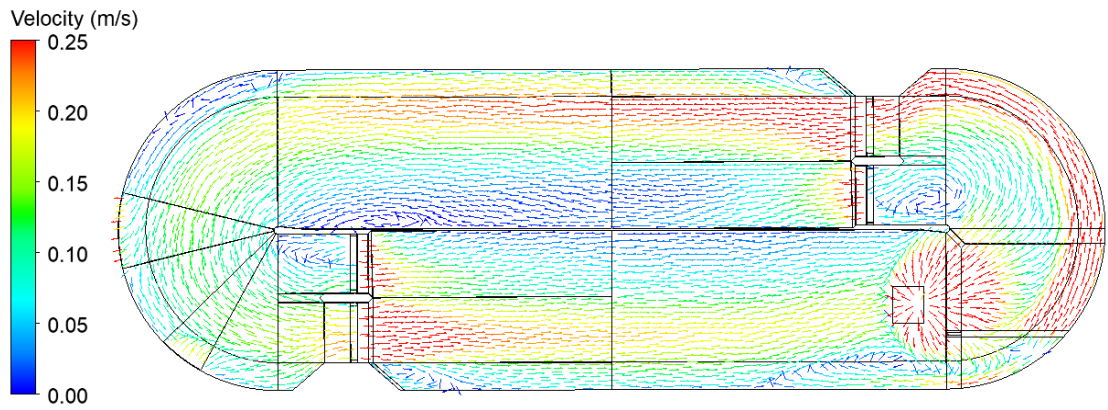


Figure 6.13 Water velocity - BSD - equal diameter discretisation

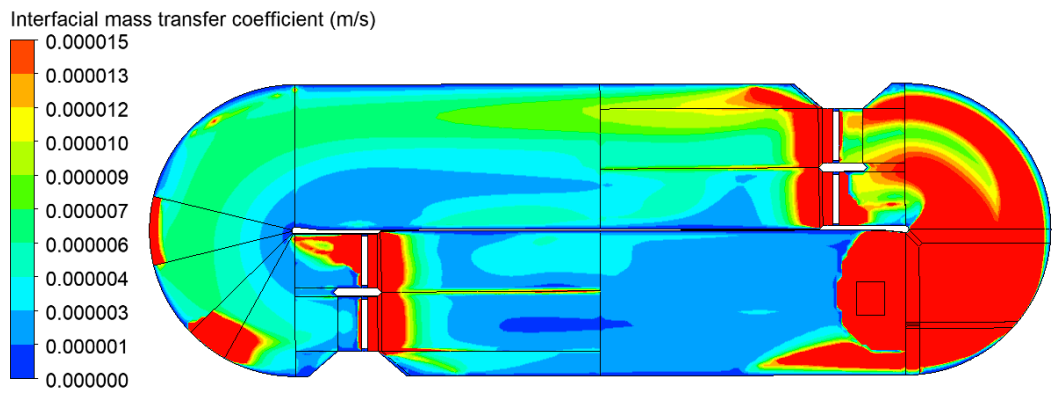


Figure 6.14 Mass transfer without BOD - equal diameter discretisation

(max =  $1.6 \times 10^{-3}$ , mean =  $1.387 \times 10^{-5}$  m/s)

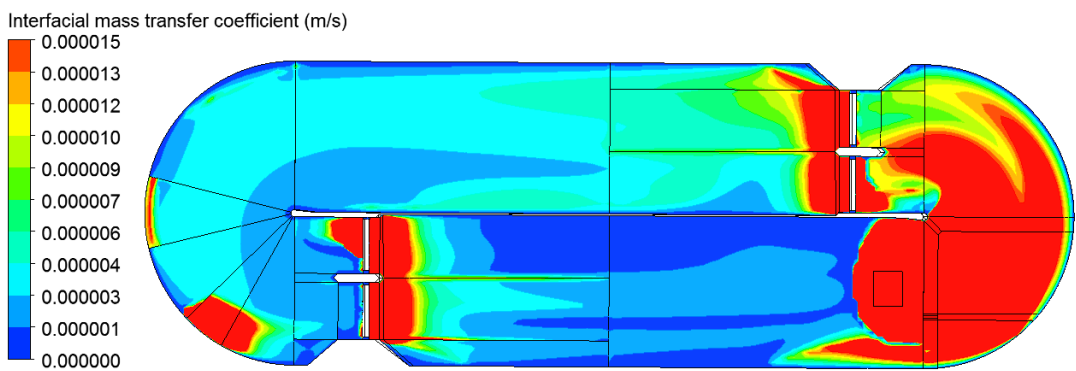


Figure 6.15 Mass transfer without BOD - equal mass discretisation

(max =  $9.4 \times 10^{-4}$ , mean =  $1.087 \times 10^{-5}$  m/s)

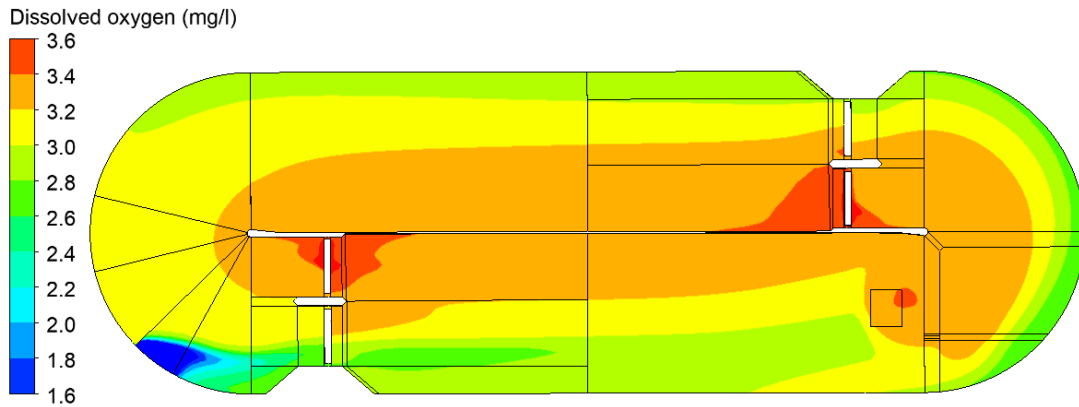


Figure 6.16 DO without BOD - equal diameter discretisation  
(max = 3.87 mg/l, mean = 3.15 mg/l)

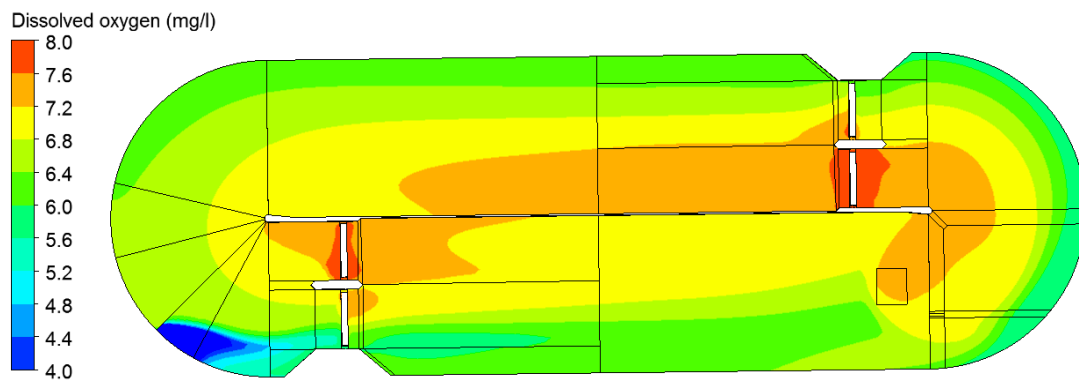


Figure 6.17 DO without BOD - molar fraction Henry coefficient (x 0.5)  
(max = 8.14 mg/l, mean = 6.81 mg/l)

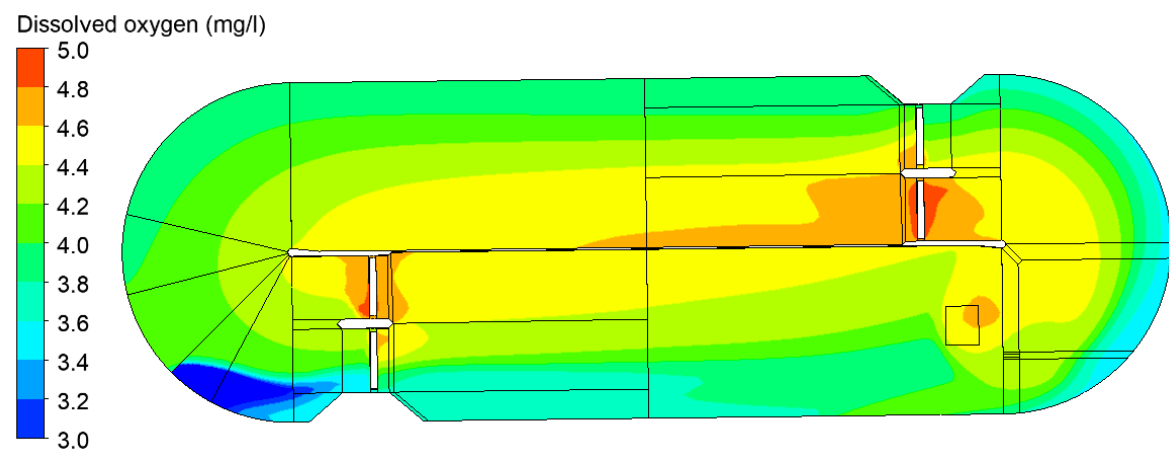


Figure 6.18 DO without BOD - mass diffusivity of oxygen in water (x 2)  
(max = 5.03 mg/l, mean = 4.23 mg/l)

#### 6.4.2 Dissolved oxygen distribution with BOD for parameters

Table 6.3 Effect of parameters on dissolved oxygen - with BOD in OD1

Parameter	Value	Unit	Mean BOD mean / max DO (mg/l)	Distributed BOD mean / max DO (mg/l)
standard (13 °C)	Table 6.1	-	0.41 / 1.26	0.42 / 1.24
summer (20 °C)	Table 6.1	-	0.37 / 1.24	0.40 / 1.25
surface aeration	12	h <sup>-1</sup>	0.39 / 1.86	0.40 / 1.77
bubble diameter	3	mm	0.38 / 1.64	0.40 / 1.62
bubble diameter	2	mm	0.39 / 2.34	0.40 / 2.32
bubble diameter	1	mm	0.38 / 3.58	0.40 / 3.64
bubble distribution	1 → 6.3 (mean=1.9)	mm	0.40 / 1.12	0.40 / 1.21
molar fraction Henry coefficient	1.7x10 <sup>9</sup>	Pa	-	0.40 / 2.07
mass diffusivity of oxygen in water	2.4x10 <sup>-9</sup>	m <sup>2</sup> /s	-	0.40 / 1.53

Comparison between the uniform and distributed BOD for the 'standard' model show that the mean (0.41 and 0.42 mg/l) and maximum (1.26 and 1.24 mg/l) DO concentrations in OD1 are very similar (Table 6.3). For some parameters (temperature and bubble size), there is little change to the mean and maximum DO, when modelling a uniform or distributed BOD (Table 6.3). The main difference is the distribution of DO (Figures 6.19 and 6.20). For a uniform BOD the lowest DO concentrations are near the central wall (Figure 6.19). For a distributed BOD the lowest DO concentrations are downstream of the influent and near the outside wall (Figure 6.20). The predicted BOD distribution in the ditch is quite similar for the different modelling parameters and quite similar for the mean BOD concentration in the ditch (standard: 18 mg/l; temperature (20 °C): 18; surface OTR (x4): 18; bubble size = 3 mm: 17; 2 mm: 17; 1 mm: 16; bubble size distribution: 16).

For summer conditions (20 °C) and uniform BOD (Figure 6.21) and distributed BOD (Figure 6.22), the mean DO in the ditch (0.37 and 0.40 mg/l) and maximum DO (1.24 and 1.25 mg/l) are similar. When surface aeration is increased fourfold there is an

increase in maximum DO to 1.86 mg/l for uniform BOD (Figure 6.23) and 1.77 mg/l for distributed BOD (Figure 6.24). The DO concentrations near the surface aerators increase the most in the ditch. Surface aeration has a bigger effect than temperature.

When bubble size is reduced to 3 mm, the maximum DO concentration increases to 1.64 mg/l for uniform BOD and to 1.62 mg/l for distributed BOD (Figure 6.25). For a 2 mm bubble size, the maximum DO increases further to 2.34 mg/l for uniform BOD, and to 2.32 mg/l for distributed BOD (Figure 6.26). For a 1 mm bubble size, maximum DO increases further to 3.58 mg/l for uniform BOD and 3.64 mg/l for distributed BOD (Figure 6.27). There is an increase in variation of DO in the ditch when bubble size is reduced when the effect of BOD is also modelled. For the smallest bubble size studied (1 mm), DO concentrations are almost zero in many parts of the ditch (Figure 6.27). The local oxygen mass transfer is increased, when bubble size is reduced (Table 6.2) especially around the aerators. Smaller bubbles are less able to transport DO by convection all around the ditch. However, the higher local DO near the aerators are due to increased local oxygen mass transfer. Overall the result is a greater spatial variation of dissolved oxygen when there is a smaller bubble size. The lowest DO in the ditch is found to be furthest downstream from the aerators (Figure 6.27).

Bubble size distribution (BSD) reduces the maximum DO from 1.26 to 1.12 mg/l for uniform BOD (Figure 6.28) and from 1.24 to 1.21 mg/l for distributed BOD (Figure 6.29). Mean BOD in the ditch with a BSD is reduced from 18 to 16 mg/l. The DO distributions for BSD (Figures 6.28 and 6.29) only show slight differences when compared to a uniform bubble size of 4 mm (Figures 6.19 and 6.20). The predicted mean bubble size in the ditch with BSD is 1.9 mm, compared to the standard model of 4 mm. There is a wide range of bubble sizes predicted by BSD from 0.99 to 6.32 mm. The mean interfacial mass transfer in the ditch is 24 % higher with a BSD.

Doubling the mass diffusivity of oxygen in water (distributed BOD) increases the maximum DO to 1.53 mg/l (Table 6.3) and makes DO more heterogeneous. Halving the molar fraction Henry coefficient (distributed BOD) increases the maximum DO to 2.07 mg/l (Table 6.3) and makes DO more heterogeneous. To determine the accuracy of these predictions there is comparison to experimental data for dissolved oxygen in the oxidation ditches at Potterne WWTP in the next chapter.

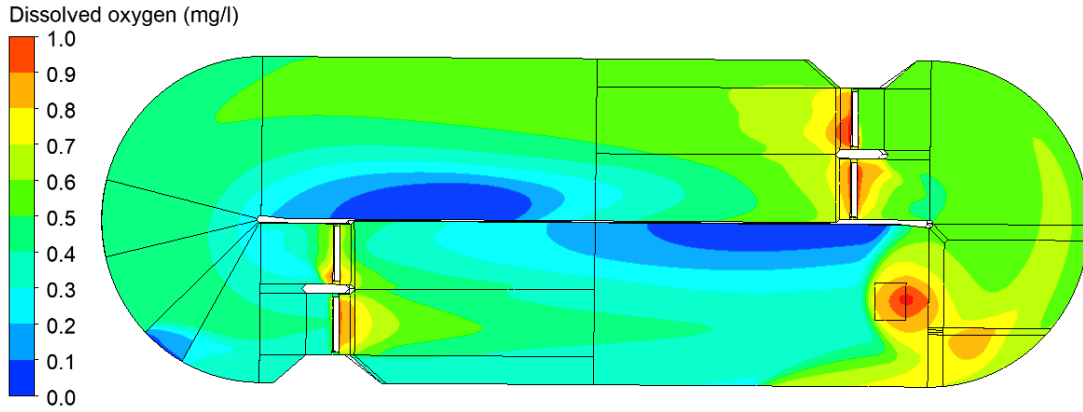


Figure 6.19 DO with uniform BOD - standard model  
 (max = 1.26 mg/l, mean = 0.41 mg/l)

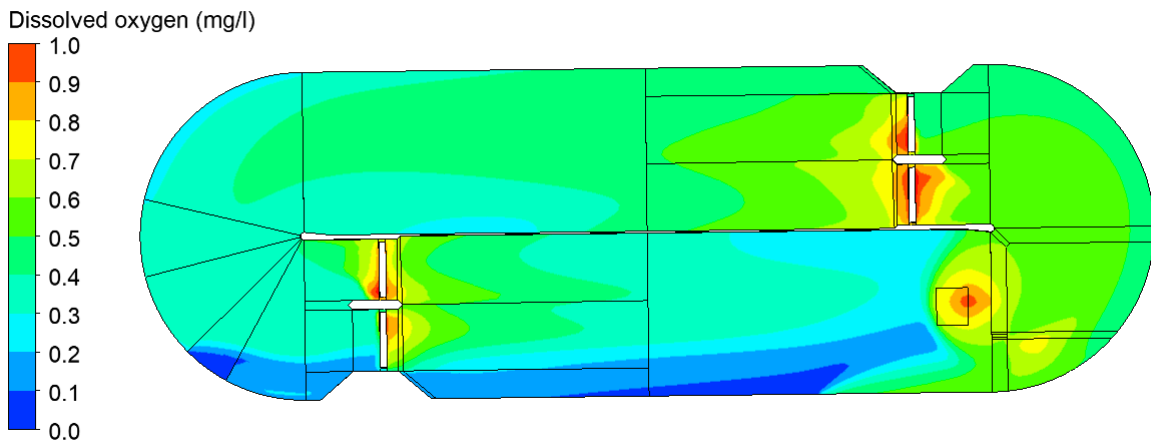


Figure 6.20 DO with distributed BOD - standard model  
 (max = 1.24 mg/l, mean = 0.42 mg/l)

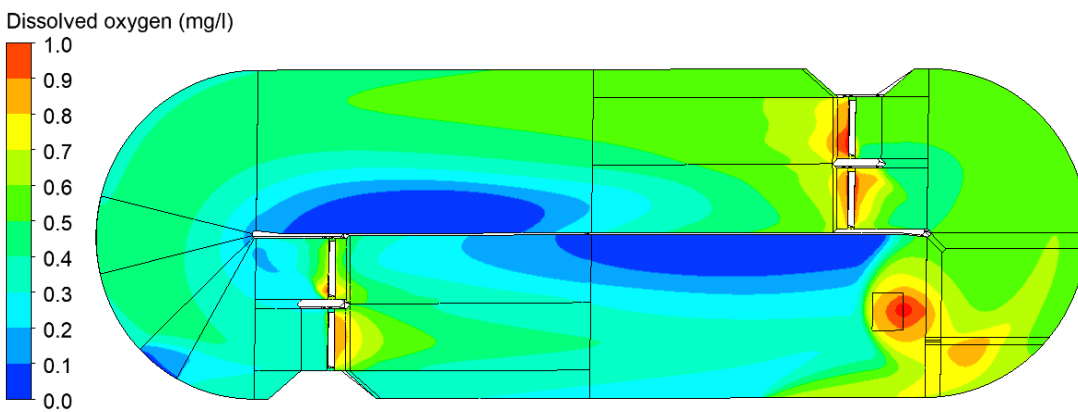


Figure 6.21 DO with uniform BOD - summer (20 °C)  
 (max = 1.24 mg/l, mean = 0.37 mg/l)

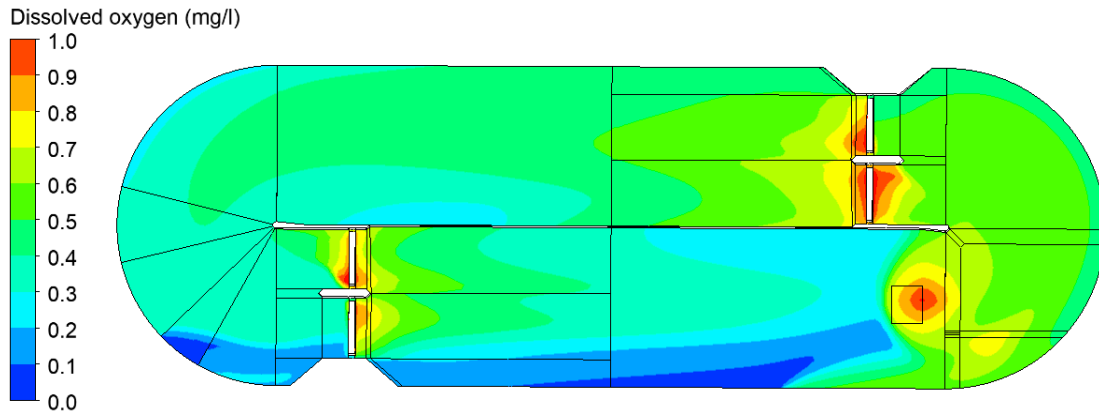


Figure 6.22 DO with distributed BOD - summer (20 °C)  
(max = 1.25 mg/l, mean = 0.40 mg/l)

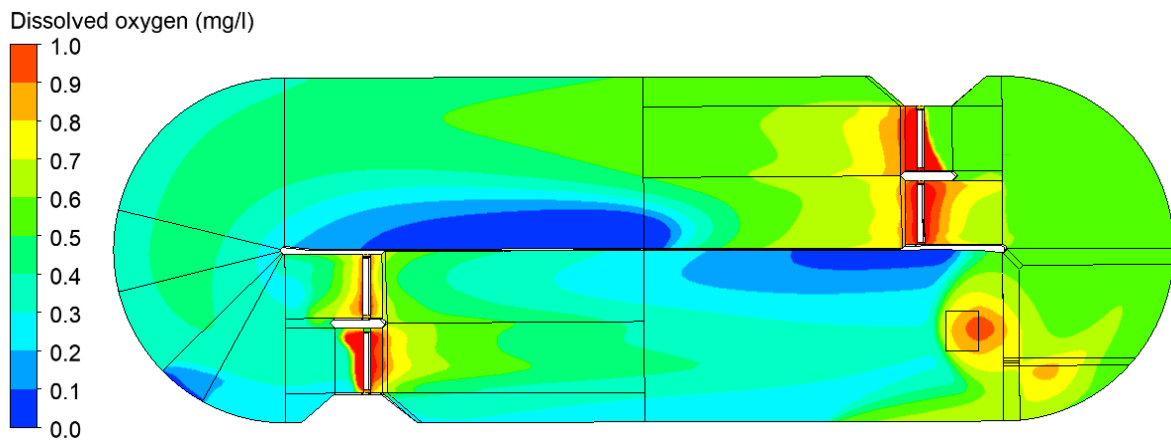


Figure 6.23 DO with uniform BOD - surface aeration (12 h<sup>-1</sup>)  
(max = 1.86 mg/l, mean = 0.39 mg/l)

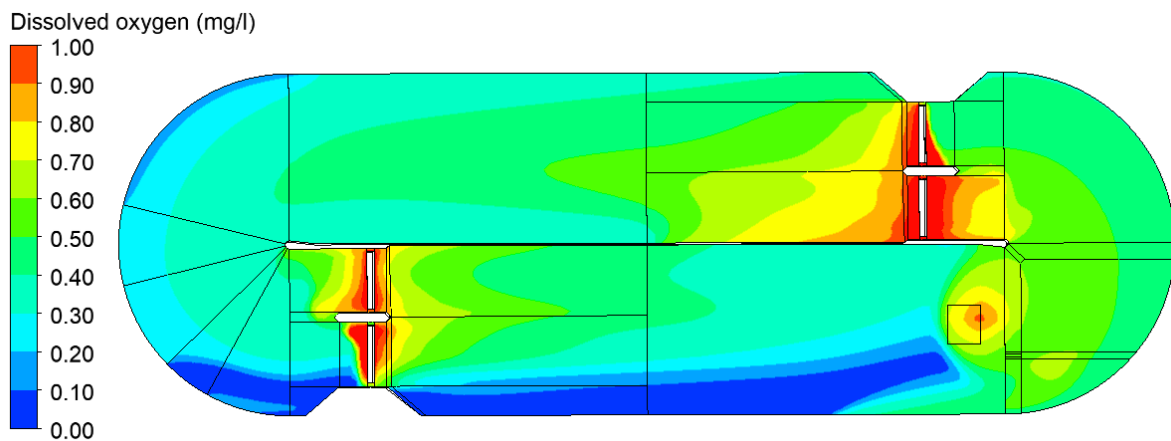


Figure 6.24 DO with distributed BOD - surface aeration (12 h<sup>-1</sup>)  
(max = 1.77 mg/l, mean = 0.40 mg/l)

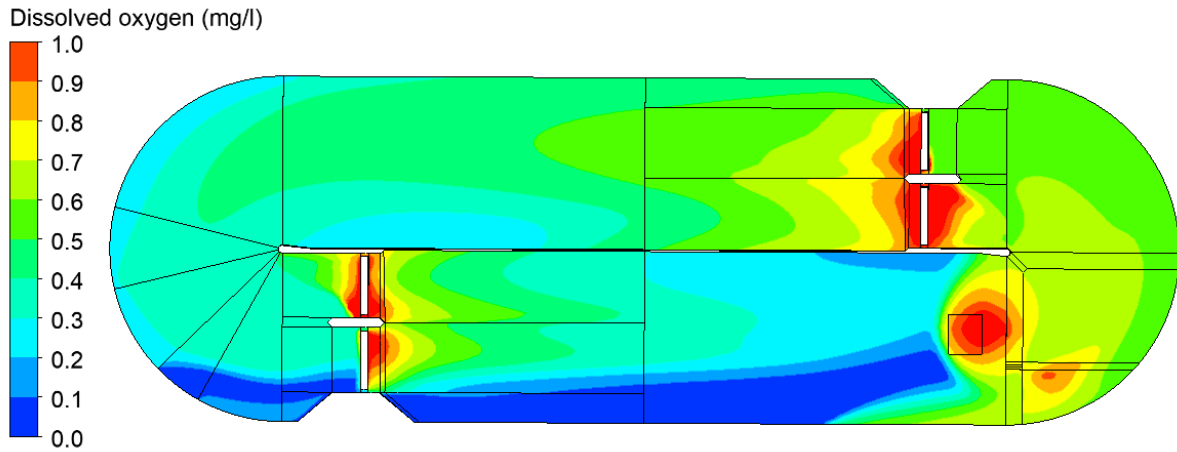


Figure 6.25 DO with distributed BOD - bubble (3 mm)  
 (max = 1.62 mg/l, mean = 0.40 mg/l)

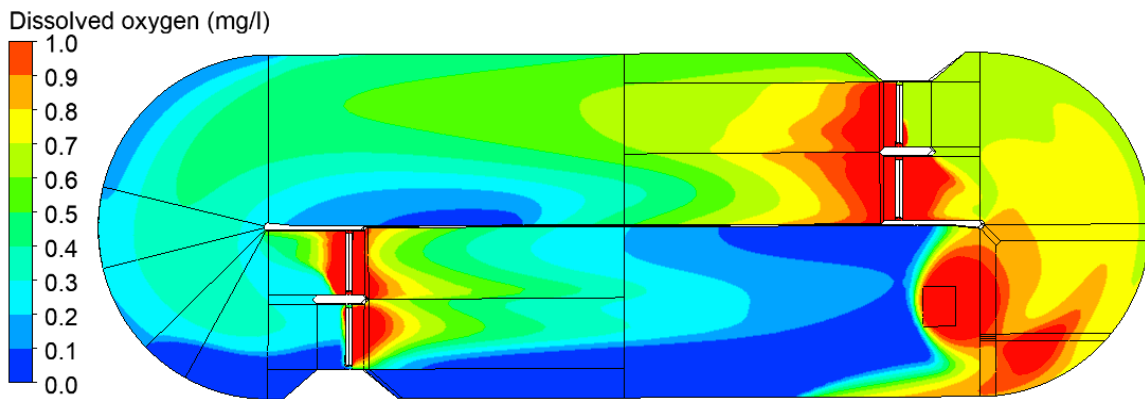


Figure 6.26 DO with distributed BOD - bubble (2 mm)  
 (max = 2.32 mg/l, mean = 0.40 mg/l)

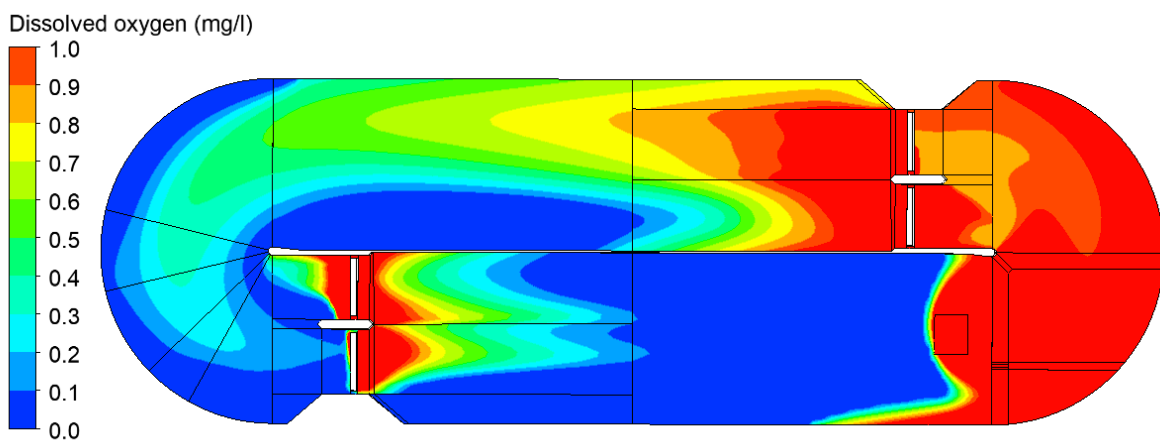


Figure 6.27 DO with distributed BOD - bubble (1 mm)  
 (max = 3.64 mg/l, mean = 0.40 mg/l)

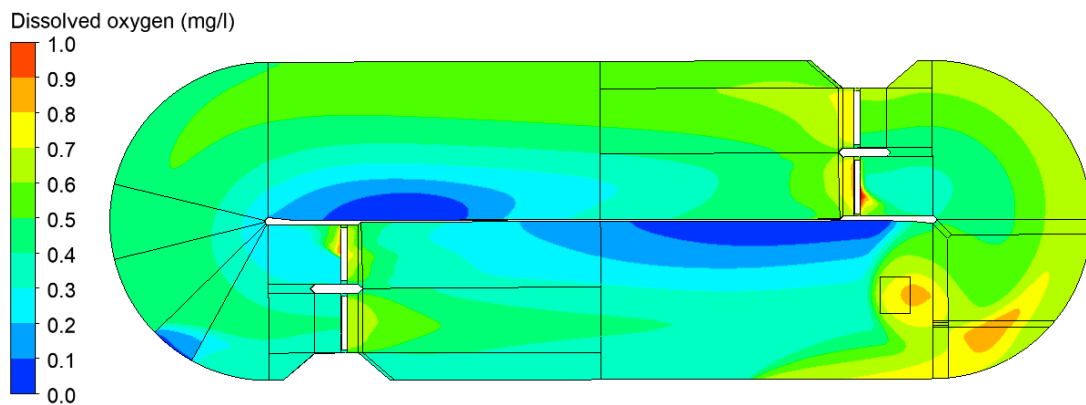


Figure 6.28 DO with uniform BOD - BSD - equal diameter discretisation  
 (max = 1.12 mg/l, mean = 0.40 mg/l)

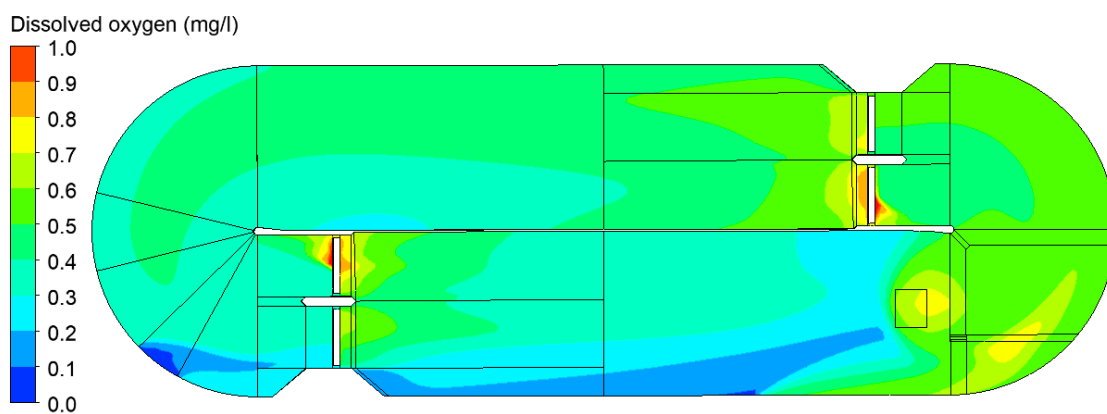


Figure 6.29 DO with distributed BOD - BSD - equal diameter discretisation  
 (max = 1.21 mg/l, mean = 0.40 mg/l)

## 6.5 Summary

The parameters that are found to have a significant effect on the dissolved oxygen are BOD distribution, temperature, surface aeration, bubble diameter, bubble size distribution, molar fraction Henry coefficient, mass diffusivity and turbulent Schmidt number of oxygen in water. When the oxygen transfer rate of surface aeration is increased fourfold, the mean DO in the ditch increases from 33 to 37 % of saturation. For an increase in temperature from 13 to 20 °C, the mean DO rises from 33 to 38 %. For this increase in temperature there is however little change to the flow pattern and DO distribution. There is an inverse linear relationship between molar fraction Henry coefficient and dissolved oxygen. There is a direct linear relationship between mass diffusivity of oxygen in water and dissolved oxygen. By decreasing mean bubble size, the total interfacial surface area of the bubbles increases, the interfacial oxygen mass transfer increases and the dissolved oxygen increases. For a 3 mm bubble size, mean DO increases from 33 to 42 % of saturation, for 2 mm to 54 %, and for 1 mm to 69 %. The variation of DO for these bubble sizes is however similar.

For the bubble size distribution (BSD), using equal diameter discretisation in the MUSIG model, the bubble size range predicted is from 0.99 to 6.32 mm, with a mean of 1.94 mm. This is a similar value to the best comparison with dissolved oxygen experimental data, which is for a mean bubble size of 2 mm (Chapter 7). The mean interfacial oxygen mass transfer in the ditch increases by 24 % with BSD, when compared to a 4 mm mean bubble size. This effect is comparable to a mean bubble size between 2 and 3 mm. However, BSD only slightly affects the DO distribution. These results suggest BSD is useful in determining the real bubble size in the ditch.

The mean and distributed BOD in the ditch are found to be quite similar for some of the parameters (temperature, surface aeration) but are more affected by bubble size. The mean and maximum DO in the ditch are affected by the different parameters (temperature, OTR of surface aeration, bubble size, BSD). Furthermore, for all of these parameters there is a significant difference in the variation of DO in the ditch, when modelling either a uniform or a distributed BOD. Therefore the bubble size distribution and the BOD distribution are found to be important parameters for the accurate prediction of the dissolved oxygen distribution in the ditch.

## 7. Experimental validation

### 7.1 Introduction

Dissolved oxygen (DO) can be measured in an aeration tank with a portable DO meter (Littleton et al, 2007a; Huang et al, 2009; Alaya et al, 2010; Le Moullec et al, 2010b; Xu et al, 2010; Karpinska et al, 2013; Lei and Ni, 2014). Bubble size can also be measured in an aeration tank by using an optical probe (Cockx et al, 2001; Fayolle et al, 2007; Le Moullec et al, 2008b) or by using high resolution camera imaging (Talvy et al, 2007; Wang and Zhao, 2009).

Portable propeller current meters can be used to measure water velocity in an aeration tank (Fayolle et al, 2007; Littleton et al, 2007a; Yang et al, 2010; Xie et al, 2014; Zhang et al, 2016). Water velocity in an aeration tank can also be measured using advanced techniques, for example, Particle Image Velocimetry (Cockx et al, 1997; Talvy et al, 2007; Wang et al, 2009; Hu et al, 2013; Ghawi, 2014), Acoustic Doppler Velocimetry (Brannock, 2003; Karpinska et al, 2013; Chen and Feng, 2014; Lei and Ni, 2014) and Particle Doppler Anemometry (Fan et al, 2010; Xu et al, 2010).

Comparison between residence time distribution (RTD) from an experimental tracer test and a numerical RTD can validate a CFD simulation. The most commonly used tracers are chemical salts (Talvy et al, 2007; Le Moullec et al, 2008b; Gresch et al, 2010; Karpinska, 2013; Ghawi, 2014; Climent et al, 2019). Other common tracers are fluorescent dyes (Makinia and Wells, 2005; Zima et al, 2009; Samstag and Wicklein, 2014). It would have been beneficial in this study to have conducted a tracer test to validate the predicted RTD and this has been proposed for future work.

In this chapter physical observation of fluid flow behaviour in two full-scale operational oxidation ditches (OD1 and OD2) at Potterne WWTP are undertaken and compared to numerical multi-phase water flow patterns in OD1 and OD2. Dissolved oxygen measurements using a portable DO meter are conducted at multiple locations near the water surface in OD1 and OD2. Numerical DO concentrations in OD1 and OD2 are compared to DO measurements.

## 7.2 Method

### 7.2.1 Experimental method

Experiments on the observation of flow patterns and the measurement of DO concentrations in operational ditches at Potterne WWTP (OD1 and OD2) are conducted in August 2018. The temperature is measured at 20.5 °C during the experiment. Therefore, one of the parameters studied has the physical properties of oxygen, air and water at 20 °C, which are the summer plant conditions.

Flow patterns are observed by sketches and photographs and videos of fluid behaviour near the water surface. It is easier to observe the flow pattern from above the ditch than at mid water depth. Dissolved oxygen measurements are also taken near the water surface. CFD simulation, observed flow patterns and DO measurements are therefore compared in the same locations in the ditches. DO measurements are taken at water depths below 0.2 m. When results are compared at water depths from 5 to 20 cm, there is less than 3 % difference in the results.

Dissolved oxygen concentration measurements are taken with a portable optical DO meter (Hach™) near the water surface, at 15 locations in ditch OD1 and at 22 locations in ditch OD2 that include the effluent. There is no measurement of water depth, which is the reason why DO measurements are not taken at multiple depths, and therefore this has been proposed for future work. The measurement of influent DO concentration is used as an inlet boundary condition in the CFD model. DO measurements are repeated for each location for better accuracy. The temperature of 20 °C during the experiment has a DO saturation concentration of 9.1 mg/l. Due to the effects of BOD, the DO concentrations in the ditches are well below this value.

The technique for measuring DO concentration is the luminescence DO method (LDO) (Roman and Felseghi, 2014; Gheorghe et al, 2018). There are no wastewater grab samples analysed in the laboratory. The portable DO meter (Hach™) has a luminescence based sensor that measures light emission characteristics. The LDO principle is based on the physical phenomenon of luminescence. Some materials emit light when excited by the stimulus of light. The intensity of luminescence and time it takes to fade are dependent on the oxygen concentration around the material.

### 7.2.2 CFD modelling

The CFD results from previous chapters are compared to experimental observations of flow patterns and the measurements of DO in the two full scale ditches (OD1 and OD2). The numerical multi-phase flow patterns and DO distributions (horizontal slice near water surface) are at the operating conditions of the ditches. Comparison with real physical experimental data is only plausible using numerical DO that includes the effect of the biochemical oxygen demand (BOD). This simulates the real situation in biological wastewater treatment. Both uniform and distributed BOD models are compared to DO measurements in OD1 using different values of parameters. Only the uniform BOD model is used to compare with DO measurements in OD2 and only by using the 'standard' model. *The theory and the methods of multi-phase and multi-component flow modelling of the flow pattern, DO distribution, BOD distribution and boundary conditions are given in the previous chapters.*

There are different parameters studied to see how closely the predictions of numerical DO concentrations compare to the measurements in one oxidation ditch (OD1). The 'standard' CFD model has a mean bubble size of 4 mm, properties at the mean annual temperature of 13 °C at Potterne WWTP and mass transfer coefficient of surface aeration is 3 h<sup>-1</sup>. The summer (experimental) conditions at 20 °C is also simulated. A further boundary condition of surface aeration of mass transfer coefficient = 12 h<sup>-1</sup> is also simulated. Different mean bubble sizes (3, 2, 1 mm) and a bubble size distribution (BSD) are simulated. To compare the numerical and measured dissolved oxygen a statistical analysis of the values at the same physical locations in the ditch are undertaken for the mean, maximum, minimum and standard deviation (SD). The parameter study in the previous chapter models different parameters for one of the ditches (OD1). Therefore the same method is used to compare numerical to measurements of DO in this chapter (Tables 7.1 and 7.2).

## 7.3 Results and discussion

### 7.3.1 Flow patterns

The water flow pattern from multi-phase flow simulation near the water surface are shown for operating conditions in OD1 (Figure 7.1) and OD2 (Figure 7.3). The sketches of observed flow patterns are shown for OD1 (Figure 7.2) and OD2 (Figure 7.4). Photographs of flow patterns at Potterne WWTP are in Figures 7.5 and 7.6.

In OD1 there is agreement between the numerical and observed flow patterns for the following phenomena. The dominant flow direction is anti-clockwise. There is stagnant flow near the effluent weir, upstream of the surface aerators and near the central wall. There is stagnant flow upstream of the diffuser and near the central wall. There is radial flow above the diffuser near the water surface. Downstream of the Maguire jet aerator there is a strong flow current near the curved outer wall. Just downstream of the jet aerator there is return flow along the right outer wall. Downstream of the jet aerator there is turbulence. Higher flow is observed near the central wall, just downstream of the surface aerators and near the influent, that is produced by the plumes from the surface aerators. While some predicted flow phenomena are not observed there is generally good validity by observation in OD1.

In OD2 there is agreement between numerical and observed flow patterns for the following phenomena. The dominant flow direction is clockwise. There is stagnant flow near the effluent weir and at the ends of the central wall. Near the influent there is upward flow from the diffusers that block the horizontal flow currents. Flow is sucked by the booster and dispersed downstream as a strong current. Just downstream there is turbulence where flow impacts a dividing wall. Further downstream there is return flow along the central wall. All the Fuch jet aerators have bi-directional flow near the water surface. The diffuser furthest from the influent weir has radial flow. The left side of the ditch has homogeneous flow. Around the curved bend at the end of the ditch the flow accelerates towards the jet aerator. There is stagnant flow upstream of a nearby jet aerator. Downstream of the jet aerators there are higher velocities. Further downstream the air from the jet aerators rise upwards and cause turbulence. There are two small pools of stagnant flow. Further downstream of the jet aerators there is stagnant flow. While some predicted phenomena are not observed there is generally good validity by observation in OD2.

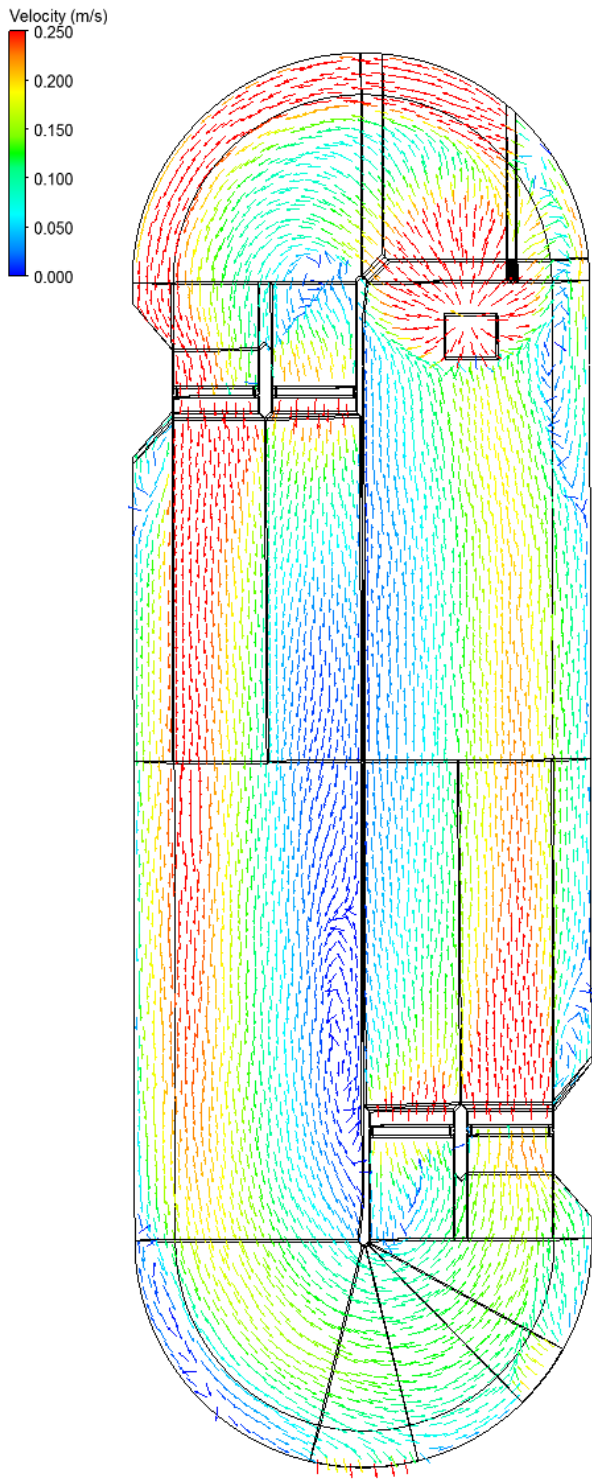


Figure 7.1 Multi-phase flow simulation of water velocity in OD1

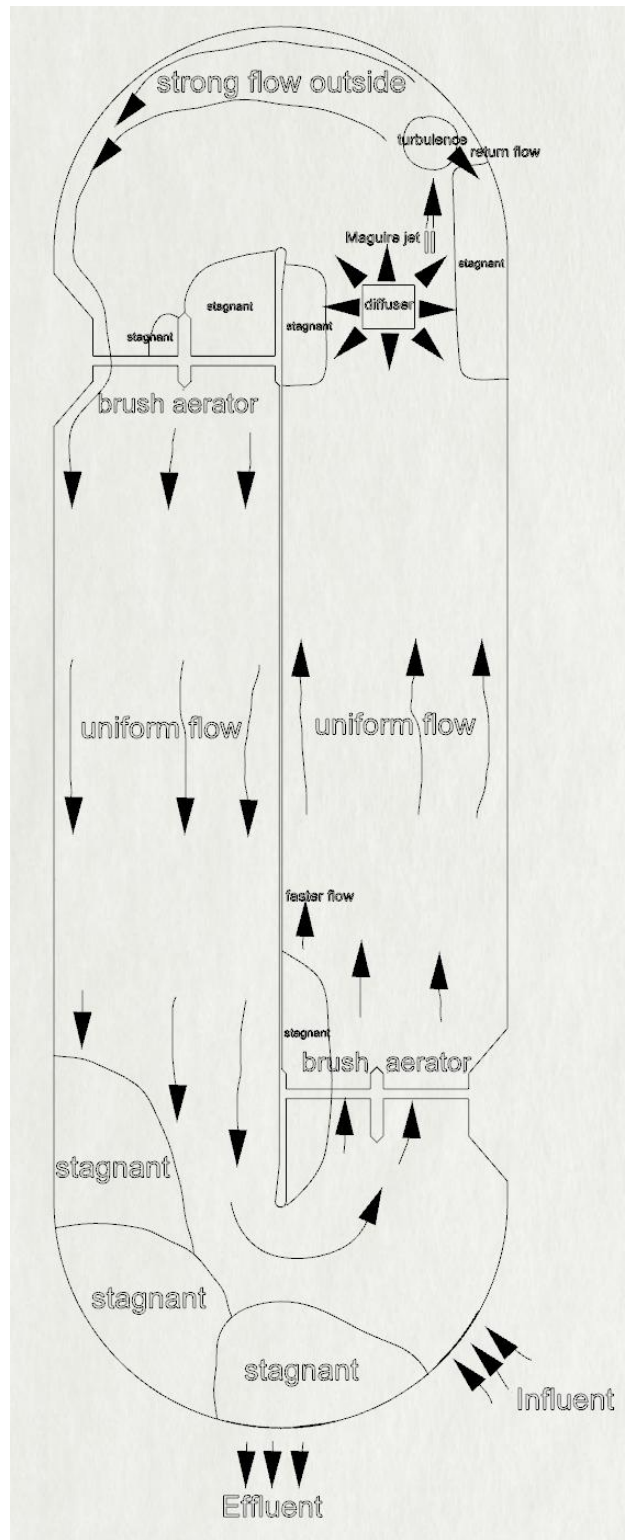


Figure 7.2 Sketches of water flow patterns in OD1 observed at WWTP

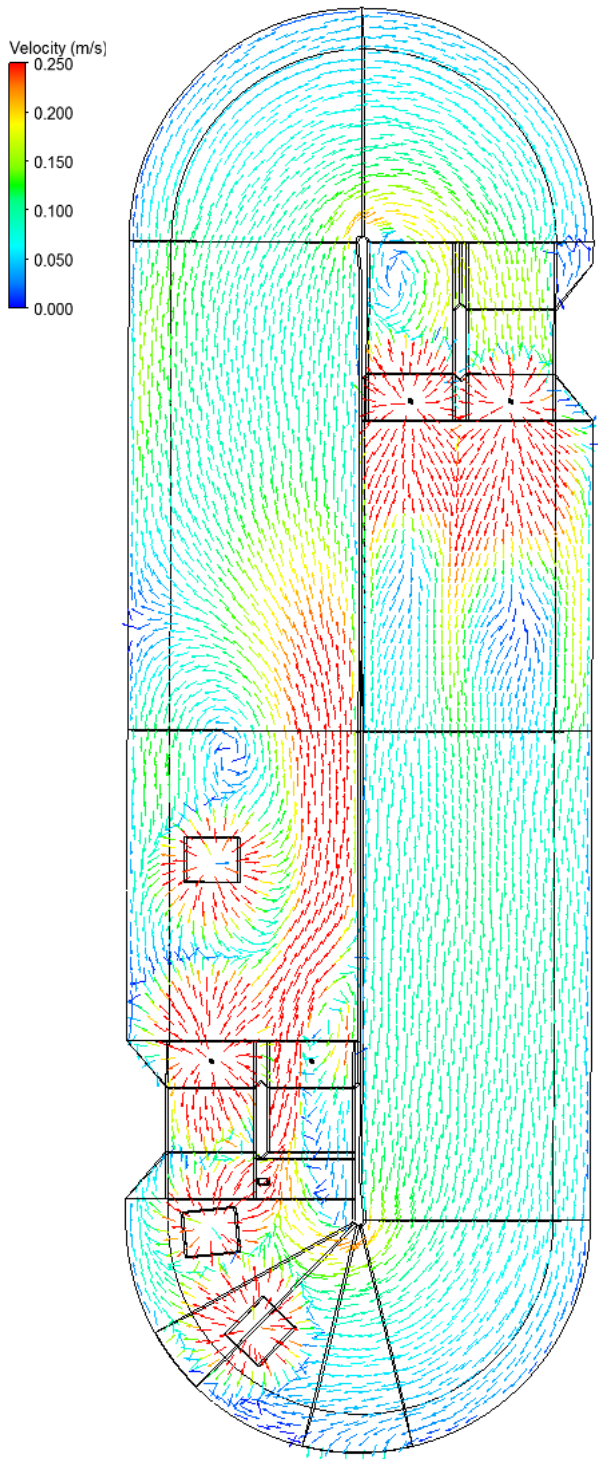


Figure 7.3 Multi-phase flow simulation of water velocity in OD2

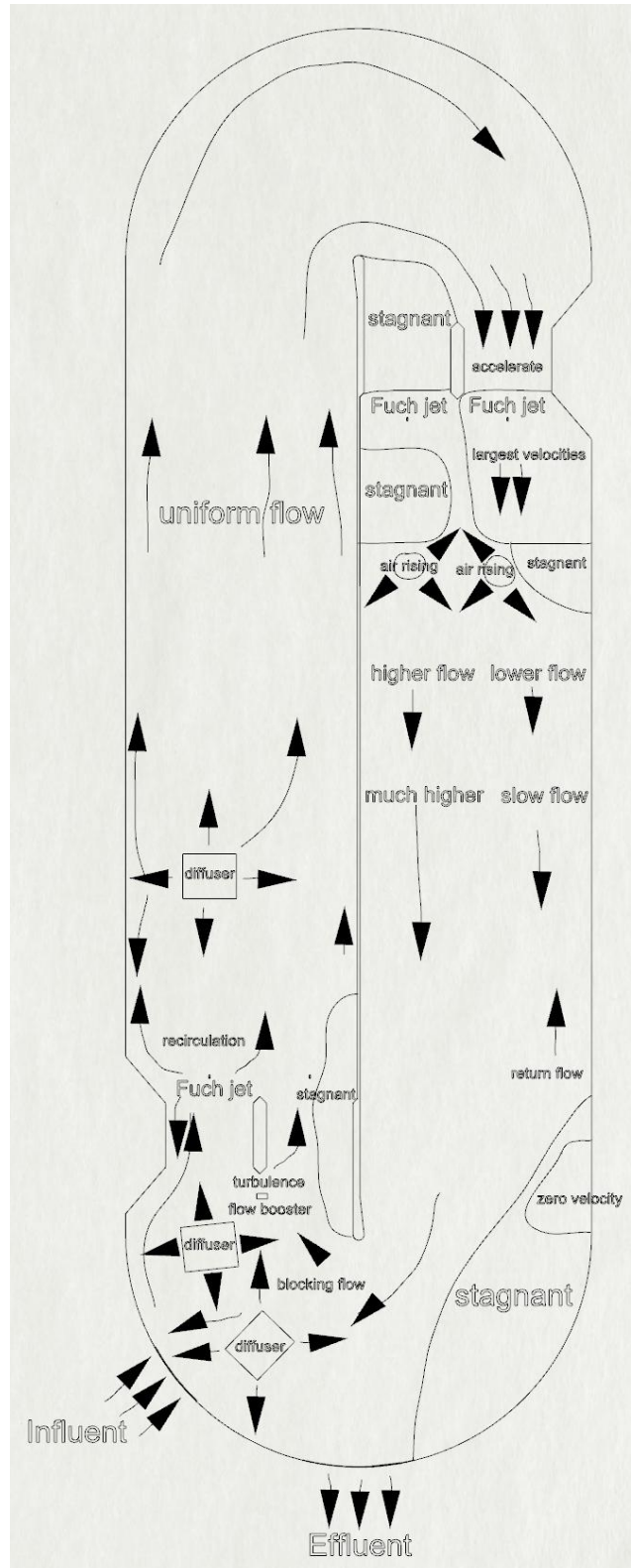


Figure 7.4 Sketches of water flow patterns in OD2 observed at WWTP



Figure 7.5 Observed flow behaviour in OD1

(from top to bottom) near effluent weir; downstream of surface aerators near influent; near diffuser; downstream of aerators



Figure 7.6 Observed flow behaviour in OD2

(from top to bottom) two diffusers and booster; booster flow impacts wall;  
jet aerator near influent; parallel jet aerators

### 7.3.2 Dissolved oxygen concentrations

Figure 7.7 shows the measurement locations for dissolved oxygen in OD1 (left) and OD2 (right) near the water surface. Figure 7.7 also shows numerical DO concentrations for operating conditions in both ditches and with a uniform BOD. There are 15 measurement locations in OD1 and 22 locations in OD2.

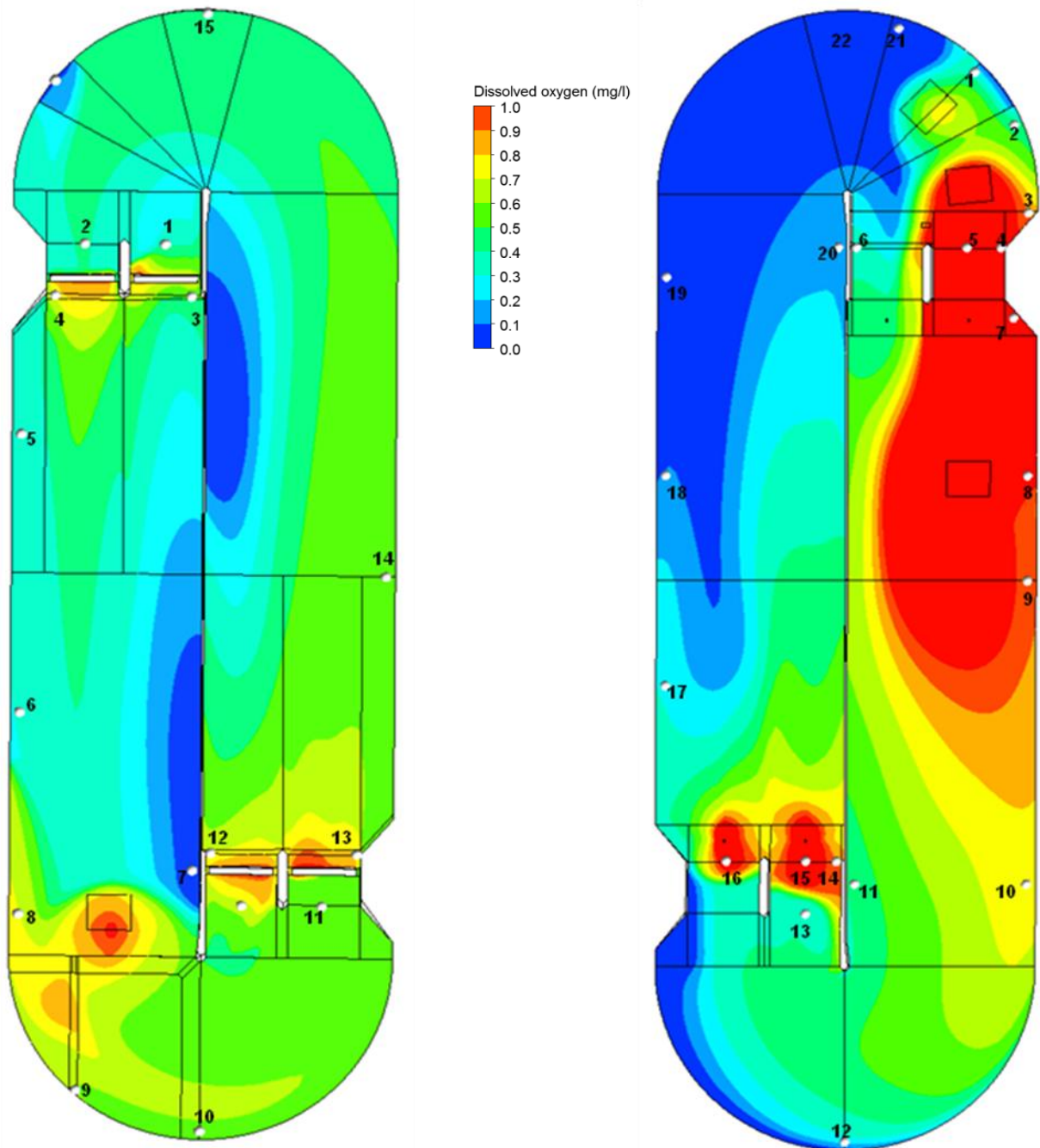


Figure 7.7 Numerical DO concentrations and measurement locations uniform BOD for OD1 (left) and OD2 (right) - operating

Table 7.1 Dissolved oxygen compared to measurements at locations in OD1

<b>Uniform BOD</b>	<b>Measure (mg/l)</b>	<b>Standard (mg/l)</b>	<b>3 (mm)</b>	<b>2 (mm)</b>	<b>1 (mm)</b>	<b>BSD</b>	<b>Temp 20 °C</b>	<b>OTR 12 h<sup>-1</sup></b>
mean points	0.44	0.51	0.48	0.55	0.62	0.49	0.43	0.46
max points	1.38	0.76	0.84	1.15	1.67	0.70	0.68	0.71
min points	0.06	0.02	0	0	0	0.04	0	0
SD points	0.44	0.20	0.23	0.36	0.63	0.19	0.17	0.17
mean ditch	-	0.40	0.38	0.39	0.38	0.40	0.37	0.39
max ditch	-	1.26	1.64	2.34	3.58	1.12	1.24	1.86
min ditch	-	0	0	0	0	0	0	0
<b>Distributed BOD</b>	<b>Measure</b>	<b>Standard</b>	<b>3</b>	<b>2</b>	<b>1</b>	<b>BSD</b>	<b>20 °C</b>	<b>12 h<sup>-1</sup></b>
mean points	0.44	0.46	0.49	0.58	0.80	0.45	0.45	0.46
max points	1.38	0.78	0.93	1.23	1.79	0.72	0.78	1.03
min points	0.06	0.07	0	0	0	0.12	0.05	0
SD points	0.44	0.20	0.28	0.40	0.64	0.17	0.20	0.28
mean ditch	-	0.42	0.40	0.40	0.40	0.40	0.40	0.40
max ditch	-	1.24	1.62	2.32	3.64	1.21	1.25	1.77
min ditch	-	0	0	0	0	0	0	0

Table 7.2 Dissolved oxygen compared to measurements at locations in OD2

<b>Uniform BOD</b>	<b>Measurements (mg/l)</b>	<b>Standard model (mg/l)</b>
mean points	0.59	0.60
maximum points	3.67	1.24
minimum points	0.03	0
SD points	1.04	0.46
mean ditch	-	0.60
maximum ditch	-	3.07
minimum ditch	-	0

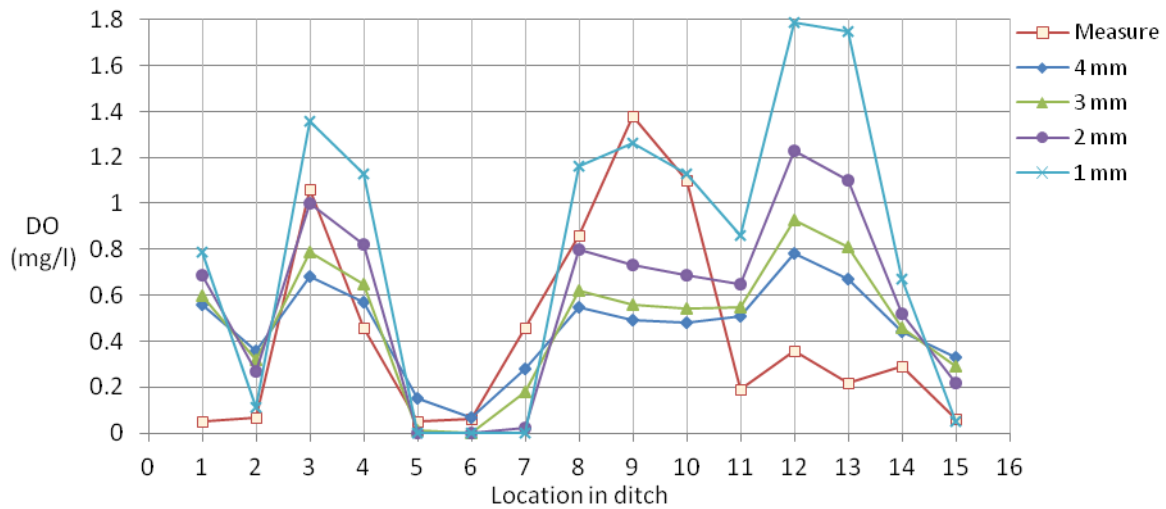


Figure 7.8 DO for mean bubble sizes - distributed BOD in OD1

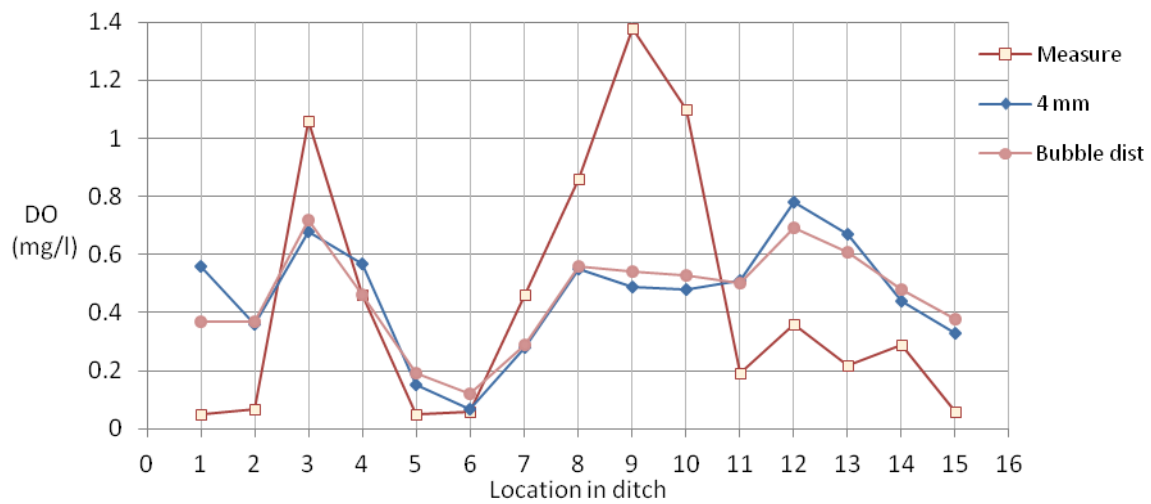


Figure 7.9 DO for BSD - distributed BOD in OD1

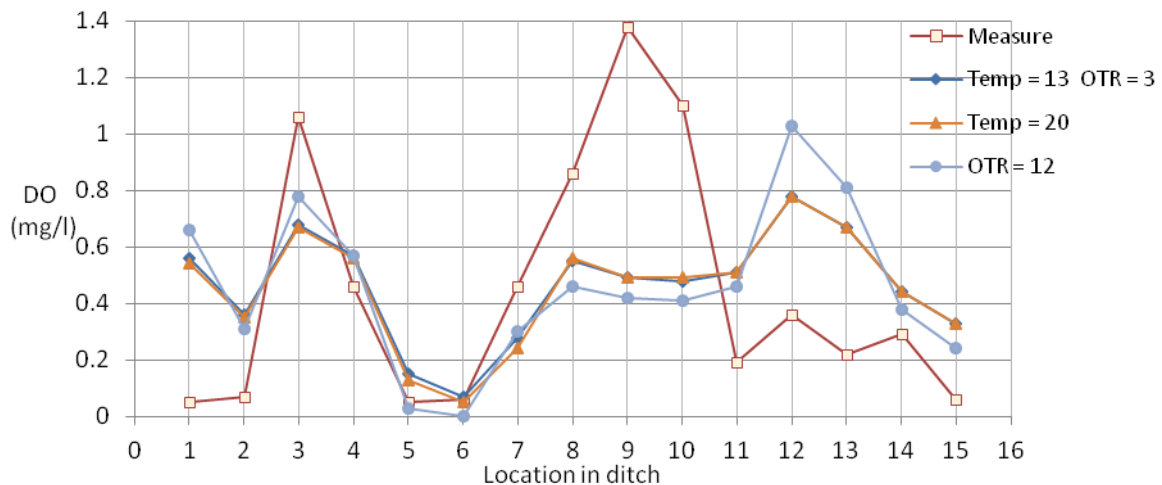


Figure 7.10 DO for temperature and surface OTR - distributed BOD in OD1

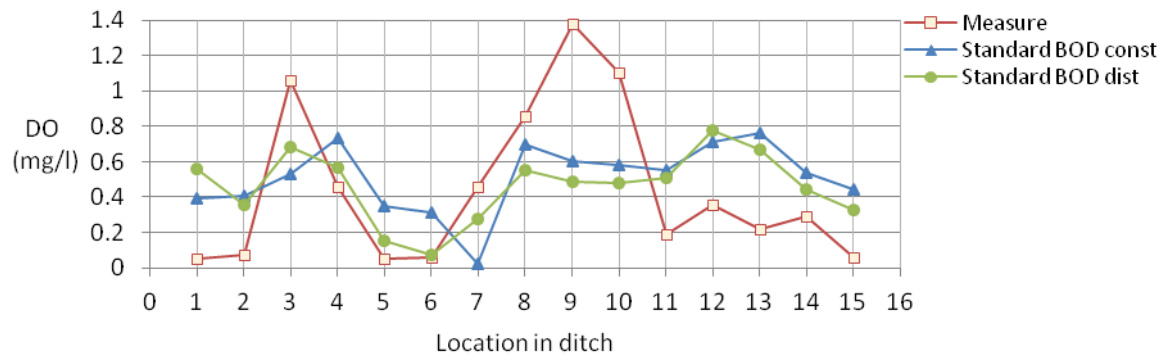


Figure 7.11 DO for standard model - uniform and distributed BOD in OD1

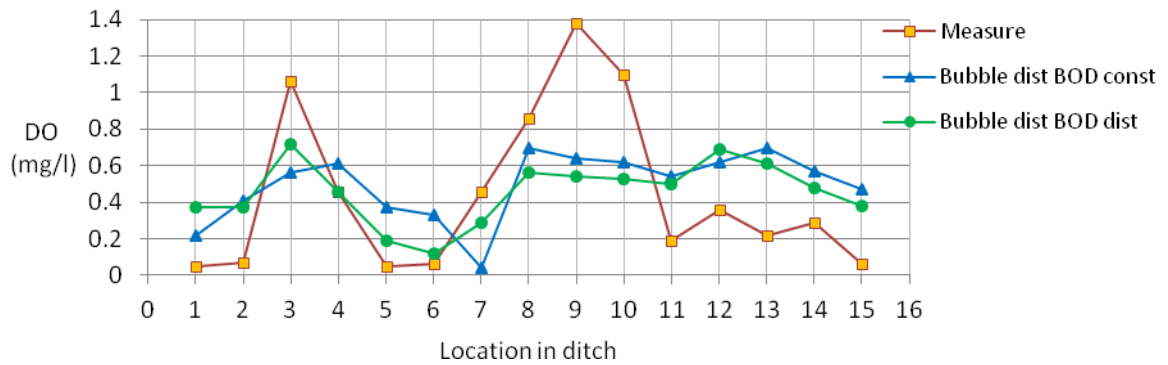


Figure 7.12 DO for BSD - uniform and distributed BOD in OD1

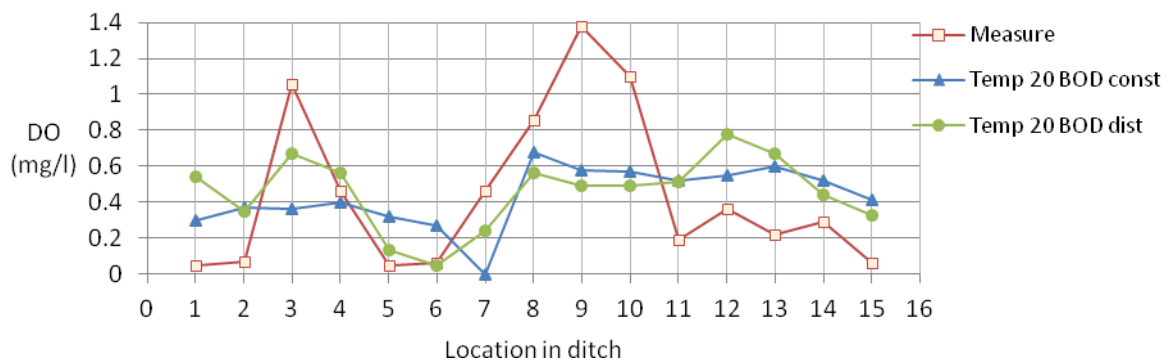


Figure 7.13 DO for temperature - uniform and distributed BOD in OD1

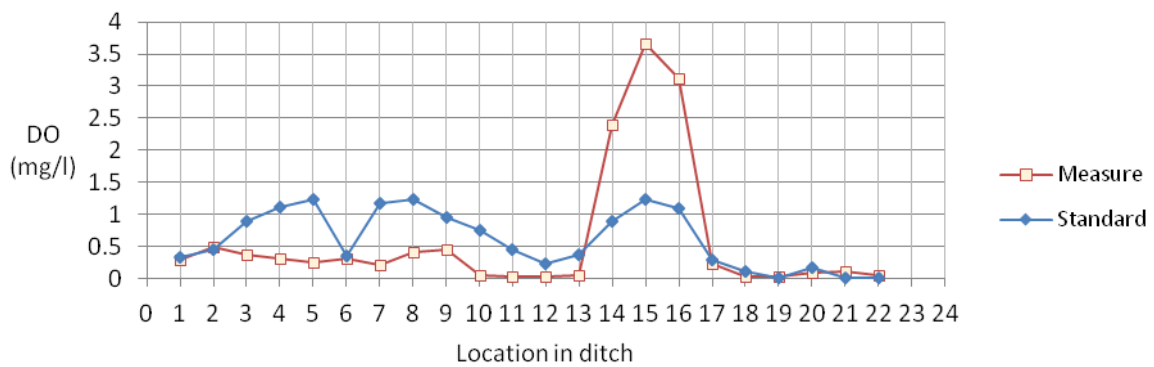


Figure 7.14 DO for standard model - uniform BOD in OD2

Table 7.1 shows the comparison between the measured and predicted dissolved oxygen concentrations (mg/l) in OD1, with uniform and distributed BOD and for different parameters. Table 7.2 shows the same comparison in OD2, but only with the standard model and uniform BOD. The 'standard' model has a mean bubble size of 4 mm, physical properties at 13 °C and mass transfer coefficient of surface aeration of 3 h<sup>-1</sup>. In OD1 the simulations are for mean bubble sizes, BSD, temperature of 20 °C during experimental conditions and surface aeration of 12 h<sup>-1</sup>. At the influent to OD1 and OD2 the DO measurements are 0.08 and 0.04 mg/l respectively. They are used in the inlet boundary condition of the CFD model.

Consider when a uniform BOD is modelled in OD1. In terms of the magnitudes of DO the numerical and physical measurements are in quite good agreement (Table 7.1). But in terms of statistical variation there is not good agreement (Table 7.1). Comparison of the 'standard' model (0.51 mg/l) with measurements (0.44 mg/l) show quite good agreement for the mean DO in the ditch, taken at the same locations in the ditch (Figure 7.7). The maximum DO concentration at these locations are standard model (0.76 mg/l) and measurement (1.38 mg/l). The standard deviation (SD) of predicted and measured DO concentrations are taken at the same locations, and are 0.20 and 0.44 respectively.

Reducing the mean bubble size to 3 mm in OD1 gives a mean predicted location value of 0.48 mg/l that is quite similar to the measured mean (0.44 mg/l). The maximum predicted location value is 0.84 mg/l compared to 1.38 mg/l. The maximum predicted DO increases from 1.26 to 1.64 mg/l. Comparison of the SD of variation improves this slightly to 0.23 (0.44). Reducing mean bubble size to 2 mm gives a mean predicted location value of 0.55 mg/l (higher than measurement) and a maximum location value of 1.15 mg/l (nearest to measurement). Comparison of the SD of variation improves this to 0.36 (closest to 0.44). The predicted maximum DO increases to 2.34 mg/l. Reducing mean bubble size to 1 mm gives higher mean and maximum predicted location values of 0.62 mg/l and 1.67 mg/l. The SD of variation is 0.63 compared to 0.44. The maximum DO in OD1 increases further to 3.58 mg/l. Simulating BSD gives a mean predicted location value of 0.49 mg/l, that is similar to a 3 mm bubble size and measurement (0.44 mg/l). The maximum location value is 0.70 mg/l compared to 1.38 mg/l. The maximum DO decreases slightly with BSD.

For the experimental temperature (20 °C), the mean and maximum DO is about the same as the 'standard' model (13 °C). Comparison of the prediction (0.43 mg/l) with measurement (0.44 mg/l) however shows better agreement for the mean dissolved oxygen at these locations. For a fourfold increase in surface aeration, comparison of the prediction (0.46 mg/l) with measurement (0.44 mg/l) shows better agreement for the mean DO at these specific locations in the ditch. With uniform BOD, as the bubble size is reduced the mean and maximum DO increases. Reducing the bubble size increases the variation (SD) of the dissolved oxygen. The closest match with the measurement data is for a 2 mm bubble size (SD of 0.36 compared to 0.44).

For the 'standard model' in OD1, when comparing uniform (Table 7.1) and distributed BOD (Table 7.2), the mean and maximum DO values are about the same. However, the distributed BOD better predicts the mean value of 0.46 mg/l at these specific locations. The SD of variation is the same for the uniform and distributed BOD. For both the uniform and distributed BOD, when the bubble size is reduced, the maximum DO increases. There is no significant effect on the mean and maximum DO with a distributed BOD. However, there is a significant increase to the SD of variation (4 mm: 0.20->0.20; 3 mm: 0.23->0.28; 2 mm: 0.36->0.40; 1 mm: 0.63->0.64; temperature: 0.17->0.20; surface aeration: 0.17->0.28). These results suggest that there is an improvement in results when simulating a distributed BOD. The best match with experimental data for both a uniform and a distributed BOD in OD1 is with a mean bubble size of 2 mm (SDs of 0.36 and 0.40). This is confirmed by the BSD which predicts a mean bubble size in the ditch of 1.9 mm. This suggests that the actual mean bubble size in OD1 may be closer to 2 mm, than what was originally thought to be accurate (4 mm).

Only the 'standard model' and uniform BOD is modelled in OD2. Comparison shows a bigger difference between numerical and measured DO in OD2 (Table 7.2). The predicted mean and maximum DO is 0.60 and 3.07 mg/l. The mean DO at these specific locations in OD2 for numerical and measurement are in close agreement (0.60 and 0.59 mg/l). However the maximum DO does not agree (1.24 and 3.67 mg/l). DO variation (SD) at these measurement locations also differ (0.46 and 1.04).

Figures 7.8 to 7.10 show graphical comparisons between the numerical and measured DO at specific locations in OD1, for the model parameters and the distributed BOD. Figure 7.8 shows that a 2 mm bubble size has the best match with measurement for the first DO peak in the graph, while the 1 mm bubble size has the best match for the 2nd peak. Figure 7.9 shows there is no significant difference between a mean bubble size and a BSD. Figure 7.10 shows there is no significant difference between a temperature of 13 and 20 °C. There is a small improvement in simulating a higher surface aeration ( $12 \text{ h}^{-1}$ ), in terms of the first peak and first trough. This is confirmed by an SD of variation of 0.28 that is closer to the measured value (0.44). Figures 7.11 to 7.13 show the graphical comparison to measured DO, between uniform and distributed BOD for different model parameters. Figures 7.11 and 7.12 show that for the standard model and BSD there is better match with the measurement at the first peak, first trough and second trough in the graph of the distributed BOD. Figure 7.13 shows a better match for the higher temperature of 20 °C at the first peak and first trough for the distributed BOD. The results suggest that the mean bubble size in OD1 may be nearer to 2 mm than was originally thought (4 mm). The results also suggest that a distributed BOD may be more accurate than a uniform BOD for determining the DO distribution in OD1.

Figure 7.14 shows the comparison between the numerical and measured DO in the other ditch OD2. The measurement locations are shown in Figure 7.7. In most of OD2 there is not good agreement for DO. However, in one part of the ditch where DO concentrations are low there is good agreement (locations 17 to 22). Near the influent there is also good agreement (locations 1 and 2). For locations 3 to 13 the predicted DO is higher than the measurements. However, they do show similar trends to measurements from locations 7 to 22. Numerical values also show a peak at the same place as the largest peak of the measurements (locations 14 to 16).

The different aerators are designed to produce different bubble sizes. The BSD predicts a range of bubble sizes from small (1 mm) to large (6 mm). There are however no measurements of bubble size. This would need to be done by either using an optical probe or by high resolution camera imaging. Measurements of bubble size at specific locations in the ditch can provide bubble size data for (1) inlet boundary conditions of the aerators and (2) validating the numerical BSD.

## 7.4 Summary

In OD1 there is overall good agreement between the numerical simulation and the physical observation in terms of the flow pattern. There is agreement for the general flow direction, radial flow pattern above diffuser and strong flow current, fluid turbulence and return flow of the Maguire jet aerator. There is agreement for the flow stagnation near the effluent, upstream of the surface aerators, near the central wall, upstream of the diffuser and near the side wall by the Maguire jet aerator.

In OD2 there is overall good agreement between the numerical simulation and the physical observation in terms of the flow pattern. There is agreement for the general flow direction, upward flow from diffusers that block horizontal flow circulating around the ditch and radial pattern above diffusers. There is agreement for the strong flow current from the booster that collides with an internal wall. There is agreement for the bi-directional flow near the water surface above the Fuch jet aerators and for the fluid turbulence caused by rising air from the jet aerators. There is agreement for the flow stagnation near the effluent, ends of the central wall, downstream of the flow booster and upstream of the Fuch jet aerators.

Comparison with real physical experimental data is only plausible by using the numerical DO concentration that includes the effect of the biochemical oxygen demand (BOD). This modelling feature considers the real situation in biological wastewater treatment. Both the uniform and distributed BOD in the ditch is compared to the DO measurements in OD1 and using different parameter values. Only the uniform BOD model is used for OD2 and with only the 'standard' model.

*Comparison between the mean numerical DO concentrations in OD1, that include the effect of BOD and experimental measurements are favourable. Comparison between the variation of DO concentration is however not as favourable. For the mean BOD in OD1, the mean DO for the standard model and the measurements are in good agreement. The maximum and variation of DO are lower than the measurements. A bubble size of 2 mm gives a mean DO that is higher than the measurements. The maximum DO and its variation is closest to measurements. The bubble size distribution (BSD) gives a mean DO that is nearer to the measurements, when compared to a mean bubble size of 4 mm. The maximum and variation of DO*

are similar to the standard model. As bubble size is reduced, mean and maximum DO increases and the variation of DO increases. The closest match to experimental data for the uniform BOD is with the 2 mm bubble size. It would have also been beneficial to have measured the DO concentrations at multiple depths in the ditches.

*For a BOD distribution in OD1*, the standard deviation of DO values compares better with the measurements than for a uniform BOD concentration. The closest match with measurement is with the 2 mm bubble size and the BOD distribution. These results suggest that a BOD distribution in a ditch has an important influence on the DO distribution and is more accurate when it is compared to a mean BOD.

*Comparison between the mean numerical DO concentrations in OD2* which include the effect of uniform BOD and the experimental measurements show a bigger difference between the predictions and measurements in OD2. However, the DO concentrations at some locations in OD2 are in agreement. There are also some similar spatial trends in DO distribution between the predictions and measurements.

The bubble size distribution (BSD) in OD1 shows a slight improvement in comparison to measurement data for dissolved oxygen, when compared to a mean bubble size. When using the homogeneous MUSIG model and equal diameter discretisation, the BSD predicts bubble sizes from 1.0 to 6.3 mm and a mean size of 1.9 mm. This compares favourably with the best agreement with experimental data, suggesting that 2 mm may be the real mean bubble size in the ditch. BSD is used to calculate the variation of bubble size from knowledge of the multi-phase flow pattern. However, by taking measurements of bubble size, by either using an optical probe or by high resolution camera imaging, this could provide data for validation of the numerical BSD. This could also be used to provide data for the different numerical inlet boundary conditions of the aeration devices. Furthermore, conducting a tracer test could provide validation for the numerical residence time distribution (RTD).

The bubble size distribution (BSD) and biochemical oxygen demand (BOD) distribution addressed in this study are important parameters when considering the fluid dynamics and dissolved oxygen distribution in an oxidation ditch. With reference to the existing published literature, there is little or no previous CFD modelling of these two parameters for aeration tanks in wastewater treatment.

## **8. Aeration system design**

### **8.1 Introduction**

The literature review has identified CFD simulation that is used for the development and design optimisation of aeration devices and aeration tank design (Karpinska and Bridgeman, 2016). The criteria for design optimisation is to improve the uniformity of the flow pattern, dissolved oxygen distribution and suspended solids distribution, increase the dissolved oxygen, increase the residence time of the aeration tank and reduce the energy consumption of the aeration process (Gillot and Heduit, 2000; Brannock, 2003; Gillot et al, 2005; Jensen et al, 2006; Kjellstrand, 2006; Thakre et al, 2008; Bhuyer et al, 2009; Fan et al, 2010; Xu et al, 2010; Gresch et al, 2011; Yang et al, 2011; Karpinska, 2013; Liu et al, 2014; Xie et al, 2014; Terashima et al, 2016; Wei et al, 2016a; Wei et al, 2016b; Zhang et al, 2016; Climent et al, 2019).

CFD simulation in this study has identified potential issues with the performance of the oxidation ditches in terms of their hydrodynamics and dissolved oxygen distribution. An analysis of how each aeration system affects the dissolved oxygen distribution is presented in Chapter 5. Moreover, the performance of each individual aerator is assessed in this chapter. Recommendations are given in this chapter to improve the hydrodynamic and aeration performance of the oxidation ditch. This is in terms of the design retrofitting of the aerators and some aspects of ditch design that have been identified in the review. There are different types of aerators studied (brush surface, membrane diffuser, hydro-jet and air jet). However, the detailed design retrofitting of each of these aerators (for example, the rotational speed of the surface aerator and pore size of the diffuser) is not the intention of this design study.

## 8.2 Theory

To calculate the efficiency of an individual aerator there are two criteria used. The factor,  $Eff_1$  is a measure of how the running costs of the supply of oxygen to an aerator can be converted into the mean dissolved oxygen concentration in the ditch.

$$Eff_1 = \frac{\text{mean\_DO}}{\text{sat\_DO} \times \text{oxygen\_s}} \quad (8.1)$$

where, mean\_DO is the mean DO in the ditch (mg/l), sat\_DO is the saturation DO concentration in water at 13 °C which is 10.5 (mg/l), and oxygen\_s is the oxygen supply to the individual aerator (kg/s). This efficiency relates to the oxygen transfer efficiency (OTE) of a submerged diffuser or jet aerator (Stenstrom and Rosso, 2010), which is calculated by the oxygen transfer rate (OTR) divided by the oxygen supply rate (equation 2.12).

The factor,  $Eff_2$  is a measure of how the mean dissolved oxygen concentration in the ditch that is delivered by an aerator compares to the theoretical mean dissolved oxygen concentration in the ditch (Stenstrom and Rosso, 2010):

$$Eff_2 = \frac{\text{mean\_DO}}{\text{theory\_DO}} \times 100\% \quad (8.2)$$

$$\text{theory\_DO} = \frac{\text{oxygen\_s} \times \text{residence\_t}}{\text{volume} \times 0.001} \quad (8.3)$$

where, theory\_DO is the theoretical DO in the ditch (mg/l), residence\_t is the predicted mean residence time of the ditch (s), which is calculated in section 4.4.3. The volume of the ditch is 2000 m<sup>3</sup>.

### 8.3 Method

*The methods for multi-phase and multi-component flow modelling of the flow pattern, DO distribution, BOD distribution and numerical boundary conditions are given in previous chapters.* The standard model has a mean bubble size of 4 mm in the ditch, temperature of 13 °C and mass transfer coefficient of surface aeration of 3 h<sup>-1</sup>. The dissolved oxygen saturation concentration in water at 13 °C is 10.5 mg/l, which is the upper limit for DO in the ditch. The aeration performance of the aerators to aerate the oxidation ditch are individually assessed in this chapter in both oxidation ditches (OD1 and OD2), without considering the effect of BOD.

Comparison between the performance of individual aerators in both ditches is given in Table 8.1. There are two efficiency criteria assessed, Eff<sub>1</sub> and Eff<sub>2</sub> that are calculated for each individual aerator. The first efficiency criteria Eff<sub>1</sub> is based on how efficiently oxygen supply to an aerator is converted into the mean DO in the ditch. The second efficiency criteria Eff<sub>2</sub> is based on how efficiently the delivered mean DO in the ditch from an aerator compares to the theoretical mean DO. The effects of the individual aerators on the flow pattern and DO concentrations are analysed. Recommendations are also made on how the design of individual aerators and ditch design can be improved in terms of the hydrodynamic and aeration performance.

## 8.4 Results and discussion

### 8.4.1 Aerator efficiency

Table 8.1 shows that the most efficient conversion of oxygen supply (running costs) to dissolved oxygen are the membrane diffusers, with  $Eff_1 = 37$  for OD1, and  $Eff_1 = 20$  for OD2. The Maguire jet aerator in OD1 is also quite efficient for this criteria,  $Eff_1 = 29$ . Brush surface aerators have a lower value of  $Eff_1 = 15$ . The least efficient are the Fuch air jet aerators in OD2 with  $Eff_1 = 8$ . The efficiency is lower for the actual operating conditions in OD1,  $Eff_1 = 11$  and in OD2,  $Eff_1 = 7$ .

The criteria,  $Eff_2$ , considers the efficiency of the delivery of mean DO compared to the theoretical DO. This is a more accurate assessment of the performance of an aerator. Surface aerators in OD1 have  $Eff_2 = 24\%$ . Less efficient are the Maguire jet aerator in OD1 with  $Eff_2 = 7\%$ . For the operating conditions of the ditches these efficiencies are higher ( $Eff_2 = 33\%$  in OD1), while in OD2 it is much better ( $Eff_2 = 83\%$ ). The mean residence times in Table 8.1 are from the numerical RTDs (section 4.4.3). Where denoted by (\*) they are predicted by single-phase flow. It is likely that multi-phase flow is more accurate (\*\*). The missing data for  $Eff_2$  in Table 8.1 is from the predicted residence times. Even though there is missing data, it is considered that aerators that provide a higher mean DO will have a higher  $Eff_2$ . The highest efficiency is therefore for the membrane diffusers (5.44 mg/l in OD1 and 8.74 mg/l in OD2), then Fuch jet aerators (5.97 mg/l in OD2), surface aerators (2.48 mg/l in OD1) and least efficient is the Maguire jet aerator (0.44 mg/l in OD1). This is the most accurate order for assessing the relative efficiencies of the aerators.

Table 8.1 Dissolved oxygen and aerator efficiencies without BOD

Case	OD	Devices	No	Oxygen supply (kg/s)	Max DO (mg/l)	Mean DO (mg/l)	Max DO (% sat)	Mean DO (% sat)	Res. time (hr)	Theory: mean DO (mg/l)	Eff1	Eff2
O2	1	surface	4	0.0163	3.07	2.48	29.2	23.6	8.87*	10.5*sat	15	24
O3	1	diffuser	1	0.0139	7.91	5.44	75.3	51.8	-	-	37	-
O4	1	Maguire jet	1	0.0014	0.68	0.44	6.5	4.2	2.33*	5.88	29	7
O5	1	ALL	6	0.0311	4.12	3.46	39.2	33.0	2.11**	10.5*sat	11	33
O7	2	diffuser	3	0.0413	9.60	8.74	91.4	83.2	-	-	20	-
O8	2	Fuch jet	3	0.0747	10.22	5.97	97.3	56.9	-	-	8	-
O9	2	ALL	6	0.1165	10.23	8.74	97.4	83.2	8.89**	10.5*sat	7	83

## 8.4.2 Aeration design

### Oxidation ditch 1

The patterns of water and dissolved oxygen distributions for individual aerators in OD1 and OD2 are shown in Figures 8.1 to 8.15 near the water surface. The benefit of the **brush surface aerators in OD1** is a homogeneous flow pattern in one flow direction around the ditch. A further benefit is it mitigates against the short-circuiting of the influent to the effluent by reversing the flow direction in the ditch. The flow pattern in Figure 8.1 is quite uniform, however there are fluid plumes that produce recirculation. A further benefit of surface aeration is to agitate the water surface and introduce air into the water. The DO distribution in the ditch is quite homogeneous which is desirable (Figure 8.2). One drawback is that the oxygen mass transfer of surface aeration is difficult to quantify. Another problem is that surface aeration does not efficiently aerate deeper water in the ditch. The brush surface aerators are one of the most inefficient types, with an oxygen mass transfer coefficient of  $3 \text{ h}^{-1}$ . When operating at  $3 \text{ h}^{-1}$ , for the operating conditions, the mean DO in the ditch is 3.46 mg/l. With a quadruple increase in surface aeration to  $12 \text{ h}^{-1}$  this increases to 3.90 mg/l.

The benefit of a **membrane diffuser in OD1** is less fluid turbulence that causes the flow pattern to spread in a tranquil manner (Figure 8.3). Diffusers do not provide a strong dominant flow direction and therefore there are low flow velocities in the ditch. The radial flow pattern has the benefit of diffusion and zonal spreading of dissolved oxygen (Figure 8.4). The mean DO is 52 % of saturation in OD1 and  $\text{Eff}_1 = 37$ , which indicate that the membrane diffuser is more efficient than the surface aerator.

The benefit of a **Maguire jet aerator in OD1** is it provides a high local DO concentration. There are however problems with flow recirculation caused by a strong flow stream (Figure 8.5). There is high DO concentration near the aerator and much lower elsewhere in the ditch (Figure 8.6). Poor oxygenation of water gives a low mean DO of just 4 % of saturation in OD1 (Table 8.1). The amount of oxygen is limited from an air saturated water source. The efficiency of providing DO from the oxygen supply ( $\text{Eff}_1 = 29$ ) is however almost as good as the diffuser ( $\text{Eff}_1 = 37$ ).

For the **operating conditions in OD1** the mean DO in the ditch is 33 % of saturation. The flow pattern is composed of plumes from the surface aerators, radial flow from the diffuser and a strong flow stream from the jet aerator (Figure 8.7). One design improvement may be to move the Maguire jet aerator to the opposite corner of the ditch, away from the diffuser and surface aerators. This could reduce its disturbance towards the radial flow (Figure 8.7) and zonal DO distribution of the diffuser (Figure 8.8). The Maguire jet aerator can be more centrally located and its flow stream in the same direction as the surface aerators (Figure 8.7). The diffuser can be moved slightly left in alignment to the surface aerators (Figure 8.7). The Maguire jet aerator causes the greatest instability to the flow and DO distribution.

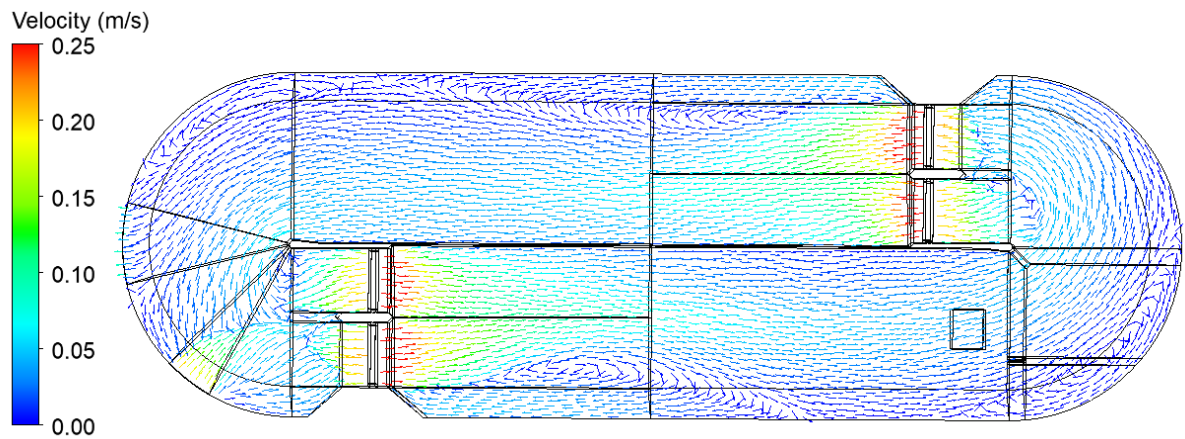


Figure 8.1 Water velocity in OD1 with surface aerators only

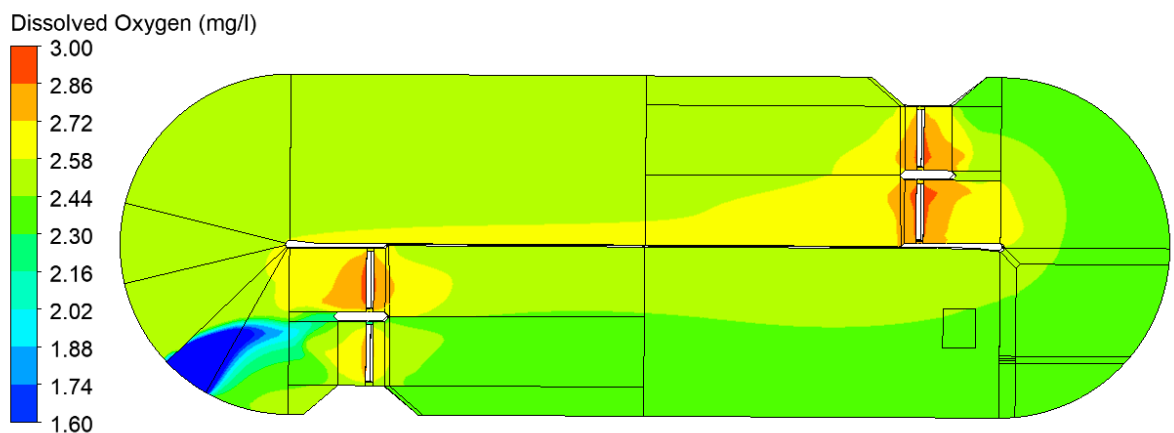


Figure 8.2 DO in OD1 with surface aerators only  
(max = 3.07 mg/l, mean = 2.48 mg/l)

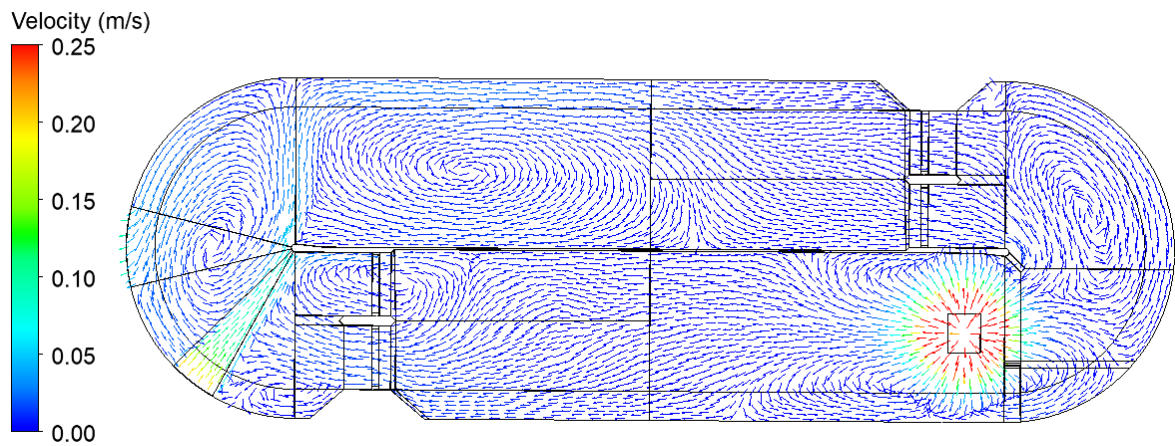


Figure 8.3 Water velocity in OD1 with diffuser only

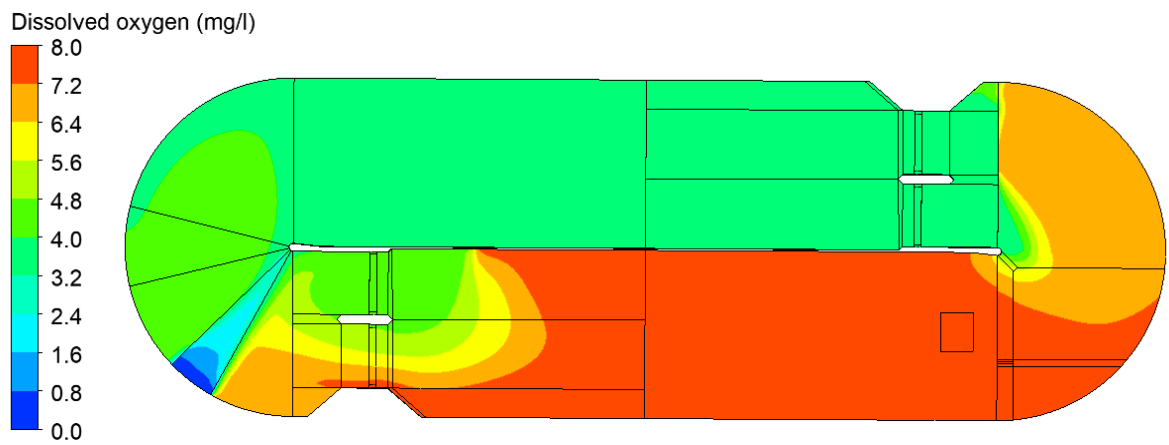


Figure 8.4 DO in OD1 with diffuser only  
(max = 7.91 mg/l, mean = 5.44 mg/l)

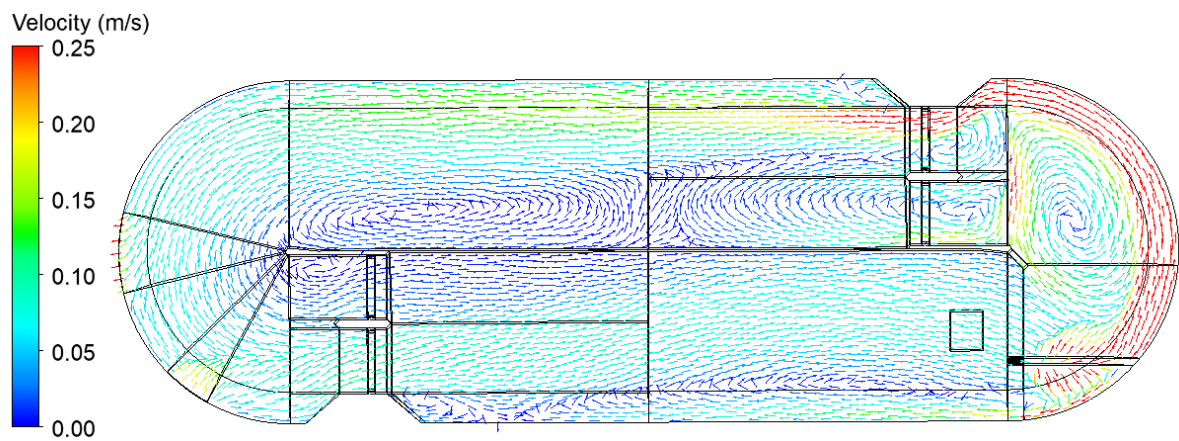


Figure 8.5 Water velocity in OD1 with Maguire jet aerator only

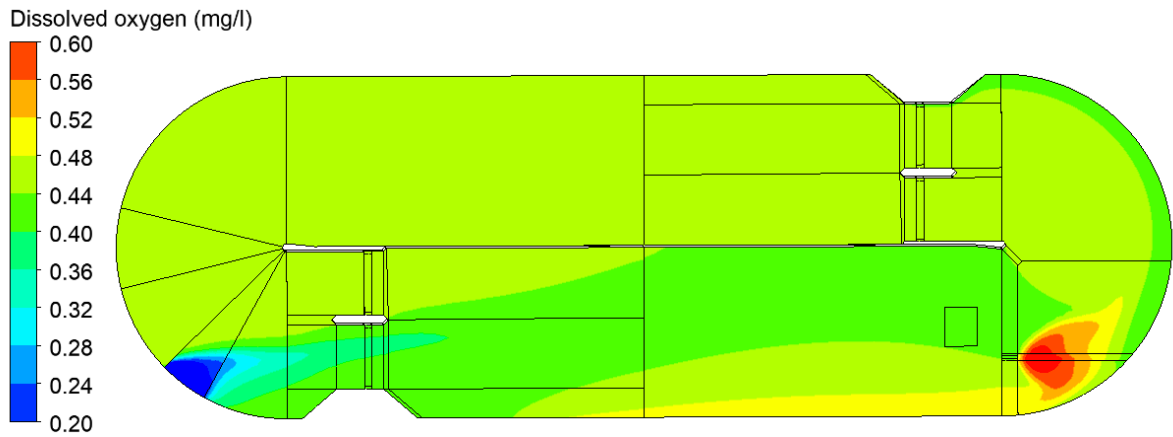


Figure 8.6 DO in OD1 with Maguire jet aerator only  
(max = 0.68 mg/l, mean = 0.44 mg/l)

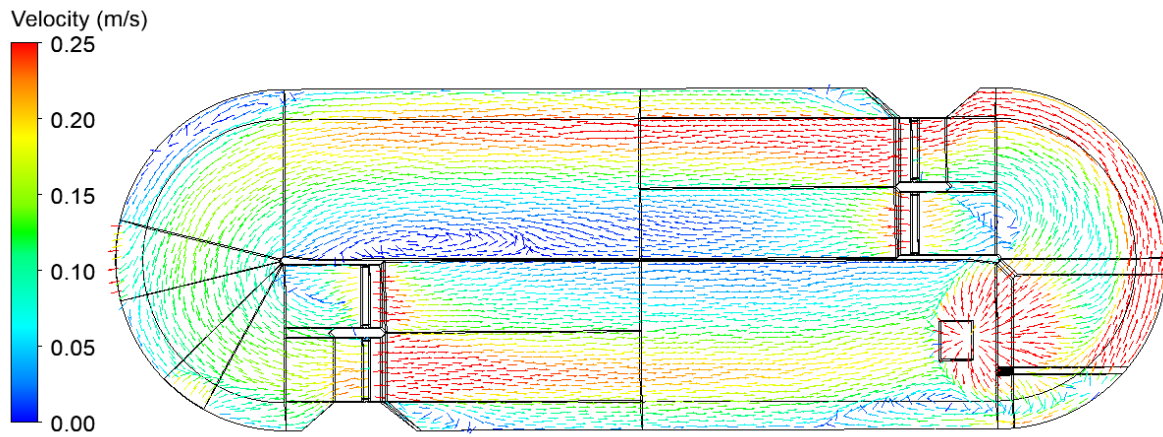


Figure 8.7 Water velocity in OD1 - operating conditions

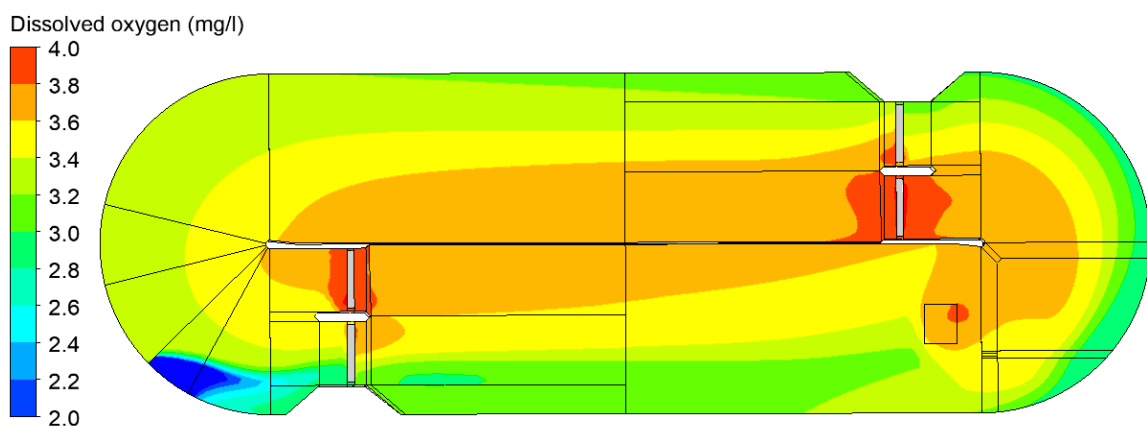


Figure 8.8 DO in OD1 - operating conditions  
(max = 4.12 mg/l, mean = 3.46 mg/l)

## **Oxidation ditch 2**

The **flow booster in OD2** does not introduce oxygen or extra flow to the ditch, but it does change the flow pattern significantly due to a strong flow stream (Figure 8.9). Its location is unsuitable as its flow stream collides with a dividing wall (Figure 8.9). It is recommended to move the booster downstream but keep it central. It is beneficial to move it away from diffusers, so its flow stream does not disturb their radial flow. It is also recommended for it to be kept away from the Fuch jet aerators.

The benefit of the **membrane diffusers in OD2** is a tranquil radial distributed flow pattern (Figure 8.10). Another benefit is a zonal dissolved oxygen pattern in OD2 (Figure 8.11). The diffusers can be moved away from the influent stream, which is interfering with their radial flow. They can also be moved away from the dividing walls and kept central in the ditch. They can be placed in a designated diffuser zone (bottom and left of ditch in Figure 8.10). The diffusers can also be kept away from the Fuch jet aerators. There are higher dissolved oxygen gradients near the influent stream and near the dividing walls in OD2 (Figure 8.11).

The benefit of the **Fuch jet aerators in OD2** is they oxygenate water with a sufficient oxygen supply (Table 8.1). One of their problems is a high inlet velocity jet of air that produces turbulence (Figure 8.12). The flow stream from the Fuch jet aerator flows downwards at an angle, but rising air makes the water flow bi-directionally near the water surface (Figure 8.12). One original design feature of a Fuch jet aerator is mono-directional water flow. However, bi-directional dispersion of DO can be desirable for the spreading of the DO (Figure 8.13). Two Fuch jet aerators in parallel provide a more uniform flow pattern (Figure 8.12). There is a large drop in DO just downstream of the parallel jet aerators due to the mixing of two opposing fluid streams (Figure 8.13). The highest DO is near the nozzles of the aerators. Fuch jet aerators provide a reasonable mean DO of 57 % of saturation. This compares to 83 % from the diffusers (Table 8.1), which also have a lower oxygen supply rate.

For the **operating conditions in OD2** the influent fluid stream interferes with the radial flow patterns of the diffusers (Figure 8.14). The flow stream from the booster collides with a dividing wall and interferes with the spreading of the DO from the diffusers. There is interference between the flow stream of the Fuch jet aerator near the influent and the diffuser downstream. The mean DO in the ditch is very high

(83 % of saturation) in OD2, when all the aerators are operating (Table 8.1). The DO distribution in OD2 (Figure 8.15) is quite homogeneous which is desirable. The exceptions are the high DO concentrations near the nozzles of the Fuch jet aerators, and near the diffuser that is furthest away from the influent. The lower DO concentrations near the two diffusers that are together is due to the dilution from the influent stream (Figure 8.15). Maintaining four operational Fuch jet aerators and keeping them as they are is recommended. Moving the three diffusers into one zonal area (bottom left) and away from the jet aerators and influent stream is recommended. Relocating the booster away from the dividing walls and maintaining a central location is desirable. When optimising the locations of the aerators the following objectives are desirable. The flow patterns and DO distributions should be as uniform as possible (Figures 8.7, 8.8, 8.14, 8.15). The mean DO in the ditch and the efficiency of the individual aerators should be increased (Table 8.1). The mean residence time of the ditch should also be increased.

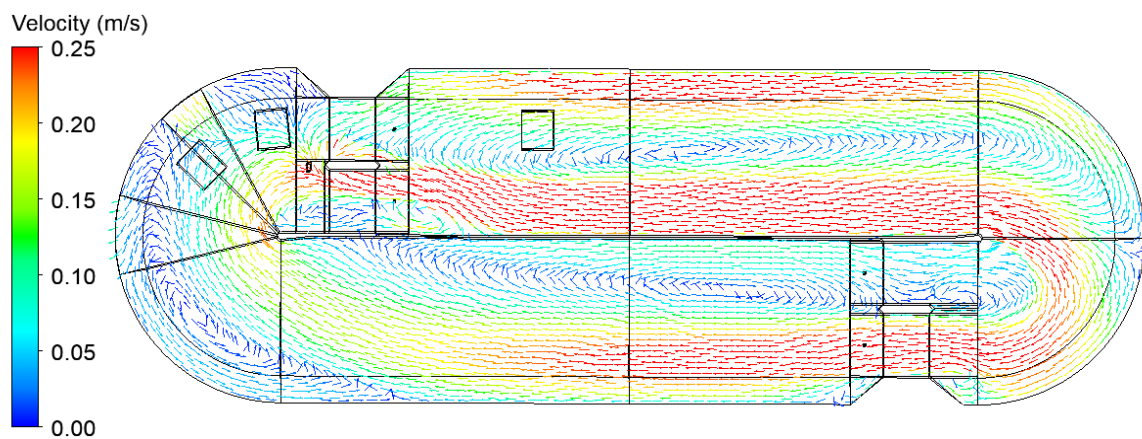


Figure 8.9 Water velocity in OD2 with flow booster only

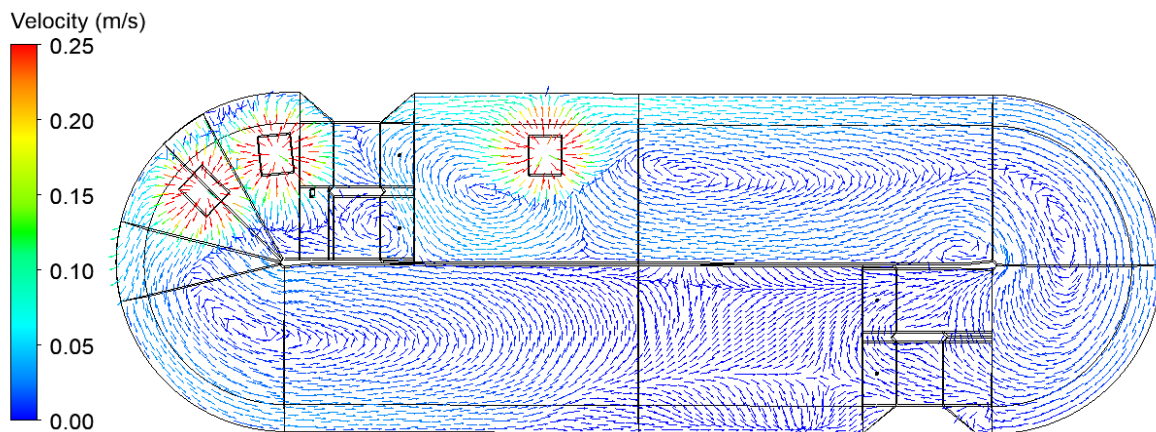


Figure 8.10 Water velocity in OD2 with diffusers only

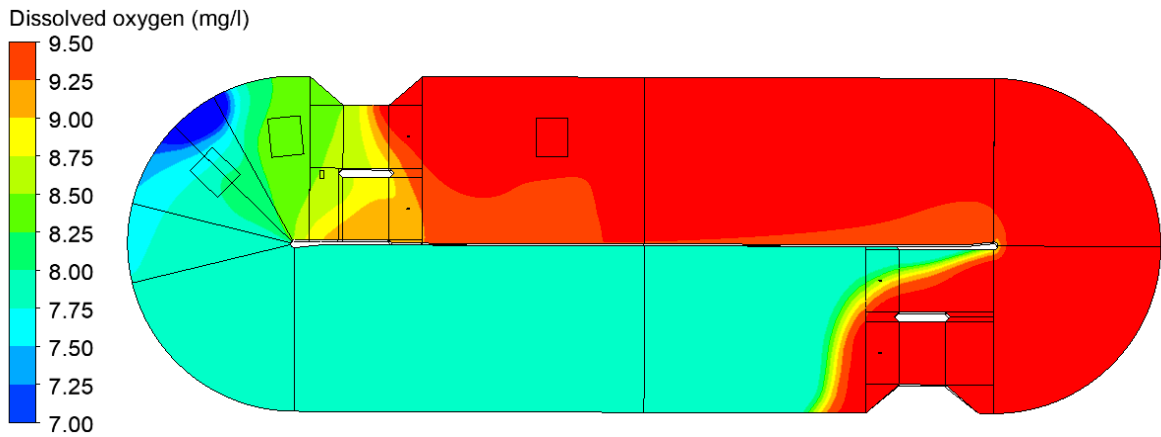


Figure 8.11 DO in OD2 with diffusers only  
(max = 9.60 mg/l, mean = 8.74 mg/l)

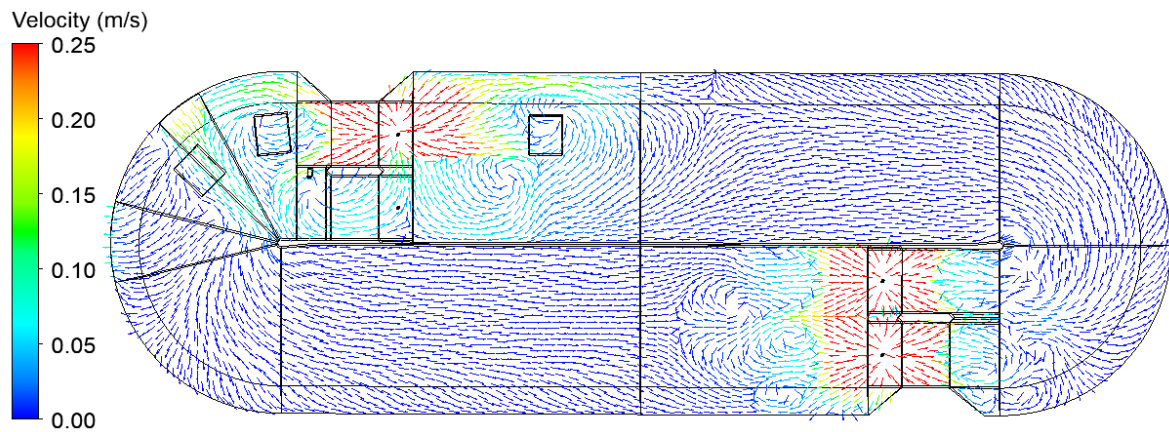


Figure 8.12 Water velocity in OD2 with Fuch jet aerators only

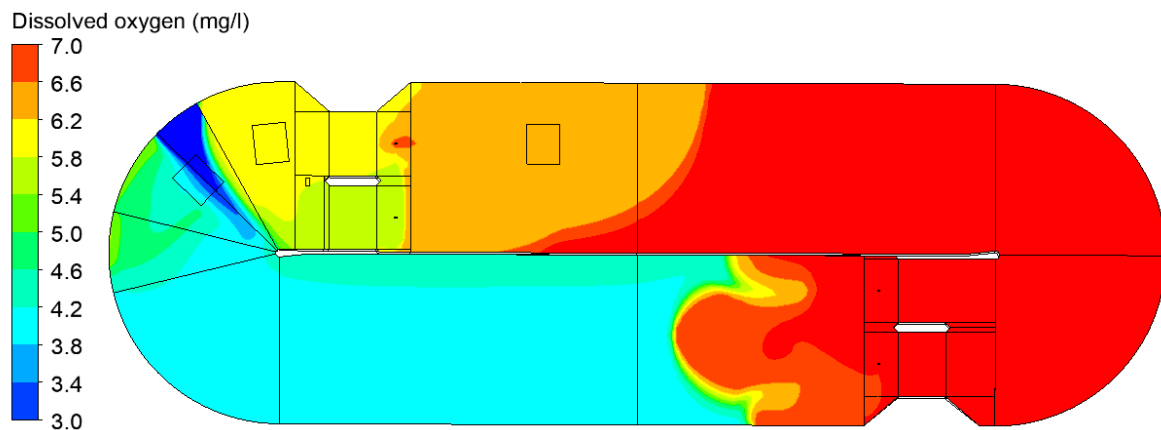


Figure 8.13 DO in OD2 with Fuch jet aerators only  
(max = 10.22 mg/l, mean = 5.97 mg/l)

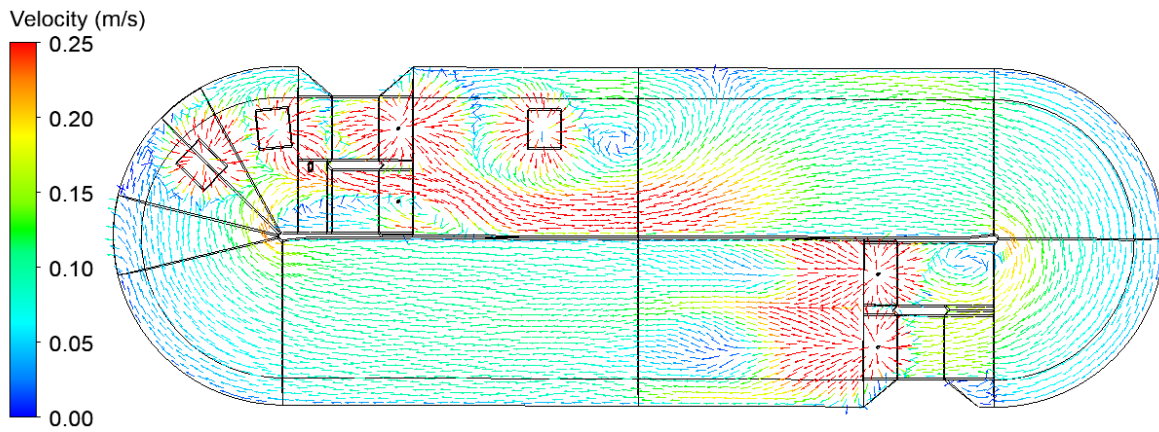


Figure 8.14 Water velocities in OD2 - operating conditions

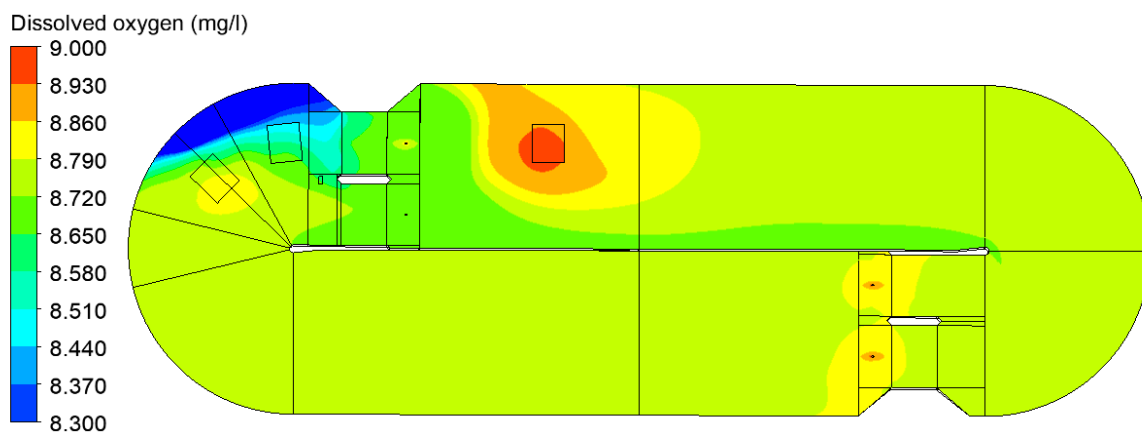


Figure 8.15 DO in OD2 - operating conditions

(max = 10.23 mg/l, mean = 8.73 mg/l)

## Comparison of OD1 and OD2 for operating conditions

For the operating conditions the mean DO in OD1 is 33 % of saturation while in OD2 it is 83 % (Table 8.1). These are similar to values for the efficiency criteria  $Eff_2$ . For the two ditches the efficiency criteria  $Eff_1$  is quite similar ( $Eff_1 = 11$  in OD1,  $Eff_1 = 7$  in OD2). In order of aeration effectiveness, best are the 3 diffusers in OD2 (83 %) and 1 diffuser in OD1 (52 %), then the 3 Fuch jet aerators in OD2 (57 %), then the 4 surface aerators in OD1 (24 %) and least is the Maguire jet aerator in OD1 (4 %).

In **OD1** design retrofitting can move the Maguire jet aerator to the opposite corner of the ditch and central and away from the diffuser and surface aerators. This is to reduce its disturbance of the radial flow (Figure 8.7) and DO spreading of the diffuser (Figure 8.8). The Maguire jet aerator has the lowest mean DO and causes the greatest instability to the flow pattern and DO distribution. The dissolved oxygen distribution in OD1 does **not show** a reasonable homogeneous pattern (Figure 8.8).

In **OD2** the influent stream interferes with the radial flow of the diffusers (Figure 8.14). The flow stream of the booster collides with a wall and interferes with the DO spreading of the diffusers. There is interference between the flow stream of the Fuch jet aerator near the influent and the diffuser downstream. Recommendation is to move the three diffusers into one zonal area, away from the jet aerators and influent. Another option is to relocate the booster away from the dividing walls. The DO distribution in OD2 **does show** a reasonable homogeneous pattern (Figure 8.15).

The improved performance of OD2 (83 %) compared to OD1 (33 %) is due to the 3 diffusers and 3 Fuch jet aerators instead of the 1 diffuser, 4 surface aerators and 1 Maguire jet aerator. It can also be attributed to a higher oxygen supply to OD2 (0.11 kg/s) compared to OD1 (0.03 kg/s). The diffusers are the most efficient aeration system. The Fuch jet aerators with a pure stream of air have merit as they supply sufficient oxygen. The bi-directional flow pattern from the Fuch jet aerators spreads DO around the ditch. For homogeneous flow around the ditch near the water surface the surface aerators in OD1 behave well. Their disadvantage is they mostly affect the distribution of DO that is nearer the water surface. The booster in OD2 produces a strong flow stream which drives flow around the ditch, but unfortunately creates flow recirculation and interferes with the flow patterns of the other aerators.

The criteria for improved aeration design is to increase the dissolved oxygen, uniformity of flow, DO and suspended solids distributions, increase the residence time of the tank and reduce the overall energy consumption (Karpinska and Bridgeman, 2016). Some of the design considerations of aeration systems are the locations of the influent and effluent weir (Jensen et al, 2006), inlet damper wall (Kjellstrand, 2006), locations and designs of baffles (Brannock, 2003; Jensen et al, 2006; Kjellstrand, 2006; Wei et al, 2016a), design of mixing impellers in terms of radius (Liu et al, 2014), submergence depth (Wei et al, 2016b), position (Brannock, 2003; Kjellstrand, 2006; Climent et al, 2019), number and rotating speed (Zhang et al, 2016), operation of surface aerators and mixing impellers (Gillot and Heduit, 2000; Yang et al, 2011; Xie et al, 2014), rotating speed of surface aerators (Fan et al, 2010), oxygen transfer rate of surface aerators (Thakre et al, 2008; Bhuyer et al, 2009), diffuser design with different bubble sizes (Terashima et al, 2016), grid diffuser spacing (Gillot and Heduit, 2000; Gillot et al, 2005; Gresch et al, 2011), air-lift oxidation ditch (Xu et al, 2010), pressurised aeration chamber and hydrojets (Karpinska, 2013).

In terms of oxidation ditch design at Potterne WWTP there are recommendations from the literature which can help optimise the hydrodynamics and aeration. It has to be considered that these recommendations apply to completely different designs than Potterne WWTP. Therefore they are only given here as general guidelines, and some of these may not be entirely suitable for the ditches at Potterne WWTP.

A vertical baffle at the inlet can guide flow and mitigate against short circuiting of the influent towards the effluent and thereby increase the residence time of the tank. The inlet and outlet weirs can be placed at opposite ends of the ditch to increase the residence time. Positioning the inlet and outlet weirs centrally splits the flow equally by the central wall and may reduce the average velocity and increase the residence time (Jensen et al, 2006). Impellers with optimal radius (Liu et al, 2014) and optimal submergence depth (Wei et al, 2016b) can make the flow distribution more uniform. Baffles that are angled downwards just downstream of the surface aerators can increase velocity at the ditch bottom, make the vertical velocity distribution more uniform which help prevent sludge deposits and increase the residence time. Baffles

can also guide DO into the bottom of the ditch, which can increase the mixture time between oxygen and water and increase oxygen mass transfer (Wei et al, 2016a).

By adjusting the position, rotating speed and number of submerged propellers, the flow distribution can be more homogeneous and problems with sludge deposits and the low velocity in the ditch bend may be improved (Zhang et al, 2016). Changes to the operation include turning on and off surface aerators and submerged impellers, which may improve the uniformity of the flow field, DO distribution (Yang et al, 2011) and suspended solids distribution (Xie et al, 2014). Suspended solids concentrations can be dispersed more evenly with a higher surface aerator rotating speed. Mixing propellers can be placed at the tank bottom to prevent sludge settling (Fan et al, 2010). The optimum location of the mixing propellers can improve the uniformity of the flow pattern (Climent et al, 2019). An even distribution of mixers and baffles along the length of a channel reactor creates several small well mixed zones in series. When flow is more uniform this increases pollutant removal (Brannock, 2003). In a channel reactor measures are studied to deal with the high velocity of the influent flow by using an inlet damper wall, mixer and baffles. The options eliminate the short circuiting stream and increase the residence time of the tank (Kjellstrand, 2006). The oxygen transfer rate (OTR) of the surface aerators can be improved by their design. In studies the curved blade rotor type is the best type with an oxygen transfer coefficient of  $11.50 \text{ h}^{-1}$ , then cage fin rotor is  $4.33 \text{ h}^{-1}$ , cage rope wound rotor is  $3.78 \text{ h}^{-1}$ , and Kessener brush rotor is the worst at  $2.94 \text{ h}^{-1}$  (Thakre et al, 2008; Bhuyer et al, 2009).

Different diffuser types produce different bubble sizes. Coarse-bubble, fine-pore, and slitted membrane diffusers have bubble sizes of 7-8 mm, 5-6 mm, and 3 mm (Terashima et al, 2016). In a channel reactor, the spatial distribution of air diffusers can lead to oscillations in the flow field (Gresch et al, 2011). In closed loop reactors these may be suppressed by slow speed mixers (Gillot and Heduit, 2000). When grid diffusers are spaced out, increasing the oxygen supply leads to a reduction in the oxygen transfer efficiency (OTE), that is caused by increased spiral flow (Gillot and Heduit, 2000). This supports the superiority of total floor coverage compared to diffusers that are placed in separate grids (Gillot et al, 2005).

## 8.4 Summary

*The overall benefits to the oxidation ditch design are as follows.* The criteria for better aeration design is higher dissolved oxygen, more uniform distribution of flow and DO, higher residence time and lower energy consumption. The Maguire jet aerator, surface aerators and booster provide a dominant flow direction in the ditch which reduces flow short circuiting. For all devices there is an increase in residence time of the ditch. For all devices there is an increase in water velocity which mitigates against undesirable sludge deposition. Dissolved oxygen is dispersed quite evenly by the surface aerators, diffusers and Maguire jet aerator. In OD1, the diffuser provides a reasonable DO, from less oxygen than the surface aerators and a much higher DO than the Maguire jet aerator. In OD2, the diffusers provide an even higher DO and from less oxygen than the Fuch jet aerators. The Fuch aerators spread DO bi-directionally and produce a homogeneous DO pattern. They provide reasonable DO from a pure air source. There is DO homogenisation by the mixing from the surface aerators, Maguire jet aerator and booster. Diffusers are the most efficient aerator as they produce the highest DO. The higher DO and better homogeneity of DO in OD2 is attributed to the diffusers, Fuch jet aerators and higher oxygen supply.

*The overall drawbacks to the oxidation ditch design are as follows.* The surface aerators produce a heterogeneous vertical distribution. The OTR of a surface aerator is difficult to quantify unless it is measured. The Maguire jet aerator produces undesirable flow recirculation. The DO produced by the Maguire jet aerator is low, because it is an ineffective aeration device from an aerated water source. The air jet from the Fuch aerator forms a complex bi-directional flow pattern. The diffusers produce local flow recirculation. The diffusers and Fuch aerators block the horizontal flow in the ditch. The booster produces undesirable flow recirculation and turbulence.

Moving the Maguire jet aerator could reduce its disturbance towards the nearby diffuser. The booster could be moved to avoid collision of its flow stream with an internal wall and reduce its interference with other aerators. Diffusers could be zoned away from Fuch jet aerators and the influent stream to avoid disturbance between aerators. In future work, the design recommendations from the literature review may also be used to improve the performance of the aeration devices at Potterne WWTP.

## 9. Conclusions and future work

### 9.1 Conclusions

- The biochemical oxygen demand (BOD) distribution and bubble size distribution (BSD) are important parameters for the dissolved oxygen (DO) distribution.
- Modelling the effect of the BOD distribution on the DO distribution is a novel approach that has not been undertaken in the literature.
- Dissolved oxygen is affected by the BOD distribution, temperature, surface aeration, bubble diameter, bubble size distribution, molar fraction Henry coefficient and mass diffusivity and turbulent Schmidt number of oxygen in water.
- Decreasing the bubble size increases the total interfacial surface area of the bubbles, which increases interfacial oxygen mass transfer and dissolved oxygen.
- The local BOD concentration depends on either the local DO concentration or the local residence time. The coupled DO-BOD modelling approach is used.
- BOD distribution when compared to mean BOD does improve the accuracy of the dissolved oxygen by better agreement with the measurements of DO variation.
- Bubble size distribution when compared to mean bubble size does improve the accuracy of dissolved oxygen by better agreement with mean DO measurements.
- The bubble size distribution predicts a mean bubble size of 1.9 mm.
- The best agreement with the measurements of dissolved oxygen is a bubble size of 2 mm, suggesting this is the probable mean bubble size in the ditch.
- There is good agreement between simulation and physical observation in terms of the flow pattern in both of the ditches at Potterne WWTP.
- There is good agreement between simulation and physical measurement in terms of the mean DO in both of the ditches at Potterne WWTP.
- The BOD distribution is quite similar for the different model parameters.
- The mean and maximum DO in the ditch is affected by the model parameters.
- In decreasing order of aeration performance are the air membrane diffuser, Fuch air jet aerator, Kessener brush surface aerator and Maguire hydro-jet aerator.
- It is recommended that the flow booster, Maguire jet aerator and membrane diffusers are relocated to reduce the flow disturbance between the aerators.

***The overall benefits for oxidation ditch design are as follows.***

- The criteria for better aeration performance is higher DO, better homogenisation of the flow and DO distribution, higher residence time and lower energy consumption.
- For all the devices there is an increase in mean water velocity in the ditch, which can mitigate against sludge deposition and provide better transport of dissolved oxygen.
- The Maguire jet aerator, surface aerators and flow booster provide a dominant flow direction in the ditch, which reduces flow short circuiting of the influent weir stream.
- For all the devices there is an increase in the residence time of the ditch.
- The diffusers provide a higher mean DO, with a lower oxygen supply than the Fuch jet aerators and surface aerators and much higher DO than the Maguire jet aerator.
- There is a desirable zonal DO pattern with the diffusers and Fuch jet aerators.
- The Fuch jet aerators provide a reasonable mean DO from a pure air source.
- The better aeration performance of oxidation ditch OD2 is due to the diffusers, Fuch jet aerators and the higher oxygen supply.
- There is improved homogenisation of dissolved oxygen in the ditches by the fluid mixing of the surface aerators, Maguire jet aerator, Fuch jet aerators and booster.

***The overall drawbacks for oxidation ditch design are as follows.***

- Oxidation ditches have a bend geometry, relative shallow depth and variable aeration sources and therefore their velocity and DO distribution is heterogeneous.
- Main causes of heterogeneous flow distribution are Maguire jet aerator and booster.
- The Maguire jet aerator causes the flow from the surface aerators to be asymmetric.
- The ineffective position of the booster produces undesirable fluid turbulence.
- The surface aerators produce undesirable heterogeneous vertical flow distribution.
- The oxygen transfer rate of surface aeration is difficult to quantify unless measured.
- The Fuch jet aerators cause water to flow bi-directionally due to a pure air jet source.
- The diffusers produce undesirable local flow recirculation.
- The diffusers and Fuch jet aerators block the general flow direction in the ditch.
- The dissolved oxygen provided by the Maguire jet aerator is low, suggesting it is an ineffective aeration device with a low oxygen supply from an aerated water stream.

## 9.2 Future work

### CFD modelling

*The bubble size distribution (BSD)* could also be helpful in understanding how the individual aeration devices deliver different bubble sizes to the oxidation ditch. The *disturbance of the water surface* can be affected by the surface aerator and the rising bubble plume and flow re-circulation from the diffuser, jet aerator and mixing impeller. To predict the shape of the water surface the surface tracking volume of fluid (VOF) model can be used. Quantifying the *transfer of atmospheric air through the water surface* and using it as an oxygen source term can be undertaken. More detailed *geometric modelling of the membrane grid diffuser* can be undertaken.

*Three phase flow modelling* considers the main phase as the liquid wastewater and the bubbles and particles as dilute disperse phases. Spherical bubbles and particles can be simplified with uniform properties. Suspended solids can incorporate discrete, flocculent, hindered and compressive settling behaviour. Bubble coalescence and particle flocculation can be coupled to the three phase flow model.

*Activated Sludge Models (ASM)* could be integrated into the CFD models that have been developed in this study. ASM can be used to predict nitrogen removal (nitrification and de-nitrification), phosphorus removal, COD removal and the growth and decay of aerobic heterotrophs and phosphorus accumulating organisms (PAOs).

### Experimental validation

Comparison between a numerical *residence time distribution (RTD)* and an experimental tracer test can be used to validate the CFD simulation. Tracer experiments can be conducted on the Potterne WWTP ditches. *Bubble size measurements* can provide bubble size distribution data for (1) aeration device inlet conditions and (2) validation of the numerical BSD. The measurement of bubble size can be undertaken by an optical probe or high resolution camera imaging. They can be measured in the ditches at Potterne WWTP at multiple locations including near the different aerators. They can also be measured in a laboratory scale ditch model.

*Fluid velocity measurements* can be used to validate the numerical velocities. A portable propeller flow meter can take measurements near the water surface and at different depths. Experiments can be undertaken on the Potterne WWTP ditches or on a laboratory scale ditch model. *Dissolved oxygen measurements* may also be taken at different water depths in the Potterne WWTP ditches. The *oxygen transfer rate (OTR) of the surface aerators* may also be measured at Potterne WWTP.

### **Aeration design and energy requirement**

It is the future intention to conduct a detailed CFD design study to be able to improve the aeration performance at Potterne WWTP. The criteria is to improve the uniformity of the flow pattern and DO distribution, to increase the residence time of the tank and to reduce the energy consumption. Aerators can be optimised individually in the oxidation ditch before combining them together. Design recommendations from the literature review can also be used to improve and optimise the design of the influent and effluent, mixing impeller, surface aerator, jet aerator and diffuser aerator.

There is a balance between how much dissolved oxygen is produced and how much energy is consumed. Aeration systems are competitively bid on the basis of oxygen transfer per unit of power or energy consumed, which is (1) mechanical power for rotors, blowers and water pumps and (2) energy power for water motion. CFD simulation can be used to evaluate an aeration device for its power and energy input, its process variables (OTR, OTE and AE) and its fluid variables of velocity and DO.

### **Graphical fluid visualisation**

Engineering fluid visualisation increasingly requires high visual fidelity photorealistic fluid animations to help demonstrate design improvements to engineers, benefit computer graphics research and provide a clearer understanding of the hydrodynamics and the energy savings. It can also help deliver a virtual reality (VR) technology. Photorealistic animations using games engine technology are being proposed. Fluid visualisation methods can be evaluated by conducting a participant usability study. The usability study can be undertaken by creating an online questionnaire that contains the graphical content of the fluid animations.

## References

- Abusam, A., Keesman, K.J., Spanjers, H., Van Straten, G. and Meinema, K., 2002. Effect of oxidation ditch horizontal velocity on the nitrogen removal process. *Official Publication of the European Water Association (EWA)*, 6, pp.1-9.
- Alaya, S.B., Haouech, L., Cherif, H. and Shayeb, H., 2010. Aeration management in an oxidation ditch. *Desalination*, 252(1-3), pp.172-178.
- Anderson, J.D. and Wendt, J., 1995. *Computational fluid dynamics* (Vol. 206). New York: McGraw-Hill.
- Ansys, Inc, 2017. ANSYS Fluent 18.0 Theory Guide.
- Barat, R., Serralta, J., Ruano, M.V., Jiménez, E., Ribes, J., Seco, A. and Ferrer, J., 2013. Biological Nutrient Removal Model No. 2 (BNRM2): a general model for wastewater treatment plants. *Water Science and Technology*, 67(7), pp.1481-1489.
- Batstone, D. J., Keller, J., Angelidaki, I., Kalyuzhnyi, S. V., Pavlostathis, S. G., Rozzi, A., Sanders, W. T. M., Siegrist, H. and Vavilin, V. A., 2002. Anaerobic Digestion Model No.1. IWA STR No.13. IWA Publishing, London, UK.
- Benfield, L. D. & Randall, C. W., 1980. Activated sludge and its process modification. In: *Biological Process Design for Wastewater Treatment*. Prentice-Hall Inc., Englewood Cliffs, NJ, USA.
- Bhuyar, L.B., Thakre, S.B. and Ingole, N.W., 2009. Design characteristics of curved blade aerator wrt aeration efficiency and overall oxygen transfer coefficient and comparison with CFD modelling. *International Journal of Engineering, Science and Technology*, 1(1), pp.1-15.
- Bokil, S.D. and Bewtra, J.K., 1972. Influence of mechanical blending on aerobic digestion of waste activated sludge. *Proc. 6th Int. Assoc. on Water Pollution Research and Control, London*, pp.421-438.
- Brackbill, J.U., Kothe, D.B. and Zemach, C., 1992. A continuum method for modeling surface tension. *Journal of computational physics*, 100(2), pp.335-354.
- Brannock, M.W.D., 2003. Computational fluid dynamics tools for the design of mixed anoxic wastewater treatment vessels. PhD thesis. University Queensland, Australia.
- Bridgeman, J., Jefferson, B. and Parsons, S.A., 2009. Computational fluid dynamics modelling of flocculation in water treatment: a Review. *Engineering Applications of Computational Fluid Mechanics*, 3(2), pp.220-241.
- Burns, A.D., Frank, T., Hamill, I. and Shi, J.M., 2004, May. The Favre averaged drag model for turbulent dispersion in Eulerian multi-phase flows. In *5th international conference on multiphase flow, ICMF* (Vol. 4, pp. 1-17). ICMF.
- Burrows, L.J., Stokes, A.J., West, J.R., Forster, C.F. and Martin, A.D., 1999. Evaluation of different analytical methods for tracer studies in aeration lanes of activated sludge plants. *Water Research*, 33(2), pp.367-374.

Burrows, L.J., West, J.R., Forster, C.F. and Martin, A., 2001. Mixing studies in an Orbal activated sludge system. *Water SA*, 27(1), pp.79-84.

Butler, E., Hung, Y., Al Ahmad, M., Yeh, R., Liu, R. and Fu, Y., 2017. Oxidation pond for municipal wastewater treatment. *Applied Water Science*, 7(1), pp.31-51.

Çengel, Y.A. and Boles, M.A., 2008. *Thermodynamics: an engineering approach*, McGraw-Hill.

Chen, L. and Feng, Q., 2014. Two-phase flow model applied in the oxidation ditch. In *Advanced Materials Research* (Vol. 838, pp. 1659-1662). Trans Tech Publications.

Clift, R., Grace, J.R., Weber, M.E., 1978. *Bubbles, Drops and Particles*. Academic, New York, pp.171-202.

Climent, J., Martínez-Cuenca, R., Carratalà, P., González-Ortega, M.J., Abellán, M., Monrós, G. and Chiva, S., 2019. A comprehensive hydrodynamic analysis of a full-scale oxidation ditch using Population Balance Modelling in CFD simulation. *Chemical Engineering Journal*, 374, pp.760-775.

Cockx, A., Line, A., Roustan, M., Do-Quang, Z. and Lazarova, V., 1997. Numerical simulation and physical modeling of the hydrodynamics in an air-lift internal loop reactor. *Chemical Engineering Science*, 52(21-22), pp.3787-3793.

Cockx, A., Do-Quang, Z., Audic, J.M., Liné, A. and Roustan, M., 2001. Global and local mass transfer coefficients in waste water treatment process by computational fluid dynamics. *Chemical Engineering and Processing: Process Intensification*, 40(2), pp.187-194.

Daigger, G.T. and Littleton, H.X., 2000. Characterization of simultaneous nutrient removal in staged, closed-loop bioreactors. *Water Environment Research*, 72(3), pp.330-339.

Dammel, E.E. and Schroeder, E.D., 1991. Density of activated sludge solids. *Water research*, 25(7), pp.841-846.

Danckwerts, P.V., 1953. Continuous flow systems: distribution of residence times. *Chemical Engineering Science*, 2(1), pp.1-13.

De Clercq, B., Coen, F., Vanderhaegen, B. and Vanrolleghem, P.A., 1999. Calibrating simple models for mixing and flow propagation in waste water treatment plants. *Water Science and Technology*, 39(4), pp.61-69.

De Gussem, K., Fenu, A., Wambecq, T. and Weemaes, M., 2014. Energy saving on wastewater treatment plants through improved online control: case study wastewater treatment plant Antwerp-S. *Water Science and Technology*, 69(5), pp.1074-1079.

De Moyer, C.D., Schierholz, E.L., Gulliver, J.S. and Wilhelms, S.C., 2003. Impact of bubble and free surface oxygen transfer on diffused aeration systems. *Water research*, 37(8), pp.1890-1904.

- Degremont, G. ed., 2007, *Water treatment handbook*. John Wiley & Sons 11th Ed.
- Dhanasekharan, K.M., Sanyal, J., Jain, A. and Haidari, A., 2005. A generalized approach to model oxygen transfer in bioreactors using population balances and computational fluid dynamics. *Chemical Engineering Science*, 60(1), pp.213-218.
- Díez, L., Zima, B.E., Kowalczyk, W. and Delgado, A., 2007. Investigation of multiphase flow in sequencing batch reactor (SBR) by means of hybrid methods. *Chemical engineering science*, 62(6), pp.1803-1813.
- Dorofeev, A.G., Nikolaev, Y.A., Kozlov, M.N., Kevbrina, M.V., Agarev, A.M., Kallistova, A.Y. and Pimenov, N.V., 2017. Modeling of anammox process with the biowin software suite. *Applied Biochemistry and Microbiology*, 53(1), pp.78-84.
- Do-Quang, Z., Cockx, A., Liné, A. and Roustan, M., 1998. Computational fluid dynamics applied to water and wastewater treatment facility modeling. *Environmental Engineering and policy*, 1(3), pp.137-147.
- Drews, R.J.L.C., Malan, W.M., Meiring, P.G.J. and Moffatt, B., 1972. The Orbal extended aeration activated sludge plant. *Journal (Water Pollution Control Federation)*, pp.221-231.
- Drews, R.J.L.C. and Greeff, A.M., 1973. Nitrogen elimination by rapid alternation of aerobic/"anoxic" conditions in "orbal" activated sludge plants. *Water Research*, 7(8), pp.1183-1194.
- Du, X., Wang, J., Jegatheesan, V. and Shi, G., 2018. Dissolved oxygen control in activated sludge process using a neural network-based adaptive PID algorithm. *Applied sciences*, 8(2), p.261.
- Dudley, J., 1995. Process testing of aerators in oxidation ditches. *Water Res.* 29 (9), 2217–2219.
- Elshaw, A., Hassan, N.M.S. and Khan, M.M.K., 2016. CFD modelling and optimisation of a Waste Water Treatment Plant Bioreactor-a case study. 3rd Asia-Pacific World Congress on Computer Science and Engineering.
- Fan, L., Xu, N., Wang, Z. and Shi, H., 2010. PDA experiments and CFD simulation of a lab-scale oxidation ditch with surface aerators. *Chemical Engineering Research and Design*, 88(1), pp.23-33.
- Fayolle, Y., Gillot, S., Cockx, A., Roustan, M. and Héduit, A., 2006. In Situ Local Parameter Measurements for CFD Modelling to Optimize Aeration. *Proceedings of the Water Environment Federation*, 2006(9), pp.3314-3326.
- Fayolle, Y., Cockx, A., Gillot, S., Roustan, M. and Héduit, A., 2007. Oxygen transfer prediction in aeration tanks using CFD. *Chemical Engineering Science*, 62(24), pp.7163-7171.

Ferrer, J., Seco, A., Serralta, J., Ribes, J., Manga, J., Asensi, E., Morenilla, J.J. and Llavador, F., 2008. DESASS: a software tool for designing, simulating and optimising WWTPs. *Environmental Modelling & Software*, 23(1), pp.19-26.

Fouad, M. and El-Morsy, A., 2014. Sludge accumulation pattern inside oxidation ditch case study. *Water Science and Technology*, 69(12), pp.2468-2475.

Frank, T., Zwart, P.J., Shi, J.M., Krepper, E., Lucas, D. and Rohde, U., 2005, September. Inhomogeneous MUSIG model - A population balance approach for polydispersed bubbly flows. In *Proceeding of International Conference for Nuclear Energy for New Europe, Bled, Slovenia*.

Ganczarczyk, J.J., 1994. Microbial aggregates in wastewater treatment. *Water Science and Technology*, 30(8), pp.87-95.

Gheorghe, G.I., Donțu, O., Băran, N., Moga, I.C., Constantin, M. and Tămășanu, E., 2018, September. Researches on the Measurement of the Dissolved Oxygen Concentration in Stationary Waters. In *International Conference of Mechatronics and Cyber-Mixmechatronics* (pp. 29-40). Springer, Cham.

Ghawi, A.H., 2014. Performance improvement of conventional aeration tanks using CFD modelling. *Kufa journal of Engineering*, 3(1).

Gillot, S. and Heduit, A., 2000. Effect of air flow rate on oxygen transfer in an oxidation ditch equipped with fine bubble diffusers and slow speed mixers. *Water research*, 34(5), pp.1756-1762.

Gillot, S., Capela-Marsal, S., Roustan, M. and Héduit, A., 2005. Predicting oxygen transfer of fine bubble diffused aeration systems - model issued from dimensional analysis. *Water research*, 39(7), pp.1379-1387.

Glover, G.C., Printemps, C., Essemiani, K. and Meinhold, J., 2006. Modelling of wastewater treatment plants—how far shall we go with sophisticated modelling tools?. *Water Science and Technology*, 53(3), pp.79-89.

Gresch, M., Braun, D. and Gujer, W., 2010. The role of the flow pattern in wastewater aeration tanks. *Water Science and Technology*, 61(2), pp.407-414.

Gresch, M., Armbruster, M., Braun, D. and Gujer, W., 2011. Effects of aeration patterns on the flow field in wastewater aeration tanks. *Water research*, 45(2), pp.810-818.

Grijpspeerdt, K. and Verstraete, W., 1997. Image analysis to estimate the settleability and concentration of activated sludge. *Water Research*, 31(5), pp.1126-1134.

Guo, L., Zhang, D., Xu, D. and Chen, Y., 2009. An experimental study of low concentration sludge settling velocity under turbulent condition. *water research*, 43(9), pp.2383-2390.

Guo, X., Zhou, X., Chen, Q. and Liu, J., 2013. Flow field and dissolved oxygen distributions in the outer channel of the Orbal oxidation ditch by monitor and CFD simulation. *Journal of Environmental Sciences*, 25(4), pp.645-651.

Haas, C.N. and Karra, S.B., 1984. Kinetics of microbial inactivation by chlorine. Kinetics in presence of chlorine demand. *Water Research*, 18(11), pp.1451-1454.

Heijnen, J.J., Hols, J., Van Der Lans, R.G.J.M., Van Leeuwen, H.L.J.M., Mulder, A. and Weltevrede, R., 1997. A simple hydrodynamic model for the liquid circulation velocity in a full-scale two-and three-phase internal airlift reactor operating in the gas recirculation regime. *Chemical Engineering Science*, 52(15), pp.2527-2540.

Henze, M., Grady C.L., Gujer, W., Marais, G.V.R. and Matsuo, T., 1987. Activated sludge model no. 1: lawprc scientific and technical report no. 1. *IAWPRC, London*.

Henze, M., Gujer, W., Mino, T. and Van Loosdrecht, M.C.M., 2000. *Activated sludge models ASM1, ASM2, ASM2d and ASM3*. IWA publishing.

Higbie, R., 1935. The rate of absorption of a pure gas into a still liquid during short periods of exposure. *Trans. AIChE*, 31, pp.365-389.

Höhne, T. and Mamedov, T., 2020. CFD Simulation of Aeration and Mixing Processes in a Full-Scale Oxidation Ditch. *Energies*, 13(7), p.1633.

Hreiz, R., Potier, O., Wicks, J. and Commenge, J.M., 2019. CFD Investigation of the effects of bubble aerator layouts on hydrodynamics of an activated sludge channel reactor. *Environmental technology*, 40(20), pp.2657-2670.

Hu, Y., Guo, Y., Zhu, W. and Chen, B., 2010, June. Numerical simulation and experiment of gas-liquid flow in aeration tanks. In *Mechanic Automation and Control Engineering (MACE), 2010 International Conference on* (pp. 2140-2144). IEEE.

Hu, Y., Chen, B. and Guo, Y., 2013. The research of gas-liquid-solid flow in aeration tanks. *BioTechnology: An Indian Journal*, 8(3).

Huang, W., Wu, C. and Xia, W., 2009. Oxygen transfer in high-speed surface aeration tank for wastewater treatment: Full-scale test and numerical modeling. *Journal of Environmental Engineering*, 135(8), pp.684-691.

Huang, W., Li, K., Wang, G. and Wang, Y., 2013. Computational Fluid Dynamics Simulation of Flows in an Oxidation Ditch Driven by a New Surface Aerator. *Environmental engineering science*, 30(11), pp.663-671.

Ishii, M. and Kim, S., 2001. Micro four-sensor probe measurement of interfacial area transport for bubbly flow in round pipes. *Nuclear engineering and design*, 205(1-2), pp.123-131.

Ishii, M. and Zuber, N., 1979. Drag coefficient and relative velocity in bubbly, droplet or particulate flows. *AIChE Journal*, 25(5), pp.843-855.

- Jamialahmadi, M., Branch, C. and Müller-Steinhagen, H., 1994. Terminal bubble rise velocity in liquids. *Chemical engineering research & design*, 72(1), pp.119-122.
- Jensen, M.D., Ingildsen, P., Rasmussen, M.R. and Laursen, J., 2006. Computational fluid dynamics modelling of hydraulics and sedimentation in process reactors during aeration tank settling. *Water science and technology*, 53(12), pp.257-264.
- Jin, B. and Lant, P., 2004. Flow regime, hydrodynamics, floc size distribution and sludge properties in activated sludge bubble column, air-lift and aerated stirred reactors. *Chemical Engineering Science*, 59(12), pp.2379-2388.
- Jin, B., Wilén, B.M. and Lant, P., 2004. Impacts of morphological, physical and chemical properties of sludge flocs on dewaterability of activated sludge. *Chemical Engineering Journal*, 98(1), pp.115-126.
- Joshi, J.B., 2001. Computational flow modelling and design of bubble column reactors. *Chemical Engineering Science*, 56(21), pp.5893-5933.
- Karamanev, D.G. and Nikolov, L.N., 1992. Free rising spheres do not obey Newton's law for free settling. *AIChE journal*, 38(11), pp.1843-1846.
- Karamanev, D.G., 1994. Rise of gas bubbles in quiescent liquids. *AIChE journal*, 40(8), pp.1418-1421.
- Karches, T. and Buzas, K., 2013. Investigation of residence time distribution and local mean age of fluid to determine dead zones in flow field. *International Journal of Computational Methods and Experimental Measurements*, 1(2), pp.132-141.
- Karpinska, A.M., Dias, M.M., Boaventura, R.R., Lopes, J.C.B., Santos, R.J., 2010. CFD Approach on the Energy Analysis of an Oxidation Ditch Aerated with Hydrojets. World Congress on Water, Climate and Energy.
- Karpinska Portela, A.M., 2013. New Design Tools for Activated Sludge Process (PhD thesis). FEUP, University of Porto, Porto, Portugal.
- Karpinska, A.M., Dias, M.M., Boaventura, R.A. and Santos, R.J., 2015. Modeling of the hydrodynamics and energy expenditure of oxidation ditch aerated with hydrojets using CFD codes. *Water Quality Research Journal of Canada*, 50(1), pp.83-94.
- Karpinska, A.M. and Bridgeman, J., 2016. CFD-aided modelling of activated sludge systems—A critical review. *Water research*, 88, pp.861-879.
- Karpinska, A.M. and Bridgeman, J., 2017. Towards a robust CFD model for aeration tanks for sewage treatment - a lab-scale study. *Engineering Applications of Computational Fluid Mechanics*, 11(1), pp.371-395.
- Karpinska, A.M. and Bridgeman, J., 2018. CFD as a tool to optimize aeration tank design and operation. *Journal of Environmental Engineering*, 144(2), p.05017008.
- Kissel, J.C., 1986. Modelling mass transfer in biological wastewater treatment processes. *Water science and technology*, 18(6), pp.35-45.

Kjellstrand, R., 2006. Hydraulic Behaviour in an Activated Sludge Tank: From Tracer Test through Hydraulic Modelling to Full-Scale Implementation.

Koot, A.C.J. and Zeper, J., 1972. Carrousel, a new type of aeration-system with low organic load. *Water Research*, 6(4-5), pp.401-406.

Kulkarni, A.A., 2007. Mass transfer in bubble column reactors: effect of bubble size distribution. *Industrial & Engineering Chemistry Research*, 46(7), pp.2205-2211.

Lauder, B.E. and Spalding, D.B., 1974. The numerical computation of turbulent flows. *Computer methods in applied mechanics and engineering*, 3(2), pp.269-289.

Lei, L. and Ni, J., 2014. Three-dimensional three-phase model for simulation of hydrodynamics, oxygen mass transfer, carbon oxidation, nitrification and denitrification in an oxidation ditch. *Water research*, 53, pp.200-214.

Le Bonté, S., Potier, O. and Pons, M.N., 2005. Toxic event detection by respirometry and adaptive principal components analysis. *Environmetrics*, 16(6), pp.589-601.

LeMoullec, Y., Potier, O., Gentric, C. and Leclerc, J.P., 2008a. A general correlation to predict axial dispersion coefficients in aerated channel reactors. *Water research*, 42(6), pp.1767-1777.

Le Moullec, Y., Potier, O., Gentric, C. and Leclerc, J.P., 2008b. Flow field and residence time distribution simulation of a cross-flow gas-liquid wastewater treatment reactor using CFD. *Chemical Engineering Science*, 63(9), pp.2436-2449.

Le Moullec, Y., Gentric, C., Potier, O. and Leclerc, J.P., 2010a. Comparison of systemic, compartmental and CFD modelling approaches: application to the simulation of a biological reactor of wastewater treatment. *Chemical engineering science*, 65(1), pp.343-350.

Le Moullec, Y., Gentric, C., Potier, O. and Leclerc, J.P., 2010b. CFD simulation of the hydrodynamics and reactions in an activated sludge channel reactor of wastewater treatment. *Chemical Engineering Science*, 65(1), pp.492-498.

Le Moullec, Y., Potier, O., Gentric, C. and Leclerc, J.P., 2011. Activated sludge pilot plant: Comparison between experimental and predicted concentration profiles using three different modelling approaches. *water research*, 45(10), pp.3085-3097.

Lesage, N., Sperandio, M., Lafforgue, C. and Cockx, A., 2003. Calibration and application of a 1-D model for oxidation ditches. *Chemical engineering research and design*, 81(9), pp.1259-1264.

Lewis, W.K. and Whitman, W.G., 1924. Principles of gas absorption. *Industrial & Engineering Chemistry*, 16(12), pp.1215-1220.

Levenspiel, O., 1998. Chemical Reaction Engineering. Wiley, New York.

Li, G., Mukhopadhyay, A., Cheng, C.Y. and Dai, Y., 2011, March. Various approaches to compute fluid residence time in mixing systems. In *ASME 2010 3rd Joint US-European Fluids Engineering Summer Meeting collocated with 8th International Conference on Nanochannels, Microchannels, and Minichannels* (pp. 295-304). American Society of Mechanical Engineers Digital Collection.

- Li, L., Lei, L., Zheng, M.S., Borthwick, A.G.L. and Ni, J.R., 2017. Stochastic evolutionary-based optimization for rapid diagnosis and energy saving in pilot and full-scale Carrousel oxidation ditches. *Journal of Environmental Informatics*, 35(1), pp.81-93.
- Littleton, H.X., Daigger, G.T. and Strom, P.F., 2007a. Application of computational fluid dynamics to closed-loop bioreactors: I. Characterization and simulation of fluid-flow pattern and oxygen transfer. *Water Environment Research*, 79(6), pp.600-612.
- Littleton, H.X., Daigger, G.T. and Strom, P.F., 2007b. Application of computational fluid dynamics to closed-loop bioreactors: II. Simulation of biological phosphorus removal using computational fluid dynamics. *Water environment research*, 79(6), pp.613-624.
- Liu, Y.L., Wei, W.L., Lv, B. and Yang, X.F., 2014. Research on optimal radius ratio of impellers in an oxidation ditch by using numerical simulation. *Desalination and Water Treatment*, 52(13-15), pp.2811-2816.
- Lo, S., 1998. Modelling of bubble breakup and coalescence with the MUSIG model. *AEA Technology,[Report] AEAT*, pp.1-17.
- Luo, H. and Svendsen, H.F., 1996. Theoretical model for drop and bubble breakup in turbulent dispersions. *AIChE Journal*, 42(5), pp.1225-1233.
- Makinia J. and Wells SA, 1999. Improvements in modelling dissolved oxygen in activated sludge systems. In Proceedings 8th IAWQ Conference on Design, Operation Economics Large Wastewater Treatment Plants 1999: Budapest, 518-25.
- Makinia, J. and Wells, S.A., 2000. A general model of the activated sludge reactor with dispersive flow—I. Model development and parameter estimation. *Water research*, 34(16), pp.3987-3996.
- Makinia, J. and Wells, S.A., 2005. Evaluation of empirical formulae for estimation of the longitudinal dispersion in activated sludge reactors. *Water research*, 39(8), pp.1533-1542.
- Mandt, M.G. and Bell, B.A., 1982. Oxidation ditches in wastewater treatment. *Ann Arbor Science, Ann Arbor MI. 1982. 169.*
- Manninen, M., Taivassalo, V. and Kallio, S., 1996. On the mixture model for multiphase flow.
- Martin, A.J., 1927 *The Activated Sludge Process*, MacDonald and Evans Publ., London, UK.
- McWhirter, J.R., Chern, J.M. and Hutter, J.C., 1995. Oxygen mass transfer fundamentals of surface aerators. *Industrial & engineering chemistry research*, 34(8), pp.2644-2654.
- Mena, P., Ferreira, A., Teixeira, J.A. and Rocha, F., 2011. Effect of some solid properties on gas-liquid mass transfer in a bubble column. *Chemical Engineering and Processing: Process Intensification*, 50(2), pp.181-188.

- Menter, F.R., 1994. Two-equation eddy-viscosity turbulence models for engineering applications. *AIAA journal*, 32(8), pp.1598-1605.
- Metcalf, E., Tchobanoglous, G., Burton, F.L. and Stensel, H.D., 2003. Wastewater Engineering, Treatment and Reuse (forth ed) McGraw-Hill. New York.
- Moore, D.W., 1965. The velocity of rise of distorted gas bubbles in a liquid of small viscosity. *Journal of Fluid Mechanics*, 23(04), pp.749-766.
- Mudde, R.F. and Van Den Akker, H.E., 2001. 2D and 3D simulations of an internal airlift loop reactor on the basis of a two-fluid model. *Chemical Engineering Science*, 56(21), pp.6351-6358.
- Mueller, J., Boyle, W.C. and Popel, H.J., 2002. *Aeration: principles and practice* (Vol. 11). CRC press.
- Nauman, E.B., 2007. Residence Time Distributions. John Wiley & Sons, Inc., New Jersey, NJ, USA, pp. 535e574.
- Nopens, I., Torfs, E., Ducoste, J., Vanrolleghem, P.A. and Gernaey, K.V., 2015. Population balance models: a useful complementary modelling framework for future WWTP modelling. *Water Science and Technology*, 71(2), pp.159-167.
- Norouzi-Firouz, H., Sarrafzadeh, M.H. and Zarghami, R., 2018. Investigating the Effect of Multiple Reference Frame Approach on the Modelling of an Oxidation Ditch. *International Journal of Environmental Research*, 12(4), pp.429-437.
- Oey, R.S., Mudde, R.F., Portela, L.M. and Van Den Akker, H.E.A., 2001. Simulation of a slurry airlift using a two-fluid model. *Chemical engineering science*, 56(2), pp.673-681.
- Olivet, D., Valls, J., Gordillo, M., Freixo, A. and Sanchez, A., 2005. Application of residence time distribution technique to the study of the hydrodynamic behaviour of a full-scale wastewater treatment plant plug-flow bioreactor. *Journal of Chemical Technology and Biotechnology*, 80(4), pp.425-432.
- Orhon, D., Soybay, S., Tünay, O. and Artan, N., 1989. The effect of reactor hydraulics on the performance of activated sludge systems—I. The traditional modelling approach. *Water Research*, 23(12), pp.1511-1518.
- Pasveer, A., 1962. Process and Device for the Purification of Sewage. CH360350. Passavant Werke, Switzerland.
- Patry, G.G. and Takács, I., 1992. Settling of flocculent suspensions in secondary clarifiers. *Water research*, 26(4), pp.473-479.
- Pereira, J.P., Karpinska, A., Gomes, P.J., Martins, A.A., Dias, M.M., Lopes, J.C.B. and Santos, R.J., 2012. Activated sludge models coupled to CFD simulations. *chemical engineering*, 2, p.3.
- Potier, O., Leclerc, J.P. and Pons, M.N., 2005. Influence of geometrical and operational parameters on the axial dispersion in an aerated channel reactor. *Water Research*, 39(18), pp.4454-4462.

- Pope, S.B., 2000. Turbulent flows. New York, NY, USA.
- Prince, M.J. and Blanch, H.W., 1990. Bubble coalescence and break-up in air-sparged bubble columns. *AIChE journal*, 36(10), pp.1485-1499.
- Qiu, Y., Zhang, C., Li, B., Li, J., Zhang, X., Liu, Y., Liang, P. and Huang, X., 2018. Optimal surface aeration control in full-scale oxidation ditches through energy consumption analysis. *Water*, 10(7), p.945.
- Ramponi, R., Blocken, B., Laura, B. and Janssen, W.D., 2015. CFD simulation of outdoor ventilation of generic urban configurations with different urban densities and equal and unequal street widths. *Building and Environment*, 92, pp.152-166.
- Ranade, V.V., 2002, Computational flow modeling for chemical reactor engineering by Vivek V. Ranade, 2002, Academic Press, San Diego, CA. Book
- Rao, A. R., 1999. "Predication of re-aeration rates in square, stirred tanks" J. Environ. Eng. 133(4), 411 – 418. 1999
- Rasmussen, M.R. and Larsen, T., 1996. A method for measuring sludge settling characteristics in turbulent flows. *Water Research*, 30(10), pp.2363-2370.
- Ratkovich, N., 2010. Understanding hydrodynamics in Membrane Bioreactor systems for wastewater treatment: Two-phase empirical and numerical modelling and experimental validation. Ghent University.
- Rauen, W.B., Angeloudis, A. and Falconer, R.A., 2012. Appraisal of chlorine contact tank modelling practices. *Water research*, 46(18), pp.5834-5847.
- Rodi, W., 1993. Turbulence models and their application in hydraulics. CRC Press.
- Roman, M.D. and Felseghi, R.A., 2014. Analysis of oxygen transfer and dissolved oxygen concentration measurement tests in a wastewater treatment plant. In *Applied Mechanics and Materials* (Vol. 656, pp. 486-494). Trans Tech Publications.
- Rosso D., Stenstrom M.K., and Larson L.E., 2008. Aeration of large-scale municipal wastewater treatment plants: state of the art. *Wat. Sci. Tech.*, 57(7), 973-78.
- Salter, H.E., Ta, C.T., Ouki, S.K. and Williams, S.C., 2000. Three-dimensional computational fluid dynamic modelling of a facultative lagoon. *Water Science and Technology*, 42(10-11), pp.335-342.
- Samstag, R.W., Wicklein, E.A., Reardon, R.D., Leetch, R.J., Parks, R.M. and Groff, C.D., 2012. Field and CFD analysis of jet aeration and mixing. *Proceedings of the Water Environment Federation*, 2012(12), pp.4113-4139.
- Samstag, R.W. and Wicklein, E.A., 2014. A Protocol for Optimization of Activated Sludge Mixing. *Proceedings of the Water Environment Federation*, 2014(13), pp.3614-3640.

Samstag, R.W., Ducoste, J.J., Griborio, A., Nopens, I., Batstone, D.J., Wicks, J.D., Saunders, S., Wicklein, E.A., Kenny, G. and Laurent, J., 2016. CFD for wastewater treatment: an overview. *Water Science and Technology*.

Sánchez, F., Rey, H., Viedma, A., Nicolás-Pérez, F., Kaiser, A.S. and Martínez, M., 2018. CFD simulation of fluid dynamic and biokinetic processes within activated sludge reactors under intermittent aeration regime. *Water research*, 139, pp.47-57.

Sato, Y., Sadatomi, M. and Sekoguchi, K., 1981. Momentum and heat transfer in two-phase bubble flow. *International Journal of Multiphase Flow*, 7(2), pp.167-177.

Schiller, L. and Naumann, Z., 1935. A drag coefficient correlation. *Vdi Zeitung*, 77(318), p.51.

Schmid, M., Thill, A., Purkhold, U., Walcher, M., Bottero, J.Y., Ginestet, P., Nielsen, P.H., Wuertz, S. and Wagner, M., 2003. Characterization of activated sludge flocs by confocal laser scanning microscopy and image analysis. *Water research*, 37(9), pp.2043-2052.

Seco, A., Ribes, J., Serralta, J. and Ferrer, J., 2004. Biological nutrient removal model No. 1 (BNRM1). *Water Science and Technology*, 50(6), pp.69-70.

Seco, A., Ruano, M.V., Ruiz-Martinez, A., Robles, A., Barat, R., Serralta, J. and Ferrer, J., 2020. Plant-wide modelling in wastewater treatment: showcasing experiences using the Biological Nutrient Removal Model. *Water Science and Technology*.

Sears, K., Alleman, J.E., Barnard, J.L. and Oleszkiewicz, J.A., 2006. Density and activity characterization of activated sludge flocs. *Journal of environmental engineering*, 132(10), pp.1235-1242.

Simonin, O., 1990, March. Eulerian formulation for particle dispersion in turbulent two-phase flows. In *Proceedings of the Fifth Workshop on Two-Phase Flow Predictions, Erlangen, Germany* (pp. 156-166).

Sokolichin, A., Eigenberger, G., Lapin, A. and Lübert, A., 1997. Dynamic numerical simulation of gas-liquid two-phase flows Euler/Euler versus Euler/Lagrange. *Chemical Engineering Science*, 52(4), pp.611-626.

Stamou, A.I., 1994. Modeling oxidation ditches using the IAWPRC Activated Sludge Model with Hydrodynamic Effects *Water science and technology*, 30(2), pp.185-192.

Stamou, A., Katsiri, A., Mantziaras, I., Boshnakov, K., Koumanova, B. and Stoyanov, S., 1999. Modelling of an alternating oxidation ditch system. *Water science and technology*, 39(4), pp.169-176.

Stenstrom M.K and Rosso, D., 2010. Aeration. Presentation. University of California.

Takács, I., Patry, G.G. and Nolasco, D., 1991. A dynamic model of the clarification-thickening process. *Water research*, 25(10), pp.1263-1271.

Talvy, S., Cockx, A. and Line, A., 2005. Global modelling of a gas-liquid-solid airlift reactor. *Chemical Engineering Science*, 60(22), pp.5991-6003.

- Talvy, S., Cockx, A. and Line, A., 2007. Modeling hydrodynamics of gas–liquid airlift reactor. *AIChE journal*, 53(2), pp.335-353.
- Terashima, M., So, M., Goel, R. and Yasui, H., 2016. Determination of diffuser bubble size in computational fluid dynamics models to predict oxygen transfer in spiral roll aeration tanks. *Journal of Water Process Engineering*, 12, pp.120-126.
- Thakre, S.B., Bhuyar, L.B. and Deshmukh, S.J., 2008. Effect of different configurations of mechanical aerators on oxygen transfer and aeration efficiency with respect to power consumption. *International Journal of Aerospace and Mechanical Engineering*, 2(2), pp.100-108.
- Thakre, S.B., Bhuyar, L.B. and Deshmukh, S.J., 2009. Oxidation ditch process using curved blade rotor as aerator. *International Journal of Environmental Science & Technology*, 6(1), pp.113-122.
- USEPA, 2000. Wastewater Technology Fact Sheet: Oxidation Ditches. EPA 832-F-00-013. US Environmental Protection Agency, Washington, DC, USA.
- Van Baten, J.M., Ellenberger, J. and Krishna, R., 2003. Hydrodynamics of internal air-lift reactors: experiments versus CFD simulations. *Chemical Engineering and Processing: Process Intensification*, 42(10), pp.733-742.
- Van Benthum, W.A.J., Van der Lans, R.G.J.M., Van Loosdrecht, M.C.M. and Heijnen, J.J., 1999. Bubble recirculation regimes in an internal-loop airlift reactor. *Chemical engineering science*, 54(18), pp.3995-4006.
- Vesilind, P.A., 1968. Design of prototype thickeners from batch settling tests. *Water Sewage Works*, 115(7), pp.302-307.
- Wallis, G.B., 1974. The terminal speed of single drops or bubbles in an infinite medium. *International Journal of Multiphase Flow*, 1(4), pp.491-511.
- Wang, H., Li, Y. and Zhao, Z., 2009. Computational study on micro-scale behaviour of bubble generated by aeration in a plug-flow aeration tank. *Water Science and Technology*, 59(10), pp.2065-2072.
- Wang, X., Ding, J., Ren, N.Q., Liu, B.F. and Guo, W.Q., 2009. CFD simulation of an expanded granular sludge bed (EGSB) reactor for biohydrogen production. *International journal of hydrogen energy*, 34(24), pp.9686-9695.
- Wang, X., Ding, J., Guo, W.Q. and Ren, N.Q., 2010. A hydrodynamics–reaction kinetics coupled model for evaluating bioreactors derived from CFD simulation. *Bioresource technology*, 101(24), pp.9749-9757.
- Wang, W., Shi, C., Yang, J., Zeng, M., Dai, Z. and Zhang, Z., 2019. Modelling performance of oxidation ditch in wastewater treatment plant by STOAT software. In *IOP Conference Series: Earth and Environmental Science* (Vol. 300, p. 032065).
- Wang, M., Mo, H., Liu, G.H., Qi, L., Yu, Y., Fan, H., Xu, X., Luo, T., Shao, Y. and Wang, H., 2020. Impact of scaling on aeration performance of fine-pore membrane diffusers based on a pilot-scale study. *Scientific reports*, 10(1), pp.1-10.

- Wei, W., Liu, Y. and Lv, B., 2016a. Numerical simulation of optimal submergence depth of impellers in an oxidation ditch. *Desalination and Water Treatment*, 57(18), pp.8228-8235.
- Wei, W., Zhang, Z., Zheng, Y. and Liu, Y., 2016b. Numerical simulation of additional guiding baffles to improve velocity distribution in an oxidation ditch. *Desalination and Water Treatment*, pp.1-10.
- Wen, C., Yu, Y., 1966. Mechanics of fluidization. In *Chem. Eng. Prog. Symp. Ser.*(Vol. 6, pp. 100-101).
- Wicklein, E.A. and Samstag, R.W., 2009. Comparing Commercial and Transport CFD Models for Secondary Sedimentation. *Proceedings of the Water Environment Federation*, 2009(10), pp.6066-6081.
- Wicklein, E., Batstone, D.J., Ducoste, J., Laurent, J., Griborio, A., Wicks, J., Saunders, S., Samstag, R., Potier, O. and Nopens, I., 2016. Good modelling practice in applying computational fluid dynamics for WWTP modelling. *Water Science and Technology*, 73(5), pp.969-982.
- Wilcox, D.C., 1998. *Turbulence modeling for CFD* (Vol. 2, pp. 103-217). La Canada
- Wu, B., 2010. CFD analysis of mixing in large aerated lagoons. *Engineering Applications of Computational Fluid Mechanics*, 4(1), pp.127-138.
- Wu, B. and Chen, Z., 2011. An integrated physical and biological model for anaerobic lagoons. *Bioresource technology*, 102(8), pp.5032-5038.
- Wu, S.Y., Zhou, D.Q. and Zheng, Y., 2012. Energy configuration optimization of submerged propeller in oxidation ditch based on CFD. In *IOP Conference Series: Earth and Environmental Science* (Vol. 15, No. 7, p. 072012). IOP Publishing.
- Xie, H., Yang, J., Hu, Y., Zhang, H., Yang, Y., Zhang, K., Zhu, X., Li, Y. and Yang, C., 2014. Simulation of flow field and sludge settling in a full-scale oxidation ditch by using a two-phase flow CFD model. *Chemical Engineering Sc.*, 109, pp.296-305.
- Xu, N., Fan, L., Pang, H. and Shi, H., 2010. Feasibility study and CFD-aided design for a new type oxidation ditch based on airlift circulation. *The Canadian Journal of Chemical Engineering*, 88(5), pp.728-741.
- Xu, Q., Yang, J., Hou, H., Hu, Y., Liang, S., Xiao, K., Wu, X., Liu, B., Hu, J., Hu, J. and Yang, C., 2018. Simulation of flow field and gas hold-up of a pilot-scale oxidation ditch by using liquid-gas CFD model. *Water Science and Technology*, 78(9), pp.1956-1965.
- Yang, L.B., Zeng, S.Y., Ju, Y.P., He, M. and Chen, J., 2008. Statistical analysis and quantitative recognition of energy consumption of municipal wastewater treatment plants in China. *Water and Wastewater Engineering*, 34(10), pp.42-45.
- Yang, Y., Wu, Y., Yang, X., Zhang, K. and Yang, J., 2010. Flow field prediction in full-scale Carrousel oxidation ditch by using computational fluid dynamics. *Water Science and Technology*, 62(2), pp.256-265.

Yang, Y., Yang, J., Zuo, J., Li, Y., He, S., Yang, X. and Zhang, K., 2011. Study on two operating conditions of oxidation ditch for optimisation of energy consumption and effluent quality by using CFD model. *Water research*, 45(11), pp.3439-3452.

Zhang, J.M., Lee, H.P., Khoo, B.C., Teo, C.P., Haja, N. and Peng, K.Q., 2011. Modeling and simulations of flow pattern, chlorine concentration, and mean age distributions in potable water service reservoir of Singapore. *Journal of Environmental Engineering*, 137(7), pp.575-584.

Zhang, T., Wei, C., Feng, C. and Zhu, J., 2012. A novel airlift reactor enhanced by funnel internals and hydrodynamics prediction by the CFD method. *Bioresource technology*, 104, pp.600-607.

Zhang, Y., Zheng, Y., Fernandez-Rodriguez, E., Yang, C., Zhu, Y., Liu, H. and Jiang, H., 2016. Optimization design of submerged propeller in oxidation ditch by CFD and comparison with experiments. *Water Science and Technology*.

Zhang, Y., Li, C., Xu, Y., Tang, Q., Zheng, Y., Liu, H. and Fernandez-Rodriguez, E., 2019. Study on propellers distribution and flow field in the oxidation ditch based on two-phase CFD model. *Water*, 11(12), p.2506.

Zima, P., Makinia, J., Swinarski, M. and Czerwionka, K., 2008. Effects of different hydraulic models on predicting longitudinal profiles of reactive pollutants in activated sludge reactors. *Water Science and Technology*, 58(3), pp.555-561.

Zima, P., Makinia, J., Swinarski, M. and Czerwionka, K., 2009. Combining computational fluid dynamics with biokinetic model for ammonia and phosphate behavior in aeration tanks. *Water Environment Research*, 81(11), pp.2353-2362.

Zuber, N., Findlay, J.A., 1965. Average volumetric concentration in two phase flow systems. *International Journal of Heat Mass Transfer* 87, 453-468.

## Appendix

This is a literature review published during the doctorate study with this citation. The abstract of the published paper is also given here.

Matko, T., Chang, J. and Xiao, Z., 2017, June. Recent Progress of Computational Fluid Dynamics Modelling of Animal and Human Swimming for Computer Animation. In *International Workshop on Next Generation Computer Animation Techniques* (pp. 3-17). Springer, Cham.

"A literature review is conducted on the Computational Fluid Dynamics (CFD) modelling of swimming. The scope is animated films and games, sports science, animal biological research, bio-inspired submersible vehicle design and robotic design. There are CFD swimming studies on animals (eel, clownfish, turtle, manta, frog, whale, dolphin, shark, trout, sunfish, boxfish, octopus, squid, jellyfish, lamprey) and humans (crawl, butterfly, backstroke, breaststroke, dolphin kick, glide). A benefit is the ability to visualise the physics-base effects of a swimmer's motion, using key-frame or motion capture animation. Physics-based animation can also be used as a training tool for sports scientists in swimming, water polo and diving. Surface swimming is complex and considers the water surface shape, splashes, bubbles, foam, bubble coalescence, vortex shedding, solid-fluid coupling and body deformation. Only the Navier-Stokes fluid flow equations can capture these effects. Two way solid-fluid coupling between the swimmer and the water is modelled to be able to propel the swimmer forwards in the water. Swimmers are often modelled using articulated rigid bodies, thus avoiding the complexity of deformable body modelling. There is interesting potential research, including the effects of hydrodynamic flow conditions on a swimmer and the use of motion capture data. The predominant approach for swimming uses grid-based fluid methods for better accuracy. Emerging particle and hybrid-based fluid methods are being increasingly used in swimming for better three dimensional fluid visualisation of the motion of the water surface, droplets, bubbles and foam."